EXPERIMENTAL INVESTIGATIONS ON CONTROLLED AUTO-IGNITION COMBUSTION IN A FOUR-STROKE GASOLINE ENGINE

A thesis submitted for the degree of Doctor of Philosophy

by

Aaron John Oakley

Department of Mechanical Engineering
Brunel University
Middlesex, United Kingdom

September 2001

Brunel University
Department of Mechanical Engineering
Middlesex, United Kingdom

Aaron John Oakley
Experimental investigations on controlled autoignition combustion in a four stroke gasoline engine
September 2001, Ph.D.

Abstract

The effects of air and exhaust gas dilution on the CAI combustion of a range of fuels including three gasoline compositions, four primary reference fuels, and two alcohols are experimentally investigated using a single cylinder research engine. Two of the three gasolines tested are manufactured from standard gasoline during engine operation by a novel fuel system, designed to improve the performance of both controlled autoignition and spark ignition engines.

A series of experimental tests are performed to establish the satisfactory combined air and exhaust gas dilution regions for each fuel. Detailed in-cylinder pressure and exhaust gas speciation measurements are taken, and the fuels are compared and contrasted for their performance in terms of power output, fuel consumption, and harmful exhaust emissions. Results show that alcohol fuels are superior to hydrocarbon fuels for controlled autoignition combustion because their autoignition characteristics are less affected by the presence of exhaust gas species. Furthermore, the timing of autoignition is shown to be of minor importance for achieving efficient and stable controlled autoignition combustion, contrary to widely held beliefs.

In addition, the novel fuel system is developed and commissioned for use on a single cylinder research engine operating with a spark ignition system. The two gasoline fuels produced by the system are evaluated individually for their knocking combustion characteristics over a range of compression ratios and spark advances. Results from these tests indicate that the fuel system used in conjunction with a specially modified production engine may allow the normal compression ratio of that engine to be increased by up to 1.0, increasing its efficiency.

Acknowledgements

First and foremost, I would like to express my sincere thanks to my supervisor, Dr. Hua Zhao for his keen interest, guidance, and moral support throughout the course of this project. Thanks are also due to him for allowing me to attend a large number of external meetings and conferences, which has deepened my knowledge and experience beyond words. I would also like to thank Professor Nicos Ladommatos, for his support and opinions during regular progress meetings.

I am indebted to a number of laboratory technicians for their expertise and assistance while commissioning the experimental test facility. For his tireless work designing and building the majority of the electronic control systems, I thank Mr. Clive Barrett. For their assistance on technical matters, and for fabricating many of the components I required for the test facility, I express deep thanks to Mr. Andy Selway, Mr. John Tierney, and Mr. Ian Hutchby. I also wish to thank Mr. Bob Webb, who has always helped me out of difficult situations when most required. I express my gratitude to my colleague and friend, Mr. John Williams for his development and assistance in commissioning the in-cylinder data acquisition system.

Thanks are due to the Ford Motor Company for providing financial assistance for this project. In particular, Dr. Tom Ma has shown great enthusiasm for the project, helping particularly with development of the fuel fractionating system, and I sincerely thank him for his input.

I would like to acknowledge the support of our partners in the 4-SPACE project (IFP, Ford, Daimler-Chrysler, PSA Peugeot-Citroen, and Heidelberg University), who provided a context for this project, and gave valuable advice upon receiving results.

I would like to thank my parents, Brian and Patricia Oakley. I could not have reached where I am today without the support that they have shown, and the sacrifices that they have made for me throughout my life.

Finally, I would like to sincerely thank my partner, Aileen, for listening and lending support throughout this project and all my other endeavours.

Nomenclature

General Abbreviations

A/F Ratio	Air/Fuel Ratio
ABDC	After Bottom Dead Centre
AC	Alternating Current
ARC	Active Radical Combustion
ASTM	American Society for the Testing of Materials
ATAC	Active Thermo-Atmosphere Combustion
ATDC	After Top Dead Centre
BBDC	Before Bottom Dead Centre
BMEP	Brake Mean Effective Pressure
BTDC	Before Top Dead Centre
CA	Crank Angle
CAI	Controlled Auto-Ignition
CAN Index	Controlled Autoignition Index
CARB	California Air Resources Board
CFR	Cooperative Fuels Research
CI	Compression Ignition
CIHC	Compression Ignited Homogeneous Charge
CN	Cetane Number
COVimep	Coefficient of Variation in IMEP
CR	Compression Ratio
DAQ	Data Acquisition
ECU	Electronic Control Unit
EGR	Exhaust Gas Recirculation
EMI	Electromagnetic Interference
EU	European Union
FBP	Final Boiling Point
FDCCP	Fluid Dynamically Controlled two-stroke Combustion Process
FID	Flame Ionisation Detection
FMEP	Friction Mean Effective Pressure
FS	Fuel Sensitivity

FTP	Federal Test Procedures
GC	Gas Chromatography
GDI	Gasoline Direct Injection
HC	Hydrocarbons
HCCI	Homogeneous Charge Compression Ignition
HPLC	High Precision Liquid Chromatography
HRR	Heat Release Rate
HSDI	High Speed Direct Injection
Hz	Hertz
IBM	International business machines
IBP	Initial Boiling Point
IC	Internal Combustion
IMEP	Indicated Mean Effective Pressure
ISFC	Indicated Specific Fuel Consumption
IVC	Inlet Valve Closure
KLSA	Knock Limited Spark Advance
KOF	Knock Occurrence Frequency
LAG	Avalanche Activated Combustion
LEV	Low Emissions Vehicle
LGV	Light Goods Vehicle
MBT	Minimum Spark Advance for Best Torque
MFB	Mass Fraction Burned
MON	Motoring Octane Number
MS	Mass Spectrometry
NDIR	Non-Dispersive Infrared
NMOG	Non-Methane Organic Gas
NTC	Negative Temperature Coefficient
ON	Octane Number
PCCI	Premixed Charge Compression Ignition
PID	Proportional + Integral + Differential
PM	Particulate Matter
PMEP	Pumping Mean Effective Pressure
PRF	Primary Reference Fuel
RON	Research Octane Number
rpm	revolutions per minute

RVP	Reid Vapour Pressure
SCR	Selective Catalytic Reduction
SI	Spark Ignition
STRAFFE	Stratified Fuel Fraction Engine
SULEV	Super Ultra Low Emissions Vehicle
TDC	Top Dead Centre
THC	Total Hydrocarbons
TLEV	Transitional Low Emissions Vehicle
TS	Toyota-Soken
UEGO	Universal Exhaust Gas Oxygen
UK	United Kingdom
ULEV	Ultra Low Emissions Vehicle
USA	United States of America
VOC	Volatile Organic Compounds
VVA	Variable Valve Actuation
WOT	Wide Open Throttle
ZEV	Zero Emissions Vehicle

General Notation

λ, lambda	Relative air/fuel ratio
γ	Ratio of specific heats
η_i	Indicated thermal efficiency
σ	Standard deviation
θ	Crank angle
τ	Arrhenius time constant
A	Constant
a	Crank radius, wet molar fraction of fuel
B	Constant
b	H/C ratio of fuel
c	O/C Ratio of fuel
c_v	Specific heat at constant volume
d	Wet molar fraction of inlet air
f	Wet molar fraction of exhaust products in inlet mixture

g	Wet molar fraction of CO_2
h	Wet molar fraction of CO
i	Numerical index, denotes intake species
j	Wet molar fraction of O_2
k	Wet molar fraction of N_2
l	Connecting rod length, Wet molar fraction of H_2O
m	Wet molar fraction of NO
m_{EGR}	Mass flow rate of EGR through cylinder
m_R	Mass flow rate of reactants
m_f	Mass of fuel contained in the cylinder
m_x	molecular mass (where x is CH_bO_c, CO_2, CO, O_2, N_2, H_2O, CH_4, H, or O)
mfb	heat release condition
N	Engine Speed
n	Constant, polytropic coefficient, number of crank revolutions per power stroke
n_f	Number of moles of fuel in the intake charge
n_R	Number of moles of reactants
n_P	Number of moles of products
n_{start}	Total number of moles trapped in-cylinder at IVC
n_t	Number of moles in-cylinder at mfb (heat release) condition
P, p	Pressure
P_c	In-Cylinder Pressure
P_i	Indicated Power
Q	Heat transfer
Q_{HV}	Lower heating value of the fuel
q	Heat transfer, Wet molar fraction of NO_2
Q_n	Net heat release
δQ_{hr}	Heat released during combustion
δQ_{ht}	Heat exchange with combustion chamber walls
R	Universal gas constant
s	Geometric length, Wet molar fraction of unburned hydrocarbons
T	Temperature
t	Wet molar fraction of H_2
dU	Systematic change in internal energy
V	Volume

V_c	Clearance volume
V_d	Displaced volume
v	Wet molar fraction of O_2 in the intake gas
W, w	Work transfer
δW	Work done by cylinder gases on the piston
x	Number of engine cycles, generic wet molar fraction

Chemical Symbols and Abbreviations

C, C_2	Carbon
CH_4	Methane
CH_bO_c	Generic fuel type
CO	Carbon monoxide
CO_2	Carbon dioxide
DME	Di-methyl ether
H_2O	Water
HCHO	Formaldehyde
HO_2	Hydrogen dioxide
MTBE	Methyl tertiary-butyl ether
NMA	N-methlanaline
NO	Nitrogen oxide
NO_2	Nitrogen dioxide
NO_x	Combined oxides of nitrogen
O	Oxygen radical
O_3	Ozone
OH	Hydroxyl radical
PTFE	Polytetrafluoroethylene
R	Radical
TEL	Tetra ethyl lead
TEM	Tetra methyl lead

Contents

Chapter 1

Introduction

Chapter 1 Introduction

1.1 Introduction

The use of Internal Combustion (IC) engines has grown exponentially since their inception in the late nineteenth century. For variable light-duty mobile applications, reciprocating IC engines utilising the Otto or Diesel cycles are now ubiquitous. However, in recent times issues such as environmental pollution and fuel cost are increasingly becoming important, precipitating massive growth in research and development of cleaner and more efficient IC engines. In addition, the search is on to find cleaner, more efficient, and economic alternatives to those currently available. There are a few prime mover technologies such as the Electric and Fuel Cell types that may become viable over the coming decades, providing they are developed sufficiently to offer comparable or better energy efficiencies than IC engines. However, to become real alternatives the new technologies must also match the versatility, power density, cost, and durability of IC engines. Furthermore, widespread changes to the fuel delivery infrastructure may be required for technologies such as the Fuel Cell. For these reasons, the IC engine is likely to remain dominant for automotive applications for at least the next two decades, and probably longer.

In the absence of viable alternatives, researchers are faced with continuously improving spark-ignition (SI) and compression-ignition (CI) technologies, to improve their efficiencies and reduce harmful emissions. With the introduction of Gasoline Direct Injection (GDI) and high-pressure direct-injection Diesel systems, a major effort in both SI and CI research is focussed on developing adequate exhaust aftertreatment systems to reduce harmful Nitrogen Oxides (NO_x), Hydrocarbons (HC), Carbon Monoxide (CO), and particulates simultaneously, while still maintaining high engine efficiencies. Despite concerted efforts, a trade-off currently exists between the ability to achieve high efficiencies, and the ability to prevent harmful exhaust emissions reaching the environment.

However, an alternative combustion technology has recently been identified that exhibits similar efficiencies as GDI and CI engines, while emitting a tiny fraction of the NO_x. Known by a number of names including HCCI (Homogeneous Charge Compression Ignition) and CAI (Controlled Autoigntion), this combustion may allow current and forthcoming efficiency and emissions targets to be met without the use of expensive,

complicated, and inefficient exhaust aftertreatment systems. The technology has already been introduced in some 2-stroke engines (HONDA ARC 250), and it is the task of current researchers to transfer it to 4-stroke engines, which must be used for forthcoming emissions targets to be met successfully. Practical applications of CAI combustion in multi-cylinder production engines have emerged over the past few years. Such systems require copious quantities of burned residual gases to be trapped in-cylinder prior to induction, which provides both the heat energy and charge dilution to achieve autoignition and controlled combustion respectively. Unfortunately, the high levels of dilution required limit the power density of such engines.

Research in this field has evolved over the past thirty or forty years, and there are currently in excess of 100 technical papers that deal with various aspects of CAI combustion. However, review of the literature indicated that there is significant scope to investigate dilution effects on CAI combustion. Given that the most viable practical systems appear to be those that use one or a combination of air and residual dilution, this has provided a focus and context for the work presented in this thesis. A parametric survey has been undertaken to investigate the air and exhaust gas dilution effects on CAI combustion characteristics for a number of fuels, including gasoline, some selected primary reference fuels (PRF), and some alcohols. Detailed measurements of combustion and emissions characteristics have allowed valuable comparisons between different fuels and operating conditions to be made, unparalleled in previous work in this area.

A novel fuelling system has been designed and patented by the Ford Motor Company. As part of the work presented here, original concepts have been developed into a fully operational prototype. The fuel system's function is to separate standard gasoline into two fuel streams by a process of distillation. The two streams have varying normal and knocking combustion characteristics when used in an SI engine, which translates to varying autoignition characteristics when used in an CAI engine. In practice, both engine types will need to be specially modified to allow strategic positioning of each fuel stream within the combustion chamber, to allow the superior attributes of each fuel to be harnessed. Thus, the fuel system may provide benefits for both SI and CAI combustion, and it has been evaluated for each.

1.2 Objectives of Project

The objectives of the project are to:

(i) Improve the understanding of the complex interplay between air and exhaust gas dilution on CAI combustion, and their effect on combustion related parameters such as the phasing of heat release, engine power, and exhaust emissions.

(ii) Design, develop, and commission a working prototype of the novel fuel system proposed by the Ford Motor Company, and evaluate it for the improvement of performance in SI engines.

(iii) Investigate the suitability of a number of fuels including gasoline, the two streams produced by the fuel system, some primary reference fuels, methanol, and ethanol for CAI combustion. Specifically, comparisons are required between fuel types to better understand how composition and structure affect CAI combustion characteristics and emissions.

(iv) Provide detailed information on a number of fuels and over a wide range of strictly controlled engine operating conditions for the calibration of CAI combustion models, which is currently an area of intense research.

1.3 Outline of Thesis

Following the introduction, chapter two contains the literature review. The review is broadly divided into four sections. Firstly, a review of current and future emissions legislation provides a context for continuing research and development of powertrain systems. Next, a section detailing the state of current technology outlines a number of competing strategies for automotive power applications. The penultimate section reviews literature relevant to spark-induced knocking combustion, which is required for the evaluation of the novel fuel system for SI combustion. Finally, a range of papers relevant to CAI combustion are covered, highlighting gaps in current knowledge, and providing a basis for the investigation of CAI combustion presented in chapters six and seven.

Chapter three details the experimental test facility used for all engine tests. The research engine with its modified fluid and combustion control systems are discussed in detail. A separate section outlines the instrumentation, incorporating both exhaust gas and in-

cylinder data acquisition. Here, the opportunity is taken to discuss the techniques used to process raw data into meaningful results.

The development and operation of the fuel system is the subject of chapter four. The system is put into context with a description of the engine concept for which it is required. A detailed description of the functionality of the fuel system follows, along with a discussion of its practicality and limitations.

Chapter five contains results of an investigation that evaluates the suitability of the novel fuel system for improving SI engine performance. The investigation concentrates on the measurement and prevention of spark-induced knocking combustion. A parametric survey of compression ratio and spark advance is undertaken for each fuel stream separately, and compared to results from standard gasoline, and some selected primary reference fuels. Extraneous figures relating to the work presented in this chapter are presented towards its end.

Chapter six describes the first investigation on the dilution effects on CAI combustion, for standard gasoline fuel. The CAI combustion test methodology and experimental procedures are fully explained here. CAI combustion is achieved under high intake temperature conditions, and in-cylinder pressure and exhaust gas speciation measurements are obtained for a range of air and exhaust gas dilution conditions. In this chapter, discussions concentrate on the quantitative comparisons between CAI and SI combustion, and the relative merits of each. Also, harmful emissions such as NO_x and HC are correlated to calculated in-cylinder temperatures.

In contrast, chapter seven attempts to draw qualitative comparisons between a total of nine different fuels, all tested under the same CAI combustion conditions. Comparisons between fuels are made by considering heat release profiles, in-cylinder temperatures, power output, and emissions levels. In order to preserve the continuity of text in this chapter, the large number of figures relevant to the work are presented towards the end.

Chapter eight contains the general conclusions and recommendations for further work. Conclusions are drawn together from separate sections contained at the end of chapters five, six, and seven, giving a broad overview of the progress made throughout this work. Recommendations for further work stem both from problems experienced during analysis

of results presented here, and from the knowledge gained that can be applied to future investigations.

Appendix A contains details of the analytical approach that has been developed for the calculation of Air/Fuel ratio and exhaust gas dilution rate given intake and exhaust speciation data only. This method was developed in response to inaccuracies incurred when using others. While an overview of this approach is contained in chapter three, here a step-by-step derivation is given.

Chapter 2

Literature Review

Chapter 2 Literature Review

2.1 Introduction – Emissions Legislation

The two main goals of current powertrain development are centred on increasing efficiencies and reducing environmental impact. In the UK, greenhouse gas emissions from the transport sector, which comprise Carbon Dioxide (CO_2), Volatile Organic Compounds (VOC), and oxides of Nitrogen (NO_x), currently account for 21% of the total. This is projected to rise to 26% by 2020 despite the best efforts of researchers to tackle the problem [1]. Global concern over how the exponential increase in economic activity is affecting our climate is reflected in the Kyoto Protocol [2]. Under this agreement, the UK has committed itself to a reduction of 12% in total CO_2 emissions by 2010, although domestic targets are as high as 20%.

Concern over the emissions from fossil-fuel powerplant can be broadly divided into two categories. Firstly, the emission of CO_2 has predominantly global implications. Many environmental studies have documented the acceleration of global temperatures over the last few decades, which has already led to the reduction of polar ice mass, and may be responsible for erratic weather patterns seen recently. Secondly, the emitted species that have predominantly local climate effects: NO_x and VOCs (emitted at ground level) react with atmospheric oxygen in the presence of sunlight to produce photochemical smog, known to cause respiratory problems. A by-product of this process is the formation of ozone, which can be lethal even in relatively small quantities. Carbon Monoxide resulting from incomplete carbon oxidation (to CO_2) is usually associated with homogeneous combustion under rich conditions, and can cause unconsciousness and respiratory failure if inhaled in sufficient quantities. Soot is generally formed as a result of inhomogeneous (diffusion rate-limited) combustion, and, along with certain hydrocarbon types (e.g. Benzene) can be carcinogenic.

Over recent years, large reductions in NO_x and VOC emissions from powerplants have been brought about by improvements in post-combustion gas treatment (after-treatment) technologies, such as catalysts. The last three decades brought about a revolution, with the introduction of legislative programmes in the United States (USA), the European Union (EU), and Japan to enforce exhaust after-treatment. The legislation is constantly being

reviewed and updated in line with developments in combustion control and after-treatment systems. The emissions legislations for passenger cars are summarised in table 1.

Euro Standard	Year	Engine Type	CO (g/km)	HC / NMOG (g/km)	NOx (g/km)	HC+NOx (g/km)	PM (g/km)
Euro II	1996	SI	2.20			0.50	
		CI	1.00			0.70	0.08
Euro III	2001	SI	2.30	0.20	0.15		
		CI	0.64		0.50	0.56	0.05
Euro IV	2005	SI	1.00	0.10	0.08		
		CI	0.5		0.25	0.3	0.025
CARB (Tier I)	2001-03		**5**	**0.25**	**0.4**		**0.08**
TLEV		Any	2.1	0.2	0.25		0.08*
LEV		Any	2.1	0.05	0.13		0.08*
ULEV		Any	1.1	0.025	0.13		0.04*
ZERO		Any	0	0	0		0
CARB (LEV II)	2004-10		**2**	**0.033**	**0.04**		
TLEV		Any					
LEV		Any	4.2	0.056	0.07		0.01
ULEV		Any	2.1	0.034	0.07		0.01
SULEV		Any	1	0.006	0.02		0.01

* After 100,000 miles

Sources [3, 4]

Table 2.1 Legislated emissions: EU and California Air Resources Board (CARB)

The EU operate a comparatively simple system: Legislation becomes effective from a certain date, and all vehicles produced after this must comply to individual Spark-Ignition (SI) or Compression-Ignition (CI) standards. The reason for disparity between the two engine types stems from technological differences in combustion regime and after-treatment systems. Legislation from the CARB is presented because it places the strictest limits on vehicle emissions in the world. The USA operates a 'fleet-averaged' emissions strategy. 'Tier 1' legislation states an average emissions level, to which the fleet must adhere. For example, individual manufacturers can sell a number of ZEVs (Zero Emission Vehicles) and TLEVs (Transitional Low Emission Vehicles) in combination to hit that average.

The figures for EU and CARB emissions levels are not directly comparable due to differences in the test drive cycle and measurements of VOC: the Federal Test Procedures (FTP) do not require the measurement of Methane in the exhaust emissions, so hydrocarbon content is defined as Non-Methane Organic Compounds (NMOG). Johnson [5] presented normalised tailpipe standards for Europe, the USA, and Japan. He showed that the US 'Tier 2' (≡ CARB LEV II) legislation being introduced in 2004 requires a

roughly similar level of HC emissions to the Euro IV (2005) standard. However, NO_x emissions will be halved compared to Euro IV. He concluded that the market penetration of Gasoline Direct Injection (GDI) and High Speed Direct Injection (HSDI) Diesel engines in the USA would be severely affected by such strict NO_x limitations, since adequate after-treatment technologies have not yet been developed. This example shows that the way in which legislation is implemented has a direct impact on the economic drivers for research and development. Consequently, GDI and HSDI technologies for passenger cars require significant enhancements before they will be adopted into the mainstream US market.

2.2 State of the Art

The ultimate goal of legislators and vehicle manufacturers alike is to produce a cheap and economical zero emission vehicle. Using current technology, there is only one type of vehicle that is truly a ZEV. It is one that employs a fuel cell to combine hydrogen and atmospheric oxygen to produce electricity, which can then be converted to mechanical energy. This vehicle is only a ZEV if the hydrogen is obtained (from water) using a renewable energy source such as sunlight. Fuel cell vehicles that 'reform' Methanol to obtain the hydrogen necessarily emit CO_2. This introduces the important concept of 'well-to-wheel efficiency'. Since limited fossil fuel reserves are used globally for almost all of our energy requirements, and atmospheric CO_2 has recently been identified as the major cause of global warming, it is on our interests to evaluate the total 'energy cost' of particular vehicle technologies for comparison. Weiss et al. [6] have undertaken such an analysis to compare existing and emerging technologies with developments projected to 2020. The total energy consumption per unit distance travelled includes the vehicle production cost, fuel production cost, and vehicle running costs. They predicted that Diesel and Gasoline hybrids will be most energy efficient, followed by electric vehicles, and then hydrogen powered fuel cell vehicles, not including vehicles with on-board reformers. Given the fuel delivery infrastructure issues that surround Hydrogen, and the limited range of the current generation of automotive batteries, they conclude that IC engines will be the predominant mobile platform for the foreseeable future.

If emissions of CO_2 are neglected, there are already a number of technologies that can be combined into an IC engine powered vehicle that result in near-zero emissions. Kishi et al. [7] and Kitagawa et al. [8] presented their SI engine strategies for meeting the US 'Tier 2' Super Ultra Low Emission Vehicle (SULEV) certification. Their approach incorporates a

number of advanced technologies such as air-assisted injection, advanced engine management, variable valve actuation for better low-speed combustion, and advanced catalyst design. Developments culminate in emissions of <0.004 g/mile NMOG and <0.02 g/mile NO_x at an engine age of 100,000 miles. Emissions at these levels are at, and in some cases, below the ambient levels that exist in urban environments. Therefore, it is entirely possible that some vehicles in the future will not only emit less of the harmful species, but also serve to clean up those that are already present.

The reduction of harmful emissions from current vehicles owes much to improvements in catalyst technology. There are two types of catalyst in mainstream use. The 3-way Catalyst is used in systems that burn a stoichiometric charge. Hydrocarbon and carbon monoxide species are oxidised, and NO_x is reduced to nitrogen and oxygen. The conversion efficiencies of HC and CO to CO_2 and H_2O for modern 'Promoted Platinum' type catalysts remains above 90% for stoichiometric to lean Air / Fuel (A/F) ratios provided a pre-catalyst gas temperature of at least 150°C is maintained. However, efficient reduction of NO_x requires A/F ratios to be controlled to within a few percent of stoichiometry [9]. In practice, carburettors are generally not suitable for such tight control of A/F ratios, and fuel injection in conjunction with closed-loop electronic engine management systems are employed. Furthermore, the presence of Lead Alkyl and Sulphur compounds has been shown to poison these catalysts, through adsorption and deposition on the substrate surface. This has led to the introduction of Unleaded Gasoline for vehicles with reduction catalysts on-board, and more recently, the introduction of low sulphur Gasoline to further reduce emissions from these vehicles. The second type is the Oxidation Catalyst, and is generally used in engines that burn an overall lean charge. It reduces tailpipe emissions of unburned HC and CO in a similar fashion, and is a simpler and cheaper construction than the Reduction type, however it has no capacity for reducing exhaust NO_x emissions.

The primary advantage of Diesel and GDI technologies is that they allow lean combustion. Part load operation is achieved by varying the fuel rate independently of the airflow rate. Conversely, conventional SI engines require a homogeneous and stoichiometric charge for complete combustion and effective aftertreatment. The only way to operate at part-load in this type of engine is to directly reduce the airflow (and fuel flow) rate. This is normally achieved by airflow throttling in the intake manifold. The throttling approach has the effect of reducing the overall efficiency of the engine by a maximum of 20% at idle conditions. Consequently, these engines are inherently less efficient than their GDI or Diesel

counterparts, which translates directly to higher specific CO_2 emissions. However, the current generation of vehicles that employ lean-burn strategies do not generally have effective aftertreatment to reduce NO_x emissions, because the technology is still in development. So, at least for the time being we are left with a trade-off between lean-burn engines, which predominantly affect the local environment, and SI (stoichiometric) engines, from which effects are felt globally through increased CO_2 output.

So, the challenge has been set: develop technologies that can combine the best attributes of lean-burn engines (efficiency) and stoichiometric engines (emissions excluding CO_2). Development of aftertreatment systems to 'clean up' the exhaust from lean-burn engines is already well underway [10]. Lean deNO_x catalysts, NO_x traps, and Selective Catalytic Reduction (SCR) are three technologies currently under development to tackle the problem. Furthermore, forthcoming Euro IV and Tier 2 legislation will require the tight control of particulate emissions, which will necessitate the addition of particulate filters to the aftertreatment systems. At present, there is only one such system that is commercially available [11]: the filter is periodically purged by post-injecting fuel so that the catalyst can raise the exhaust temperature sufficiently for carbon oxidation (~550°C) to CO_2 in the filter. This system imposes a fuel penalty of 3-4% overall, and requires advanced engine management algorithms. Current problems with lean-burn aftertreatment systems are not insurmountable, but will probably always result in fuel penalties, which tends to negate the reason for using a lean burn approach in the first place. Furthermore, aftertreatment systems suffer from durability problems and are not as robust as the engines themselves.

There is another technology that offers a different approach. The technology is based on a new combustion process known as HCCI, or CAI in the current research. CAI is a combustion regime different from conventional SI or CI concepts. CAI combustion involves the autoignition of a premixed combustible charge. It requires the autoignition of the cylinder contents combined with a means of controlling the subsequent heat release rate. The practical means of obtaining autoignition is to ensure that local in-cylinder temperatures at the end of charge compression are raised above the autoignition temperature of the reacting species under the prevailing chemical conditions. Furthermore, combustion rates are limited by large quantities of excess air and/or exhaust gas dilution.

The theoretical and practical roots of modern CAI combustion research can be attributed to Semenov [12, 13, 14], although it wasn't until Onishi et al. [15, 16], and subsequently

Noguchi et al. [17], who were studying the causes of 'run-on' combustion in two-stroke engines, that the full potential of CAI combustion was realised. Firstly, CAI lends itself to highly diluted combustion, which allows the possibility for Diesel-like efficiencies. Secondly, the charge is homogeneous and combustion occurs at low temperatures (<1800 K), which can result in negligible particulate and NO_x emissions. So, this technology holds the possibility to overcome the efficiency problems of conventional SI engines, without necessarily requiring expensive and complicated aftertreatment systems. The first (and only) production engine that uses CAI technology is the Honda ARC 250 2-stroke engine [18]. Two-stroke engines particularly lend themselves to the CAI combustion regime because the cycle ensures that hot combustion residuals are available during fresh-charge induction and compression, tending to promote auto-ignition. Honda reported that increases in efficiency of up to 29% combined with a reduction of up to half of the THC emissions could be achieved with their technology. Despite the apparent suitability of the two-stroke engine, it still has several drawbacks that preclude its mainstream use for light-duty automotive applications. Peculiarities of the gas-exchange process in the two-stroke engine ensure that maximum torque is a strong function of engine speed, which can lead to driveability problems. Furthermore, the absence of a low cylinder pressure during induction adds the requirement for fresh charge to be pumped into the cylinder. If this is achieved conventionally via the crankcase, then lubricants must be added to the fuel to avoid excessive engine wear, which inevitably lead to higher exhaust THC emissions. Conversely, pumping can be achieved externally which complicates the system and reduces overall efficiencies through increased pumping work. In any case, at high loads, the simultaneous opening of exhaust and intake ports can lead to the charge 'short-circuiting' from intake to exhaust ports during the induction process, which dramatically increases the exhaust hydrocarbon emissions. This can be mitigated to some extent by the inclusion of a specially shaped piston to encourage 'loop scavenging' within the cylinder. Many of these complications can be overcome with the developing GDI technologies [19]; it remains to be seen whether the implementation of GDI enables two-stroke engines to serve a wider market.

The complications of the two-stroke cycle have prompted the development of CAI combustion for four-stroke engines. Najt and Foster [20] were the first to achieve CAI in a four-stroke single cylinder engine, using elevated intake charge temperatures and ultra-lean mixtures. Until recently, this approach has been adopted by most researchers in the field to study phenomena associated with choice of fuel, mixture composition, and temperature

and pressure histories. However, the limited speed and load ranges over which CAI combustion are acceptable remains a major shortfall, prompting new approaches such as those explained by Lavy et al. [21] and Kimura et al. [22, 23] to hybridise CAI with SI and CI concepts respectively. These approaches essentially take the best attributes of CAI and marry it with existing technologies to produce a powertrain that, on average, produces fewer emissions. The drawback of such hybrids is in the increased hardware and level of engine management required for their implementation.

Justification for the assertion that CAI is a newly discovered combustion process arises when one makes comparisons with SI and CI concepts. Unlike SI combustion, CAI ignition does not rely on the spark event for initiation or phasing of combustion. Instead, Ignition occurs when local in-cylinder conditions are favourable for auto-ignition of at least some of its contents, akin to the ignition in CI combustion. In CI engines, the rate of heat release relies on the physical process of fuel and air mixing by diffusion. On the other hand, in SI engines the rate of heat release relies on heat transfer from the exothermic flame-front to raise the temperature of the adjacent unburned stoichiometric mixture and propagate combustion. Heat release in CAI combustion is predominantly a function of mixture composition, temperature, and pressure, which determine the chemical reaction rates of the various species in the mixture.

Interest in CAI combustion was sparked by Onishi et al. [16] in 1979, and has been gathering momentum ever since. The complicated nature of this combustion has led to a number of acronyms being proposed by various researchers to describe it alongside SI and CI regimes. Onishi et al. [16] used Active Thermo Atmosphere Combustion (ATAC), and Noguchi et al. [17] rather immodestly named it Toyota-Soken (TS) combustion. Later, Najt and Foster [20] named it Compression Ignited Homogeneous Charge (CIHC) combustion. Thring [24] was first to propose the now globally accepted acronym of HCCI. Ishibashi et al. [25] named their two-stroke concept Active Radical Combustion (ARC), making the assumption that radical species present in the combustion residuals are instrumental in promoting auto-ignition. Aoyama et al. [26] developed the term HCCI into Premixed Charge Compression Ignition (PCCI), to make it more generally applicable. Duret and Venturi [27] named the two-stroke regime Fluid Dynamically Controlled Two-Stroke Combustion Process (FDCCP), attempting to stress the importance of mixture control on this combustion. Most recently, Lavy et al. [21] have renamed the process Controlled Auto-Ignition (CAI) combustion. Although HCCI is the most generally used term, it does

not reflect the generic nature of this combustion, since it assumes that the ideal state is one of homogeneity, and that this is what one strives for. There are two conditions that any term that we use must fulfil:

(i) It should be compatible with the classical classification of combustion regime by ignition type e.g. SI and CI.

(ii) It shall reflect the generic nature of the combustion, and include all the means of achieving it without precisely defining in-cylinder charge conditions. SI and CI classifications are successful precisely because they make no attempt to describe the complexities of the systems developed to implement their combustion type, yet one can still ascertain the basic technologies required for either.

With respect to these two points, terms such as HCCI, ARC, FDCCP, and ATAC fail either because they are not compatible with CI and SI, or that they refer to specific charge conditions that need not be attained to achieve this combustion (e.g. HCCI need not be homogeneous). PCCI is a more generic term, and could be considered sufficient. However, historically, the term 'premixed' has referred to systems that incorporate port injection or carburetted technologies, and some confusion may arise with DI systems running this type of combustion. CI is sufficient to describe the auto-ignited nature of this combustion, but does not separate it sufficiently from the existing CI combustion and associated technologies. Therefore, a better description of the ignition regime would be Auto-Ignition, or AI. This type of analysis has led Lavy et al. [21] to rename the combustion as Controlled Auto-Ignition (CAI) since it fulfils both of the above requirements. The term can describe approaches from GDI, SI, and CI technologies without reform. Terms such as HCCI can be considered as subsets to CAI: HCCI is analogous to homogeneous CAI. In the author's opinion, the term CAI is superior to any that have been suggested in the past, and it shall be adopted throughout the rest of this work.

So far, a brief analysis of the emissions legislation driving developments in automotive powertrain technology has been presented. A review of existing technologies and those under development has provided a context for the continued research into CAI combustion, and how it can be implemented in four-stroke engines to meet forthcoming emissions regulations. Before the author can delve into the complexities of CAI combustion itself, it is necessary to review the associated research area of 'spark-knock' and auto-ignition in SI engines. This is a much older and more widely researched field of IC engines, and much

can be learned from the application of this knowledge to CAI technology. The next section shall deal with auto-ignition and knocking phenomena in SI engines, followed by a section detailing the progress of research in the area of CAI combustion.

2.3 Knocking Combustion in Spark-Ignition Engines

Ricardo [28] first suggested that a process of autoignition is responsible for the audible 'knocking' combustion that occurs under some engine operating conditions. Other mechanisms proposed at this time included one of 'detonation', in which the flame front is accelerated through the charge and forms a leading pressure wave, which is then internally reflected, exciting the engine structure and causing the audible knocking noise [29]. With the introduction of optical techniques employed by Withrow and Boyd [30], Miller [31], and Male [32], who obtained qualitative data to support the autoignition theory, Ricardo's assertion became widely accepted.

Autoignition occurs in the unburned part of the cylinder charge, usually termed the 'end-gas'. If the pressure and temperature histories of the end-gas are sufficiently severe, then autoignition will take place. The pressure and temperature histories of the end-gas are dependant on the pressure rise due to piston compression and normal flame propagated combustion (that follows spark ignition), and heat transfer to the combustion chamber walls. However, knock will only occur as a result of auto-ignition if two further conditions are met:

(i) The reactions that follow auto-ignition consume the unburned charge at sufficient rate to induce in-cylinder pressure differentials.
(ii) There is sufficient heat release before the arrival of the flame front to transmit any pressure waves generated to the cylinder walls.

If these two conditions are met, then the combustion chamber walls will be excited at their natural frequency, resulting in audible knock [33]. As in normal combustion, the occurrence of knock is subject to cyclic variations brought about by changes in end-gas geometry and composition. Under light knocking conditions, knock occurrence competes with normal flame consumption. Only cycles that are observed as having the shortest total combustion duration burning actually knock [34], since combustion that includes charge

consumption by normal flame propagation and autoignition in the end-gas will occur faster than combustion by flame propagation only.

The occurrence of knock is particularly relevant to SI engine operation because it directly constrains engine performance. It usually occurs under Wide-Open-Throttle (WOT) conditions, when pressure and temperature histories are most severe. Thus, compression ratio is limited, and since the maximum thermal efficiency of the Otto cycle is mainly dependant on compression ratio, this is also limited. Furthermore, knocking combustion can lead to engine damage in the form of piston crown and cylinder head erosion, severely reducing the engine's life [35]. Lee and Schaefer [35], and Zhao et al. [36] have also shown that combustion chamber wall surface temperatures are increased under knocking conditions, increasing heat transfer from the system, and tending to lower cycle efficiency.

So, it is of practical importance for researchers to understand the causes of knocking combustion and take measures to eliminate it. Advances in combustion chamber design to reduce the duration of normal flame propagation are termed 'fast-burn' approaches. These include the use of pent-roof, central-spark, or two-spark designs to reduce flame travel, and increasing turbulence through induced 'swirl', 'tumble', or 'squish' to increase the flame speed [37]. These approaches allow higher compression ratios to be achieved because they limit the time allowed for autoignition to take place by consuming the end-gas earlier in the cycle. Other approaches have included the careful blending of fuel and the addition of fuel additives such as tetraethyl lead to raise the fuel's autoignition resistance, although this practice has recently been phased out due to the forced introduction of reduction catalysts, which are poisoned by tetraethyl lead. The choice of fuel blend plays a vital role in developing efficient combustion systems that avoid engine knock, and this will be dealt with in the next section.

2.3.1 Fuel Effects on Autoignition and Knocking Combustion

2.3.1.1 Research and Motoring Octane Numbers

For practical purposes, the suitability of a particular fuel or fuel blend for automotive applications must be quantified. In the case of the SI engine, there are standards that define the fuel anti-knock quality, to which commercially available fuel blends must adhere. Thus engine manufacturers, legislators, and consumers can be satisfied that the automotive

systems sold are operated with the correctly specified fuel. The development of these standards is chronicled in references [38, 39, 40, 41]. Fuel anti-knock (or octane) quality is determined in a Co-operative Fuels Research (CFR) engine using the American Society for Testing Materials (ASTM) procedures D-2699 and D-2700, which are colloquially known as the Research Octane and Motor Octane tests respectively. These tests are similar, but expose the test fuel to different engine operating conditions. Thus, a Research Octane Number (RON) and a Motor Octane Number (MON) are obtained, which can qualitatively predict the knock behaviour of the fuel over a wide range of real-engine conditions. The conditions that conspire to produce different RON and MON in both tests are summarised in table 2.2.

Engine Parameter	Research Method	Motor Method
Engine Speed (rpm)	600	900
Intake Temperature (°C)	52	149
Spark Advance	13° BTDC	19-26°BTDC

Table 2.2 Experimental engine conditions for RON and MON tests

In both tests, there are two Primary Reference Fuels (PRFs) that are used to measure other fuels against. These fuels are normal Heptane (n-Heptane), and Isooctane (Trimethylpentane[2,2,4]). They were chosen because they represent two extremities of anti-knock quality: n-Heptane and Isooctane have low and high knock resistances respectively. Automotive fuels are tested in a CFR engine to the RON and MON standards, and results are compared to results of mixtures of n-Heptane and Isooctane. The fuel is designated an octane number (ON) relative to the volumetric mixture of PRFs giving similar knocking tendency. For example, if the test fuel has a similar knocking tendency to a mixture of 80% Isooctane and 20% n-Heptane in the RON test, then it is designated 80 RON. Thus, one desired quality of an automotive fuel for SI engines is to have a high ON, as these are most resistant to knock.

So, a fuel's propensity to auto-ignite can be measured quantitatively using empirical standards designed to regulate fuel specifications. However, these standards make no attempt to address the fundamental issues regarding the chemistry and thermodynamics of spark-induced autoignition. There has been a huge array of work on the fundamental

aspects of autoignition, which will be addressed in the following subsection and in section 2.3.2.

2.3.1.2 Fuel Structure Effects

Studies on fuel structure effects have been instrumental in the classification of hydrocarbons. Generalisations that can be made between different groups of hydrocarbons as to the autoignition and combustion chemistry has aided in the development of complex models to predict the behaviour of real-world fuels such as Gasoline and Diesel [46]. Lovell [47] presented results from the collaborative API Research Project 45, which remains the most comprehensive work on the effects of fuel structure on autoignition behaviour. There are over 300 individual hydrocarbons studied, and results show that autoignition behaviour is related to hydrocarbon structure as follows:

Aromatics:

Almost all of the aromatics contained within Gasoline have an octane value exceeding 100. Octane numbers do vary and are dependent on the positioning of additional side chains on the benzene ring. Generally, more carbon atoms present in the side chain leads to reduced octane number. However, if this chain is branched the knocking resistance tends to increase.

Paraffins:

Although some of the shorter-chain paraffin hydrocarbons have similar octane values to aromatics, the majority exhibit much lower values. Generally, the longer chain paraffins exhibit poorer knock resistance. However, increased branching of the chain (e.g. methyl groups) tends to increase octane number. This is demonstrated by the difference between the straight-chain n-Heptane (n-C_7H_{16}), and Isooctane or [2,2,4] Trimethylpentane. The prefix [2,2,4] indicates the presence of branched methyl groups on the straight-chain structure of pentane.

Olefins:

Olefins containing two or more double bonds exhibit higher knock resistance than ones containing single double bonds. However, there are some exceptions to this, including acetylene, ethylene, and propylene. Similarly to the paraffins, the addition of side branches tends to increase knock resistance.

2.3.1.3 Effects of Fuel Additives

Organometallic Antiknock Compounds

Tetraethyl lead (TEL) and Tetra methyl lead (TEM) are the most well known of this class of compounds. All organometallic antiknocks operate by decomposing at the appropriate temperature in the engine cycle to form a cloud of catalytically active metal oxide particles. These particles interrupt the reactions that lead to autoignition, delaying its occurrence until the end-gas is consumed in the normal fashion by the propagating flame-front. Although TEL and other organometallic compounds are now outlawed in developed countries such as in the US and Europe due to environmental concerns, their use is still wide spread among the developing countries because of the reduced cost of refining those Gasolines [48]. The primary concern over the use of these compounds is that they are never consumed completely during the course of combustion. Thus, combustion chamber deposits can build up if proper 'scavenging' additives are not also included. Furthermore, deposition of these compounds on catalyst surfaces obstructs their operation. Anything left in the exhaust flow is eventually emitted into the environment with associated health effects.

Organic Antiknock Compounds

Organic antiknocks are favourable because they are consumed during the combustion process, having minimal effects on catalyst operation and the environment. Mackinven [49] presented a study on the relative benefits of various 'ashless' (organic) antiknock additives, showing that N-methylaniline (NMA), aromatic compounds containing nitrogen or oxygen, iodine and aliphatic iodine compounds, and selenium compounds were all effective for increasing the blending anti-knock quality of Gasoline. However, he also concluded that, at that time, none were as cost-effective as TEL or the further processing of Gasoline to increase octane number.

However, since the phasing out of lead alkyl compounds, other blend components have been used widely to increase the octane quality of Gasoline. These include oxygenates such as Methanol, Ethanol, Methyl Tertiary-Butyl Ether (MTBE), Ethyl Tertiary-Butyl Ether (ETBE), and aromatic compounds.

Other Species That Influence Knock

Of the many thousands of compounds that either inhibit or promote knock, there are two of particular interest to this work:

(i) *Oxides of Nitrogen (NOx).* Kawabata et al. [50] presented a study on the influence of NOx concentration in residual and EGR gases on the occurrence of autoignition. They showed that as NO concentration in the unburned charge is increased, the timing of autoignition is advanced. Since NO is only normally found in the unburned charge as a result of mixing with the residual gases or EGR, it is interesting because the overall affect of EGR is to slow combustion, whether flame-propagated or auto-ignited.

(ii) *Ozone (O_3).* A little known work by Brooks [51] was first to examine the effect of low concentrations of ozone in the unburned charge. He showed that ozone significantly promotes knocking combustion. Concentrations as low as 0.5% by volume can induce a reduced octane of 17 ON in a 77 RON fuel.

Although not directly related, these studies are particularly relevant to our work on CAI combustion, since it is autoignition that we wish to promote, and the utilisation of either NOx or Ozone in the unburned charge may help to increase the speed/load range over which CAI combustion can currently be achieved.

2.3.2 Autoignition Chemistry and Knocking Combustion Prediction Models

2.3.2.1 Chemistry of Autoignition

The process of autoignition can be thought of as a number of discreet chemical reactions that occur between fuel and oxidiser (*chain initiation*), which generate a pool of radicals for consumption in the subsequent combustion or *chain propagation* reactions. *Degenerate-branching* reactions that occur after *chain initiation* in some hydrocarbons can either form stable molecules or radicals. The rates at which these reactions occur, and the type of species generated, are intimately dependent on the temperature and pressure histories of the mixture. The basic hydrocarbon oxidation process due to Semenov [42] is as follows:

1.	$RH + O_2 \rightarrow \dot{R} + H\dot{O}_2$		*Chain Initiation*
2.	$\dot{R} + O_2 \rightarrow R\dot{O}_2$		
3.	$\dot{R} + O_2 \rightarrow Olefin + H\dot{O}_2$		
4.	$\dot{R}O_2 + RH \rightarrow ROOH + \dot{R}$		*Chain Propagation*
5.	$\dot{R}O_2 \rightarrow R'CHO + R''O$		
6.	$H\dot{O}_2 + RH \rightarrow H_2O_2 + \dot{R}$		
7.	$ROOH \rightarrow R\dot{O} + \dot{O}H$		*Degenerate Branching*
8.	$R'CHO + O_2 \rightarrow R'CO + H\dot{O}_2$		
9.	$\dot{R}O_2 \rightarrow$ Destruction		*Chain Termination*

Figure 2.1 Basic hydrocarbon oxidation process: a dot denotes an active radical. Each dash denotes the number of free bonds on the organic radical R.

Heywood [43] describes how this generalised oxidation process can result one or a combination of four types of combustion behaviour:

(i) *Slow reactions* normally occur at low temperatures (<200°C), requiring a long time and not normally associated with combustion in engines.

(ii) *Cool Flames* result in some hydrocarbons when the mixture is raised to 300-400 °C, these can occur singularly or in multiple waves depending on conditions. These reactions only consume a small fraction of the fuel and result in small temperature rises.

(iii) *Two stage ignition*: under the right conditions, cool flame reactions are succeeded by a hot flame, in which the chemical energy of the fuel is normally released rapidly in an explosion. The period of low reactivity between cool and hot flames is associated with some of the *Chain propagation* reactions approaching a state of equilibrium, in which both forward and backward reaction rates are similar. This type of behaviour is normally associated with low octane paraffins such as n-Heptane. It is also sometimes termed 'Negative Temperature Coefficient' (NTC) behaviour, because the reaction rate between first and second stage ignition is reduced despite increasing gas temperatures.

(iv) *Single Stage Ignition*: This occurs in fuels where no cool flame reactions are observed. Instead, high-temperature autoignition precedes extremely rapid combustion of the entire mixture. This behaviour is normally seen in Olefin and aromatic hydrocarbons [44].

For a number of years, researchers have been developing models to predict combustion phenomena such as flame propagation and autoignition behaviour. Studies that help to determine reaction paths and the intermediate species involved in autoignition can be broadly divided into four categories [45]; (i) pre-combustion heat release studies, (ii) rapid sampling valve studies, (iii) spectroscopic investigations, and (iv) fuel effect studies. Heat release studies have shown that there is a general, but not universal, inverse correlation between octane number and heat release prior to autoignition. Litzinger [45] also concluded that any heat released during cool flame reactions seriously reduces the knock resistance of the fuel due to an implicit rise in end-gas temperature. Rapid sampling valve studies are useful because they can measure quantities of stable intermediate reactants at different stages in the engine cycle very accurately through the application of Gas Chromatograph (GC) techniques. Litzinger [45] reports that these studies have helped to confirm the role of low temperature oxidation kinetics (cool flames) in auto-ignition chemistry. Spectroscopic investigations provide the most information about autoignition chemistry because the role of radicals can be determined. The advancing field of laser

diagnostics has broadened the scope in this area, and provides much information for combustion model development.

2.3.2.2 Knocking Combustion Prediction Models

The knowledge of fuel structure effects combined with intermediate species data obtained from experiments provides a sound basis for the development and calibration of knocking combustion prediction models. There are three types of models that have been developed to predict the onset of autoignition and knocking combustion. These can be summarised as follows:

(i) *Induction time correlations* use an Arrhenius type function (Equation 2.1) to fit model predictions to experimental data. The onset of autoignition / knocking combustion is obtained by integrating the function over time to include the time dependant histories of pressure (p) and temperature (T). A, B, and n are constants.

$$\tau = Ap^{-n} \exp\left(\frac{B}{T}\right) \qquad \text{Equation 2.1}$$

(ii) *Detailed Chemical Kinetic Models.* These types of models attempt to follow all of the elementary reactions that take place during the autoignition process. To this end, hundreds of species are considered, and in excess of 1000 reactions are required, even for a single hydrocarbon fuel such as Isooctane [52]. With current limitations on computational power, this code is unsuitable for full boiling range fuels such as Gasoline and Diesel, which contain many hundreds of hydrocarbons. However, these model types are extremely useful for fundamental observations, and may be used to calibrate less accurate *Reduced Kinetic* models.

. (iii) *Reduced Chemical Kinetic Models.* The Shell model [53] is an example of this. It is a generalised kinetic model based on a degenerate branched-chain mechanism for hydrocarbon oxidation. It uses general chemical entities to represent individual species. Due to its simplified nature, this model has been used to predict the behaviour of fuels such as Gasoline. It is also useful for more detailed combustion models, for which autoignition is only a small part.

2.3.3 Effects of Engine Operating Conditions on Knocking Combustion

Knocking combustion is affected by engine operating conditions to the extent that the temperature and pressure histories of the end-gas will vary if conditions are changed. Knowledge of the relevant importance of each operating variable can give insight into how the temperature and pressure histories of the end-gas are affected by each, and the best means of practically abating knock. Recognition of the importance of engine operating conditions stems to the earliest research on octane rating [38-41], which resulted in tests designed to rate fuels at two sets of conditions and qualitatively predict autoignition behaviour over the full range of conditions.

2.3.3.1 Fuel Effects - Fuel Sensitivity

The arithmetic difference between RON and MON is termed 'Fuel Sensitivity' (RON-MON). It is a measure of how the autoignition resistance of a fuel changes between two specific engine conditions. In general terms, the motor method is considered more 'severe', because its inlet temperature exceeds the research method considerably, inducing a raised temperature history. However, the research method is operated at a lower engine speed than the motor method, allowing more time for the reactions leading to autoignition. PRFs by definition have zero fuel sensitivity, since they are the fuels by which all others are measured in the RON and MON tests. Fuels that have lower MON than RON have positive fuel sensitivity, indicating that as engine operating conditions become more severe, their resistance to knock worsens. Fuels with negative fuel sensitivity exhibit the opposite effect. Leppard [44] was first to explain the fundamental reasons for observed fuel sensitivities in different hydrocarbon classes. He showed that of the paraffins, most had either zero or negative sensitivity, except those having RONs in excess of 100, which displayed distinctively positive fuel sensitivities. However, the majority of paraffins contained in Gasoline are below 100 RON. On the whole, olefins and aromatics have higher research octane quality than paraffins, but possess positive fuel sensitivities. On the basis of paraffinic behaviour being normal, olefin and aromatic behaviour predicts that these fuels are *derated* under MON conditions due to their poorer autoignition resistance. However, Leppard [44] asserts that the aromatic and olefin behaviour should be considered as normal, and that paraffins are *super-rated* at MON conditions, where they show abnormally high resistance to autoignition. Aromatics and olefins do not generally exhibit two-stage ignition over the temperature range that occurs in the end-gas during normal

engine operation. On the other hand, most paraffins do exhibit two-stage ignition, especially if their octane rating is low (i.e. less than 100). The period of low reactivity between the first and second stages of ignition increases with intake temperature between RON (52 °C) and MON (149 °C) conditions, and with increases in engine speed. On the other hand, the time to autoignition for olefins and aromatics decreases monotonically with increasing intake temperature. These are the primary reasons for the *super-rated* behaviour of paraffins under MON conditions.

Work has been carried out by several researchers to quantify how specific changes in operating conditions affect knocking combustion. These effects are summarised in the following sections

2.3.3.2 Spark Advance

The effect of spark advance on the occurrence of knock is well documented. As the spark is brought earlier, so is combustion phasing, resulting in higher end-gas temperatures and pressures occurring closer to Top Dead Centre (TDC) on the compression stroke. Russ [55] reports that an increase in octane number of the fuel allows an approximately equal increase in spark advance to avoid knocking combustion (1 ON/ 1 °CA). Gluckstein and Walcutt [56] studied spark advance relationships with end-gas temperature, and concluded that increases in spark advance were proportional to increases in end-gas temperature for the fuels and conditions they chose. Reducing spark advance is the most practicable means of avoiding knock, and has resulted in closed loop systems consisting of a knock-sensor mounted in the engine block to detect the onset of knock and retard the spark accordingly.

2.3.3.3 Intake Temperature

The effect of raising intake temperature is to raise the charge temperature history while slightly reducing the pressure history due to lower charge density. Leppard [44] reports that this has a more pronounced effect on paraffins than for aromatics and olefins, because the NTC region is widened, resulting in a delayed auto-ignition response. This effect is also noted in the work of Taylor [57]. Russ [55] comments that in general, if an increase of 7K is induced, then the fuel's octane must be raised by approximately 1 ON (1 ON/7 K).

2.3.3.4 Coolant Temperature

Raising coolant temperature has a similar effect on charge temperature as raising the intake temperature. During induction and part of compression, heat is transferred from the cylinder walls, raising charge temperature and lowering its density. When charge temperature is raised above the wall temperature (through compression), heat transfer from the charge is comparatively reduced at higher coolant temperatures. All of this adds up to higher end-gas temperatures preceding autoignition. Russ reports that an increase in coolant temperature of 10K requires the fuel octane increase of 1 ON to avoid knock (1 ON/10 K). Leppard [58] reports a similar response of 1 ON/9 K.

2.3.3.5 Compression Ratio

Compression ratio sets both the pressure and temperature ratio that exists before and after compression. As such, it is instrumental in the occurrence of knock. Currently, production port-fuel injected SI engines are limited to a compression ratio of 10-11, so that end-gas temperature and pressure histories are never too severe to induce knock. The ideal compression ratio is somewhere in the region 12-14, beyond which, limitations of the practical cycle such as blow-by and heat losses to the cylinder head become more important. Furthermore, a higher compression ratio requires stronger engine components and structure, which can severely limit the maximum speed of the engine. Modern GDI engines are capable of achieving compression ratios of up to 12, because of an increased charge cooling effect compared to port-fuel injected engines. Work by Caris and Nelson [59], Thring and Overington [60], and Russ [55] are in general agreement that an increase in compression ratio of 1 requires approximately a 5 ON increase in the fuel to avoid knock.

2.3.3.6 Intake Pressure

Changes in intake pressure are essentially analogous to changes in compression ratio (excluding temperature effects), except in one important respect. In most SI engines there is a certain degree of 'valve overlap' that occurs at the end of the exhaust stroke and the beginning of induction. During this period both intake and exhaust valves are open. If the intake manifold pressure is reduced relative to the exhaust manifold pressure, as is often the case, exhaust flows back into the cylinder. The increased presence of exhaust gas

increases the charge temperature and dilutes it to a certain extent. On the other hand, if the intake manifold is supercharged then the overlap period will aid in scavenging the cylinder and removing more exhaust than would normally be the case. There is some disparity as to the effect of intake pressure on knock occurrence, probably due to the peculiarities in gas exchange process that will occur between different experimental systems and at different engine speeds. However, Russ [55] draws the conclusion that, on average, an increase in 10kPa requires an ON increase of 3-4 over the range 85-105 kPA absolute manifold pressure.

2.3.3.7 Exhaust Backpressure

The effect of exhaust backpressure is relatively insignificant. Increases lead to more in-cylinder residuals, which simultaneously raises the charge temperature and dilution rate. Russ [55] reports an approximate rule of thumb of 1 ON increase per 30 kPa exhaust backpressure. This trend is interesting because recent developments in aftertreatment systems that will tend to boost exhaust backpressure (catalysts and particulate filters) in GDI systems may lead to the requirement for higher-octane fuels.

2.3.3.8 Air/Fuel Ratio

The effect of A/F ratio on knocking combustion cannot be widely examined in SI engines, since they normally require close-to-stoichiometric mixtures for complete and satisfactory combustion. This is particularly relevant to modern SI engines that require stoichiometric exhaust catalysis to meet current emissions legislation. However, studies that have been carried out [55, 61] show a maximum fuel octane requirement occurs at an equivalence ratio of 0.95. In general, octane requirement decreases at a rate of 2 ON per A/F ratio either side of this value.

2.3.3.9 Summary

Any engine operating condition that is changed results in changes to the end-gas temperature and pressure histories, to a greater or lesser degree. If the changes are sufficient for the particular charge composition, then this can induce autoignition in the end-gas, which may lead to knock. The author has shown that the physical and chemical processes that lead to knock are extremely complex, and very difficult to predict

accurately. However, introducing this subject has provided some of the key fundamentals that are equally applicable in the fledgling research area of CAI combustion. In CAI combustion the entire charge is made to behave as the end-gas, and is without the additional complexities that flame propagation brings to the analysis of spark-knock.

2.4 CAI Combustion

Nikolai Semenov and his colleagues carried out pioneering work in the field of ignition chemistry in the early 1930's. Of this work, Semenov's Chemical, or Chain theory of ignition remains as the foundation for modern autoignition theories [62]. This theory postulates that autoignition occurs when the number of *chain initiating* reactions that occur at distinct 'chemical centres' within the charge, exceeds the number of *chain terminating* reactions. Furthermore, pressure and temperature effects on the chemical reaction rates of intermediate species determine their specific reaction paths. Ultimately this model can explain all the mechanisms of hydrocarbon oxidation, including cool flame, single-stage, and two-stage autoignition.

Semenov recognised that the SI and CI concepts of combustion are ultimately dominated by physical processes, and set about devising a combustion regime that could take advantage of a chemical-kinetics controlled process. Thus, the LAG (Avalanche Activated Combustion) combustion process was devised [12], and subsequently developed [13, 14] for use in IC engines. The concept comprises a pre-chamber and a main chamber [63]. During induction the pre-chamber receives a rich charge, while the main chamber receives a lean charge. Combustion is initiated in the pre-chamber in the normal fashion, using a spark discharge. The rapid expansion of gases in the pre-chamber forces partially oxidised intermediates and radicals such as OH, CH, C_2, H, CHO, HO_2, and O into the main chamber via a small orifice. During this process, the flame is extinguished. Mixing in the main chamber provides the lean charge with both the heat, and the composition required for bulk autoignition. Subsequent heat-release is controlled by the initial dilution rate of the main chamber contents. This combustion regime is widely accepted as an early form of CAI combustion [63].

At the time that Gussak et al. [13, 14] were developing the LAG process for practical use in IC engines, Onishi et al. [15, 16, 64, 65] presented a series of papers documenting developments of a lean combustion regime to stabilise the idle operation of two-stroke

engines. Initially, Onishi and his colleagues set about analysing the causes of abnormal combustion that occur as a result of the two-stroke cycle. However, their work identified that the abnormal combustion could be controlled through the use of exhaust and intake throttling, and resulted in vastly reduced NOx, CO, and VOC exhaust emissions [16]. Until this point, the CAI combustion regime was considered as a novel peculiarity, with no real benefits. However, the knowledge that it can dramatically reduce exhaust emissions sparked the interest of many researchers, and has led to the recognition that this technology is viable with any other currently being proposed for future IC engines.

Over the past few decades, there have been a few hundred papers dealing with the various aspects of CAI combustion. Approaches have usually taken the form of developments of SI or CI strategies to achieve CAI in those engines and with suitable fuels. The development of CI technologies to facilitate CAI combustion necessarily has a different set of constraints to the development of SI technologies, primarily due to the different behaviours of SI and CI fuels (Gasoline and Diesel). Furthermore, a plethora of work on CAI combustion has dealt with the kinetic modelling aspects of CAI combustion, which is not directly relevant to the author's own experimental work presented later. The remainder of this review shall concentrate (without strict limitation) on experimental approaches that develop SI technologies for CAI combustion, because this is the area in which the author's own work is most applicable.

2.4.1 Current Four-Stroke Strategies

Broadly speaking, there are four strategies that have been adopted by researchers to enable CAI combustion in the four-stroke engine. The goal of each is to adjust the temperature and pressure histories beyond those normally experienced by the cylinder charge, so that autoignition is achieved. A further requirement of each strategy is charge dilution to prevent excessive heat-release rates. These strategies can be divided and summarised as follows:

(i) *Intake Pre-heating*

This approach is used to raise the temperature history of the charge without significantly affecting the pressure history. Early examples of this included work by Najt and Foster [20], and Thring [24] who both used intake temperatures in excess of 300°C to achieve autoignition. Aoyama et al. [26] have also shown that intake

air heating can significantly increase the lean limit A/F ratio, with a penalty of increasing the rich limit A/F ratio also. The intake temperature required for autoignition is intimately dependant on compression ratio, intake pressure, and the heat transfer characteristics of the cylinder and charge. Although this is a useful method for research purposes, the practicality of charge heating has yet to be proved. The transient nature of automotive engines requires that the associated air throughput also be transient. Any system that heats the intake air prior to induction will have an associated thermal inertia, making temperature control extremely complex. Heating the air also has implications for maximum power because of the reduction in volumetric efficiency [26, 66]. Furthermore, unless heat is obtained using wasted energy (coolant, exhaust), this approach will reduce engine efficiency.

(ii) *Raised Compression Ratio*

Another means of achieving the required autoignition temperature is by raising the compression ratio. This approach has been used widely [63, 67, 68] and is particularly relevant to CI strategies [22, 23]. Increases in compression ratio change both pressure and temperature histories of the cylinder contents. Thring [24] reports that if compression ratio is too high, then the dilution required to limit the heat release rate is excessive. Ultimately, this reduces the maximum load under which CAI combustion can be achieved. Christensen et al. [68] performed a detailed study looking at the compression ratio required for various Gasoline/Diesel and Isooctane/Heptane blends for different inlet air temperatures. They showed that regardless of fuel type, as compression ratio is increased, the inlet temperature required for CAI combustion is reduced. With ignition timing maintained at TDC, increases in compression ratio combined with reductions in inlet air temperature lead to increased combustion duration. They assert that the reduction in average cycle temperature is the main reason for this trend. However, it is difficult to separate the trend of increased compression ratio from that of reduced charge temperature to define the exact role of compression ratio alone.

(iii) *Variations in Fuel Blend*

Olsson and Johansson [69] recently presented a strategy that uses variations in the quantity of two separate fuel components combined with supercharging to control CAI combustion over a wide speed/load range. The fuels employed were Isooctane and Heptane. Their strategy employed advanced engine control techniques,

requiring closed-loop control of intake temperature and heat-release characteristics. Although it works reasonably well in principle, there are some issues remaining that question the transient capability of such a complex system.

(iv) *Variable Valve Actuation (VVA)*

In recent years, many systems have been developed that use mechanical VVA to modify combustion under certain conditions [70-72]. These are useful in four-stroke SI engines to optimise the gas exchange process over a wider speed range, and to improve combustion stability under low load conditions. Such systems are also useful for achieving CAI combustion. Lavy et al. [21], Li et al. [73], and Law et al. [74] have all recently published approaches to CAI combustion that utilise the heat energy and dilution properties of in-cylinder residuals. Significant quantities of burned gases are trapped in the cylinder during the exhaust stroke prior to induction of the fresh charge, providing the right conditions for autoignition and controlled heat-release at the end of compression. These techniques require heavily modified valve timing, lift, and durations. The systems described by Lavy et al. [21] and Li et al. [73] are designed for hybridisation with SI combustion to ensure that the current speed/load range of SI engines can be achieved in the new hybrid engine. Consequently, a complex VVA and control system is required, the likes of which are not yet available commercially. However, the approach of Law et al. [74] uses an electro-hydraulic valve actuation system, which is infinitely more versatile than the conventional mechanical variety. Such systems are the subject of intense research and may become available within the next few years. Electro-hydraulic and electromagnetic VVA systems are considered as an enabling technology for CAI combustion [75]. When these systems become available, CAI combustion achieved using burned gases as a means of control will become much more viable.

In combination with one or more of these four main strategies, supercharging the inlet manifold has been shown to be an effective method of achieving CAI conditions. Aoyama et al. [26] increased the charging efficiency of their four-stroke single cylinder engine from a normally aspirated 85%, to 120%. They showed that higher loads could be achieved with minimal effects on exhaust NOx emissions, because the rate of charge dilution need not be reduced to achieve the higher loads, as is normally the case. In addition, Christensen et al.

[76] have reported loads up to 14 bar IMEP, which are easily sufficient to match the maximum torque output of modern SI engines.

2.4.2 Speed and Load Considerations

The limitations of CAI combustion with regard to engine speed and load have already been briefly discussed. Here, more detailed analyses on the CAI range will be presented.

Studies on the speed range by Onishi et al. [16] using a forced air-cooled, single cylinder 2-stroke (NiCE-10) showed that at low loads, CAI can be achieved over the full speed range of their engine (1000-4000 rpm). This was subsequently confirmed by Noguchi et al. [17] using a two-stroke horizontally opposed uniflow-scavenging engine. Studies carried out on a modified Honda ARC 250cc production engine by Lavy et al. [21] showed that provided its exhaust timing is advanced (to trap more residuals), and that transfer and exhaust port throttling of up to 97.5% were employed, this engine can operate at loads as low as 1 bar IMEP over its entire speed range (1000-4500 rpm). Lida [77] conducted studies using a similar engine as Onishi et al. [16], but modified to incorporate a ceramic cylinder head to reduce heat rejection. The compression ratio used was 6.0 as oppose to Onishi's 7.5. In his studies, he reports that the minimum speed attainable in CAI combustion mode with Gasoline fuel was 2200 rpm. It is unclear as to why the range does not extend down to 1000 rpm as other authors [16, 17, 21] have found, but it may be due to the reduced compression ratio.

Each of the above studies recognises that the speed range attainable is very much dependant on load. Onishi et al. [16] and Noguchi et al. [17] used the term *delivery ratio* as an indicator of engine load in their two-stroke engines. *Delivery ratio* is defined as the ratio between inducted mass and the inducted mass under ideal gas-exchange conditions given the geometry of the cylinder [54]. It is analogous to *volumetric efficiency* used commonly in four-stroke engine terminology. Onishi et al. [16] and Noguchi et al. [17] report that the maximum delivery ratio attainable is approximately 0.4, which is equivalent to light load operation. Particularly as engine speed is increased beyond 2500 rpm, maximum loads are reduced. However, Lavy et al. [21] do not report an appreciable reduction in maximum load with increased engine speed in the Honda ARC engine. The maximum load achieved by this engine in CAI combustion mode remains approximately constant at 3-3.5 bar IMEP. The disparity is probably as a result of improvements in gas exchange between the

initial work of Onishi et al. [16] and Noguchi et al. [17] and the manufacture of the production Honda ARC engine.

The above studies all recognise that idle operation at low speed is not possible in the CAI two-stroke engine. Onishi et al. [16] presented a possible reason for this: under low load (low delivery ratio) conditions, the dilution by exhaust gases is excessive resulting in a large reduction in mean in-cylinder gas temperature. Consequently, the temperature required for bulk autoignition cannot be achieved.

The work of Lavy et al. [21] and Li et al. [73] has resulted from an attempt to model the gas exchange process that allows CAI combustion in two-stroke engines, and apply this knowledge to four-stroke engines. However, the means of achieving the combustion are vastly different, and result in a different set of constraints on the speed / load region. In both cases, the speed range attainable varies from 1000-3500 rpm. Lavy et al. [21] report a respectable maximum load of over 5 bar IMEP at 1000rpm, while Li et al. [73] give theirs as just over 4 bar IMEP. In each case, as the engine speed is increased the maximum load attainable is linearly reduced. Li et al. [73] attribute this to the reduction in volumetric efficiency that occurs at higher engine speeds as a direct result of the chosen valve durations. As with two-stroke studies, idle operation is not achievable at low speeds. They assert that low load operation at any speed is problematic due to the low exhaust gas temperatures that they observed in this region (~325 °C).

In a more fundamental study, Fergusen [78] reported that engine speed does not have any measurable effect on CAI combustion durations, unlike the case of SI combustion. If the reaction rates remain fixed relative to engine speed then the absolute time available for pre-combustion reactions is reduced with increasing engine speed. Thus, to ensure properly phased combustion, the mixture composition, temperature or pressure must be altered to compensate. Thring [24] carried out a brief investigation into the effects of engine speed on homogeneous CAI combustion at elevated intake temperatures. He found that he was unable to obtain CAI combustion at speeds higher than 2000 rpm, and reached similar conclusions to Fergusen [78]. Modelling work by Najt and Foster [20] tends to support this argument. Their work showed that as engine speed is increased, the initial charge temperature must also be increased to compensate for the reduced time allowed for the reactions leading to autoignition. Furthermore, they state that only by using initial charge

temperatures sufficient to cause single-stage instead of two-stage ignition, will the ignition trend with engine speed be minimised.

Christensen et al. [68] conducted studies on homogeneous CAI in a four-stroke single cylinder engine operated at various intake temperatures and using various fuels (Isooctane, Ethanol, and Natural Gas). They reported that loads between 4 and 5 bar IMEP could be achieved depending on fuel type. They observed knock-like pressure oscillations on the pressure transducer output wave, which may have been responsible for them limiting the load in each test, to prevent engine damage. However, this was not explicitly stated.

Cycle-by-cycle variations in combustion phasing and total heat release have been shown to correlate with brake torque variations, which directly affect vehicle driveability [79]. In CAI combustion, cyclic variations arise from changes in mixture composition and temperature, and charge formation. Furthermore, in multi-cylinder engines variations between cylinders can occur as a result of unequal distributions of air and fuel in the inlet manifold, and temperature gradients occurring in the engine structure that affect heat transfer. It is important for developers to design systems that minimise cyclic variability to promote the smooth operation of the engine, and optimise its performance in terms of emissions and efficiency. Most studies that have dealt with CAI combustion cyclic variability [16, 17, 63, 77] have concentrated on the variation in maximum cylinder pressure that occurs between successive cycles. These studies have shown that the cyclic variability determined by maximum pressure for CAI combustion is normally much lower than that seen for SI combustion. From this, they have concluded that CAI combustion is much smoother. However, Matekunas [80] has shown that, at least for SI combustion, the relationship between variability of maximum in-cylinder pressure and torque variations is complex; it does not necessarily follow that low cyclic variations in maximum pressure lead to low cyclic variations in torque output.

Two methods that can reliably relate combustion parameters with torque variations are (i) heat release analysis, and (ii) IMEP analysis. In (i), techniques are used to define the start and end of combustion. If the cyclic variability of these parameters is low, then it follows that the variations in brake torque output will also be low, since variability is almost entirely dependant on combustion phasing. Heat release analysis shall be discussed in detail in section 3.3.1.2. A statistical approach to measuring successive IMEPs (ii) gives a further combustion characteristic known as Coefficient of Variation in IMEP (COVimep)

as defined in Equation 3.6. This parameter is in common use to describe torque variability occurring as a result of variable combustion.

Lida [81] used heat release analysis to compare combustion variability between SI and CAI combustion modes in a NiCE-10 two-stroke engine equipped with a ceramic cylinder head. He conclusively showed that the cyclic variability in the start of combustion, end of combustion, and combustion duration was significantly lower in the CAI operating mode than in the equivalent SI mode in this engine. Comparisons of the total heat release between cycles showed that the variations were equivalent for CAI and SI modes. So, for CAI combustion in two-strokes, combustion is significantly smoother. However, two-stroke SI combustion at part load is inherently more unstable than the equivalent four-stroke combustion because of the increased presence of burned gas residuals. To the author's knowledge, there has not yet been any work comparing the cyclic variability of CAI and SI combustion in four-stroke engines in terms of heat release or COVimep, where the differences are likely to be reduced.

2.4.3 Heat Release Characteristics

Heat release analysis is an invaluable tool used by many researchers [16, 17, 20, 26, 63, 66-68, 77, 81-85] to characterise CAI combustion and contrast it to similar results from SI or CI combustion regimes. A number of generalisations can be made about CAI combustion characteristics, which set it apart from conventional types.

Onishi et al. [16] and Noguchi et al. [17] both showed that the period between ignition and end of combustion (combustion duration) was significantly reduced for CAI compared to SI combustion in the two-stroke cycle. Onishi et al. [16] also showed that the maximum heat release rate was increased by up to 30% under the conditions they chose. Lida et al. [81], using a modified version of Onishi's engine, showed that combustion duration can be reduced by up to 30% by using a ceramic cylinder head as oppose to the conventional aluminium type. They also found that this configuration promoted more advanced ignition and better combustion efficiency, presumably due to the low heat transfer characteristics of the ceramic material.

A study by Christensen et al. [82], showed that as the rate of air dilution was decreased in their four-stroke homogeneous CAI engine, heat release rates in excess of 400 J/°CA could

be obtained, reducing the combustion duration (10-90% burn CA) to approximately 3 °CA, which is extremely short compared to the SI equivalent of 13 °CA. Generally speaking, whether two- or four-stroke operation is employed, durations for CAI combustion are much shorter than is found conventionally in SI engines, and depend heavily on charge temperature and composition (dilution). The mechanisms of heat release have been discussed in detail in previous sections. However, Onishi et al. [16] provided a good qualitative explanation for why CAI combustion heat release can be faster than conventional SI combustion. Figures 2.2a and 2.2b show the generalised models for SI and CAI combustion respectively. In each case, the x-axis represents the fraction of total mixture mass (m), and the y-axis represents the specific heating value of the in-cylinder charge. In SI combustion, each element of charge must combust fully while in the hot reaction zone (flame) represented by *dw*. On the other hand, combustion occurs almost simultaneously in all parts of the charge in CAI combustion, and *dq* represents the total heating value of intermediate reactants that continue the chain branching reactions. Thus, the minimum SI combustion duration is limited spatially by the physics of flame propagation, while minimum CAI combustion duration is limited chemically by kinetic reaction rates.

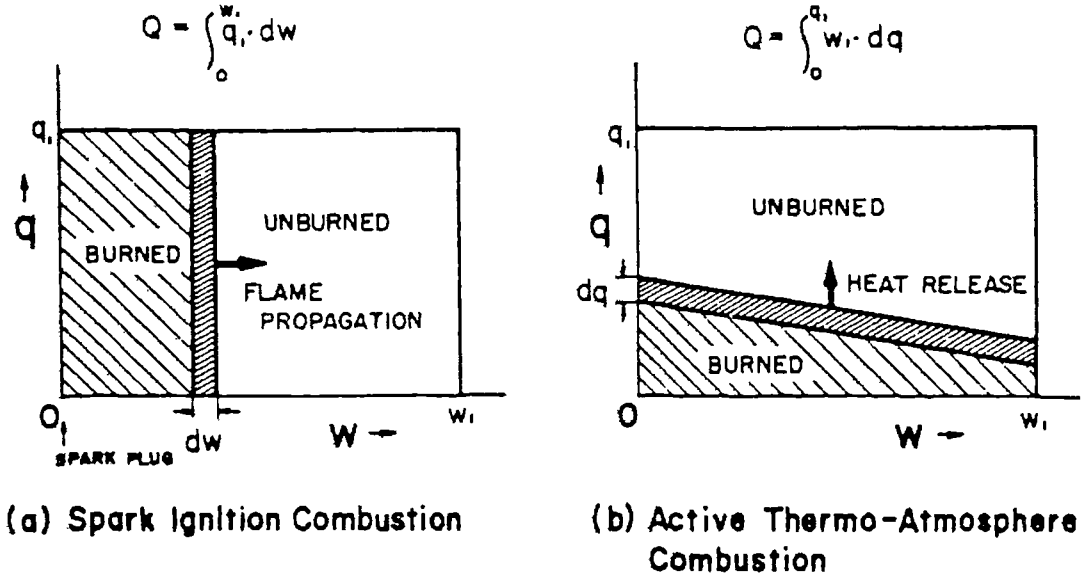

(a) Spark Ignition Combustion

(b) Active Thermo-Atmosphere Combustion

Figure 2.2 Ideal models of spark-ignition and CAI (ATAC) combustion (Onishi et al. [16])

The ignition timing of CAI combustion is another characteristic that is of major importance. The Otto cycle is based on the ideal air standard cycle, in which combustion occurs at Top-Dead-Centre (TDC) and at constant volume, or in other words, in an infinitely short time frame. Therefore, the short combustion durations associated with CAI combustion facilitate a more idealised engine cycle providing the phasing of combustion can be kept optimal. There are many parameters that affect ignition timing in various ways, and these shall be dealt with in subsequent sections. However, at this point it would be prudent to point out general differences that occur between two- and four-stroke regimes, as observed from heat release analyses in those papers. Work by Onishi et al. [16], Noguchi et al. [17], and Lida et al. [81] presenting heat release analyses of the two-stroke CAI regime show that ignition timings are normally well before TDC. In the most extreme case, Lida et al. [81] showed that ignition can be phased to 30° before TDC, with heat-release completed before TDC, without any adverse affects. This said, the completion of combustion before TDC on the compression stroke must surely affect engine efficiency. In general, the two-stroke cycle happily accommodates early ignition, despite subsequent rapid heat release rates.

Studies completed on four-stroke engines have generally used combustion timings that occur very close to TDC. Christensen et al. [68] used a combination of variable compression ratio and inlet temperature to adjust ignition to TDC for various fuel blends. This approach recognises the importance of correct combustion phasing to obtain highest efficiencies. Moreover, advanced ignition can lead to very high in-cylinder pressures, extremely short combustion durations, and knock-like pressure oscillations [68]. The two-stroke engines studied by Onishi et al. [16], Noguchi et al. [17], and Lida [81] have compression ratios of approximately 6.5, much lower than those used in four-stroke studies. Lower compression ratios lead to lower heat release rates and in-cylinder pressures. This is the primary reason that the two-stroke engines can operate with comparatively advanced ignition without adverse effects.

2.4.4 Effects of Charge Composition

2.4.4.1 Air/Fuel Ratio

NO_x emissions from CAI combustion engines can easily match those emitted from current generation SI engines fitted with reduction catalysts. This knowledge allows the possibility for more efficient lean combustion to be employed without the necessity for complicated exhaust aftertreatment systems that are still in development. To this end, many papers have studied the effects of changing the air dilution rate on combustion parameters.

Although the LAG system developed by Semenov and Gussak [12-14] was designed to run an overall lean charge, they did not specifically investigate the effects of air dilution on combustion. Onishi [16] presented the range of A/F ratios that facilitated CAI combustion with Gasoline fuel in his two-stroke engine operated at a constant speed of 2000 rpm. He showed that the range spanned 11-22, although this is reduced at the low and high loads of the CAI operating region. The A/F ratio giving the widest load range was given as 16.5. This indicates that CAI combustion is ideally operated slightly lean of stoichiometric in their two-stroke engine. In the Methanol study by Lida et al. [81], they showed that ignition timings were most advanced at stoichiometric A/F ratios, while combustion durations decreased monotonically as the mixture was enriched. Total heat release was also highest at stoichiometry, showing that combustion efficiency drops significantly under even slightly rich conditions. Their results also indicate that combustion stability is best when the engine is operated slightly lean.

Thring [24] studied the effect of A/F ratio and external EGR rate on the attainable CAI operating region at elevated intake temperatures (~400°C) for Gasoline and Diesel fuels. Generally speaking, the rich ($\lambda<1$) and lean ($\lambda>1$) limits were constrained by misfire and output power restrictions respectively. At the lean limit, the power produced as a result of combustion was not sufficient to exceed 0 bar BMEP on Thring's single cylinder research engine. However, this limit is arbitrary because the FMEP of a research engine is artificially high when compared to that of production engines. Thring found that the region of operation was largest when the engine was operated rich or lean. Close-to-stoichiometric combustion led to extremely fast heat release rates and knock-like symptoms, which could only be attenuated with the addition of copious quantities of external EGR. In their study of homogeneous CAI in an optical single cylinder research

engine, Aoyama et al. [26] were able to achieve A/F ratios in the range 33-44, limited by knocking combustion and misfire respectively. At A/F ratios in excess of 40, CAI combustion produced significantly lower IMEP than either GDI or Diesel combustion regimes operating at similar dilution ratios. Since all of these regimes use a similar airflow, it can be concluded that the combustion efficiency of homogeneous CAI is comparatively reduced in this region, resulting in lower load. Najt and Foster [20] note that the dependence of autoignition timing on dilution rate leads to conflicting benefits with a requirement for fine tuning: ignition is improved under lower dilution conditions, but this leads to unacceptable heat release rates. Conversely, to obtain reasonable heat release profiles, the ignition must be retarded beyond optimal by increased dilution.

2.4.4.2 Fuel Effects

Najt and Foster [20] used their four-stroke homogeneous CAI combustion research engine to study the fuel effects on combustion. They looked at differences that occur between paraffinic and aromatic fuels. They noted that the main differences that are observed relate to the low temperature oxidation kinetics (< 950K) that lead to autoignition. Subsequent heat release in both fuel types is governed by high temperature (>1000 K) kinetics for which the reaction paths are similar, resulting in similar heat release rates.

Lida [77] tested methanol and gasoline individually in a low heat rejection NiCE-10 engine. He found that methanol facilitated combustion at much lower speeds and loads than could be obtained with gasoline. Furthermore, methanol exhibited significant differences in combustion characteristics: earlier ignition, shorter duration combustion, and higher maximum heat release rates were observed, compared to gasoline. He also found that while a region of overlap between SI and CAI combustion exists with gasoline, it was not observed with methanol. Methanol also showed a propensity for hot surface ignition at the upper load end of its CAI region, as a direct result of using a ceramic cylinder head. In an optical analysis of CAI and SI combustion, Lida [77] showed that the generation of OH radicals precedes heat-release in CAI combustion, and their appearance is much earlier when compared to conventional SI combustion. This tends to confirm the importance of the hydroxyl radical in the low temperature kinetics that lead to autoignition.

Diesel fuels ([24, 67, 68]) intrinsically have a low resistance to autoignition, but their viscous nature and high flash point means that they are resistant to vaporisation at ambient

temperatures when port injection is used. When injected directly in the cylinder using standard CI injection systems, injection must occur during induction or early compression to obtain a sufficiently homogeneous air/fuel mixture to allow CAI combustion. Poor vaporisation leads to an inhomogeneous mixture, and results in pockets of the charge burning by a diffusion-rate limited process, with associated combustion products such as particulates and NO_x. In their study, Christensen et al. [68] showed that using Diesel instead of Gasoline can result in the combustion efficiency dropping by as much as 10%.

Flowers et al. [84] conducted a study using Propane and a dimethyl-ether (DME)/methane blend in a homogeneous CAI engine at a compression ratio of 16 and intake temperatures ranging 130-175 °C. They showed that as A/F ratio is leaned, the phasing of peak heat-release was linearly retarded, regardless of fuel and engine operating conditions. However, the gradient of retardation with increased A/F ratio was much more pronounced for propane than for the DME/methane blend. The authors speculate that there may be two reasons for this. Firstly, methane has a negative partial pressure coefficient, so as its concentration is increased, its reactivity is comparably reduced. Secondly, they state that methane can act as a 'radical sink', tending to lower the overall reaction rate.

Duret and Lavy [86] presented qualitative results from an extensive study of the fuel effects on CAI combustion. They used a 2-stroke engine to quantify the suitability of a host of fuels in terms of a Controlled Autoignition Number (CAN) index. The index is defined by accounting for the engine operating range (speed/load) attainable using each type of fuel. They found that the most suitable fuels were blends of oxygenates and hydrocarbons, followed by pure oxygenates, and lastly hydrocarbons. This would tend to support the work of Aoyama et al. [26] in his gasoline/methanol studies. Furthermore, they asserted that the suitability of a fuel for CAI combustion shows no correlation to its RON or MON, or its fuel sensitivity. While this approach has empirical value, it does not attempt to address the fundamental aspects of why different fuel types exhibit different behaviour, and is severely limited in that the results are only generally applicable to the two-stroke process in their engine. Duret and Lavy [86] gave no specific details of the fuels tested, making comparisons with other work difficult.

2.4.4.3 Burned Gas Recycling

Studies that deal with the recycling of burned gases can be broadly divided into two categories: those that study residual gas effects, and those that deal with externally circulated exhaust gas (EGR).

Residual Gas Effects

All work that has been presented on two-stroke engines, and developments by Lavy et al. [21, 86], Li et al. [73], and Law et al. [74] of the four stroke CAI combustion process, rely on the recycling of residual burned gases. In his original study, Onishi [16] explains that there are three conditions that must be met for attainment of two-stroke CAI combustion:

1. The quantity of mixture and the air-fuel ratio supplied to the cylinder must be uniform cycle-to-cycle.
2. The scavenging directivity and velocity also must have cyclic regularity to ensure the correct conditions of the residual gases remaining in the cylinder.
3. The temperatures in the combustion chamber must be suitable.

In point 2, they recognise that the mixing of residuals with fresh charge is a major factor that decides whether CAI combustion occurs or not, although they do not go as far as explaining the ideal residual gas/fresh charge conditions required for optimum CAI combustion. Onishi et al. [16] also point out that there is a specific region in which CAI can be expected to occur. Under low load conditions, despite an abundance of residual gas, its temperature is not high enough to raise the fresh charge temperature to that required for autoignition (after compression). Similarly, under higher load conditions, the residual gas quantity is reduced, with a corresponding reduction in heating effect. Consequently, the charge does not reach the temperature required for autoignition after compression. Fortunately in the two-stroke regime, when the in-cylinder conditions move outside of those required for CAI combustion, the engine can be reverted to SI combustion with little change in configuration.

In later work carried out by Lavy et al. [21], the Honda ARC 250cc engine was modified to include transfer port throttling, which significantly increased the speed/load region attainable. They showed that control of the instantaneous scavenging velocity of fresh

charge throughout the induction process is important for CAI combustion. Without transfer port throttling, the scavenging velocity of the intake charge was highly variable with sharp peaks and pronounced backflow into the transfer port. Conversely, the velocity of intake charge when transfer throttling is applied is much smoother with minimal backflow. They point out that this tends to increase the stratification between fresh charge and residual gases by reducing the degree of large-scale in-cylinder turbulence. Clearly, control over the mixing process between fresh charge and residuals is important for the optimisation of the two-stroke process.

Law et al. [74] presented two methods of burned gas recycling that can be used to obtain the in-cylinder conditions required for CAI combustion. Their first method requires early closure of the exhaust valve during the exhaust stroke. This traps a fixed quantity of burned residuals in the cylinder. During the rest of the exhaust stroke and part of the intake stroke, both intake and exhaust valves remain closed. During this period, the cylinder contents are compressed and re-expanded, effectively acting like a gas spring. Only when the in-cylinder pressure balances the intake manifold pressure (approx. 1 atmosphere) is the intake valve opened to induct the fresh charge. Thus, there is a significant quantity of hot residuals to provide the heating effect and achieve autoignition, and to dilute sufficiently and control the subsequent heat release rate. This approach would appear similar to that of Lavy et al. [21] and Li et al. [73], although in both of these works, the authors circumvented explanation of their exact method of achieving CAI, presumably due to commercial considerations. The second method of Law et al. [74] utilises their electrohydraulic valve actuation to hold the exhaust valves open for a full 360 °CA during the exhaust and induction strokes. Inlet valve timing remains essentially unchanged. In this way, exhaust gas is stored in the exhaust manifold during the induction stroke prior to re-induction during the intake stroke, along with fresh charge from the inlet manifold. Careful control over exact valve timings varies the rate of hot exhaust gas dilution to control the onset of autoignition. Extensive results comparing the two methods are not supplied, so no conclusions can be drawn as to the suitability of one or the other. However, it is clear that there are two major differences between the methods:

1. Whether the burned gases are stored in-cylinder (method 1) or in the exhaust manifold (method 2) will have an impact on the heat transfer that occurs. Re-compressed residual gases will suffer heat losses to the cylinder head, while

exhausted and re-inducted gases will suffer heat losses both to the cylinder head and exhaust manifold.

2. Each method will result in a different regime of mixing between fresh and burned gases. It may be possible to limit the mixing that occurs as a result of method 1, using intake port throttling in a similar fashion to Lavy et al. [21] in their two-stroke studies, as this has been found to have positive effects in the two-stroke engine. However, it is difficult to see how mixing can be controlled using method 2 without specifically altering the flow patterns of re-induction from both exhaust and intake manifolds.

Using method 1, Law et al. [74] have showed that CAI can be achieved using residual rates in the region of 36-59%. Their results showed that as residual rate is increased, both the onset of autoignition and peak-pressure CA are advanced monotonically. This result is significantly different from results given by Nakano [85] and Christensen et al. [83], indicating that introduction of homogeneous external EGR tends to retard ignition and slow heat release. Law et al. [74] explain their results by dividing the pressure cycle into three distinct phases: compression, pre-autoignition, and combustion. They propose four mechanisms by which the combination of fresh charge and trapped residuals can lead to CAI combustion. These four mechanisms include the importance of pressure and temperature, and intermediate combustion products whether stable or radical, that are present in the residuals or in the charge as a whole as a result of pre-combustion reactions. They do not conclude that any one of the four mechanisms is responsible for CAI combustion in their engine, due to insufficient data. Furthermore, in these mechanisms they do not include the possibility for the importance of residual gas stratification, as Onishi et al. [16], Lavy et al. [21], and Li et al. [73] have found in their two- and four-stroke studies.

Zhao et al. [87] have produced an interesting study on the CAI combustion of a 60 RON PRF in an optical engine operating at low speed (500 rpm), a compression ratio of 10:1, and elevated intake temperature of 205 °C. The engine configuration had a shrouded side valve arrangement so that high swirl could be induced and optical measurements taken of the whole combustion chamber from above. In their engine, they showed that the high swirl and directivity of the intake flow induced a core of hot residuals to remain at the centre of the combustion chamber during the intake stroke. During CAI operation, they

photographed ignition occurring at the interface between fresh charge and burned residuals in a toroidal pattern. Subsequent combustion propagated from the centre outwards, apparently unaffected by the high in-cylinder swirl. They noted that autoignition sometimes occurred near to the cylinder wall before the arrival of propagated combustion, probably as a result of pressure and temperature increases in this part of the charge arising from combustion. This study lends weight to the idea that residual stratification is important in engines that operate a regime that relies on high temperature residuals to initiate combustion. If too much mixing occurs between fresh and burned gases, local temperatures will not be high enough for a long enough period to facilitate autoignition.

Homogeneous EGR effects

Thring [24] was first to investigate the effect of homogeneous EGR on CAI combustion variables. He showed that exhaust gas dilution was effective in slowing down combustion sufficiently to allow stoichiometric operation. Excessive EGR rates tended to retard ignition beyond acceptable limits, resulting in misfire in some cycles.
Christensen et al. [83] also performed an investigation into the effects of external EGR. In their tests, they chose to fix the ignition timing close-to-TDC. To achieve this, they increased inlet charge temperature as increases in EGR were made. They showed that EGR was effective for attenuating knocking combustion by reducing the rate of heat release and maximum in-cylinder pressure, and increasing combustion duration. Furthermore, they showed that increases in EGR positively affect combustion efficiency up to rates of approximately 50%, beyond which combustion efficiency drops. However, these results are mitigated by the fact that intake temperature is increased at higher EGR rates to compensate for retarded autoignition timing. Increased intake temperature would also tend to increase combustion efficiency, so the relative importance of either intake temperature or EGR dilution cannot be determined.

Nakano et al. [85] state that the proper way of determining the effect of EGR aimed at controlling the combustion is to carry out investigations at constant load, or fixed fuel flow. By doing this, the ideal EGR conditions to obtain best stability, efficiency, and hydrocarbon and NO_x emissions may be determined for each engine load and speed. This idea recognises that ignition timing is not important in itself, but merely an indicator of the emissions and stability requirements to which the engine must adhere. The results from Nakano et al. [85] show that EGR is effective for both retarding ignition timing and

reducing heat release rates. Using a detailed reaction model, they predict the relative effects of EGR dilution, and intake temperature on the timing of auto-ignition for a isooctane / heptane / toluene mixture, supposed to be representative of a Gasoline type fuel. They show quantitatively that intake temperature strongly affects autoignition timing, a trend that is more pronounced as conditions approach stoichiometric from lean. They also show that to obtain similar ignition timing for a range of A/F ratios and constant fuelling rate, EGR rate and intake temperature must be increased as the mixture is made richer.

A more fundamental modelling study presented by Zhao et al. [88] attempts to separate the various effects that EGR can have on CAI combustion. In this study, the individual effects of EGR are categorised as follows:

(i) *Charge heating effect*

EGR admitted to the intake manifold is likely to be of higher temperature than the fresh charge. The transfer of heat that occurs between the two gases is defined as the *charge heating effect.*

(ii) *Dilution effect*

This arises as the EGR replaces reactive oxygen with non-reactive species such as carbon dioxide and water vapour. The reduction of air/oxygen by EGR is termed the *dilution effect*

(iii) *Thermal effect*

The increased presence of water vapour and carbon dioxide raises the average specific heat capacity of the charge; this is termed the *thermal effect.*

(iv) *Chemical effect*

Stable combustion products contained within the EGR can participate in the chemical reactions that lead to autoignition and subsequent combustion. This is termed the *chemical effect.*

The *charge heating* property was investigated by increasing intake temperature with no EGR present. They showed that increased intake temperature leads to advanced ignition, as other authors have found. In further study, only the *thermal* property of EGR was found to have any effect on ignition timing (causing retardation), with no contribution from *dilution*

or *chemical* properties, despite the apparent reactivity of some EGR species. However, while the *chemical* property of EGR was found to significantly reduce combustion durations, the opposite effects of the *dilution* and *thermal* properties conspired to cause an overall effect of increased duration with EGR.

2.4.4.4 Summary

This section has shown that the effects of charge composition are many and varied. Whether dilution is obtained using air or recycled burned gases, and how these hot or cold gases are mixed with fresh charge has a profound effect on the resulting combustion. It is likely that in a practical production CAI engine, a wide selection of these dilution and mixing techniques may be used to provide adequate control over the chemical kinetics to achieve efficient and properly phased combustion, and the reduction in exhaust emissions that CAI combustion promises in four-stroke engines. Thus far, the emissions that result from this combustion have only been dealt with in general terms. The next section shall outline how operating variables can affect emissions, as observed from the work presented so far in this area.

2.4.5 Engine-out Emissions

2.4.5.1 Efficiency (CO_2 Emissions)

Onishi et al. [16] were first to report that a stationary generator equipped with their CAI engine could achieve savings in fuel consumption in the region of 50% compared to a two-stroke, and 25% compared to a four-stroke engine. Later, Noguchi et al. [17] reported that increases in net indicated thermal efficiency of around 8% were achieved compared to a conventional SI two-stroke regime.

Thring [24] performed a study on the effects of air and exhaust gas dilution on the fuel consumption observed in his four-stroke engine. He found that increasing EGR rates up to 30% tended to reduce the fuel consumption, although this effect is most pronounced at close-to-stoichiometric A/F ratios. He also showed that at high EGR rates, best fuel consumption was obtained at the leanest conditions he chose ($\lambda \approx 2$), with values as low as 200 g/kW.h.

Aoyama et al. [26] looked at the effects of changing A/F ratio, charging efficiency, and Intake temperature on the fuel consumption of CAI, Diesel, and GDI combustion regimes. They found that in a small A/F ratio window of 30-40, CAI improved on Diesel and GDI by as much as 5% in terms of fuel efficiency, while giving similar output power. Also, CAI marginally achieved its best fuel consumption when intake temperatures were reduced to ambient, and at lower ($\lambda \approx$ 2-3) A/F ratios. Charging efficiency appeared to have little effect on the CAI fuel consumption, unlike the diesel case, where comparable values (to CAI) were only achieved at charging efficiencies greater than 100%. From these results Aoyama et al. [26] concluded that CAI combustion could display similar efficiencies to modern HSDI Diesel regimes under specific conditions.

Christensen et al. [68, 82, 83] have performed a series of studies which detail the effects of Intake temperature, A/F ratio, compression ratio, and EGR rate on engine efficiencies for a number of fuels including Ethanol, Natural Gas, Isooctane, and blends of Gasoline and Diesel. They showed that for constant load operation, best efficiency could be obtained at higher intake temperatures. However, at their highest load operation, highest efficiency could only be achieved when the intake temperature was reduced to avoid excessive knocking combustion occurring as a result of advanced ignition and high heat release rates. They reported maximum net indicated thermal efficiencies of 48%, 43% and 45% for isooctane, ethanol, and natural gas respectively, always occurring at the highest loads attainable. In their studies of the effects of EGR dilution on the same three fuels [83], they showed that increases in EGR always led to increases in net indicated efficiency. However, these tests were performed under constant fuelling conditions. Thus, increases in EGR bring about a reduction in A/F ratio, which has been shown by themselves and others to independently increase engine efficiency. But these results do show that higher efficiencies can be obtained if one replaces air dilution with exhaust dilution for a similar load and fuelling rate. When Christensen et al. [68] studied compression ratio effects on the CAI combustion of Gasoline and Diesel blends, they showed that best efficiencies were obtained with pure gasoline and at the highest compression ratios they used (22:1). From analysis of the combustion efficiencies from these tests, they concluded that the addition of Diesel fuel to the blend adversely affects vaporisation resulting in much poorer combustion. In similar tests, they found that addition of heptane to isooctane limited compression ratio, thus placing restrictions on the maximum efficiencies attainable.

Flowers et al. [84] studied the effect of combustion phasing on net indicated efficiency using propane and a DME-in-methane blend. They showed experimentally that retarding the peak heat release crank angle yielded linear increases in engine efficiency in the range 4 °BTDC to 10 °ATDC for both fuels. This occurred despite model predictions that a maximum efficiency would occur slightly after TDC, beyond which retarding the combustion would reduce engine efficiency.

In their first paper on the subject, Lavy et al. [21] showed that a 3-4 % reduction in fuel consumption could be achieved under stoichiometric CAI combustion conditions, when compared to SI combustion in the same engine. They indicated that improvements of up to 8% are attainable under slightly lean conditions. However, in a later paper, developments have yielded a low-load reduction of up to 18% of fuel consumption compared to an engine operated under the EU urban drive cycle conditions. Li et al. [73] use a similar engine configuration to Lavy et al. [21,86], but report improvements in fuel consumption in the order of 30% under near idle conditions. As load is increased, the fuel saving is reduced linearly. They claim two reasons for these improvements: (i) a reduction of throttling losses in the CAI combustion regime, since this engine is also designed to operate under stoichiometric fuelling conditions, and (ii) the combustion that they observe occurs almost at constant volume, which is more ideal when compared to normal SI combustion. It is not clear why Duret and Lavy [86], and Li et al. [73] claim vastly different improvements, but it is more probable that they used different base engine data for comparisons than any significant differences exist between combustion in their respective engines.

On the whole, improvement in powertrain efficiency is the major driving force behind CAI technology. It should be noted that those studies that use intake heating never include the fuel penalty that this incurs in the efficiency calculations, mainly because it is thought that in practice the heat energy required can be obtained from waste sources around the engine such as exhaust gas and coolant flow. However, studies have shown that the efficiency of CAI combustion can at least match that obtained in modern HSDI Diesel engines under certain conditions, which allows CAI combustion a window of opportunity for development before technologies such as fuel cell vehicles, electric vehicles, and hybrids become viable to the wider market.

2.4.5.2 HC, CO, and NOx Emissions

One of the major attractions of CAI combustion is that it can reduce emissions of NO_x in the region of 90-98% [66]. This reduction is attributable to the absence of high temperature reaction zones that are normally present in SI and CI combustion regimes. Because of the homogeneous nature of CAI combustion, peak combustion temperatures are related directly to engine load, which in turn determines the exhaust NO_x concentration. On the other hand, in four-stroke engines CAI combustion typically leads to higher CO and HC emissions due to the decreased temperature of the combustion reactions [66]. This problem is compounded by the need for air or exhaust gas dilution to prevent excessive heat release rates.

Onishi et al. [16] reported that while they gained efficiency from employing CAI combustion, they also reduced emissions considerably. CO and HC emissions were reported at low levels of 50 ppm and 0.03% respectively, made possible by the use of a two-way catalyst. NO_x emissions showed slight increases at higher loads, ranging from 10 to 40 ppm, but given that these values are not significantly affected by the catalyst operation, one can see they are extremely low. In the study by Noguchi et al. [17] using methanol fuel in a low heat rejection two-stroke engine, they showed that both NO_x and formaldehyde (HCHO) emissions tend to increase as conditions approach stoichiometric from lean. Lavy et al. [21] compared the CAI and SI pre-catalyst emissions characteristics from the Honda 250 ARC engine. They showed that both HC and NO_x emissions were reduced by approximately 35% at an engine speed of 2500 rpm and 1.75 bar IMEP load. Better HC emissions were attributed to an 80% increase in combustion stability under these conditions, resulting in an elimination of misfire.

Aoyama et al. [26] presented comparisons of emissions from CAI, CI, and GDI regimes on a volumetric basis. Although a gravimetric analysis is normally required for comparisons between modes of engine operation, in this case the airflow through the engine remains fixed for each. Their results showed massive reductions of 80-99% NO_x could be achieved with CAI combustion compared to CI and GDI operating at the same load. As with the study of Noguchi et al. [17], decreasing the A/F ratio led to increases in NO_x emissions. On the other hand, HC emissions were very high, in the order of 10 times those of the CI regime, and significantly higher than GDI. HC emissions tended to rise with increasing air dilution, resulting in 3% of the exhaust gas comprising hydrocarbons at an A/F ratio of 60.

In the study of isooctane, ethanol, and natural gas by Christensen et al. [82], NO_x emissions were so low that they presented comparisons with SI combustion on a logarithmic scale. Generally speaking, specific NO_x emissions were recorded at 100 times below those of SI combustion for each fuel. For isooctane, NO_x emissions showed a curious minimum between 1 and 3 bar IMEP. At very low and high loads, NO_x levels tended to increase by a factor of about 2. Between all the fuels, the general trend was for highest NO_x emissions to occur at higher loads, and for higher intake temperatures. They conclude that NO_x at the levels recorded are as good or better than post three-way catalyst emissions normally measured from SI engine exhausts. HC and CO emissions show similar trends – as load is increased (lower A/F ratio), these emissions are exponentially reduced. However, HC levels are always at least twice those found from (pre-catalyst) SI combustion, and CO levels only approach reasonable levels at loads in excess of 2 bar IMEP for isooctane and ethanol, and 3 bar IMEP for natural gas. Higher intake temperatures tend to lead to lower HC and CO emissions regardless of engine load. In their study of EGR on the same fuels, Christensen et al. [83] showed that EGR is extremely effective at reducing NO_x emissions at higher fuelling rates for Isooctane and Ethanol, but did not affect those for natural gas, which showed low values for all the conditions they chose. This exemplifies an important difference between air and exhaust gas dilution: if higher air dilution is employed to reduce NO_x emissions, then the engine load (and fuelling rate) are reduced unless supercharging is used, since best efficiency requires maximum airflow. However, EGR rate can be increased at a fixed fuel rate to optimise combustion phasing and reduce NO_x considerably. Thus, EGR dilution allows higher loads than air dilution. Christensen et al. [83] also showed that EGR tends to decrease HC emissions with minimal effect on CO.

Li et al. [73] presented absolute values for pre-catalyst emissions from CAI combustion and numerically compared these with a similar SI engine. They showed that NO_x emissions can be reduced anywhere from 90-99%, with the best reductions obtained at low load. Unlike other studies, CO emissions improved on those of SI combustion by 10-40%, with the best reductions obtained at higher loads. However, HC emissions were always worse, with increases from 50-160% reported. HC emissions were particularly bad under low load operation. They postulate that low temperature combustion may be responsible for higher HC emissions observed under these conditions. None of the emissions from their CAI engine showed a particular trend with engine speed.

2.5 Summary

Protecting our environment from the ravages of mankind is of utmost importance if we wish to continue inhabiting our planet in the way we have become accustomed. The burning of fossil fuels for power generation and transportation is accelerating, resulting in local and global climate changes that will affect us in unpredictable ways. Public attitudes are rapidly changing and this is reflected in the policies of governments that regulate our economic activity. In developed nations, tough legislation has been imposed to reduce the impact of fossil fuel burning on the environment. Specific targets for new automobiles have led to the widespread introduction of catalyst technology, and continue to drive technological developments. Ultimately, the question of energy efficiency is also one of economics. New technologies can only emerge if they are cheaper and easier to produce and operate than existing ones. Consequently, there are a number of alternatives such as fuel cell and electric vehicles that require a great deal more development before widespread adoption. However, improvements in the short term can be made on existing technologies such as SI and CI concepts, for which there is an abundance of knowledge.

A technology has emerged in recent years, which combines the best attributes of both CI and SI technologies to allow possibility for an efficient and clean power source for transportation without complicated and expensive exhaust aftertreatment systems that are currently in development. Active research centres in Europe have tagged this technology Controlled Auto-Ignition (CAI) combustion. Currently the most efficient powertrain systems for light transportation are those of the HSDI Diesel class. However, it is SI technology with associated exhaust aftertreatment that exhibits the lowest emissions of harmful NO_x, CO, VOC, and particulate species. Researchers have shown that CAI combustion can operate at similar efficiencies to HSDI Diesel engines, while emitting a tiny fraction of the NO_x and particulate emissions, after which the reduction of CO and VOC is relatively trivial.

From the literature study, it is clear that a number of areas require further investigation. Although the general role of dilution using burned residuals or air is known, the exact nature of how the interplay between air and exhaust gas dilution changes combustion has not been investigated fully. Furthermore, there have been no published studies that look at a wide range of fuels operated under the same conditions to determine differences in combustion that exist. Although Duret and Lavy [86] determined a Controlled Autoignition (CAN) index, there has been no attempt to quantify the general suitability of particular fuel blends and grades such as the RON and MON tests that exist for SI combustion, and the Cetane Number (CN) test that exists for CI combustion. During the course of the rest of this work, the author shall attempt to address some of these questions.

Chapter 3

Experimental Test Facility

Chapter 3 Experimental Test Facility

3.1 The Ricardo E6 Engine

3.1.1 General Description

An experimental test facility was set up and commissioned so that the experimental work described in this thesis could be undertaken. Figure 3.1 shows the base engine, which is a Ricardo E6. The engine is of the single-cylinder, twin poppet-valve four-stroke type. Its normal speed range is between 1000 and 3000 rpm. The engine has a capacity of 557 cc, a stroke of 111.1 mm, and a bore of 76.2 mm. It is versatile for experimental purposes because its compression ratio is continuously variable from 4.5:1 to 18:1 by means of a worm gear that controls the height of the cylinder head relative to the crankshaft. The cylinder, with its hardened cast iron liner is telescopic, as is the shaft that drives the valve train from the crankshaft. Compression ratio may be changed during normal engine operation, and is measured via a calibrated micrometer mounted at the side of the cylinder.

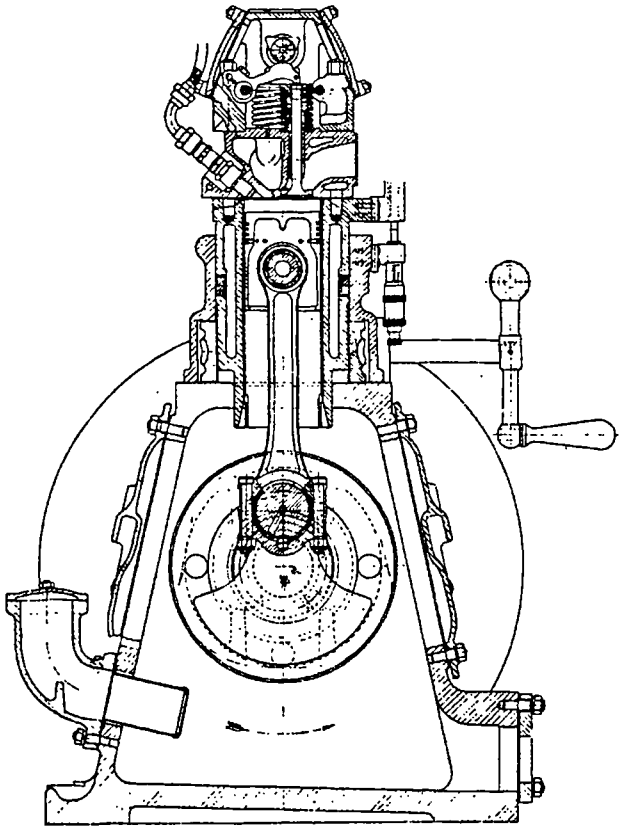

Figure 3.1 Ricardo E6 single cylinder research engine

The lubricating system is of the wet sump type, from which oil is taken via a crankshaft driven pump. Oil is delivered separately to the crank- and camshaft so that the big-end bearings and cam surfaces can be lubricated by means of radial feeds. The camshaft drivetrain is lubricated in a similar manner, with additional oil fed directly onto the bevel gear mating surfaces. An electrical heater is immersed in the sump oil to reduce the engine's cold start period, and a mains-water fed heat exchanger is externally fitted to allow accurate manual control of oil temperature during normal engine operation. Liberal cooling areas are provided in both the cylinder head and barrel. Coolant is circulated around the engine at a high flow rate to ensure uniform temperature distribution. Details of modifications to the original coolant system for the purposes of these tests shall be dealt with in section 3.2.2.

The valve timings operated in this engine can be considered as approximately standard to that in most four-stroke fixed-timing engines. As normal, the timings are set as a compromise between low-load combustion stability, which requires minimal exhaust backflow (valve overlap), and optimised gas exchange over the entire speed range of the engine. Intake valve opening and closing timings are 8 °BTDC and 36 °ABDC respectively. Exhaust valve opening and closing times are 43 °BBDC and 6 °ATDC respectively. These timings yield a valve overlap period of 14° around TDC on the induction stroke, and prevent excessive exhaust backflow when the intake manifold pressure is low relative to the exhaust.

3.1.2 Combustion Chamber Geometry

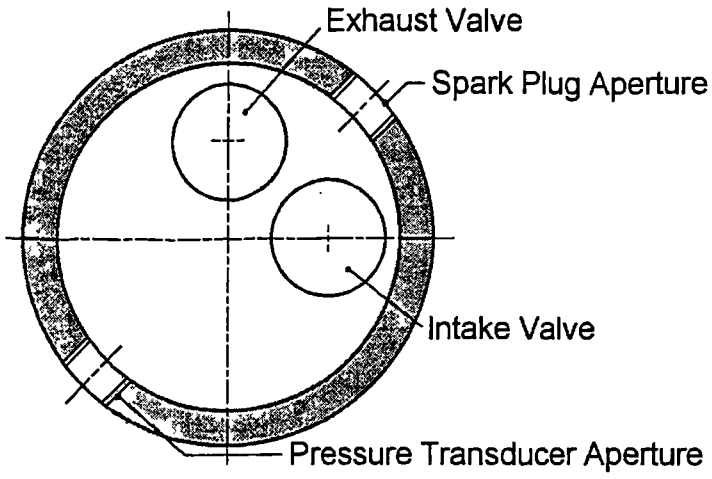

Figure 3.2 Combustion chamber geometry

Figure 3.2 shows a plan view of the Ricardo E6 combustion chamber. It is cylindrical in shape, the ends being formed by the flat surfaces of the cylinder head, piston, and inlet and exhaust valves. The 14mm spark plug aperture is situated between the valves, and there is another M14 tapping placed opposite to accommodate a pressure pick-up. This design ensures that the maximum flame travel during SI operation is minimally affected by changes in compression ratio.

3.1.3 Exhaust System

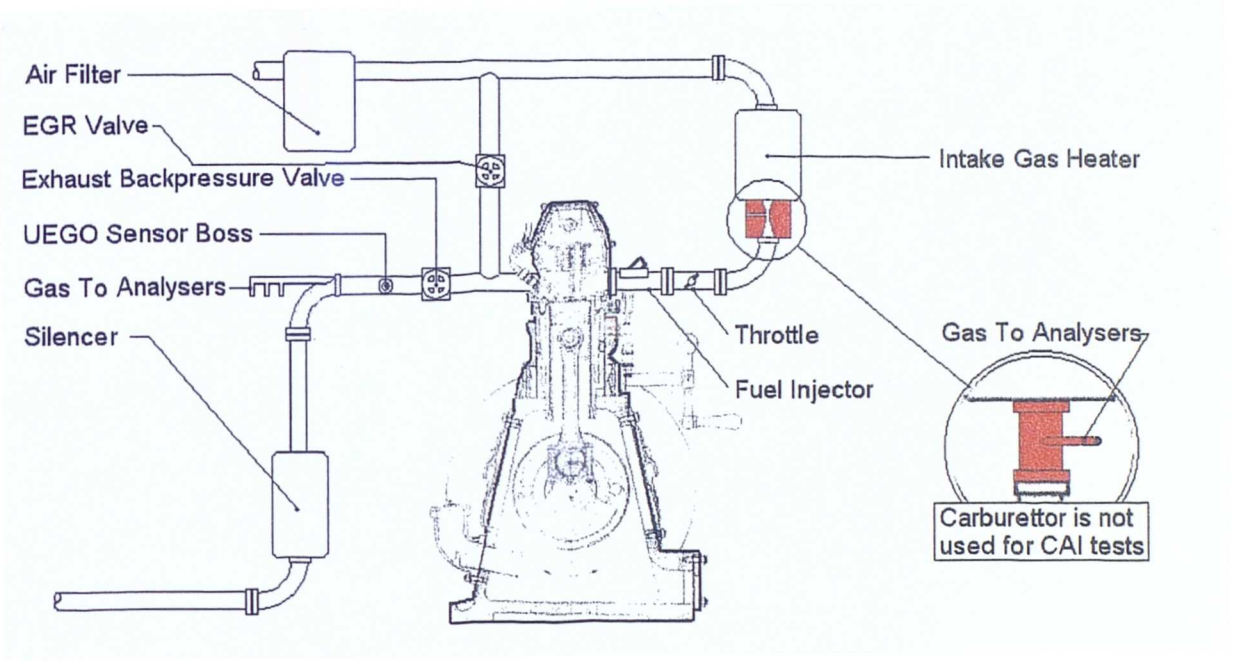

Figure 3.3 Ricardo E6 intake and exhaust systems

A schematic showing the intake and exhaust systems used for these tests is shown in figure 3.3. Beyond the exhaust port, the exhaust gases are divided into two streams. The main stream passes through a gate valve, which is used to control the exhaust backpressure. A gauge is mounted externally to measure the positive exhaust pressure relative to atmosphere ahead of the gate valve. After this, there are several features fitted to the exhaust pipe to facilitate the measurement of exhaust gas. These include gas tap-off points for external analysers, and a welded boss to accommodate a Universal Exhaust Gas Oxygen (UEGO) sensor. Exhaust then passes through a silencing box, and into atmosphere. The second stream of exhaust (exiting the exhaust port) is connected directly to the inlet manifold via another gate valve, allowing facility for the inclusion of EGR in the intake mixture. When EGR is used, it is inducted before the intake gas passes through

the heater or throttle body, ensuring enough time for proper mixing of intake and EGR gases before induction.

3.1.4 Intake Systems

The tests that are described in this work can be divided into two categories: SI, and CAI tests. SI tests have been undertaken to evaluate the operation of a novel fuel system, as described in detail in chapter 4. This system requires the use of a constant depression venturi placed in the intake stream for fuel metering purposes. On the other hand, the CAI tests performed did not require the venturi. Consequently, there are two incarnations of the intake system shown in figure 3.3, each used at different stages of testing.

Air is first passed through the intake filter from atmosphere. If required, EGR gas is added via the EGR pipe and the mixture then passes through a 3kW heater (Secomak Ltd. Model 632). The heater is closed-loop controlled using a sophisticated Proportional + Integral + Differential (PID) controller. Feedback is obtained via a thermocouple that is mounted downstream of the heater. The heater is capable of raising the gas temperature at its exit to a maximum of 400 °C, and under steady state operation can control this temperature to within ± 1°C. Heat losses that occur in the remaining section of manifold limit the intake port temperature to approximately 320 °C. Beyond the heater, for the SI tests described in chapter 5, a constant depression type carburettor is fitted as a means of fuel metering. For the CAI tests described in chapters 6 and 7, this carburettor is replaced by a plain pipe, which is flanged at either end. After this, the intake gas passes by a manually controlled throttle. The throttle is calibrated so that it can be set anywhere between 0° opening, and 60° opening corresponding to WOT, and to an accuracy of 0.5°. A standard Bosch port fuel injector is mounted approximately 100mm upstream of the intake valve, and is directed toward the valve to reduce wall-wetting phenomena.

3.2 Engine Control Systems

The systems required to control combustion and engine operation can be subdivided into four categories: fuelling, ignition, cooling, and engine speed. A great part of this work has been dedicated to developing the novel fuelling system, and so this shall be dealt with in detail in chapter 4. The remaining three control systems are explained here.

3.2.1 Spark Ignition System

Originally, the engine had a magneto type ignition system fitted to the camshaft with a manual control over ignition timing ranging from 45 °BTDC to TDC on the compression stroke. However, preliminary testing indicated that this system did not have the range of spark-timings required for the current research, and that the spark timing event itself was not repeatable on a cyclic basis. Thus, it was decided that a more modern battery-coil ignition would be fitted to achieve better control.

A crankshaft encoder is now fitted to the engine. The optical sensor on this encoder sends two signals to a control box. The first is known as a 'trigger', and is sent once per crankshaft revolution. The second is known as a 'clock', and this is sent 360 times per crankshaft revolution. Thus the control box can determine a reference point in the cycle from the trigger signal, and relate it to any other point using the clock signal. The control box is a modified 'Dial-a-Time' unit, originally manufactured by Lucas Engineering Ltd.. Using this unit, the spark timing is set within the range of 79 °BTDC to 45 °ATDC, and to a highly repeatable accuracy of 0.5 °CA. When the signal to spark is given by the unit, it drives a contact open in the 'low tension' circuit of the coil. The collapse of current in the coil induces a high voltage in the 'high tension' side of the coil, forcing a spark to jump the gap between the electrodes in the spark plug, and initiate combustion.

3.2.2 Coolant System

The original coolant system consisted of a centrifugal pump that circulated coolant through a mains-water cooled heat exchanger and then the engine. Accurate control of the cylinder head temperature relied on setting the rate of cooling in the heat exchanger to compensate for changes in the heat rejection rate from the cylinder contents, resulting from changes in engine load. Furthermore, full-load operation could only raise the coolant temperature to approximately 70 °C, which is well below that experienced in production engine types. The system was inadequate, and so a closed-loop controlled, heated coolant system was designed and commissioned.

The coolant system used for all testing is presented schematically in Figure 3.5. In this system, coolant enters the heat exchanger from the centrifugal pump as before. The rate of cooling in this unit is controlled by a PID temperature controller, which obtains feedback

from a thermocouple situated at the coolant exit from the engine. The controller regulates the rate of cooling by adjusting the flow rate of mains water through the heat exchanger using an on/off valve. Ideally, an analogue valve should be used, but those were found to be prohibitively expensive. After the heat exchanger, the coolant enters a 3 kW liquid heater, which is operated continuously. After passing through the engine, the coolant temperature is measured before re-entry to the pump. Using this system, the coolant temperature can be maintained automatically at any temperature between 40 and 85 °C, to an accuracy of ± 0.2 °C under steady state operation. Thus, the use of a 'digital' on/off mains valve to the heat exchanger has proved adequate for this purpose. The system could have been designed so that the mains water operates continuously, and temperature control is achieved through adjusting the power to the liquid heater. However, the heat exchanger has a greater capacity for cooling than the heater has for heating. Therefore the coolant system's response to inputs from the controller is faster if control is on the heat exchanger. Most importantly, the coolant temperature can be automatically maintained independently of engine load or fuelling rate.

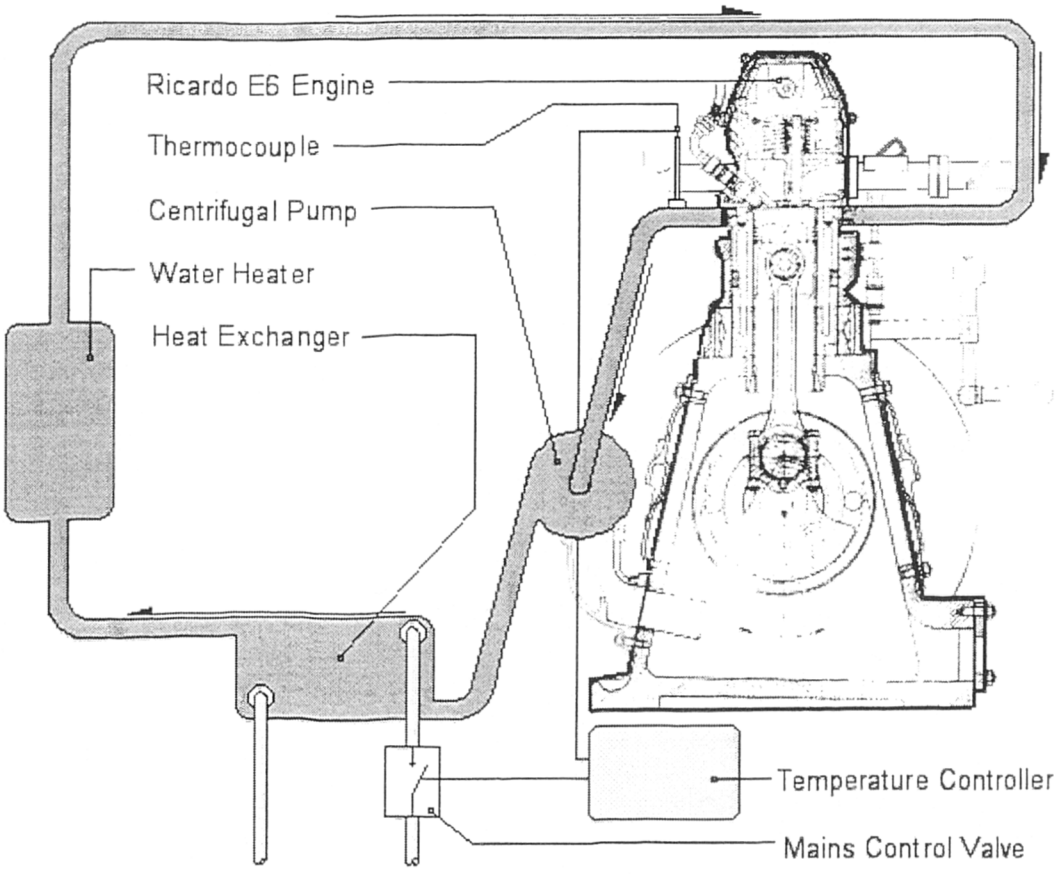

Figure 3.5 Thermostatic liquid cooling system

3.2.3 Speed Control

The engine is coupled to a Laurence Scott 'NS' type Swinging Field AC Dynamometer. The dynamometer is supplied with 3-phase, 440V at 50 Hz from mains. Speed control is achieved using a separate oil-cooled regulator, which is operated manually using a hand wheel. Although closed-loop speed control would be preferable, it requires large alterations to the dynamometer installation. Manual speed control is maintained throughout the tests to a good accuracy as measured from the clock output of the crankshaft encoder.

3.3 Measurement Systems

3.3.1 Computer Data Acquisition

3.3.1.1 In-Cylinder Pressure Measurement

In-cylinder pressure measurement is frequently used in automotive research. The pressure variation over the engine cycle can be used to quantify a number of engine operating characteristics. These include gas exchange phenomena, combustion events such as ignition and instantaneous burning rates, and knocking combustion phenomena. Pressures exerted as a result of combustion also give information about the engine load, cycle-by-cycle variations, and the cyclic loading of different components of the engine for fatigue and vibration analysis.

The real-time in-cylinder pressure measuring system described in this section is used in all experimental work to help characterise combustion, whether it be normal SI or CAI combustion, or abnormal misfire or knocking combustion. Furthermore, it has proved an invaluable tool in the development and commissioning of ancillary engine controls such as fuelling, spark, coolant, and intake temperature subsystems.

A water-cooled pressure transducer (Kistler type 7061B) is mounted in the engine block opposite to the spark plug. This transducer is of the piezoelectric variety, capable of measuring gauge pressures in the range 0-100 bar. Transducers that are not water-cooled are prone to 'thermal shock', in which an incorrect pressure measurement may result as exhaust gas is forced past the transducer during the exhaust stroke. The transducer is connected via a high impedance shielded cable to a charge amplifier (Kistler type 5001).

The charge amplifier is used to amplify the transducer voltage, and is calibrated such that the numerical voltage output from the amplifier corresponds to a predetermined in-cylinder pressure level.

The transducer is calibrated using an oil-filled 'dead weight' testing machine. Known pressures are applied to the transducer, and the charge amplifier output is adjusted so that it corresponded to 10 bar/V, over a range of 10V (100 bar). Maximum in-cylinder pressures that normally occur in an SI engine are in the region of 60 bar, under extremely severe conditions. Thus, the calibrated range should be adequate for all testing requirements.

3.3.1.2 Computer Data Acquisition System (DAQ)

Hardware

The computer DAQ operates as a real-time displaying, measuring, and logging device for the in-cylinder pressure readings. It requires three input signals for correct operation: the charge amplifier output, the clock signal, and the trigger signal. As discussed already, a crankshaft encoder generates the clock and trigger signals for use by the spark and fuelling systems. The clock and trigger are required by the DAQ system so that the pressure output can be sampled at regular intervals (1 °CA), and its phasing relative to the four-stroke cycle can be established. The clock and trigger signals are transferred to the DAQ system via an electronic interface in the computer. The electronic interface is required for two reasons:

(i) The combined loading of the inputs for fuel, spark, and DAQ system on the crankshaft encoder output is high, resulting in a much lower signal voltage, which affects the threshold operation of transistor switches in those respective circuits.

(ii) The DAQ system is situated approximately 3 metres from the crankshaft encoder output. Electromagnetic Interference (EMI) generated by the spark-ignition system, and various temperature control systems around the engine cause voltage spikes to be generated and superimposed on the clock and trigger signals, causing the DAQ system to misread the correct trigger position and clock speed.

Figure 3.6 shows the electronic circuit that is used to transport the signal from the encoder to the DAQ system. The circuit consists of a 'line driver' and a 'line receiver' for both clock and trigger signals. Amplifiers are used to raise the differential signal voltage to 10V, and 100 Ω resistors are situated across the receiver inputs to lower their impedance, thus raising the signal current to reduce the effects of EMI. Inputs to the 'line driver' are in the order of 1 MΩ, which reduces loading on the crankshaft encoder output signals. Outputs from the receiver are fed directly to the DAQ card in the computer. The various parts of the system are screened to further reduce EMI problems. This system has proved effective for ensuring the DAQ receives a well-conditioned encoder input.

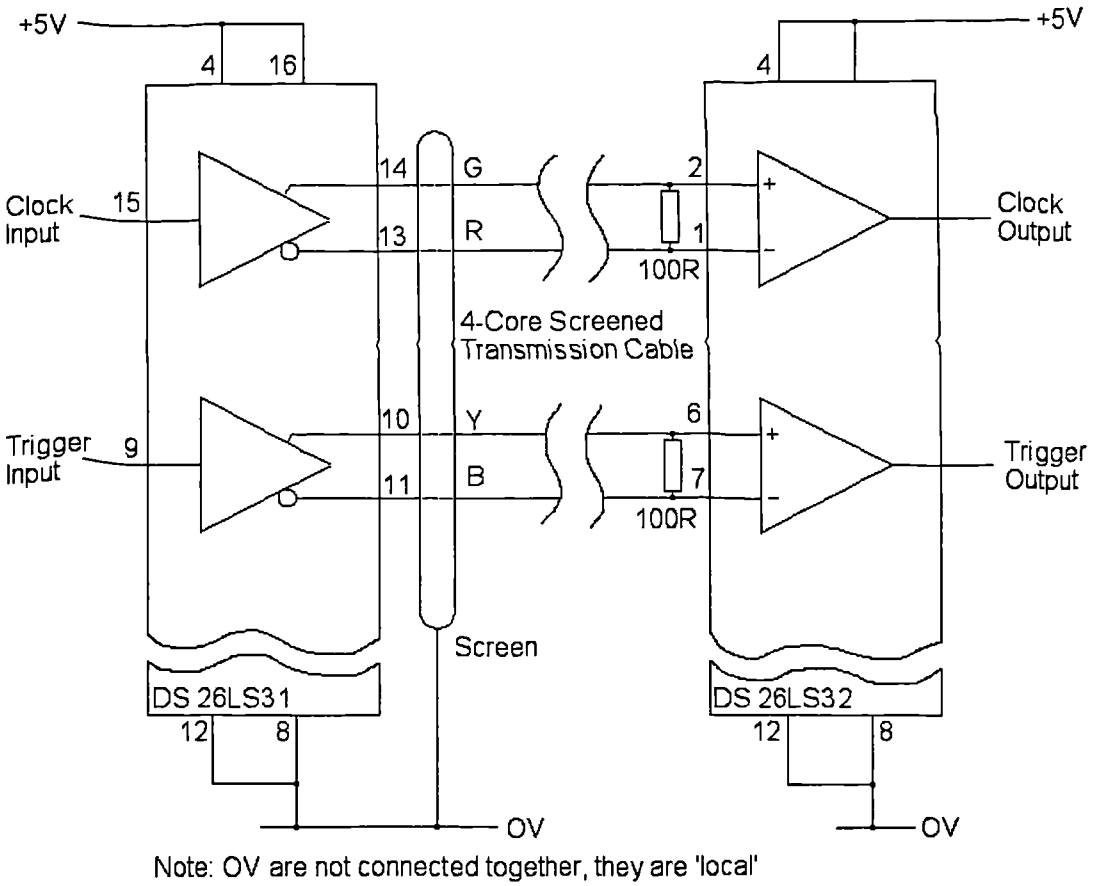

Figure 3.6 Reduced interference interface, showing differential line driver and receiver

The DAQ card is a National Instruments™ type PCIMIO16-1, designed for use in IBM compatible, Pentium™ level personal computers (PC). This card was purchased along with the National Instruments Labview™ software, from which real-time data analysis software can be developed for specific data acquisition requirements. The computer in which the

DAQ card is installed is a Pentium II™ 400 MHz, deemed adequate for real-time analysis of pressure data.

Software

This section outlines the main functions of a program written by John Williams of Brunel University for the analysis of combustion from in-cylinder pressure data. The program performs an array of functions including heat-release analysis, IMEP and COVimep calculation, and knocking combustion analysis. This section introduces the fundamentals of these analytical procedures and how they are performed, so that the general applicability of the software can be demonstrated.

Determination of the Absolute In-cylinder Pressure

The pressure signal sampled by the DAQ card is a gauge pressure. Before calculations can be performed, the pressure must be converted to the absolute scale. To do this, an accurate reading of the absolute in-cylinder pressure at some point in the cycle must be taken. It is normal for this measurement to be taken upstream of the inlet valve, in the inlet manifold. Thus, the cylinder pressure is assumed to equal the manifold pressure at Inlet Valve Closure (IVC). The value of this pressure is dependant on atmospheric conditions, the engine speed, and the nature of the restrictions occurring upstream of the measuring point.

Prior to each set of experiments, the manifold pressure was ascertained by motoring the engine at 1500 rpm and attaching a digital pressure gauge capable of measuring absolute pressure. The in-cylinder IVC pressure was then assumed to be equal to the average reading from the gauge. This value is then input as a constant on the DAQ software.

Cylinder Pressure and Volume Calculations

Figure 3.7 is a screen shot of the main screen during data acquisition. There are four charts that update in real-time on a cyclic basis, as the pressure signal is sampled. The chart at the top left of the figure shows in-cylinder pressure (P_c) versus CA. Using the trigger signal, the software displays the full engine cycle with TDC on the compression stroke phased so that it occupies the centre of the chart.

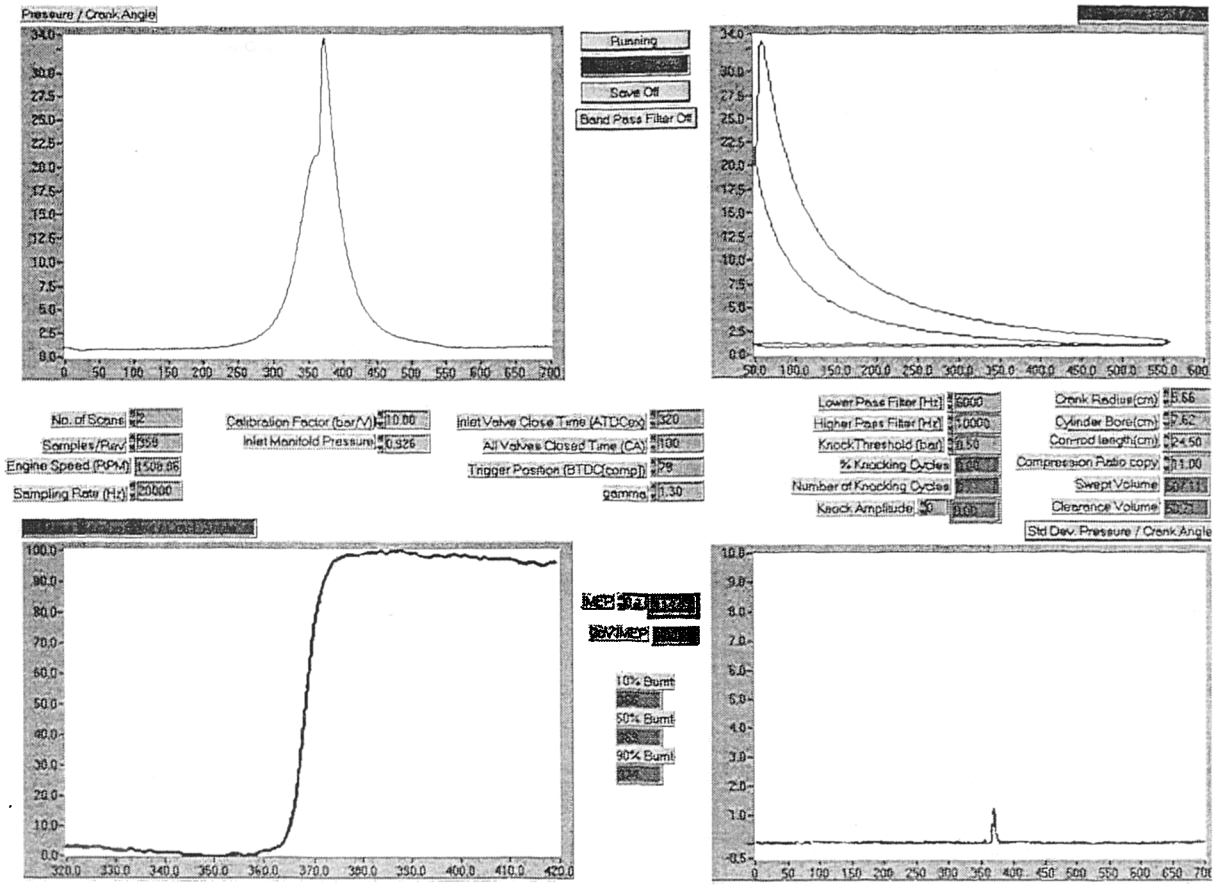

Figure 3.7 Screen image showing the DAQ software main interface

The chart to the top-right of figure 3.7 can be toggled to either show the pressure (P_c) versus cylinder volume (V), or the log(P_c) versus log(V) chart. Cylinder volume is calculated directly from the clock signal (CA) using equations 3.1 and 3.2:

$$V = V_c + \frac{\pi B^2}{4}(l + a - s) \qquad \text{Equation 3.1}$$

where V_c is the clearance volume, B is the cylinder bore diameter, l is the connecting rod length, a is the crank radius, and s is the distance between the crank axis and the piston pin axis, defined as

$$s = a\cos\theta + \sqrt{(l^2 - a^2\sin^2\theta)} \qquad \text{Equation 3.2}$$

where θ is the crank angle to the vertical. Log (Pc) versus log (V) representation is useful for calculating the polytropic coefficients of compression and expansion in the actual

engine cycle. The in-cylinder pressure and volume during the compression and expansion strokes in an IC engine are related by the general expression for a polytropic process:

$$P_c V^n = C \qquad \text{Equation 3.3}$$

where n and C are constants. Taking logs and rearranging

$$\log(P_c) = -n\log(V) + \log(C) \qquad \text{Equation 3.4}$$

Thus $\log(P_c)$ plotted against log(V) yields a straight line of gradient –n, and intercept log(C). The polytropic coefficient (n) can be used to relate pressure, volume, and in-cylinder charge temperature through use of the ideal gas law.

Engine Load Calculations

Knowledge of how pressure changes with cylinder volume is vital for calculating the Indicated Mean Effective Pressure (IMEP), which is the best indication of engine load in single-cylinder research engines. Referring to the top-right chart of figure 3.7, IMEP is calculated by integrating around the curve to obtain the area enclosed on the diagram, and multiplying it by the inverse of the displaced volume, V_d. However, in practice this calculation is performed numerically using a step interval equal to the sampling interval.

$$IMEP = \frac{1}{V_d}\oint p.dV \qquad \text{Equation 3.5}$$

It should be noted that the software calculates the net IMEP, which includes work done on the piston during the compression and expansion strokes, and work done by the piston during the exhaust and induction strokes. If IMEP values are calculated for a number of consecutive cycles, a property defining its variability can be established; this is known as the COVimep. Variability in IMEP results directly from combustion variability from cycle to cycle. Therefore, COVimep is a good indicator of both combustion stability as well as brake torque variations.

$$COV_{imep} = \frac{x\sigma_{IMEP}}{\sum_{1}^{x} IMEP_i}$$ Equation 3.6

where x is the total number of complete cycles for which IMEP has been calculated, and σ_{imep} is the standard deviation in IMEP.

Heat Release Analyses

Heat release analysis remains the most useful method of characterising combustion events within both spark-ignition and diesel engines. It works by computing the amount of heat that would have to be added to the cylinder to produce the observed pressure variation. The first law of thermodynamics is applied to the cylinder contents, which represents a closed system during the combustion event:

$$\delta Q_{hr} = dU + \delta W + \delta Q_{ht}$$ Equation 3.7

Where δQ_{hr} is the heat released during combustion, dU is the systematic rise in internal energy, δW is the work done by the system on the piston, and δQ_{ht} is the heat exchange with the chamber walls.

Assumptions include:

(i) Single zone combustion chamber. Therefore the reactants and products are fully mixed, and no temperature gradients exist.

(ii) There is no difference in the properties of the reactants and products.

Each of the terms needs to be evaluated:

$$\delta W = pdV$$ Equation 3.8

$$dU = mc_v dT$$ Equation 3.9

From the equation of state for an ideal gas ($pV = mRT$):

$$mdT = \frac{1}{R}[pdV + Vdp] \qquad \text{Equation 3.10}$$

Combining Equations 3.9 and 3.10 in terms of dU, and substituting terms into Equation 3.8 gives:

$$\frac{dQ_n}{d\theta} = \frac{dQ_{hr}}{d\theta} - \frac{dQ_{ht}}{d\theta} = \frac{\gamma}{\gamma - 1} p \frac{dV}{d\theta} + \frac{1}{\gamma - 1} V \frac{dp}{d\theta} \qquad \text{Equation 3.11}$$

Where $dQ_n/d\theta$ is the net heat release rate, and $\gamma = c_p/c_v$, the ratio of specific heats. Therefore, using the measured and corrected pressure array, the calculated volume array, an estimation of average ratio of specific heats value during compression and expansion, and arrays that define the rates of change of pressure and volume with respect to crank angle, the net Heat Release Rate (HRR) may be obtained. By integrating Equation 3.11 with respect to crank angle, a cumulative heat release function is obtained, from which the normalised burned mass fraction can be calculated. Burned mass fraction (MFB) curves can then be used to quantify ignition timing, combustion duration, and in the case of SI operation, the 'flame development angle', and the 'rapid burn angle', defined as the 0-10% MFB CA and the 10-90% MFB CA respectively.

The bottom-left chart of Figure 3.7 shows the real-time graphical output of the software for MFB curves. The curve is normalised to the range 0-1 to remove effects of varying total heat release with engine load.

Knocking Combustion Analyses

Audible knocking combustion can arise from the autoignition and rapid consumption of all or part of the cylinder charge. Spatial charge consumption can exceed the velocity of sound during this process, which sets up pressure oscillations that are internally reflected within the combustion chamber. Pressure wave energy is dissipated at the combustion chamber walls, exciting the structure at its natural frequency. The in-cylinder transducer is capable of measuring the pressure oscillations to a high accuracy, and the intensity measured does not depend greatly on the specific location of the transducer [34]. The technique requires

finding the frequency range in which the measured knock intensity is highest. For the Ricardo E6 combustion chamber, this frequency is in the region of 6-8 kHz.

During normal combustion analysis, the pressure-sampling rate is defined by the crankshaft encoder clock signal, which produces 360 pulses per crank revolution. This equates to a sampling frequency of approximately 9 kHz at an engine speed of 1500 rpm. If the pressure signal contains frequencies of up to 8kHz that are of interest, then the sampling frequency must be at least double this value to prevent 'signal aliasing'. Thus, a sampling frequency of at least 18 kHz is required to accurately measure the knocking oscillations. Since this cannot be provided by the crankshaft encoder, the software uses the internal computer clock to generate a 20 kHz sampling frequency, adequate for our purposes. Although the internal clock is required for knock analyses, it is not generally suitable for sampling under normal combustion conditions. It has the disadvantage that the sampling points in the engine cycle are only linked positionally once per crank revolution, on the trigger pulse. This leads to slight inaccuracies in matching a particular pressure to a particular CA, as the crank speed does not generally remain constant from one instantaneous point to the next.

Once the pressure sample has been collected at high frequency (Figure 3.8a), the resulting vector is fed into a digital band-pass filter, which removes frequencies below 6 kHz and above 10 kHz. This results in separating the knock trace from the low-frequency pressure trace, and high-frequency noise (Figure 3.8b). An intensity threshold is manually set to separate knocking from non-knocking cycles. If the knock trace exceeds this threshold (0.5 bar), then the software indicates that knocking combustion has occurred.

Cyclic variations within the combustion chamber, caused by variations in gas motion, homogeneity, and mixture composition from cycle to cycle, in turn lead to cyclic variations in knock intensity and can determine whether knock occurs at all. Consequently, when measuring incipient and non-destructive knock phenomena within the engine, a sample number of cycles will contain both knocking and non-knocking cycles. When sampling a number of engine cycles, the software calculates the ratio of knocking cycles to the total number sampled, and this is termed the Knock Occurrence Frequency (KOF). The KOF is a good measure of whether the engine is deemed 'knocking' or not. For the purposes of the tests carried out in this study, combustion is reported as 'knocking' if the KOF exceeds 10% for an intensity threshold of 0.5 bar.

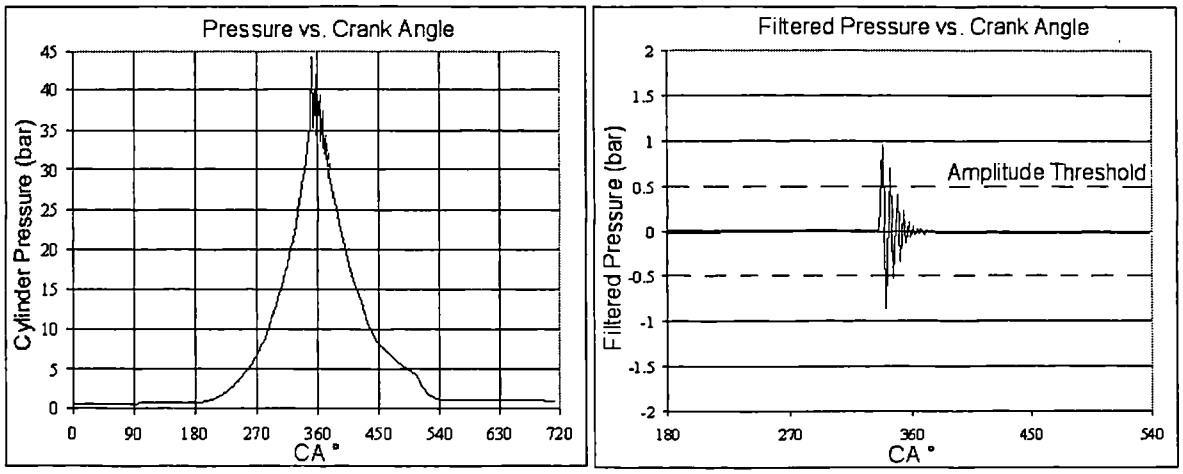

(a) (b)

Figure 3.8 (a) Pressure transducer output, and (b) filtered signal for knock analysis

Data File Output

The program is capable of recording all of the outputs described previously in tabular form. In theory, the number of successive cycles that can be recorded is not limited. However, computing power and storage capacity do limit practical operation. Tests have proved that the storage of 300 cycles takes approximately 60 seconds, dependent on engine speed and pressure-sampling frequency. The file sizes amount to 7 MB and 17 MB for the engine (9 kHz) and computer generated (20 kHz) pressure-sampling frequencies respectively, when the engine is run at 1500 rpm. Storage in an ASCII format allows quick data-access using packages such as Microsoft Excel™, or for more in depth manipulation and analysis, using Mathworks MATLAB™.

3.3.2 Exhaust Emissions

3.3.2.1 CO_2, CO, and O_2 Measurements

A Richard Oliver K650 Emissions Analyser is installed and used to take measurements of CO, CO_2, and O_2. This analyser is of the type used in the U.K. Ministry of Transport regulatory tests on privately owned Light Goods Vehicles (LGV) and Motorcycles. The analyser receives cooled exhaust gas from the engine exhaust stream via a silicon rubber sample line, a water trap, and a combined condensate and particulate removal filter. The

'dry' gas entering the analyser is split for analysis to an infrared absorption cell, and a galvanic cell.

The combined non-dispersive infrared (NDIR) absorption cell is used to measure CO, CO_2, and hydrocarbons. Dried exhaust gas is passed through the cell, which has optical access at either end. At one end of the cell, a broad-band infrared source emits energy into the cell. Infrared radiation (IR) is absorbed by a wide range of molecules, including carbon monoxide, carbon dioxide, and most hydrocarbons. However, each molecule type tends to absorb radiation of discrete wavelengths. Thus, the presence of absorbing gases can be detected by measuring the reduction of IR at the opposite end of the cell from the source. To measure the gas concentrations, IR output from the cell is first passed through a band-pass filter to remove unresponsive frequencies. There are four band-pass filters corresponding to the filtration requirements of CO_2, CO, HC, and a reference which passes IR energy that none of the other three absorbs. The reference theoretically never changes, and so gas absorption can be determined from changes in sample gas composition. The filters are mounted on an oscillating piezoelectric crystal, which cycles each filter through the source beam at a known frequency. The result is a cycling IR beam, whose energy is inversely proportional to the relevant gas concentrations. This beam then enters a 'LUFT' detector, where its remaining energy is absorbed. A similar arrangement to measure the gas concentrations of a reference gas (air) results in absorption on the opposite side of the 'LUFT' detector. The absorbed energy on both sides causes a pressure rise in the gases contained in the 'LUFT' detector. The difference in pressure is measured physically using a diaphragm that separates the detector gases, resulting in a measurement of gas concentration relative to the reference. The measurement accuracies of CO and CO_2 using this technique are limited to $\pm$ 0.06% and $\pm$ 0.5% respectively. This technique can measure quantities of unburned hydrocarbons present in the gas. However, its accuracy is limited as the exhaust gas contains a range of different hydrocarbon species, which have widely varying absorption spectra. The technique of Flame Ionisation Detection (FID) is preferred for hydrocarbon measurement, which is detailed in later in this section.

Oxygen concentration is measured using a galvanic cell. This comprises a gold plated anode and a silver plated cathode immersed in a potassium chloride gel, which acts as the electrolyte. The anode is fixed to a PTFE membrane, through which the sample gas is diffused. Oxygen is reduced electrochemically, and the resulting oxygen ions traverse the electrolyte at a rate proportional to the oxygen concentration and the applied potential

difference across the electrodes. Thus, the measured current gives a value for oxygen concentration to within ±0.1%. Although the cell is sensitive to concentrations of other species such as carbon dioxide, oxygen sensitivity is in the order of 100 times greater than anything else. The majority of the inaccuracy arises from the 'zeroing' procedure that uses oxygen from ambient air. The concentration of oxygen in ambient air varies with humidity and pollution, and is usually in the range 20.7 to 20.9%.

Using dry measured values of CO, CO_2, HC and O_2, the analyser approximately calculates the exhaust A/F ratio and Lambda. The method used is only generally applicable for analysing combustion that occurs at close-to-stoichiometric A/F ratios, resulting in a restricted analyser range of 5-30 A/F ratios.

Range calibration of the analyser is normally carried out at 6-monthly intervals. A specially formulated gas containing known values of propane, carbon monoxide, and carbon dioxide is passed through the analyser to adjust the detector responses for each. The analyser is periodically zeroed during normal operation, at intervals of approximately 30 minutes. 'Zero Grade Air' is used for this purpose by drawing air from atmosphere through an activated carbon filter, which removes any VOC species from the sample.

3.3.2.2 NO_x measurements

A 'Signal 4000VM' chemiluminescent NO_x analyser is used to quantify exhaust NO_x concentrations. The system comprises a heated sample line to prevent water condensation, the analyser unit, and an external vacuum pump to control the sample flow. The chemiluminescence technique relies on the emission of light from activated nitrogen dioxide (NO_2) to quantify the NO_x concentration.

Exhaust gas from IC engines typically contains NO and NO_2. The sample is first passed through a particulate filter. Then, NO_2 contained in the sample is catalytically converted to NO. 'Zero Grade Air' is drawn from a gas bottle and passed through an electrical discharge, which converts some of its oxygen to ozone (O_3). The sample gas and the gas containing ozone are then introduced to a reaction chamber. Further reactions combine the NO and O_3 species to form NO_2 in an excited state, and oxygen. The activated NO_2 can return to its normal state either by light emission or by collision with another molecule. The reaction path is summarised in Equation 3.12:

$$NO + O_3 \rightarrow \overset{*}{NO}_2 + O_2 \rightarrow NO_2 + O_2 + photon$$ Equation 3.12

The reaction chamber is maintained at a low pressure to prevent excessive molecular collisions, and promote light emission. The low pressure also limits the strong deactivating effects of carbon dioxide and water vapour on nitrogen dioxide. The small amount of light produced is proportional to the combined concentration of NO and NO_2 (NO_x), and is measured by a photomultiplier before amplification.

The model 4000VM analyser requires three gas bottles for normal operation. When the analyser is first switched on, a warming period is followed by calibration before samples can be measured. Calibration requires the use of a 'zero' gas containing 'Zero Grade Nitrogen', and a 'span' gas containing 500 ppm of NO in a balance of nitrogen. Once the unit is calibrated properly, the third bottle containing 'Zero Grade Air' is used for ozone production inside the analyser, as explained above. The response time of the analyser is in the region of 2 seconds, and gives readings to an accuracy of ±1% of the span calibration.

3.3.2.3 Unburned Hydrocarbon Measurements

A 'Signal 3000HM' total hydrocarbon analyser is employed to quantify the exhaust hydrocarbon concentrations using the FID technique. When hydrocarbons are burned, electrons and positive ions are formed. If this combustion occurs in the presence of an electric field, a current is generated which is proportional to the number of carbon atoms contained in the sample, which can be measured accurately. To ensure a correct measurement, the sample must be burned in a non-ionising flame. It is usual to use hydrogen fuel burned in air for this purpose. Studies have shown that the detector response is not entirely dependent on the number of carbon atoms present in the mixture, but varies slightly with species type and molecule size. Some variances that occur between different molecular structures are summarised in Table 3.1 [91]. A more complete treatment of FID theory and limitations can be found by referring to Cheng et al. [92].

Molecular Structure	Relative Response
Alkanes	0.97-1.05
Aromatics	0.97-1.12
Alkynes	0.99-1.03
Alkenes	1.07
Carbonyl Radical (CO-)	0
Oxygen in Primary Alcohol	0.23-0.68

Table 3.1 Typical responses of a flame ionisation detector to different molecular structures, normalised with respect to propane [91].

In the 'Signal 3000HM' system, exhaust samples are drawn from the manifold using a heated sample line to avoid condensation and absorption of water and hydrocarbon species respectively. The sample gas is mixed with the FID fuel and a stoichiometric quantity of high purity air. The mixture is combusted in a diffusion flame, which resides in an electric field equivalent to approximately 100V. If hydrocarbons are present in the sample gas, an ion current forms which is measured by an internal galvanometer.

As with the NO_x analyser, this unit requires 3 gas bottles for normal operation. After a period of warming, ignition of the FID flame commences. Gas is fed from one cylinder containing a binary mixture of hydrogen (40%) and helium (60%), and another containing 'Zero Grade Air'. The use of highly pure air is of paramount importance to ensure that ion detection is not impaired. Once the unit reaches normal operating temperatures, calibration is performed using the 'Zero Grade Air' cylinder as zero gas, and a mixture of propane (1500ppm) in a balance of non-reactive nitrogen to adjust the correct range.

The FID technique is limited because individual hydrocarbon species concentrations cannot be determined. The measurement of total hydrocarbon concentration results in a value expressed in ppm carbon (C_1), or methane (CH_3), since this is the simplest expression of quantity. It is of little use to express the hydrocarbon concentration as more highly structured molecules (C_aH_b), since no information on the hydrogen/carbon ratio of the sample exists. The quantification of individual VOC species requires the use of more sophisticated techniques such as Gas Chromatography (GC) or High Precision Liquid Chromatography (HPLC) in combination with FID or Mass Spectrometry (MS).

3.3.3 Temperature Measurement

Thermocouples are situated in various places around the engine, for both measurement and control purposes. The following is a list of measured quantities:

Property	*Situation*
Intake gas temperature:	exit of intake heater and in the intake port
Exhaust gas temperature	exhaust port
Coolant temperature	at inlet and exits points of the engine block
Oil temperature	at inlet of oil cooler (cooler not used)

In addition to these, there are a number of thermocouples used for measurement and control of the novel fuel system described in chapter 4.

3.4 Post-processing of Gas Analyses for A/F ratio and EGR Calculation.

The SI tests detailed in later chapters were all carried out at close-to-stoichiometric A/F ratios. For this reason, the Richard Oliver K650 gas analyser was adequate for determination of A/F ratio to ensure stoichiometric operation. Furthermore, no EGR was used, so there was no requirement to calculate the EGR rate. However, during the CAI tests, extreme air and exhaust gas dilutions were used to characterise the combustion of various fuels under those conditions. Under these circumstances, the A/F ratio calculated by the K650 analyser was insufficient, since it has a full range reading of 30:1, equating approximately to $\lambda=2$ for Gasoline. There is facility for the installation of a UEGO sensor, which is capable of measuring A/F ratio in the range $0.5<\lambda<10$. However, although this sensor has a catalytic surface to remove VOC and CO species through reaction with oxygen, this reaction is not 100% efficient, resulting in slight inaccuracies. This is compounded by the fact that hydrocarbon emissions are a significantly higher fraction of the initial fuel input for CAI combustion than for SI combustion, as studies have shown. Another method for calculating A/F ratio is by measuring the intake air flow rate at a given temperature and pressure, the fuel flow rate directly. There are two reasons why this was not used: firstly, the intake structure must be fully leak-tight for an accurate air flow reading, the intake heater was not designed for this purpose and would have required

extensive modification. Secondly, while the fuel injector can be calibrated accurately, air flow measurements must be taken over several minutes to obtain an average reading. This method extends the experimental time considerably, which is obviously undesirable.

It was concluded that, in any case, the K650 analyser was required to determine the EGR rate by comparing intake and exhaust carbon dioxide concentrations. Instead of using both the K650 analyser and the UEGO sensor, which rely on entirely different technologies, it would be more prudent to take readings of CO_2, CO, O_2, and HC from the exhaust and intake (excluding HC) flows using the K650 and Signal FID analysers, and use combustion equations to calculate the in-cylinder A/F ratio and EGR rate simultaneously. Providing the readings of individual species concentrations are accurate, this method exceeds the accuracy of any other.

Although there are many books that deal with combustion calculations and the determination of A/F ratio, the author was unable to find any literature that combines EGR into the equations. Problems arise because if one introduces EGR into the cylinder, not all EGR species are unreactive, and some contribute actively toward combustion, altering the A/F ratio. Thus, an accurate determination of EGR rate must be obtained to calculate A/F ratio. Lacking any adequate literature, the simultaneous calculation of A/F ratio and EGR rate from known quantities of intake and exhaust species was set about from first principles.

Only the main derivation steps shall be presented here, with a full derivation contained in Appendix A. The analysis begins by equating reactants and products for a general fuel type with oxygen, and for a certain EGR rate. The combustion equation can be written explicitly as:

$$n_R[aCH_bO_c + d(O_2 + 3.773N_2) + (g_iCO_2 + h_iCO + j_iO_2 + k_iN_2 + l_iH_2O + m_iNO + q_iNO_2 + s_iCH_4 + t_iH_2)] \Rightarrow n_P(g_eCO_2 + h_eCO + j_eO_2 + k_eN_2 + l_eH_2O + m_eNO + q_eNO_2 + s_eCH_4 + t_eH_2)$$

Equation 3.13

For a precise definition of each of the variables, refer to appendix A. Defining a volumetric EGR rate (f) and assuming lean CAI combustion conditions such that concentrations of H_2, NO, and NO_2 are negligible, Equation 3.13 can be simplified, and rewritten:

$$n_R[aCH_bO_c + d(O_2 + 3.773N_2)] = (n_P - n_R f)(g_e CO_2 + h_e CO + j_e O_2 + k_e N_2 + l_e H_2O + s_e CH_4)$$

Equation 3.14

The fuel composition is known (b,c), as are the dry concentrations of CO_2, CO, and O_2 in the inlet and exhaust (v_i', g_e', h_e', j_e'). The variables v_i', g_e', h_e', j_e', and s_e are measured using the appropriate analysers. The general relationship

$$x = (1 - l)x' \qquad \text{Equation 3.15}$$

defines the dependence of wet and dry (measured) molar fractions on the H_2O molar fraction in the inlet or exhaust (wet). Providing l_e can be found, d, g_e, h_e, and j_e are known. Solution requires assuming 100 moles of dry exhaust products (n_P = 100).

The unknowns are a, d, n_R, k_e, and l_e. Five exclusive equations are required for solution of the combustion Equation 3.14. Analysis of the hydrogen and carbon mass balances yield the equation for H_2O concentration in the exhaust:

$$l_e = \frac{b(g_e' + h_e') + s_e(b - 4)}{[2 + b(g_e' + h_e')} \qquad \text{Equation 3.16}$$

Thus the wet molar concentration of H_2O in the exhaust can be calculated from measured concentrations of CO_2, CO, and CH_4 in the exhaust stream, and knowledge of fuel composition. Equation 3.16 is analogous to the equation presented by Heywood [93]. Important differences are that (i) lean mixture means that CO concentrations are very low, and (ii) hydrocarbons are measured here as CH_4, not converted to concentrations of unburned HC with the same C/H ratio as the intake fuel. Further analysis of the EGR relationships, intake and exhaust O_2 concentrations, and an oxygen balance yield a system of four simultaneous equations in four unknowns (a, d, f, and n_R):

$$\begin{bmatrix} e_i' & 0 & (1-l_e)g_e'+l_e g_i' & 0 \\ -v_i' & -1 & l_e j_e'-l_e v_i'-j_e' & 0 \\ c & 2 & (1-l_e)(2g_e'+h_e'+2j_e')+l_e & -n_P[(1-l_e)(2g_e'+h_e'+2j_e')+l_e] \\ 1 & 0 & (1-l_e)(g_e'+h_e')+s_e & -n_P[(1-l_e)(g_e'+h_e')+s_e] \end{bmatrix} \begin{bmatrix} a \\ d \\ f \\ n_R^{-1} \end{bmatrix} = \begin{bmatrix} g_i' \\ -v_i' \\ 0 \\ 0 \end{bmatrix}$$

Equation 3.17

Once Equation 3.17 is solved, A/F ratio can be found by considering the intake and EGR excess air, the injected fuel, and the EGR hydrocarbon content:

$$A/F\ Ratio = \frac{138.25(c + f(1-l_e)g_e')}{a(12.011+1.008b+16c)+16.043fs_e}$$

Equation 3.18

All of the EGR rate data presented in this report is done so on a gravimetric basis. Many CAI combustion studies that have considered EGR have presented measurements on a volumetric basis. While this is fine for entirely homogeneous combustion (such as is presented here), it has become clear that when burned gas residuals are used to initiate and control the combustion event, a volumetric representation of EGR is not sufficient to express the EGR rate. This is because the mass of EGR used is dependent on its temperature and pressure for a known volume, and these quantities may well not be known. So, it has been decided that EGR presented an a gravimetric basis is of more use to future researchers in the field, even though the gravimetric and volumetric rates are approximately numerically equal in this study (due to charge homogeneity). EGR rate is determined by considering the relationship:

$$EGR_m = \frac{\dot{m}_{EGR}}{\dot{m}_{EGR} + \dot{m}_r}$$

Equation 3.19

The composition of major components contained in EGR and reactant gases is known from solution of Equation 3.17. These are

$$\begin{aligned} m_{EGR} &= n_R f(g_e m_{CO_2} + h_e m_{CO} + j_e m_{O_2} + k_e m_{N_2} + l_e m_{H_2O} + s_e m_{CH_4}) \\ &= n_R f(44.01g_e + 28.01h_e + 32j_e + 28.16k_e + 18.016l_e + 16.043s_e) \end{aligned}$$

Equation 3.20

$$m_R = n_R(am_{CH_bO_c} + d(m_{O_2} + 3.773m_{N_2})$$
$$= n_R[a(12.011 + 1.008b + 16c) + d(32 + 3.773 * 28.16)$$

Equation 3.21

Equations 3.20 and 3.21 are then replaced into Equation 3.19 for the determination of gravimetric EGR rate.

The simplest way to employ these A/F ratio and EGR calculations is by programming a spreadsheet to perform them automatically. The computer used for data acquisition of pressure data has also been used for this. An extensive spreadsheet has been developed, used to manually log all of the inlet and exhaust species concentrations during experimentation. It also has facility for the input of fuel composition, required for the A/F ratio and λ calculations. The software then automatically calculates λ and gravimetric EGR rate, and plots the results on a relevant chart for immediate review.

3.4.1 Post Processing of Data for Calculation of Gravimetric Emissions

Raw emissions data obtained from the engine are received on a volumetric basis (ppm, %). The quantity of any species is therefore dependant on the total exhaust flow rate. In SI engines, excluding speed considerations, the exhaust flow per cycle is dependent on engine load, ultimately determined by the intake throttle position. On the other hand, Diesel and un-throttled CAI engines exhibit roughly constant exhaust flow per cycle characteristics, determined only by restrictions imposed by intake design and valve configuration. A technique is required to normalise emissions from each of these engine types, so that realistic comparisons can be made. The best way to achieve this is by expressing emissions on a gravimetric basis, since it is an absolute measurement. The most common practice is to normalise the volumetric emissions to the indicated- or brake-power delivered by the engine. For the research engine used here, indicated specific emissions are most useful, and so post processing is employed to evaluate these.

The first requirement is to calculate the indicated power of the engine (P_i), this is found from the relationship:

$$P_i = \frac{IMEP.V_d N}{n}$$

Equation 3.22

where V_d is the displaced volume per engine cycle, N is the engine speed, and n is the number of crank revolutions for each power stroke (2 for a four-stroke cycle). The indicated specific fuel consumption (ISFC) is of interest to evaluate efficiency characteristics of the engine, and this is defined as

$$ISFC = \frac{\dot{m}_f}{P_i} \qquad \text{Equation 3.23}$$

where $\dot{m}_f$ is the mass flow rate of fuel, evaluated from injector calibrations that are performed frequently between experimental tests. Calibrations change with fuel type and injector wear. Indicated specific values of NO_x, HC, and CO are calculated in a similar fashion

$$ISNO_x = \frac{\dot{m}_{NO_x}}{P_i}, \quad ISHC = \frac{\dot{m}_{HC}}{P_i}, \quad ISCO = \frac{\dot{m}_{CO}}{P_i} \qquad \text{Equations 3.24}$$

The generic equation used by the spreadsheet software combines Equations 3.23 with 3.24 to form a more easily handled formula for specific emissions calculations

$$IS(x) = \frac{[(n_P - n_R f) * vol(x) * m_{(x)}}{n_R a(m_c + bm_H + cm_O)} * ISFC \qquad \text{Equation 3.25}$$

where (x) is the emission of interest, vol(x) is the quantity of that emission expressed as a molar fraction, and $m_{(x)}$ is its molecular mass.

So, to perform calculations of indicated specific emissions, the spreadsheet contains data on the calibrated fuel flow rate, and IMEP as calculated by the DAQ system. In the latter case, data from the DAQ output files are transferred manually after experimentation, since no direct links exist between the DAQ and spreadsheet software.

3.5 Summary

Details of the single cylinder research engine used for all of the experimental tests have been presented. Significant upgrades to the gas-exchange, spark-ignition, and coolant systems have been undertaken to ensure the precise control of engine related parameters during the following experimental tests. Exhaust gas speciation and in-cylinder pressure measurement systems have been installed to accurately record the effects of changing operating conditions. Strategies for the determination of the state of heat release during combustion, and for the severity and frequency of knocking combustion have been outlined. Finally, a method of simultaneously calculating A/F ratio and EGR rate using intake and exhaust gas speciation data only has been developed from first principles.

Chapter 4

Prototype Fuel System Design and Development

Chapter 4 Prototype Fuel System Design and Development

4.1 Introduction

A major part of this project is to develop and evaluate a novel fuelling system, first invented and patented (UK Patent Number GB197-0386) by the Ford Motor Company. In the following section, the Stratified Fuel Fraction Engine (STRAFFE) concept is introduced, giving an overview of how the system is used to modify combustion. In later sections, a detailed description of the fuel system's construction and operation is presented. In the following chapter the system is commissioned and its operation is evaluated with the engine operating in SI mode.

4.2 Stratified Fuel Fraction Engine (STRAFFE) Concept

IC engines rely on the release of the fuel's chemical energy to produce mechanical power. The formulation of gasoline fuel has significant effects on combustion and pollutant formation within the cylinder. Furthermore, its particular properties have a significant effect on the driveability and performance attributes of the engine, such as reliable cold starting, fast warm-up, rapid transient response, knock-free combustion, and durable operation. To meet all of these requirements, gasoline fuel is a carefully formulated blend of many hundreds of hydrocarbons and additives, to give the best compromise for all round performance. The STRAFFE concept proposes to use gasoline fuel in a more flexible manner, by targeting the superior properties of separate fuel components present in the blend to match specific engine attributes. For example, the lighter fractions contained in gasoline are highly volatile and more ignitable, better suited to cold start operation and lean burn. On the other hand, the heavier fractions are more resistant to knocking combustion. This has led to the STRAFFE concept, which attempts to stratify the charge by fuel components, rather than by the A/F ratio of the averaged components, as is the case in conventional stratified-charge engines. According to this concept, all of the gasoline fuel is consumed completely during combustion just like in conventional engines. However, strategic positioning of specific fuel components within the combustion chamber may facilitate improvements in engine efficiency, performance, emissions, and driveability. Examples of the type of fuel stratification that can be achieved using conventional port-injected or GDI strategies are presented in Figure 4.1. In Figure 4.1a, light fractions are

inducted for a short period during cold-start operation to improve the homogeneity and ignitability of the cylinder charge. Figure 4.1b shows how the heavier fractions may be stratified to occupy the end-gas region of the cylinder during high-load operation. The higher resistance to autoignition of the heavier fractions combined with a more ignitable light fraction in the centre region (faster flame development angle) leads to a higher knock resistance, possibly allowing increases in the engine's compression ratio, which translates directly to higher thermal efficiency. There is also the possibility to operate this configuration in a lean mode, since the lighter fractions are more easily spark-ignited.

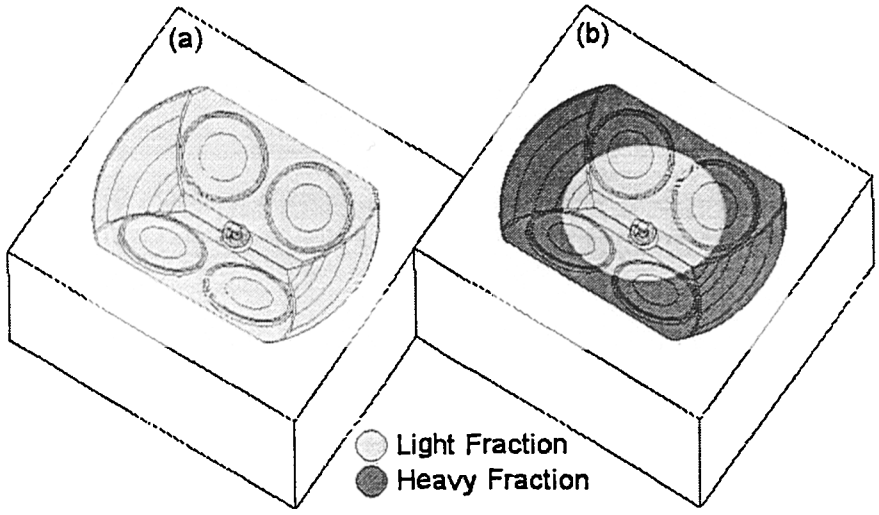

Figure 4.1 STRAFFE concept strategies, showing (a) cold start, and (b) WOT fuel patterns

Leaving the stratification technique to one side, the STRAFFE concept requires a fuel system that can deliver equal quantities of two gasoline components that have significantly differing properties. Furthermore, a production version of this system must cope with the highly transient fuelling requirements of modern automotive engines. The simplest incarnation of the fuel system would be one that uses two fuels, obtained from separate reservoirs. These fuels can be delivered to the vehicle using separate pumps at the garage forecourt. Obviously this would require significant changes in the fuel distribution infrastructure and major collaboration with oil companies, which is not warranted at this stage. The more favourable option is to develop an on-board system that can separate gasoline as required by the engine. The system can be used to evaluate the potential benefits of the STRAFFE concept, and help to economically justify whether an on-board system is preferable or not.

Distillation is the proposed technique of separating gasoline into two fuel streams using an on-board system. The Ford Motor Company commissioned Saybolt UK Ltd. to investigate the distillation properties of a European standard gasoline (BS EN 228), and subjected the resulting distillates to a number of tests for octane quality and composition. Their Results are shown in Table 4.1.

Under preliminary tests, Saybolt UK Ltd. were asked to establish the temperature at which 50% (by mass) of the Type 2 (Table 4.1) gasoline was vaporised. Their tests showed that half of the fuel vaporised at a temperature of 90°C, when at atmospheric pressure. After this, they produced a quantity of Type 1 gasoline (light fraction) by evaporating standard gasoline to 90°C and re-condensing the vapour in a separate vessel. Type 3 Gasoline is what remained of the original gasoline after this process. Thus, standard gasoline was split equally into two separate fuels by distillation.

	Type 1 - Light Fraction Distilled from Type 2 (IBP* - 90°C)	Type 2 BP Premium Unleaded Gasoline BS EN 228		Type 3 - Heavy Fraction Distilled from Type 2 (90°C - FBP*)
		MIN	MAX	
Composition				
Aromatics	11.8	34.1		69.1
Paraffins	79	58.3		24.3
Olefins	9.2	7.6		6.6
Total lead (g/l)			0.013	
Total Sulphur (%m/m)	0.01		0.05	0.04
Properties				
Research Octane Number (RON)	90	95		99.4
Motor Octane Number (MON)	84	85		87.1
Fuel Sensitivity (RON-MON)	6	10		12.3
Density 15°C (kg/m^3)	669	725	780	830
Vapour Pressure (kPa)	103	45	80	7

* IBP = Initial Boiling Point FBP = Final Boiling Point

Table 4.1 Specification and Properties of Unleaded Gasoline (BS EN 228) and Selected Distillates.

Tests on the composition of each of the gasoline types yielded some interesting results. Of the species present in standard gasoline, most paraffins were evaporated into the light fraction, while most aromatics remained in the heavy fraction. The olefinic content of light and heavy fractions were measured as roughly the same. Furthermore, sulphur compounds were found to be mostly present in the heavy fraction after the distillation process.

Fuel octane tests showed that the heavy fraction, containing more aromatic compounds, had a raised RON of 99.4, while the paraffinic light fraction had a RON of 90.0. This indicates that it is possible to gain significant benefits by stratifying the heavy fraction to occupy the end-gas region, raising the knock-resistance of the entire charge. It is interesting to note that the MON values measured for each of the fuels are similar. This would suggest that under more severe engine operating conditions, the benefits gained from employing the STRAFFE concept for the avoidance of knocking combustion may be minimal. The light fraction is more volatile with a lower density and higher Reid Vapour Pressure (RVP) than standard gasoline. The opposite is true for the heavy fraction. These tests have shown that under laboratory conditions the fundamental ideas behind the STRAFFE concept are valid. It remains for a prototype system to be developed and evaluated under real engine operating conditions.

4.3 Fuel Fractionating System

The fuel system described in this section was developed from the patent GB197-0386, held by the Ford Motor Company. The system was developed over a period of 12 months from original concept designs contained within the patent. A great deal of modifications were necessary to make the concept work in practice. Despite taking many forms, only the final version of the prototype shall be presented here. However, a detailed discussion of each of the major components will give insight into the practical constraints on each element in the system.

4.3.1 Functionality and Limitations

The primary function of the fuel fractionating system is to receive standard gasoline at atmospheric pressure and ambient temperature, and deliver equal quantities of 'light' and 'heavy' fractions separately to the intake manifold of the engine. There are two fundamental requirements that the system must meet to ensure satisfactory operation:

(i) The composition of each fraction must remain constant, regardless of fuel flow rate through the fuel system.

(ii) The fuel flow rate is ultimately a function of required engine operating conditions. Thus, the system must produce fractions on a continuous and transient basis, according to engine demand.

With respect to (i), although the composition of the resulting fractions can be kept constant for a single gasoline, the composition of 'standard specification' gasoline varies geographically and between oil companies, since fuel composition is not currently subject to legislation. This factor may affect the operation of the system, but cannot be determined without full investigation using a working prototype. With respect to point (ii), although adequate transient response of the system is paramount for satisfactory operation, evaluating and optimising it requires extensive application of control theory, and is beyond the scope of this study. So, the fuel system has been designed, built, and commissioned on the Ricardo E6 engine to evaluate its performance under steady state operation and for type 2 gasoline with the specific composition as listed in Table 4.1. Testing of different gasolines and for transient effects can be performed later if the concept appears to show promise.

4.3.2 Description of Operation

Figure 4.2 shows a schematic of the prototype fuel fractionating system, as installed for evaluation on the Ricardo E6 engine. For clarity, the system has been subdivided into three parts: measurement, control, and fuel fractionating subsystems.

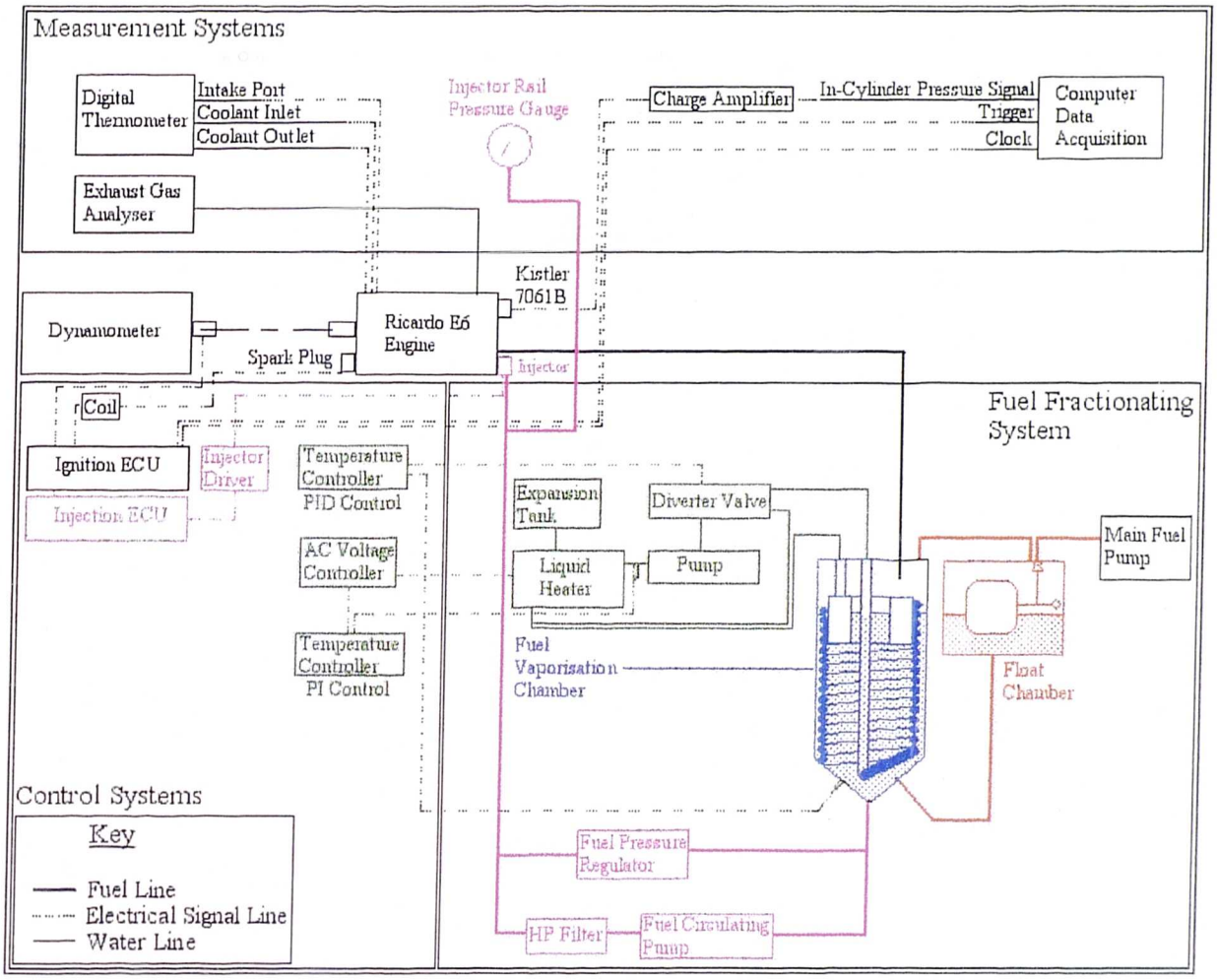

Figure 4.2 Schematic of the fuel fractionating system with associated measurement and control systems

4.3.2.1 Float Chamber

Standard gasoline fuel enters the system from the laboratory supply via a calibrated burette, which is used to determine the total fuel flow rate through the system. As shown in red in figure 4.2, fuel is admitted to the float chamber, which is used to regulate the level of liquid fuel in the vaporisation chamber to ensure constant volume conditions. The float chamber is connected to the vaporisation chamber in two places. A vapour connection ensures that both vapour spaces are subject to the same pressure conditions, which is required for fuel level control. A liquid connection feeds fuel to the base of the vaporisation chamber.

4.3.2.2 Fuel Vaporisation Chamber

The fuel vaporisation chamber is shown in blue in figure 4.2. This is where the separation of light and heavy fraction streams takes place. Liquid fuel in the chamber is maintained at a constant temperature, as measured at the base of the chamber, opposite to the fuel inlet. The chamber pressure is also maintained at a constant value using a venturi, as discussed later. Maintaining a constant chamber temperature and pressure are paramount for ensuring that the composition and relative flow rates of light and heavy fractions out of the system are constant over time and for a varying total fuel flow rate. The gasoline can be considered as a mixture of a number of discrete liquids, each with its own heat capacity and boiling point. If the gasoline composition, its temperature, and its pressure remain fixed, then thermodynamic principles dictate that a fixed fraction of the gasoline will be evaporated. So, fuel entering the chamber is raised to the fractionating temperature through conduction and convection from the chamber contents. As the temperature is raised, the lighter fractions are made to vaporise, while the heavier fractions gain only sensible energy. Once separation has been achieved, the light fraction exits the chamber at the top as a vapour, and the heavy fraction exits the base as a liquid.

Fuel Temperature Control

The vaporisation chamber temperature is regulated using a separate control system. In practice, it is envisaged that the heat energy required for fuel fractionating can be derived from waste coolant heat. It is to the systems advantage that the coolant temperature in modern production engines is regulated to around 90°C, meeting the fractionating requirements for equal output fuel streams. In this prototype, an independent coolant circuit has been designed to simulate operation of a practical one, as shown in green in figure 4.2. The coolant circuit contains an equal mixture of ethyl glycol and water, to simulate the heat capacity, viscosity, and heat transfer properties of fluids used in practical coolant systems. Coolant first passes through a 3 kW liquid heater. The exit temperature from the heater is regulated by an external PI controller to 90 ± 0.2 °C. Coolant then enters a centrifugal pump, after which it meets a diverter valve. The operation of this valve is tightly controlled using a PID controller. The vaporisation chamber fuel temperature is measured, and the PID controller determines whether heat addition is required or not. If not, then the coolant is returned to the inlet of the liquid heater. Otherwise coolant is passed through a copper coil, which is immersed in the fuel contained within the

vaporisation chamber. Coolant is then passed back to the inlet of the liquid heater. This system allows accurate control of the vaporisation chamber temperature to within ± 0.1 °C under steady state conditions.

The fuel temperature is measured some distance away from the surface of the immersed coil to ensure a correct measurement. Unfortunately, the fuel contained in the chamber has a very low flow rate compared to its volume, and is essentially stagnant. Because of this, temperature gradients exist between the coil surface and the thermocouple. The fuel temperature as measured at the base of the chamber is maintained at 65°C, which was found experimentally to be the correct temperature to ensure equal light and heavy fraction flow rates. However, fractionation still occurs at 90°C, since this is the temperature at the interface between the immersed coil and the fuel.

Vaporisation Chamber Pressure Control

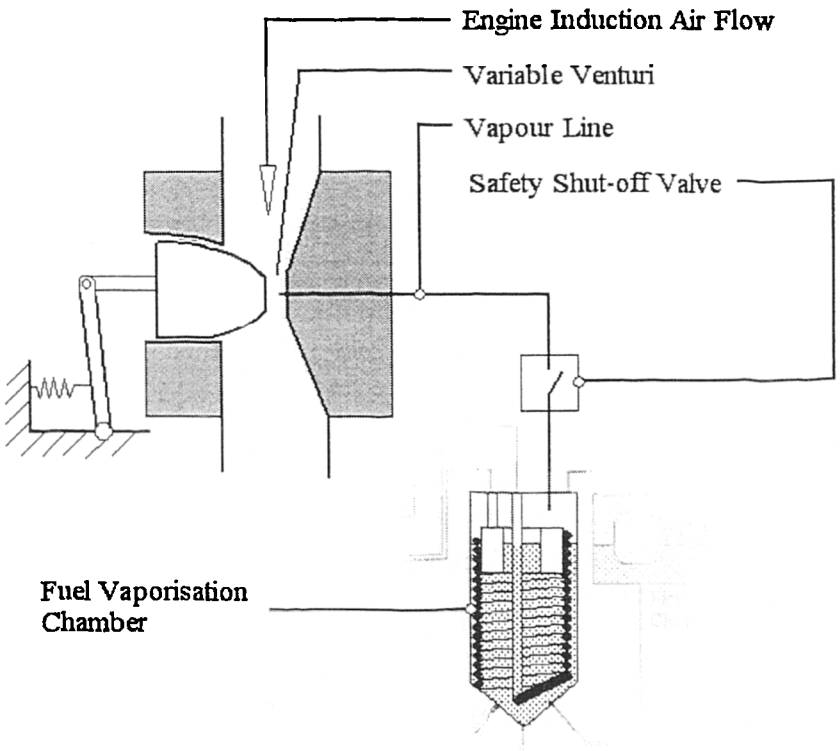

Figure 4.3 Vaporisation chamber pressure control showing the vapour line and the constant depression carburettor

Figure 4.3 shows how the vapour exiting the top of the chamber is metered into the intake air flow of the engine. Vapour exiting the vaporisation chamber is fed into the metering jet

of a constant depression type carburettor. The carburettor is designed to maintain a pressure of approximately 0.9 bar absolute at its throat, regardless of the induction air flow rate. This arrangement is suitable because the vaporisation chamber pressure is maintained at a constant value regardless of engine load and total fuel flow rate through the system. Unfortunately, it does place an extra restriction in the intake manifold, resulting in a lower maximum volumetric efficiency. A shut-off valve is situated in the vapour line between the chamber and the venturi for safety purposes during system shutdown.

4.3.2.3 Injected Fuel Metering Circuit

Fuel exiting the base of the vaporisation chamber enters a fuel injection circuit, as shown in pink in figure 4.2. Fuel first passes through a Bosch positive displacement circulating pump, and then a high-pressure filter. A spur carries the fuel to a standard Bosch port injector for delivery to the intake manifold of the engine. Excess fuel is circulated past a pressure regulator, which maintains the rail pressure at 2.7 bar gauge, relative to the intake manifold downstream of the throttle plate. This arrangement ensures that the pressure drop across the injector nozzle is constant regardless of intake manifold pressure, which varies with engine speed and load. Thus, for a particular injector opening time, a known quantity of heavy fraction fuel is delivered to the engine. In conventional systems, the pressure regulator outlet returns fuel to the main tank to ensure that it is cooled sufficiently before returning to the 'hot' engine bay. This prevents vapour locks forming in the low-pressure areas of the fuel circuit, which can interrupt injector delivery. However, in this system, excess fuel from the rail is passed directly back to the intake of the circulating pump. It is unnecessary to return the heavy fraction to the main tank because all of its light fractions have already been removed, precluding the formation of vapour locks.

The vaporisation chamber temperature and pressure are fixed, which in turn determines the composition of light and heavy fractions, and the relative rate at which they are produced. The temperature is set to 65°C, and the pressure is set to 0.9 bar absolute, ensuring that equal quantities of light and heavy fraction are generated. Therefore, the only part of the system that controls the total flow of fuel though the system is the injector. A lengthened injector pulse width increases the flow of heavy fraction, which in turn increases the quantity of light fraction evaporated in the main chamber because more gasoline is inducted at its base. An increase in inducted gasoline will lead to a reduction in the measured temperature at the base of the vaporisation chamber, and the coolant flowrate

through the coil will be increased to compensate. Thus, the system is fully self-controlled, and should produce equal quantities of light and heavy fractions under all engine operating conditions required for testing

4.3.3 Practical Design Constraints

During the course of prototype development, a number of configurations were tested and rejected. While it is not relevant to detail the unsuitable configurations in this study, some general points on the choices leading to the final strategy are warranted. The system as commissioned on the Ricardo E6 engine is shown in figure 4.4.

4.3.3.1 Float Chamber

For adequate operation of the whole fuel system, the gasoline fractions must be produced and delivered to the intake manifold on a continuous basis. While this can be ensured with the heavy fraction by fuel injection, production and delivery of the light fraction as a vapour requires a continuous intake fuel flow to the vaporisation chamber. However, the float valve operates in an on/off pattern, which inherently prevents the continuous flow of fuel. There are two simple methods to helping the float mechanism achieve a more stable flow:

(i) Match the maximum flow through the float valve to the usual flow requirements of the system. This approach cannot be used in this case because the maximum flow requirements of the system (at WOT) far outstrip those found usually (at low load), which would result in insufficient flow through the float chamber and fuel starvation.

(ii) Increase the on/off frequency of the valve. This can be achieved easily by reducing the surface area to volume ratio of the fuel. If the surface area is reduced, then a unit change in volume will produce a larger change in fuel height within the column.

A hollow cylindrical aluminium insert is placed within the vaporisation chamber to reduce the combined surface area of fuel within the vaporisation and float chambers. Although this reduces the total vapour/liquid surface area, which may have adverse effects on fuel

evaporation, it is thought that most vaporisation occurs at the coil/fuel boundary in a similar fashion to a domestic kettle.

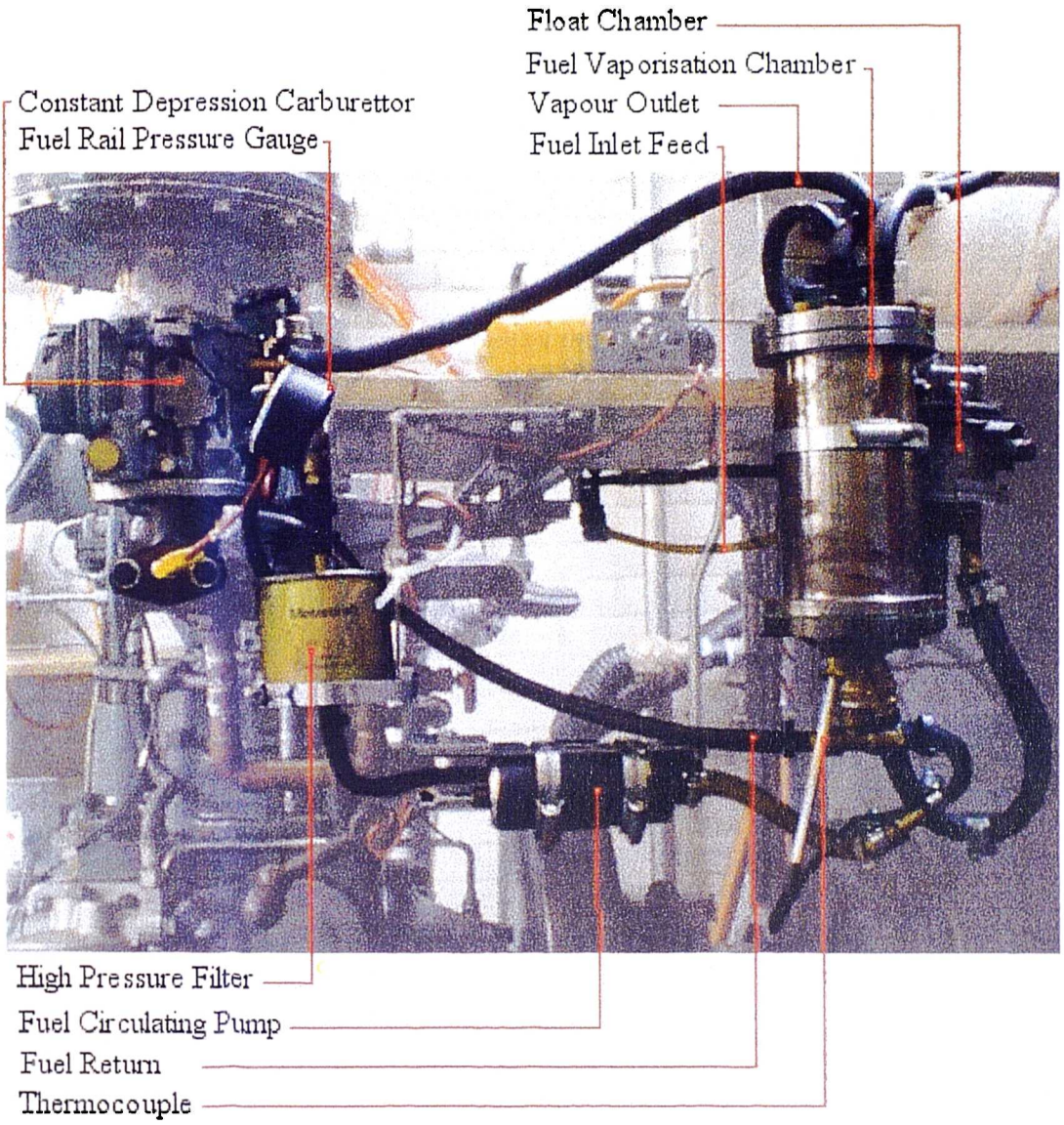

Figure 4.4 Prototype fuel fractionating system installed on the Ricardo E6 engine

4.3.3.2 Method of Heat Addition

A range of different coolant/fuel heat exchange strategies were tested during the course of prototype development. There are a number of requirements that the final system fulfils to ensure stable the production of light fraction fuel:

(i) Heat addition must take place within the vaporisation chamber. The original patent described a system in which gasoline was heated in an external circuit before re-

entry to the chamber. This caused problems with heat transfer in the chamber, since it acted as a large heat sink, reducing the vaporisation rate significantly.

(ii) The coolant temperature must be controlled accurately to within ± 0.5 °C. Earlier systems used simpler on/off control to regulate the coolant temperature, which resulted in large oscillations of both coolant temperature and vapour production.

(iii) A highly efficient heat exchanger arrangement is required. In earlier systems, a coolant jacket around the vaporisation chamber was used to transfer heat. The exposed surface area was too small to transfer the required heat and produce enough light fraction fuel. In other attempts, fuel was circulated inside the coil resulting in vapour forming on the inside surface of the coil, which adversely affected heat transfer to the liquid fuel. In the current system, the copper coil has a large surface area, conducive to large heat transfers. Furthermore, vapour forming at the coil surface is immediately expelled to the vapour space at the top of the chamber.

The amount of fuel submerging the coil has significant effects on the stability of vapour production. A trade-off exists between a large volume of fuel, which facilitates stable and non-oscillating vapour production, and a small volume of fuel, which gives better transient response to changes in total fuel flow requirements. The thermal inertia of the chamber increases with an increasing volume of liquid fuel. A high thermal inertia tends to stabilise heat transfer between coolant and fuel. Unfortunately, 'fresh' gasoline entering the chamber rapidly diffuses into the fuel already present, and consequently takes a longer time to fully come into contact with the coil surface, where vaporisation (to 90°C) takes place. A longer time to obtain light fraction from intake gasoline translates directly to a poorer transient response. However, the aim in this work is to obtain a working prototype for steady-state evaluation of the resulting fuels, so the fuel height within the chamber has been set to the maximum allowable to give the most stable operation.

4.3.3.3 Heat Loss Considerations

The original patent suggests a system that incorporates the vaporisation chamber 'in-line', between the pressure regulator and the fuel circulating pump. Thus, circulating fuel enters the top of the chamber from the regulator and exits its base to the fuel pump. The heat

transfer from the pump, fuel-rail components, and regulator was extremely high under these circumstances, since the system attempted to raise the temperature of the whole circuit in order to vaporise the light fraction. In the final prototype, the vaporisation chamber is a 'spur' off of the main flow of circulating fuel. This yields three benefits:

(i) The heat losses in the pump and fuel rail components are minimised, because reheating of the circulating fuel is not required.

(ii) The transient response of the system is vastly improved because 'fresh' gasoline entering the vaporisation chamber has a much longer residence time, facilitating complete light fraction separation before the liquid fuel exits the chamber.

(iii) Vapour bubbles are not carried to the inlet of the fuel circulating pump, as is the case with the in-line system. Vapour bubbles at the pump inlet cause an unstable fuel rail pressure, leading to an unstable fuel injection rate.

4.4 Summary

The STRAFFE concept has been introduced as a method for using gasoline fuel in a more targeted manner, which may allow improvements in engine operation. While the STRAFFE concept could be realised in a number of ways, an on-board fuel system is the cheapest and most effective means to investigate its validity. To this end, a prototype fuel fractionating system has been developed from initial concept designs, and installed on the Ricardo E6 engine. The particular arrangement used has been optimised for steady state operation, so that the properties of each fuel fraction produced can be determined in an experimental programme.

Chapter 5

Evaluation of The Fuel Fractionating System

Chapter 5 Evaluation of the Fuel Fractionating System

5.1 Commissioning of the Fuel Fractionating System

Commissioning of the fuel system was carried out using the Ricardo E6 single cylinder engine and associated measurement and control systems as laid out in chapter 3. The fuel system was operated so that it delivered light and heavy fractions to the engine intake manifold, to form a stoichiometric charge for consumption by the engine. At the beginning of prototype development, two objectives were set that define successful operation of the fractionating system:

(i) At least 50% of the total fuel flow to the engine must be inducted via the venturi.
(ii) Oscillations in fuel flow rate must be kept to a minimum under steady state operation.

With respect to (i), the rate of vaporisation was obtained by measuring the total fuel flow at the burette, and subtracting the (heavy fraction) fuel flow through the injector. Injector calibration was carried out beforehand using a sample of heavy fraction fuel. With respect to (ii), there are a number of ways that oscillations in fuel flow rate can be observed around the engine. The most obvious of these is the changes of engine output power that accompany variations in stoichiometry. In the Ricardo E6 engine this effect is manifested by variations in torque output and engine speed, since speed is not automatically regulated. However, these do not quantify the stability of fuel delivery to the engine. The technique used was to observe fluctuations in A/F ratio as measured by the Richard Oliver K650 exhaust gas analyser. The fuel system's operation was deemed adequate when the analyser showed that variations in exhaust gas stoichiometry over time were lower than the resolution of measurement (lambda to 2 d.p.). It should be noted that any oscillations observed were as a result of changes in vapour production only, since variations in the injection rate are extremely small.

5.2 Composition and Properties of the Gasoline Fractions

A further measure of the system's ability to separate light and heavy fractions adequately can be obtained through compositional and octane analysis of the light and heavy fractions

produced during normal operation. This is not a simple procedure because samples of each fraction must be sent away for analysis, preferably to Saybolt UK Ltd. to ensure that similar procedures are employed as for the original laboratory tests. While the heavy fraction can easily be stored for transit, the light fraction must be re-condensed after production.

A subsystem consisting of a water cooled heat exchanger, and 5m of 4mm copper coil immersed in iced water is used to condense the vapour fraction beyond the exit of the vaporisation chamber, as shown in figure 5.1. Liquid light fraction exiting the coil is then passed into a fuel storage container, which is also situated in iced water. This container has a second tube fitted to its lid to allow light fractions that do not condense to escape to atmosphere, preventing pressure build-up in the system. Some preliminary tests indicated that approximately 1-2% of the light fraction was unavoidably lost with this arrangement.

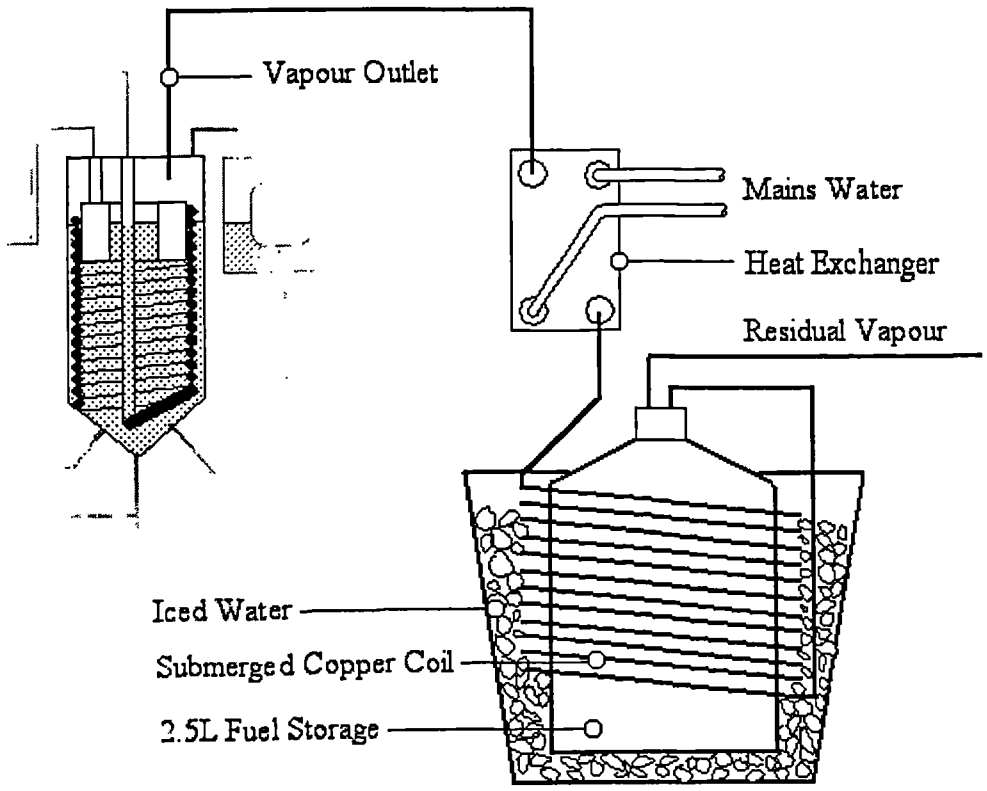

Figure 5.1 Vapour condensing subsystem for light fraction storage

In total, approximately 30 litres of light and heavy fraction each were produced over a number of days, and stored in appropriate sealed containers. For each fraction, the contents of all the containers are emptied into one large one, thoroughly mixed and then replaced

into the smaller ones for storage. This ensures that any slight variations in fuel system operation from day to day do not result in differences in fuel composition between containers. 5 litres of each fraction were sent to Saybolt UK for analysis. The remaining light and heavy fraction fuels were used in the engine tests described in Chapter 7.

	Gasoline	Light fraction		Heavy fraction	
		*Laboratory	**Fuel System	*Laboratory	**Fuel System
% of total fuel	100	~49	~48	50	50
Paraffins (% vol)	58.3	79	72.1	24.3	42.6
Olefins (% vol)	7.6	9.2	12.4	6.6	9.9
Aromatics (% vol)	34.1	11.8	15.5	69.1	47.5
RON	94.7	90	93.5	99.4	98
MON	84.5	84	85	87.1	86.5
Fuel Sensitivity (RON-MON)	10.2	6	8.5	12.3	11.5

*Laboratory Distilled Fractions ** Fuel System Fractions

Table 5.1 Comparison of composition and properties of light and heavy distillates of gasoline using two methods of production.

Table 5.1 shows the comparisons of composition and properties between light and heavy fraction fuels for the original laboratory tests, and for the fuel streams generated by the prototype fuel system. Examining the composition, the prototype system light fraction does not contain as many paraffins, and contains more aromatics than the light fraction produced under laboratory circumstances. Similarly, the heavy fraction produced by the fuel system contains more paraffins and less aromatics than in the corresponding heavy fraction produced in the laboratory. It would appear that the resolution of fuel fractions produced has been 'blurred' in the online system. This has had a profound effect on the properties of each fuel fraction. The light fraction produced by the prototype system has a RON of 93.5, compared to 90 RON obtained in the laboratory. Similarly, the Heavy fraction RON has been reduced from 99.4 to 98. Thus the (research) octane spread between fractions has more than halved from 9.8 to 4.5. As was found originally, the MON spread between fractions is low, but reduced even more from 3.1 to 1.5. The fuel sensitivity of the light fraction produced using the fuel system is slightly increased due to its increased aromatic content. In a similar fashion, the fuel sensitivity of the heavy fraction produced using the fuel system is reduced due to its increase of paraffinic species.

An explanation for the cross-contamination of the fuel fractions arises when one considers the difference in production techniques between the laboratory and the fuel system. In the

laboratory, there is infinite time allowed for the distillation of gasoline into the required fractions. Thus, the temperature and pressure conditions need to only just be sufficient to evaporate 50% of the gasoline over a long time period. However, the online fuel system does not have the luxury of time to allow the full separation of the fractions under similar pressure and temperature conditions to those used in the laboratory. Fuel entering the base of the vaporisation chamber has a finite 'residence time' in which to gain sensible and latent heat. Thus, to achieve a rate of 50% vaporisation the temperature and pressure conditions must be more severe, to promote quick fractionation. In the laboratory tests, 50% of the fuel was evaporated at a temperature of 90°C and atmospheric pressure. However, in the fractionating system, while the coolant temperature is maintained at 90°C, the pressure induced by the constant depression venturi is approximately 0.9 bar, providing more severe conditions for vaporisation. The more severe conditions allow a greater concentration of aromatic species to vaporise, while a finite liquid fuel residence time ensures that more paraffins are retained in the heavy fraction as it exits the base of the chamber, before they have had chance to gain sufficient latent heat and vaporise.

Clearly, this effect will become more pronounced under higher fuel flow conditions, because the fuel residence time is reduced. Knocking combustion in SI engines normally occurs at WOT and at low to medium engine speeds. The STRAFFE concept requires stratification of the heavy fraction to occupy the end-gas region of the combustion chamber under those engine conditions, so that the maximum compression ratio of the engine can be increased. The fuel flow requirement of the engine under these conditions is approximately one quarter to one half of the maximum required at high speed and WOT.

The only practical means of increasing the resolution of the fuel fractions is to increase the time that gasoline is exposed to heating at the required temperature. This can be achieved in the prototype system by increasing the surface area of the heat exchanger, increasing the volume of fuel in the vaporisation chamber to increase its residence time, or by introducing forced liquid convection around the chamber. Each of these methods will increase the time that each element of liquid fuel is exposed to the hot coil surface, allowing the temperature and pressure conditions in the chamber to be less severe while still producing 50% vapour.

While the system's performance has not yet been optimised, there are a number of routes that can be taken to do this. The system does produce equal quantities of light and heavy fractions at a sufficient rate for consumption by the Ricardo E6 engine operated at WOT

and 3000 rpm. The fractions produced show a significant (if not optimal) octane spread, indicating that benefits can be gained by employing the STRAFFE concept. Thus, the system is ready for testing in the Ricardo E6 engine using SI combustion, to quantify properties of the light and heavy fractions in terms of normal and knocking combustion characteristics. Once the benefits of the STRAFFE concept have been well established, economic decisions can be made as to the applicability of such a fuel system for modern production engines.

5.3 Test Objectives and Methods

Although octane testing is a good method for quantifying the behaviour of fuels with regard to knocking combustion, it only does so under very specific engine operating conditions. Furthermore, it provides no information on a fuel's combustion characteristics. An experimental programme has been devised to investigate the combustion characteristics of the light and heavy fractions separately. At this point, it would be unwise to implement the charge stratification elements of the STRAFFE concept, since this adds extra complexity to the analysis of results, and firm conclusions cannot be drawn as to the nature of combustion for each fuel fraction individually. Therefore, the fuel system is utilised in such a way that a stoichiometric charge containing only light or heavy fraction fuel is delivered to the engine cylinder. Analyses of the heat release and knocking characteristics of combustion can be done individually for each fraction, providing information on the best means of charge stratification for a STRAFFE engine.

A range of engine test conditions is required to provide sufficient information about each fuel fraction under SI operation. There are a host of engine parameters that can be varied to achieve this. These include:

- Compression Ratio
- Spark Advance
- Inlet Air Temperature
- Cylinder Head (coolant) Temperature
- Throttle Position
- Engine Speed
- A/F Ratio
- Valve Overlap and Timing (varies residual gas rate)
- Oil Temperature

The effects of changing each of these variables on knocking combustion have been discussed in detail in chapter 2. The timing of the spark event probably is the easiest variable to change, and has the most profound effect on heat release and knocking combustion characteristics. In all SI engines, this is the primary means of controlling combustion over the engine speed and load range, to ensure that combustion phasing is always optimal. Consequently, the spark advance must be one of the experimental variables. While a range of spark timings is desirable, it has an optimum value imposed by two conflicting effects:

(i) If combustion is initiated relatively late, the peak in-cylinder pressure is retarded and reduced, resulting in a lower work transfer from the cylinder gases to the piston during the expansion stroke. Thus, less energy is obtained from the same cylinder charge, lowering torque output.

(ii) If combustion is initiated relatively early, a significant additional pressure rise occurs before TDC. The compression stroke work transfer from the piston to the in-cylinder gases (pumping work) is increased, resulting in a drop of torque output. Early combustion can significantly increase the peak in-cylinder pressure and temperature, and lead to autoignition of the end-gas and knocking combustion.

The result of these conflicting effects is a property of combustion known as Minimum spark advance for Best Torque (MBT). There are usually a number of spark advances that give torque values that are very similar around the MBT point. Thus, it is normal for spark advance to be retarded 1 or 2°CA without significant penalty, to help avoid knocking combustion that can occur if the timing is over-advanced.

One of the potential benefits of applying the STRAFFE concept is to facilitate an increase in engine compression ratio by strategic positioning of the heavy fraction mixture within the cylinder. Therefore, it is proposed that this be one of the variables of the experiment. An increase in compression ratio has a twofold effect on combustion:

(i) In-cylinder turbulence may be increased, leading to faster combustion rates.

(ii) End-of-compression pressures and temperatures are increased, which facilitate faster combustion, but also promote autoignition of the end-gas before the arrival of the spark-ignited flame front.

So, heat release and autoignition characteristics are affected by changes in compression ratio, making it an ideal experimental variable. Furthermore, the Ricardo E6 engine allows its compression ratio to be changed while the engine is running, which simplifies the experimental procedure.

	Parameter		Value
Variables	Fuel		Light Fraction Heavy Fraction Standard Gasoline (BS EN 228) PRF 90 RON PRF 95 RON PRF 100 RON
	Spark Advance	(°CA)	Variable for MBT and Knock
	Compression Ratio		7, 8, 9, 10, 11, 12, 13
Fixed Conditions	Engine Speed	(rpm)	1500
	Intake Manifold Pressure	(bar)	0.93 absolute
	A/F Ratio (Lambda)		0.95
	Intake Charge Temperature	(°C)	40
	Coolant Tempretaure	(°C)	70
	Oil Temperature	(°C)	55
	EGR Rate		0
	Injection Timing	(°CA)	79 BTDC Compresion Stroke

Table 5.2 List of experimental parameters for SI tests on the gasoline fractions and the primary reference fuels

Therefore, a parametric experimental programme studying the effects of spark advance and compression ratio on the heat release characteristics of light and heavy fractions is proposed. Meanwhile, all other engine variables are fixed to the values shown in table 5.2. Similar tests are carried out on a selection of Isooctane/Heptane PRFs. Results from the PRF tests shall be used as a benchmark for the analysis of the combustion characteristics of the gasoline fractions.

5.4 Experimental Procedure

5.4.1 Fuels

The three gasoline fractions are tested in the specific order: standard gasoline, light fraction, and then heavy fraction. This order has been chosen to ensure that no fuel contamination occurs between tests. While standard gasoline is being tested, the coolant circuit of the fuel fractionating system is not heated, and the vaporisation chamber is isolated from the venturi pressure. Thus, gasoline passes unaltered through the float and vaporisation chambers, and to the inlet of the fuel injection circuit. When testing the light fraction fuel the vaporisation system is operated in the normal manner, except that heavy fraction fuel is injected into storage containers for later use. However, during system warm-up and stabilisation any heavy fraction produced has an incorrect composition, and is discarded. Once the light fraction tests are finished, the fuel system contains only heavy fraction. For the heavy fraction tests, the system is operated in a similar manner as for the standard gasoline tests, with heavy fraction fed manually into the system from a tank. Using stored instead of newly produced heavy fraction ensures that the fuel is compositionally opposite to the tested light fraction, and that problems regarding the disposal of light fraction when only heavy fraction is required for the test are not encountered. Once the gasolines have been tested, PRF fuels are carefully blended and tested individually.

5.4.2 Engine Related Procedures

At the start of each test, the engine is started and motored to the speed of 1500 rpm. At this point, the oil heater is switched on and remains on until it reaches the set temperature of 55°C, after which it is maintained by heat rejection from the engine. The data acquisition system and analysers are also switched on, and checked for correct operation. The spark system is engaged, and the engine is now ready for fuel admission.

Depending on the particular fuel being tested, the fuel system is operated in either the 'cool' or the 'hot' mode. If light fraction is required (hot mode), then the control systems that regulate the high temperature operation of the fractionating system are switched on, and the system is allowed to stabilise at its set temperature of 65 °C. In this hot mode, the injector is removed from the intake manifold and the remaining orifice in the manifold is

blocked. During system warm-up, the injection is switched on, and the rate of light fraction production gradually increases until the intake charge of the engine is rich enough to support combustion. The system is left for 1 hour before any testing takes place to allow it (and the engine temperatures) to stabilise. All heavy fraction produced in this period is then discarded prior to testing.

All other fuels require the fractionating system to operate in the 'cool' mode. In the cool mode, high temperature operation of the vaporisation chamber is not required, and it is isolated from the venturi pressure using the safety shut-off valve. The fuel system needs no time to stabilise, and is ready for testing immediately. However, engine temperatures still need to reach operational values, so 1 hour is allowed for this.

For each fuel, a number of measurements are taken for a range of spark advances and compression ratios. This is done by first setting the engine and data acquisition (DAQ) system to the correct compression ratio, starting with 7 upwards. The spark advance is retarded to 10° BTDC, and measurements of combustion heat release and IMEP are recorded after a settling period. This is repeated for more advanced spark timings in steps of 10°CA, until MBT is reached. Around the MBT point, the measurement resolution is increased so that results are taken in steps of 0.5, 1, or 2 °CA spark advance. This procedure ensures that a highly accurate MBT spark advance is obtained, from which ignition and heat release measurements from each fuel can be compared.

At some compression ratios, as the spark timing is advanced, the end-gas temperature and pressure histories result in conditions that are favourable to knocking combustion. While this normally occurs at more advanced timings than MBT, MBT can occur under knocking combustion conditions. Since the knocking characteristics of each fuel are under investigation, the DAQ system is used to ascertain if and when knocking combustion occurs. So, as well as the MBT spark advance, data is recorded for the spark advance that causes 10%, 50%, and 90% Knock Occurrence Frequency (KOF), as defined in Chapter 3. Once a full range of spark advances have been applied at one compression ratio, the compression ratio is increased on the engine and the DAQ system, and the process is repeated in integer steps until a value of 13:1 is reached.

5.5 Discussion of Results

5.5.1 Load Considerations

5.5.1.1 IMEP Measurements

Figure 5.2 shows how the IMEP varies with spark advance and compression ratio for the standard gasoline. For each compression ratio, a maximum IMEP is obtained at MBT. Greater spark advance causes the Pumping Mean Effective Pressure (PMEP) to rise, resulting in lower power output. Retarded spark advance results in late combustion, the work done on the piston during the expansion stroke is reduced due to the increasing speed of the piston through its stroke, also resulting in lower IMEP measurements. Increasing compression ratio has the effect of increasing IMEP for fixed spark advance. This occurs because the thermal efficiency of the cycle is increased.

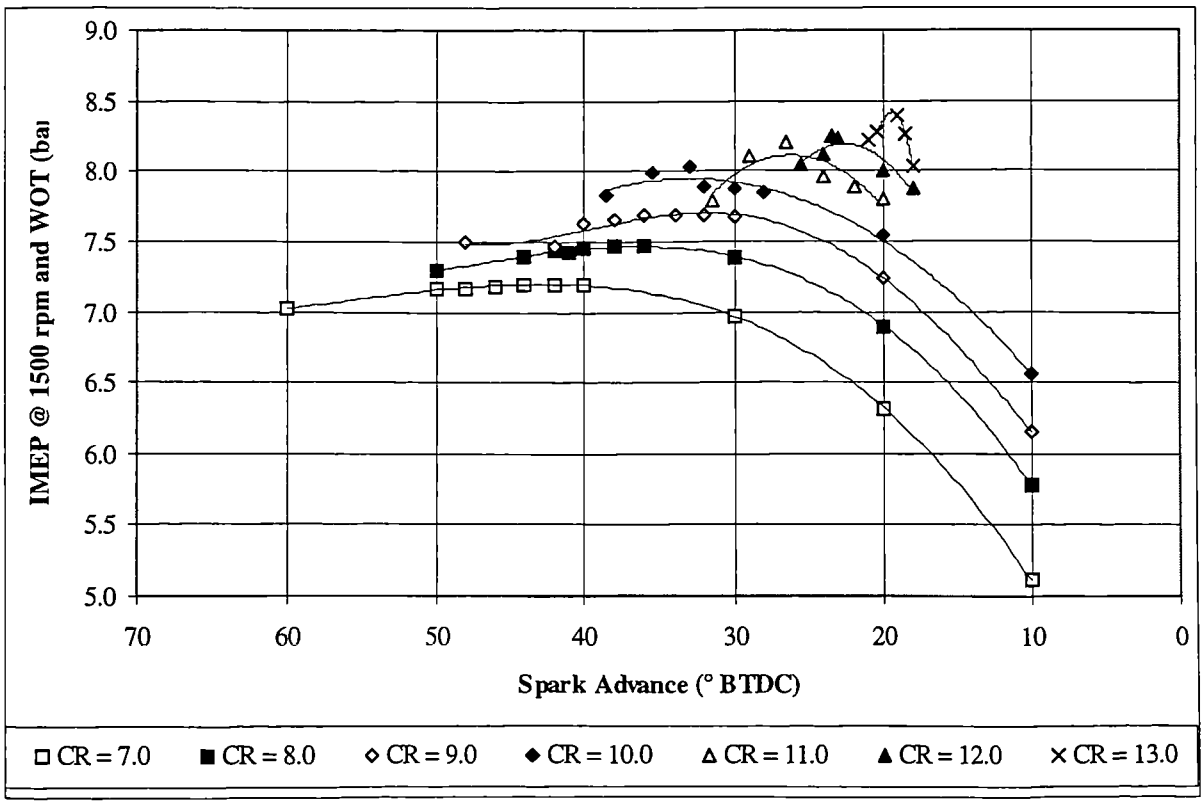

Figure 5.2 Net IMEP curves with varying compression ratio (CR) for standard gasoline.

Each of the six fuels under consideration has been tested for IMEP measurements at MBT with varying compression ratio. The IMEP measurements for each of the fuels are

presented at the end of this chapter, figures 5.9 to 5.14. The trends for each of these fuels do not differ greatly from those presented in figure 5.2. However, when one compares the IMEP values at MBT for all fuels and over all compression ratios, some important differences are observed between fuels. Figure 5.3 shows how IMEP at MBT varies with compression ratio for each of the six fuels tested.

For each fuel, IMEP increases for increasing compression ratio, up to a compression ratio of 10.0. Beyond this, fuels with a lower octane (Light Fraction, PRF 90 RON) exhibit a reduction in IMEP. Other fuels also exhibit a reduction in the rate of increase of MBT torque with compression ratio in this region. The trends for all fuels can be explained by the occurrence of knocking combustion at higher compression ratios and MBT. However, the effect is most pronounced with the low octane fuels, since knocking combustion at MBT occurs earliest in the cycle, and is more severe in their cases. Increasingly intense knock leads to a rise in PMEP and a reduction in load under these conditions.

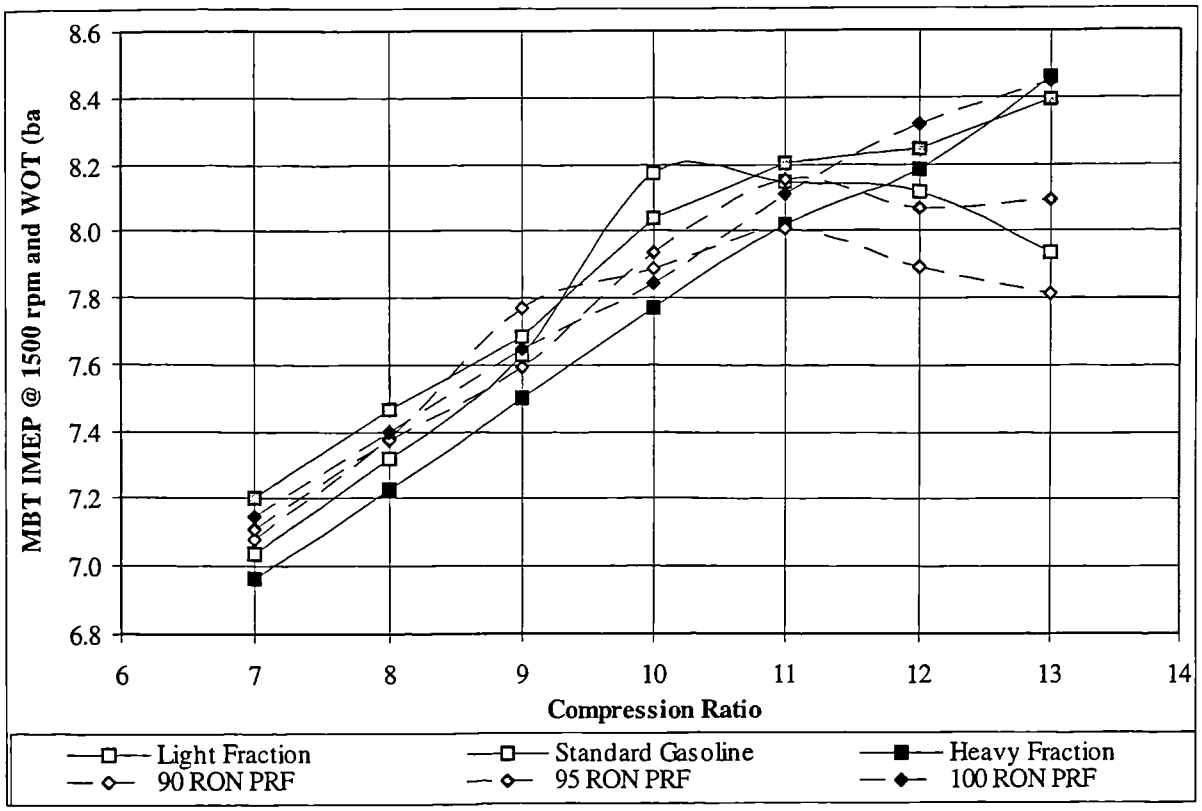

Figure 5.3 Net IMEP at MBT trends for various compression ratios and fuels

These results have also been analysed to establish if there are differences in engine power output for different fuels. Of the gasoline fractions, standard gasoline appears to produce a higher IMEP output than either the heavy or light fractions at lower compression ratios,

where knocking combustion does not occur for any of the fuels. This appears to be contradictory, since light and heavy fractions together make up the gasoline used for testing. The transport and mixture properties of light and heavy fractions are different because of the difference in volatility and phase when introduced to the engine intake manifold. While this can explain differences between light and heavy fractions, it does not account for standard gasoline's apparent superiority. A more reasonable explanation can be found by examining the absolute differences in IMEP for the three gasoline fractions. While it is usually much lower, the maximum difference in net IMEP between the fractions under non-knocking conditions is approximately 0.4 bar at a compression ratio of 10. This is approximately 5% of the total IMEP for each of the fractions. Differences in absolute IMEP could be explained by experimental error, since they are so small. Experimental error can arise from slight differences in engine speed, stoichiometry, and variations of intake air temperature and humidity, despite efforts to minimise these.

The PRF fuels exhibit very similar IMEP values at MBT for the lower compression ratios. As compression ratio is increased, the IMEP of the 90 RON PRF suffers first, followed by that of the 95 RON PRF. As with the heavy fraction, the 100 RON PRF exhibits a near-linear relationship between IMEP and compression ratio, since these fuels do not tend to knock at high compression ratio and MBT, unlike the lower octane fuels.

5.5.1.2 COVimep Measurements

Study of the combustion variability can provide useful information on the quality of combustion for each of the fuels when the engine is operating at MBT conditions. Furthermore, COVimep values can be used to precisely quantify the stable operation of the fuel fractionating system. For each test point, the DAQ system has been set to record a total of 300 consecutive engine cycles. This represents a time period of 24 seconds when the engine is operated at 1500 rpm. So, in terms of fuel fraction delivery, measurements of COVimep can show the combined effects of:

(i) Changes in nominal stoichiometry over time. This is particularly relevant to the light fraction fuel delivery, since the stability of vapour production is highly dependant on the fuel system's ability to control the vaporisation chamber temperature, pressure, and fuel induction rate. All other fuels are injected using

standard injection technology, which should not lead to significant stoichiometry changes over time.

(ii) Degree of charge homogeneity. A highly inhomogeneous charge can result in large changes in the quality and duration of flame development from the ignition kernel, which is observed as fluctuations in IMEP. This effect is particularly relevant to the heavy fraction, which contains all of the least volatile species normally contained in gasoline.

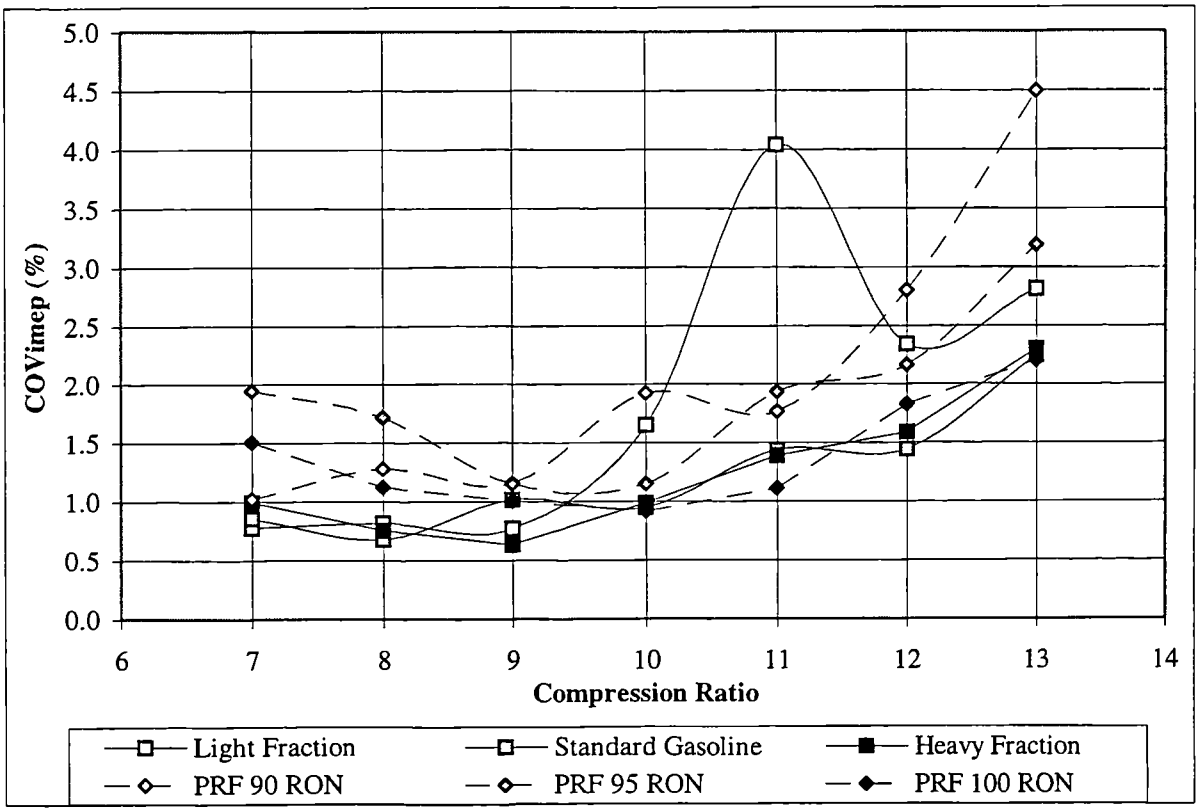

Figure 5.4 COVimep at MBT for a Number of Fuels and Compression Ratios

Figure 5.4 shows how the COVimep varies between fuels and over the full range of compression ratios tested. Each of these measurements corresponds to optimal MBT operation, where COVimep values are lowest. The first thing to note is that all tests yield COVimep values that are well within the normally acceptable limits of around 5%. Anything above this value is unacceptable because the vehicle driver can then feel the resultant brake torque variations. Generally speaking, COVimep reaches a minimum at a compression ratio of approximately 9.0 for all of the fuels. At lower compression ratios, ignition quality is impaired due to lower in-cylinder temperatures and pressures. At higher

compression ratios, the occurrence of knocking combustion in a small number of cycles can lead to slightly higher COVimep. This effect is obviously more pronounced for the lower octane fuels, which exhibit a greater degree of knock at the higher compression ratios and MBT. The only result that stands out particularly from other trends is that for the light fraction fuel at a compression ratio of 11.0. The averaged heat release profile under these conditions as shown in Figure 5.15 (at the end of the chapter) is not remarkably different from the other fuels. The most reasonable explanation for this is that the stoichiometry had changed over time, as discussed in point (i) above, although this cannot be confirmed.

5.5.2 Heat Release Analyses

Heat release results are available for all of the fuels and conditions under consideration. However, only those results relating to MBT conditions shall be presented in this work, because combustion is optimal. The full set of MBT results are presented at the end of this chapter, Table 5.3 and Figure 5.15.

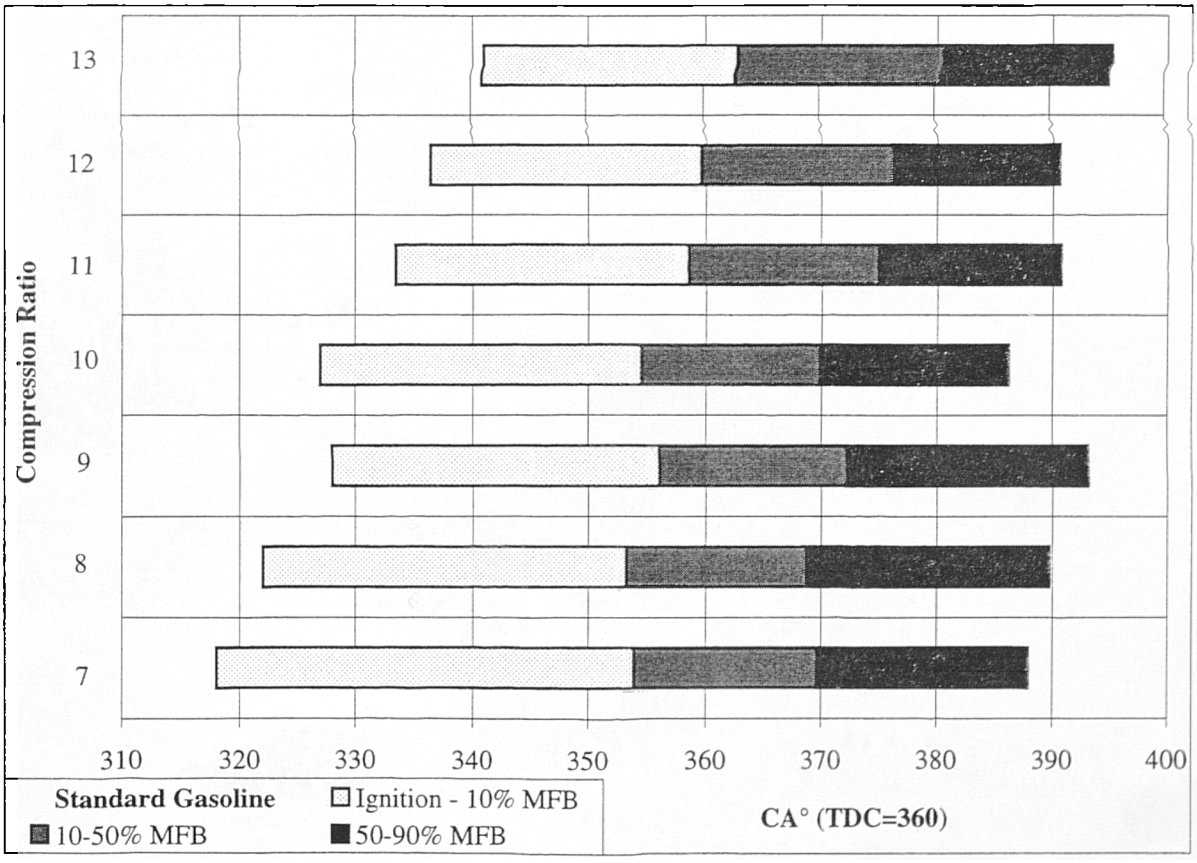

Figure 5.5 Heat release analysis at MBT and a number of compression ratios for standard gasoline (1500 rpm, WOT)

There are some general trends to which all fuels adhere. Figure 5.5 shows the MBT heat release results for standard gasoline for the full range of compression ratios, shown on the vertical axis. The horizontal axis represents time measured on a crank angle basis. The left-hand extent of each bar denotes the spark-ignition timing, as input at the ignition controller. The bars are subdivided into 3 sections. The left-most section indicates the period between ignition and 10% mass fraction burned, also known as the 'flame development angle'. The centre subsection of each bar indicates the elapsed period between the 10% and 50% mass fraction burned, and the right subsection denotes the period between 50% and 90% mass fraction burned. The total period between 10% and 90% mass fraction burned is also known as the 'rapid burn angle'.

Considering the overall period between ignition and completion of combustion, it is clear that as compression ratio is increased, combustion duration is reduced from around 70 to 50 °CA. This occurs as a result of an increase in in-cylinder turbulence, and a higher temperature and pressure environment for combustion, which both promote an increased flame speed. Generally speaking, ignition must be retarded with increased compression ratio, to compensate for the increased speed of combustion. However, the result for compression ratio 10 appears to be anomalous, since ignition is further advanced than for compression ratio 9. Results indicate that the flame development angle is most affected by increased compression ratio, and the rapid burn angle is only affected slightly. A higher in-cylinder temperature and pressure at ignition may be the cause of better mixture ignition quality.

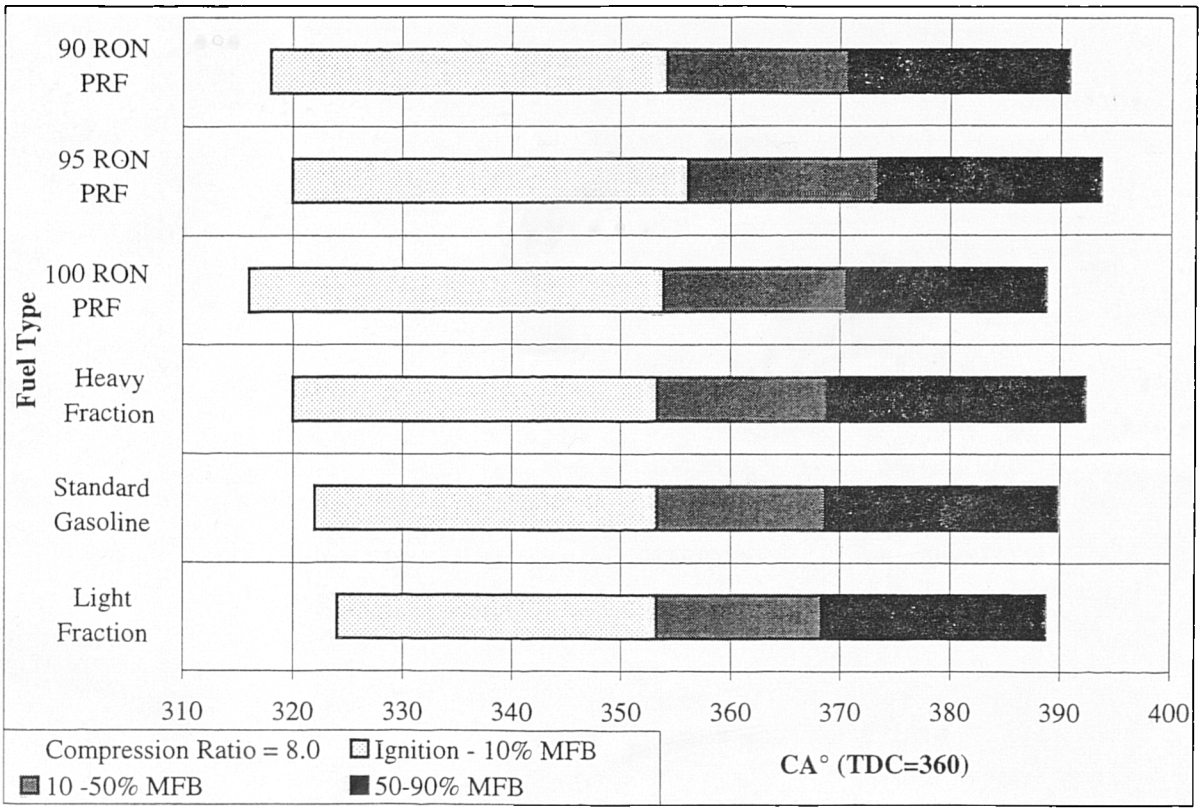

Figure 5.6 Heat release analysis at MBT for a number of fuels (CR = 8.0, 1500 rpm, WOT)

Figure 5.6 shows the heat release profiles of each of the six fuels with the engine operating at MBT and a typical compression ratio (8.0). Some general observations can be made that are true at any compression ratio. Examining the gasoline fractions, the combustion duration for the light fraction is shorter than that for gasoline, which is shorter again than that of the heavy fraction fuel. Shorter combustion duration requires a more retarded spark timing for MBT conditions. Thus, generally speaking, the light fraction spark timings are considerably more retarded than those for the heavy fraction at any compression ratio. The shorter combustion duration for the light fraction is the combined effect of reduced flame development and rapid burn angles. It is interesting to speculate, and there are two possible reasons why this occurs:

(i) The average laminar flame speed of the light fraction species may be higher than that of the heavy fraction species. While this may be true, it is extremely difficult to quantify due to the complex chemical nature of the gasoline fractions. However, Davis and Law [89] performed a study of the laminar flame speeds of a number of paraffins, olefins, and cyclic compounds such as aromatics using the counter flow twin-flame technique. They showed that cyclic compounds such as benzene,

toluene, and cyclohexane possess similar laminar flame speeds to straight chain alkanes such as n-heptane and n-butane, but were in the order of 5-10% faster than branched-chain paraffins such as isooctane and isobutane. From this, it can be asserted that the aromatic heavy fraction probably possesses an equal or faster laminar flame speed than the paraffinic light fraction, despite the results presented here.

(ii) The light fraction admitted to the engine intake manifold as a vapour forms a more homogeneous charge, promoting fast ignition and combustion. Conversely, standard gasoline and the heavy fraction are injected near the intake port. Both contain significant quantities of low volatility species that do not readily form a completely homogeneous charge when mixed with the intake air. Measures taken to eliminate this effect include the phasing of injection to occur just after intake valve closure, so that the intake charge has a further three engine strokes before induction. However, in hindsight a more effective technique would have been to situate the injector much further upstream of the port, to promote greater charge mixing within the intake manifold.

The results of Davis and Law [89] are in direct contradiction to the results presented here. Therefore, the best explanation for the faster heat release of the light fraction arises from its higher volatility, which allows it to form a more homogeneous charge. In any case, the light fraction metered as a vapour is beneficial for spark ignition and to reduce combustion duration. This effect in combination with fuel stratification (STRAFFE) will tend to reduce the overall combustion duration of the stratified fuel charge, effectively increasing the overall fuel octane.

Although not as obvious, the PRF fuels exhibit similar tendencies to the gasoline fuels, as shown in figure 5.6. Generally speaking, as the quantity of heptane in the fuel increases, its combustion duration is reduced, leading to a retarded ignition timing required to obtain MBT. All PRF fuels are injected upstream of the intake port. Furthermore, n-heptane and isooctane have similar volatilities, so charge homogeneity is not a factor as it was for the gasoline fuels. An explanation for these trends arises from the work of Davis and Law [89], who showed that the laminar flame speed of n-heptane is in the region of 10% faster than that of the branched-chain isooctane when burned under stoichiometric conditions.

So, for a similar compression ratio (turbulence level), the PRF 90 RON fuel should burn at a faster rate than the PRF 100 RON fuel, as it does in most cases.

5.5.3 Knocking Combustion Analyses

With the knock intensity threshold set at 0.5 bar, 300 cycles have been recorded for the spark advance causing 10, 50, and 90% Knock Occurrence Frequency (KOF) for each fuel and compression ratio. Figure 5.7 shows the relationship between spark advance to cause a fixed KOF, and compression ratio for the light fraction fuel only. The trends shown in this figure are repeated for all of the fuels, as presented at the end of this chapter, figures 5.16 to 5.20.

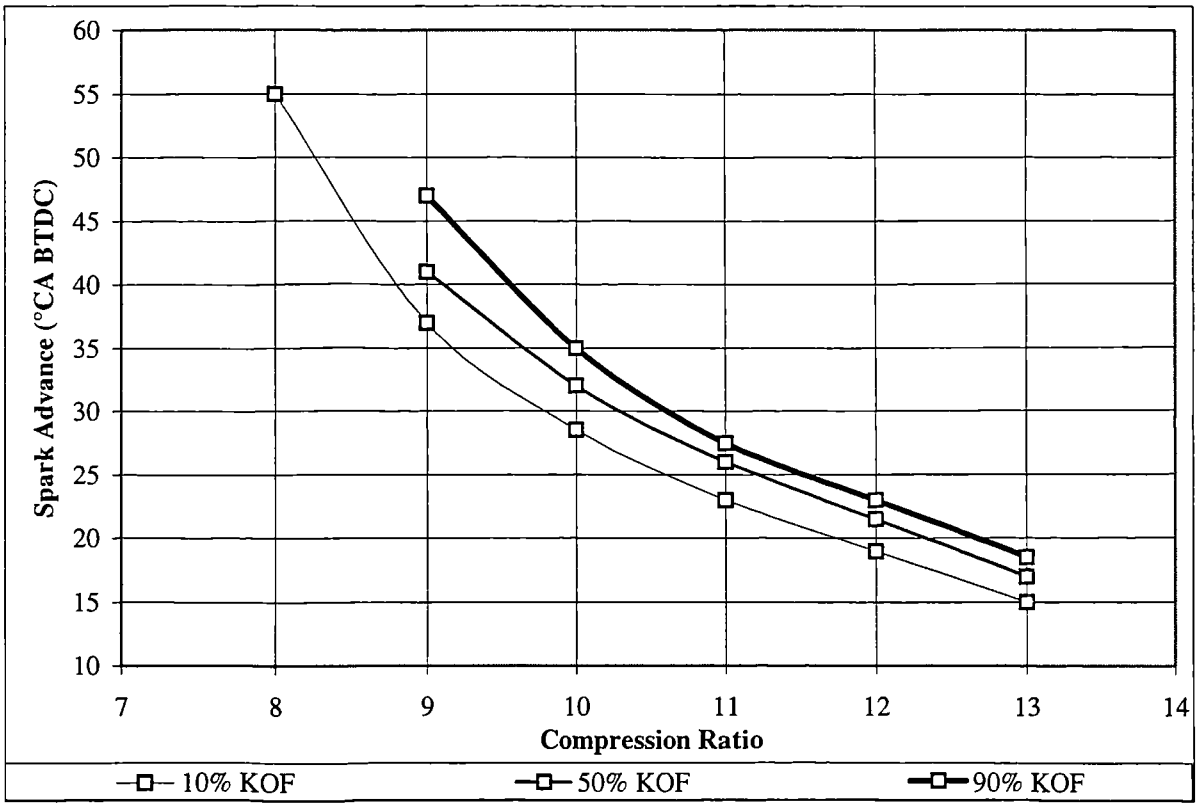

Figure 5.7 Spark Advance to Cause Knocking Cycles as a Function of Compression Ratio for the Light Fraction

Predictably, as the compression ratio is increased, the spark advances to cause 10, 50, and 90% KOFs are retarded significantly. Also, the range of spark advance between 10 and 90% KOF decreases with increasing compression ratio. Although results were taken for

compression ratios 7 and 8, the knock intensity did not rise above the 0.5 bar threshold required for registration in most cases.

A comparison is required between each of the gasoline fractions to provide more information on their relative knocking combustion characteristics. Furthermore, results from the PRFs can be used as a benchmark to compare the gasoline fractions against. Figure 5.8 shows the spark advance to cause 10% KOF for all six fuels as a function of compression ratio.

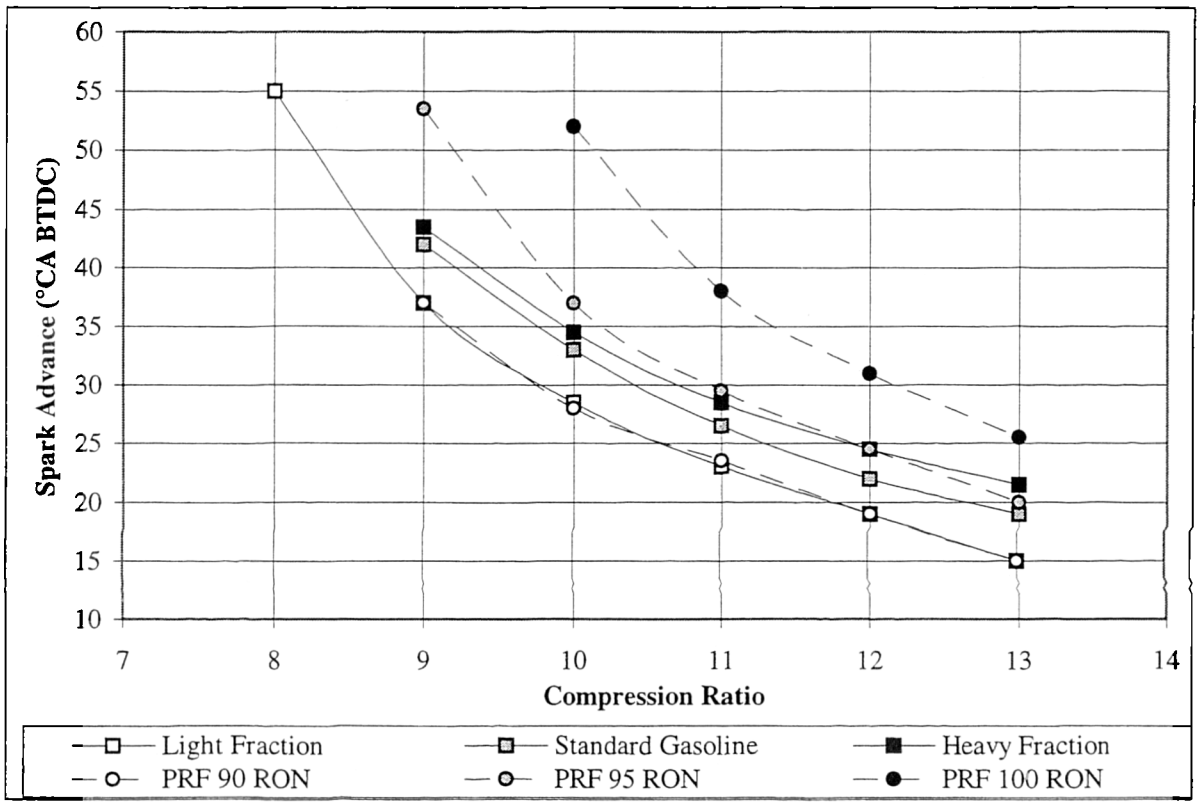

Figure 5.8 Spark Advance to Cause 10% KOF as a Function of Compression Ratio for a Number of Fuels

The gasoline fractions clearly react to changes in compression ratio in a different manner to the PRFs. The trends for the three gasoline fractions are much closer together, as their respective RON test values would predict. However, the heavy fraction performs considerably worse than even the 95 RON PRF at compression ratios up to 12, given that its spark timing is considerably more retarded. However, the light fraction would appear to have very similar knocking combustion characteristics to the 90 RON PRF.

The most important result from Figure 5.8 is in the difference between standard gasoline and heavy fraction results. Differences between these two fuels translate to performance improvements that may be gained from changing the engine configuration from the standard homogeneous charge to the STRAFFE arrangement. In this case, the end gas mixture is changed from gasoline/air to a heavy fraction/air mixture. A fast burn engine normally operating at a compression ratio of 12 would benefit most, because stratification of the heavy fraction would allow a higher compression ratio of 13 for a similar Knock Limited Spark Advance (KLSA). Similarly, this approach would only yield modest benefits for a slow burn engine normally operating at a compression ratio of 9. In this case, an increase in compression ratio of approximately 0.2 is facilitated before the heavy fraction mixture reaches its KLSA.

When one compares results between the PRFs and the gasoline fractions, it is clear that the relative octane spread between the gasoline fractions is comparitavely low at approximately 2.5 ON, at a compression ratio of 9. The octane spread increases with compression ratio to 7 ON at a compression ratio of 13. This trend tends to reinforce the assertions made in the previous paragraph, that the STRAFFE concept would be applied best in fast burn engines.

5.6 Summary

The fuel streams produced by the online system were analysed by Saybolt UK Ltd., and compared to their original test results. Comparisons have shown that separation of the fractions in the online system is not optimal, and cross-contamination occurs as the combined result of severe vaporisation chamber pressure / temperature conditions, and an inefficient coil / fuel heat transfer arrangement. However, the fractions do show a large enough difference in properties to facilitate an experimental programme designed to observe differences in their normal and knocking combustion characteristics. The following conclusions can be drawn from those tests:

(i) Trends for IMEP with compression ratio show that the light fraction combustion becomes severely knock limited at higher compression ratios. The heavy fraction only experiences mild knock under similar conditions. This shows that the octane differences between the fractions translate directly to compression ratio constraints on the engine.

(ii) Measurements of COVimep for each fraction under a number of conditions prove that the fuel fractionating system is capable of stable and non-oscillating fuel delivery under steady state operation. Values for COVimep are well below the acceptable limit of 5% in all test cases.

(iii) The light fraction burns faster than standard gasoline, which in turn burns faster than the heavy fraction. Review of the relevant literature has shown that there is not necessarily a chemical reason for this trend. However, an explanation arises when one considers that the highly volatile species contained in gasoline are more likely to form a homogeneous charge, because they have more time to mix with air when in the vapour phase. A stoichiometric homogeneous charge burns faster than one that is inhomogeneous, because its combustion is never diffusion-rate limited. This effect is beneficial to the SRAFFE concept, because the period between ignition and 50% mass fraction burned will be comparably reduced if the light fraction is stratified to occupy the region around the spark-plug. Although the 50-90% period will be increased slightly (because the heavy fraction burns slower than gasoline), this period only represents one quarter to one third of the overall combustion duration. The combined effect of a faster ignition-50% burn and a slower 50-90% burn is to slightly reduce the overall combustion duration, allowing less time for end-gas autoignition that may lead to knocking combustion.

(iv) The KLSA for the light fraction is always more retarded than that of the heavy fraction, with standard gasoline lying roughly in between. Results indicate that a fast burn engine would benefit most from the application of the STRAFFE concept, perhaps allowing for an increase of compression ratio of up to 1.0.

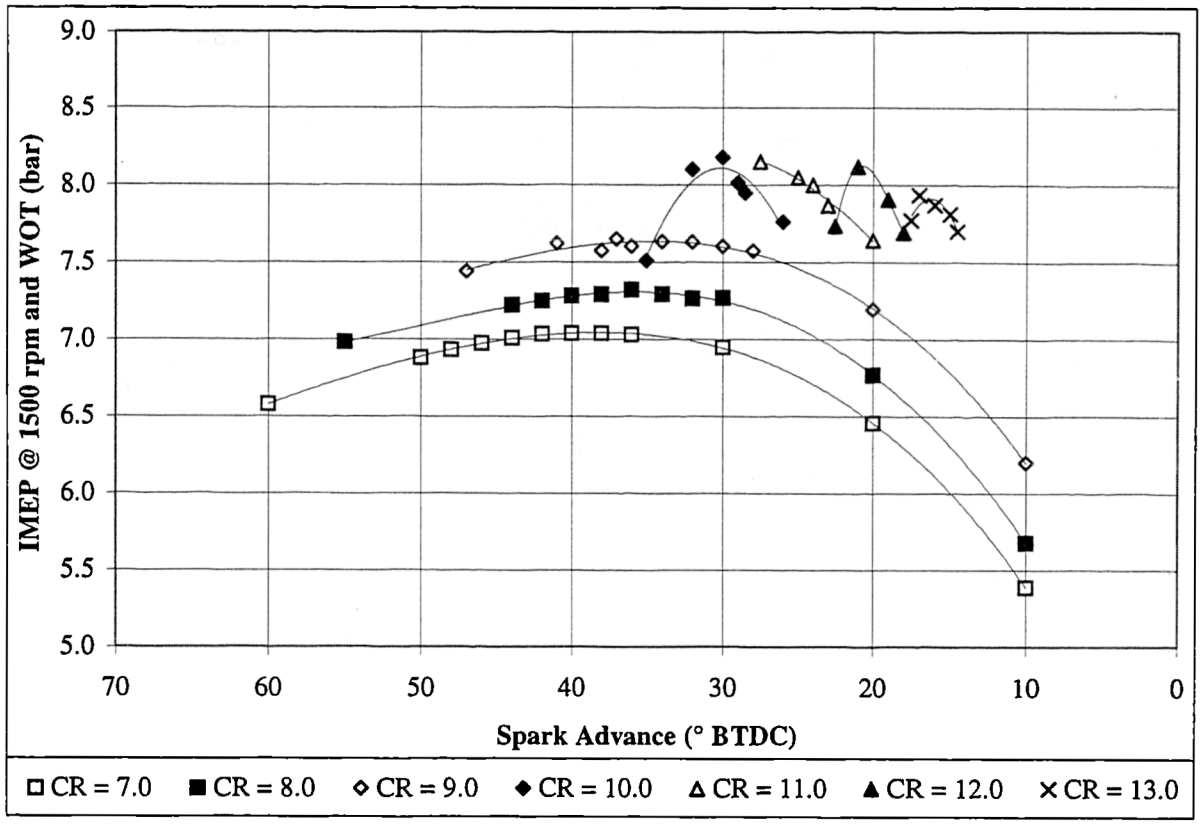

Figure 5.9 **Light fraction: IMEP variation with spark advance for a number of compression ratios**

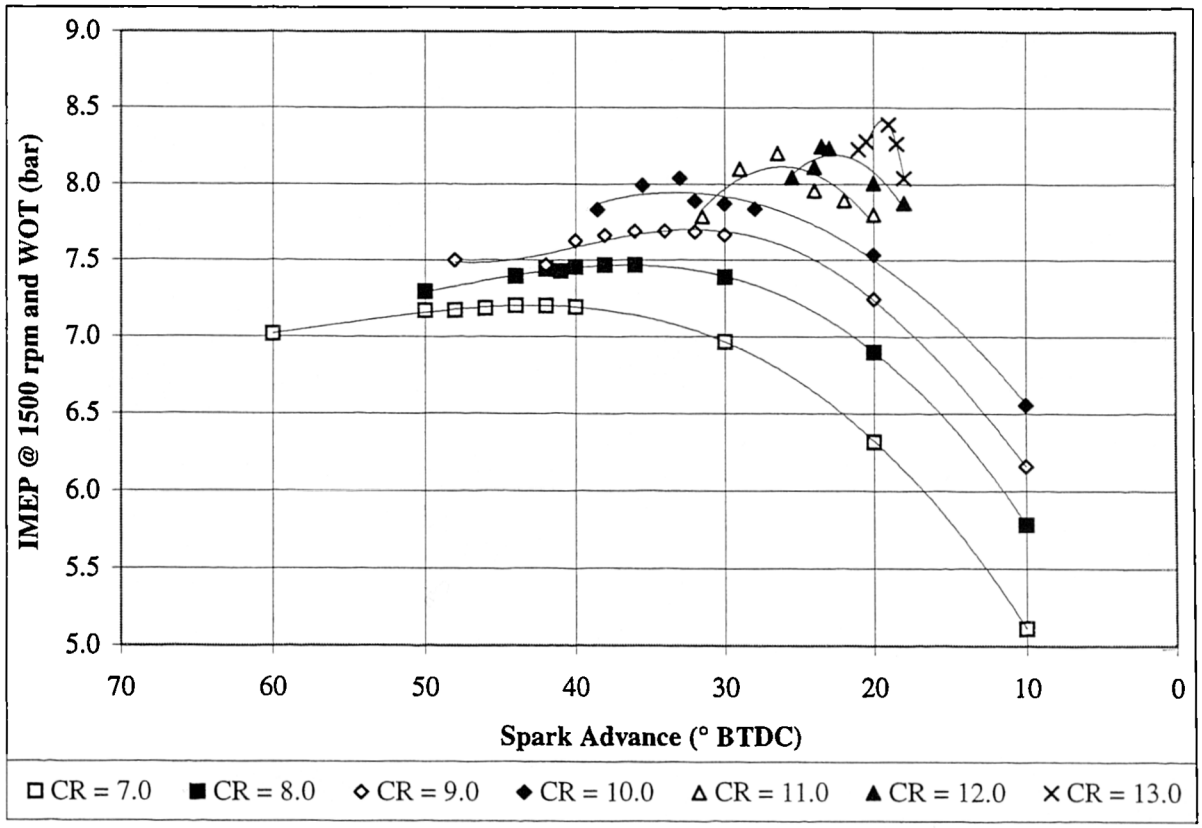

Figure 5.10 **Standard gasoline: IMEP variation with spark advance for a number of compression ratios**

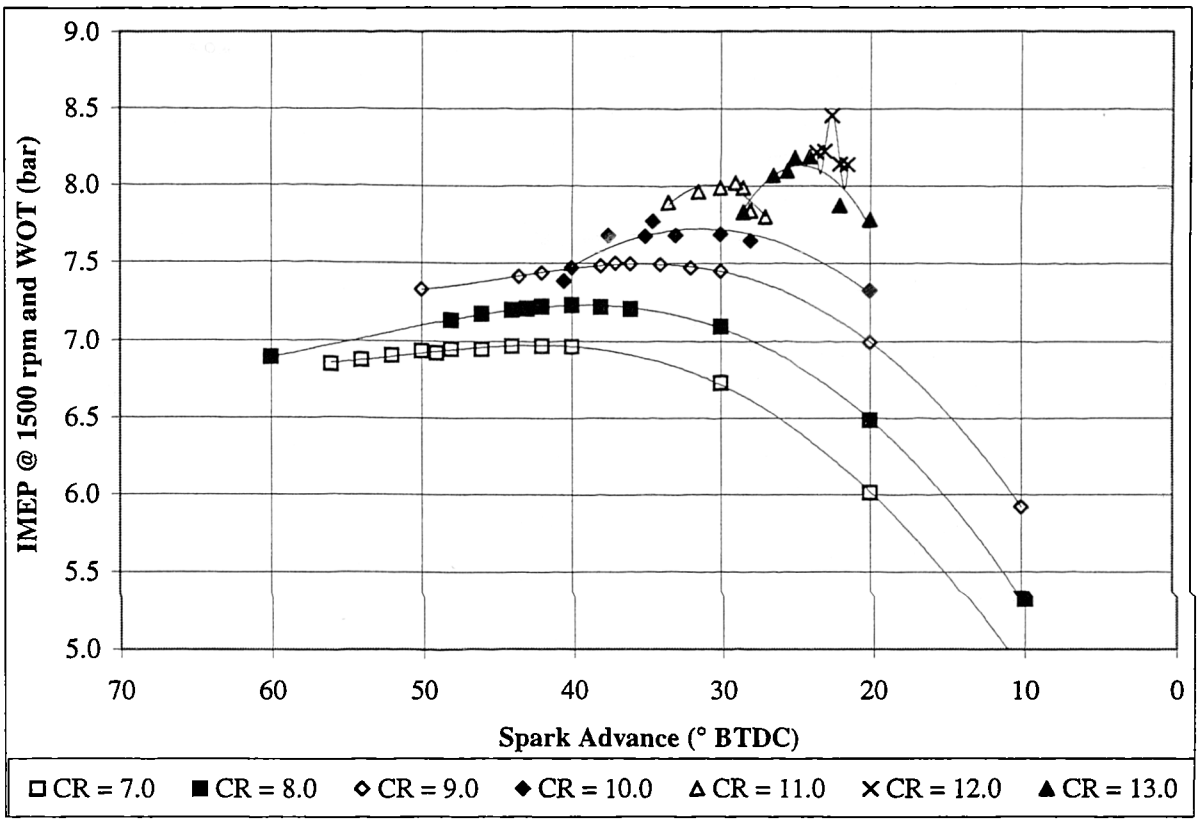

Figure 5.11 **Heavy fraction: IMEP variation with spark advance for a number of compression ratios**

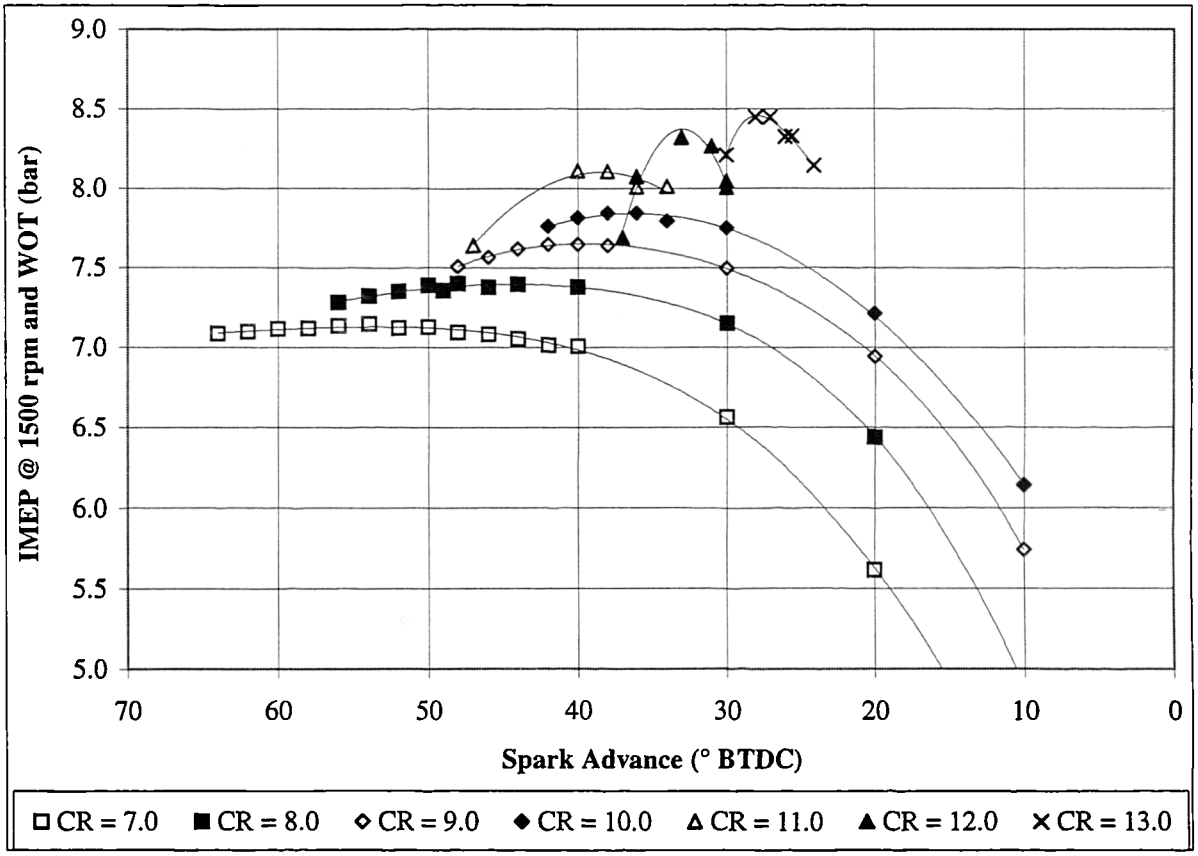

Figure 5.12 **PRF 100 RON: IMEP variation with spark advance for a number of compression ratios**

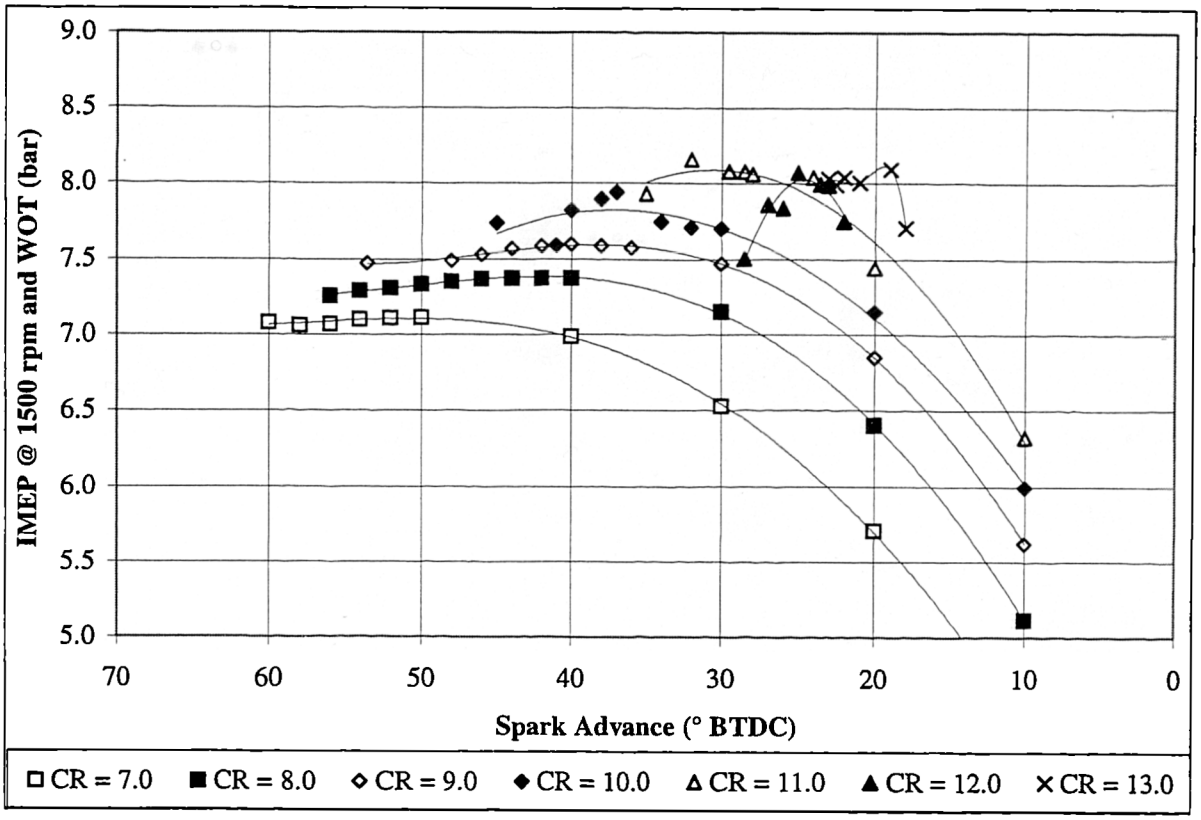

Figure 5.13 **PRF 95 RON: IMEP variation with spark advance for a number of compression ratios**

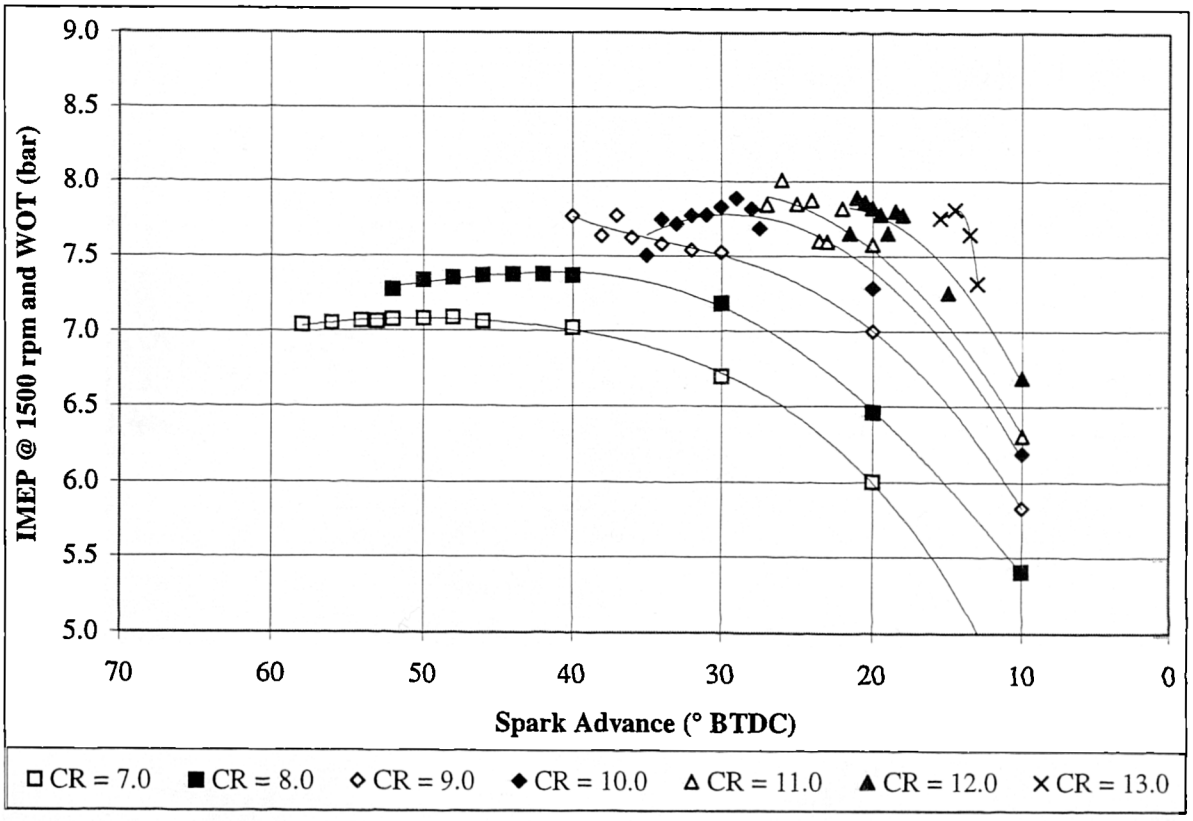

Figure 5.14 **PRF 90 RON: IMEP variation with spark advance for a number of compression ratios**

CR	Ignition Timing (°CA)	10% MFB (°CA)	50% MFB (°CA)	90% MFB (°CA)	IMEP (bar)	COVimep (%)
Light Fraction						
7	322.0	353.8	369.5	389.0	7.04	0.78
8	324.0	353.2	368.4	388.7	7.32	0.82
9	326.0	352.3	367.2	385.2	7.63	0.77
10	330.0	356.5	371.9	386.2	8.17	1.65
11	332.5	357.2	372.2	395.5	8.15	4.04
12	339.0	361.8	378.4	390.5	8.12	2.34
13	343.0	363.7	381.1	394.4	7.93	2.81
Standard Gasoline						
7	318.0	353.9	369.7	387.9	7.20	0.86
8	322.0	353.3	368.7	389.8	7.47	0.68
9	328.0	356.1	372.3	393.1	7.68	1.02
10	327.0	354.5	369.9	386.2	8.04	0.95
11	333.5	358.6	375.0	390.8	8.20	1.44
12	336.5	359.6	376.3	390.6	8.25	1.45
13	341.0	362.7	380.7	395.2	8.39	2.24
Heavy Fraction						
7	318.0	354.3	370.3	389.0	6.97	0.99
8	320.0	353.3	369.0	392.3	7.23	0.76
9	323.0	352.7	367.7	391.3	7.50	0.63
10	325.5	354.0	369.2	391.2	7.77	0.99
11	331.0	357.1	373.2	391.4	8.02	1.39
12	335.0	359.2	375.7	392.7	8.18	1.59
13	337.5	360.1	377.7	390.7	8.46	2.31
PRF 100 RON						
7	306.0	352.6	369.6	388.7	7.15	1.51
8	316.0	353.9	370.7	388.7	7.40	1.12
9	320.0	353.2	369.7	388.9	7.65	1.01
10	324.0	353.0	369.6	389.2	7.85	0.92
11	320.0	350.8	366.9	388.1	8.11	1.11
12	327.0	353.7	369.6	384.3	8.32	1.83
13	333.0	356.9	374.0	388.4	8.45	2.20
PRF 95 RON						
7	310.0	355.0	372.7	392.2	7.11	1.95
8	320.0	356.2	373.5	393.6	7.37	1.72
9	322.0	354.5	371.3	392.6	7.59	1.15
10	323.0	354.0	370.4	389.1	7.94	1.15
11	328.0	356.4	373.3	388.1	8.16	1.94
12	335.0	359.9	378.8	396.1	8.07	2.16
13	341.0	363.8	384.7	403.8	8.09	3.19
PRF 90 RON						
7	312.0	352.8	369.2	387.1	7.08	1.02
8	318.0	354.2	370.8	390.7	7.38	1.28
9	323.0	355.0	371.4	387.5	7.77	1.15
10	331.0	359.1	376.4	391.5	7.89	1.92
11	334.0	359.9	377.8	391.1	8.01	1.77
12	339.0	361.6	381.0	394.9	7.89	2.80
13	345.5	366.2	389.8	407.3	7.81	4.49

Table 5.3 **Measurements of heat release, IMEP, and COVimep for a number of fuels and compression ratios. In each case, measurements are taken at MBT. Engine is operating at 1500rpm and WOT, SI combustion.**

The following figure is derived from results presented in Table 5.3. It graphically shows the ignition timing, and 10, 50, and 90% mass fraction burned CA for each fuel and compression ratio tested. For each compression ratio, results between fuels are directly comparable since they are obtained while the engine is operating at MBT.

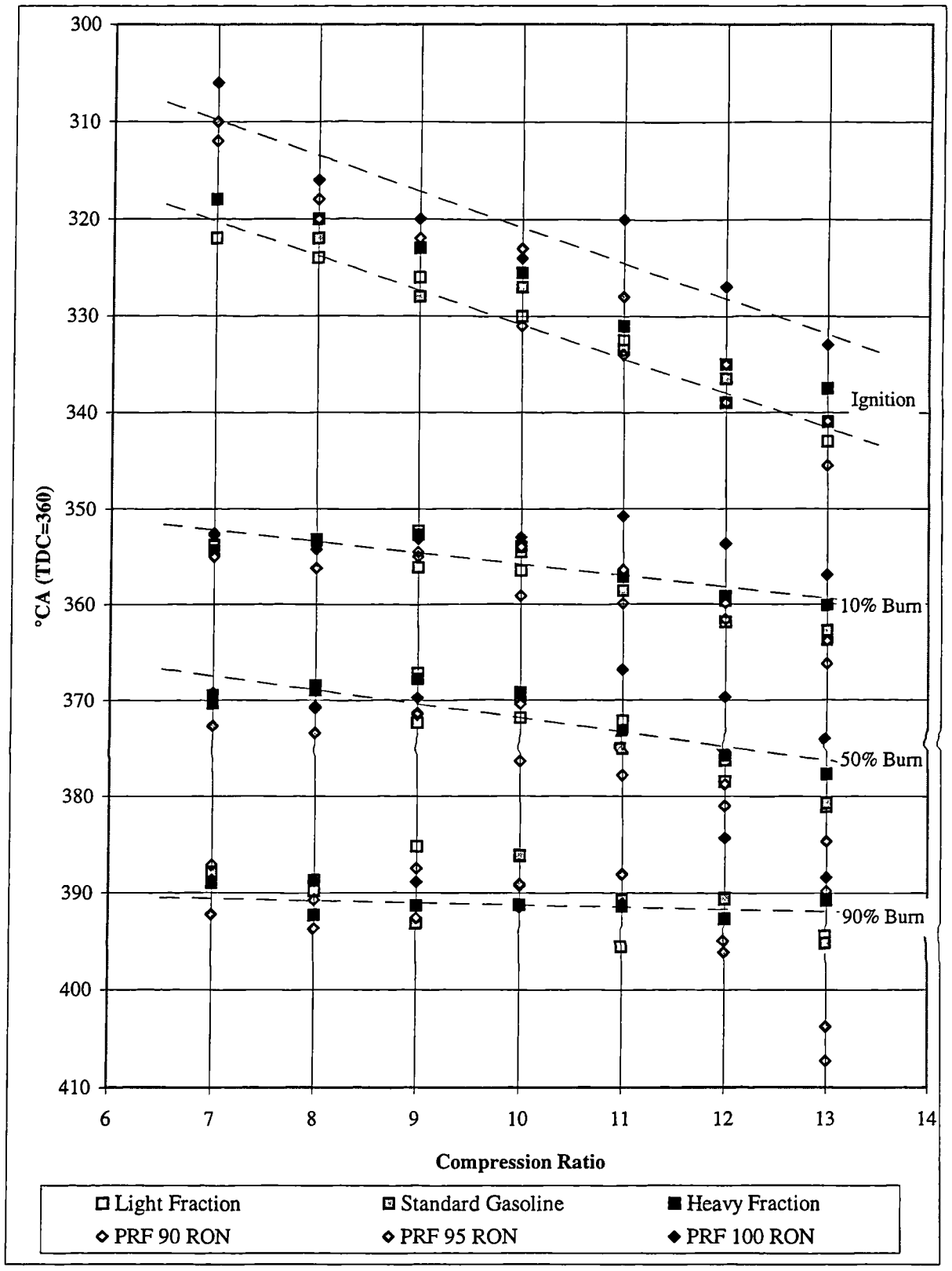

Figure 5.15 **Ignition and burn history for a number of fuels and compression ratios, with the engine operating at MBT**

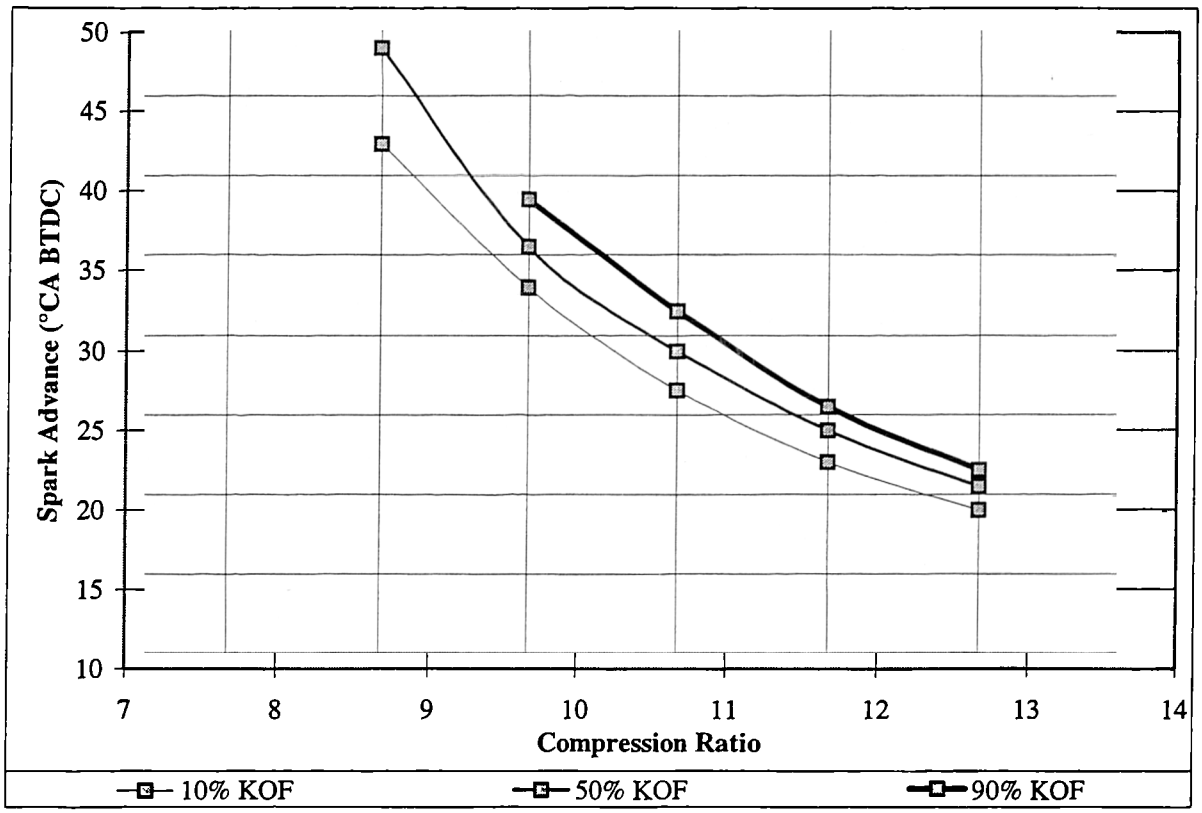

Figure 5.16 **Spark advance to cause knocking cycles as a function of compression ratio for standard gasoline**

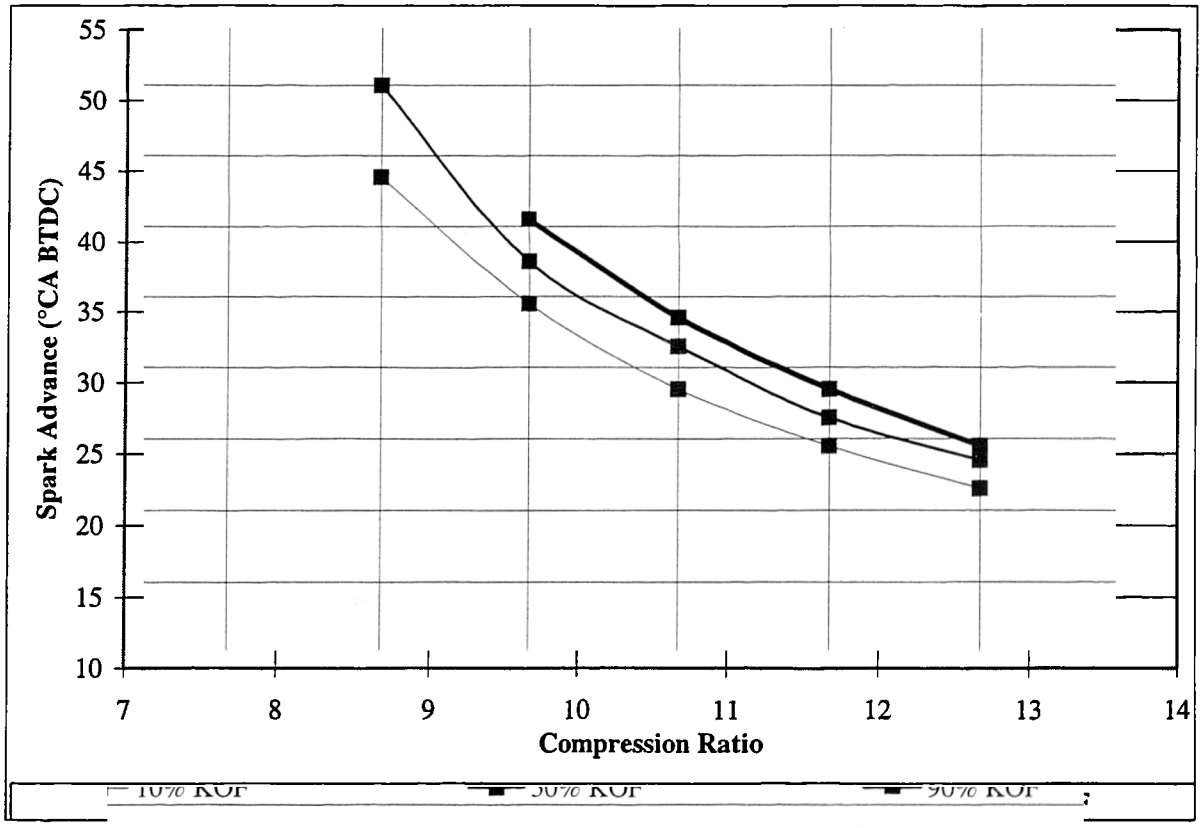

Figure 5.17 **Spark advance to cause knocking cycles as a function of compression ratio for the heavy fraction**

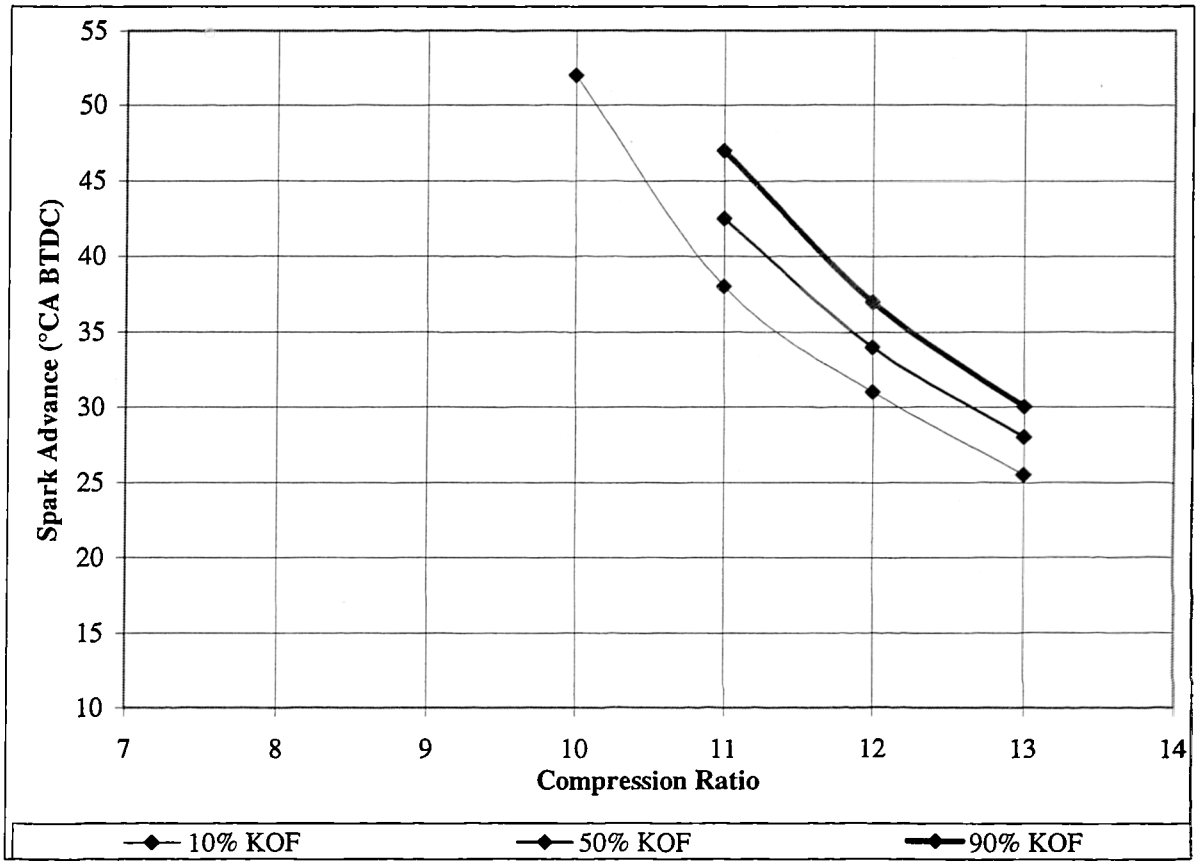

Figure 5.18 **Spark advance to cause knocking cycles as a function of compression ratio for the PRF 100 RON (isooctane)**

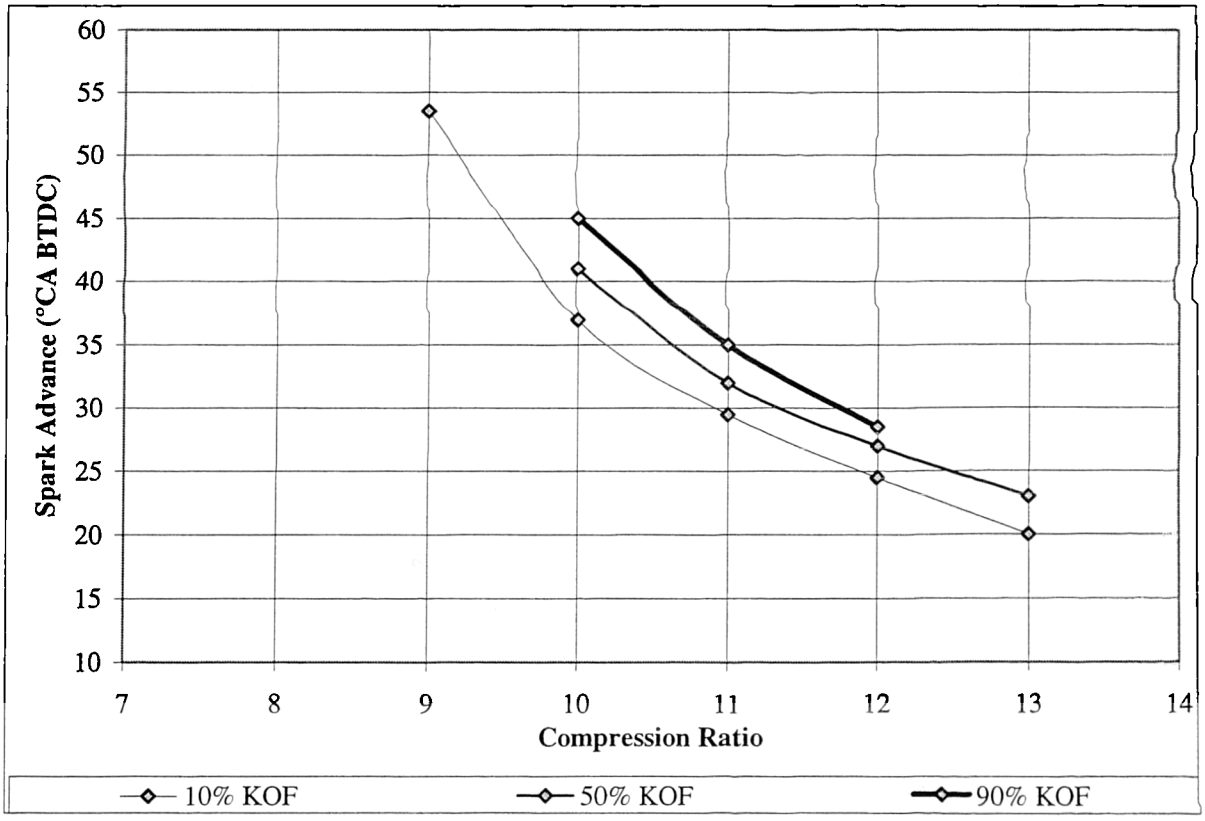

Figure 5.19 **Spark advance to cause knocking cycles as a function of compression ratio for the PRF 95 RON**

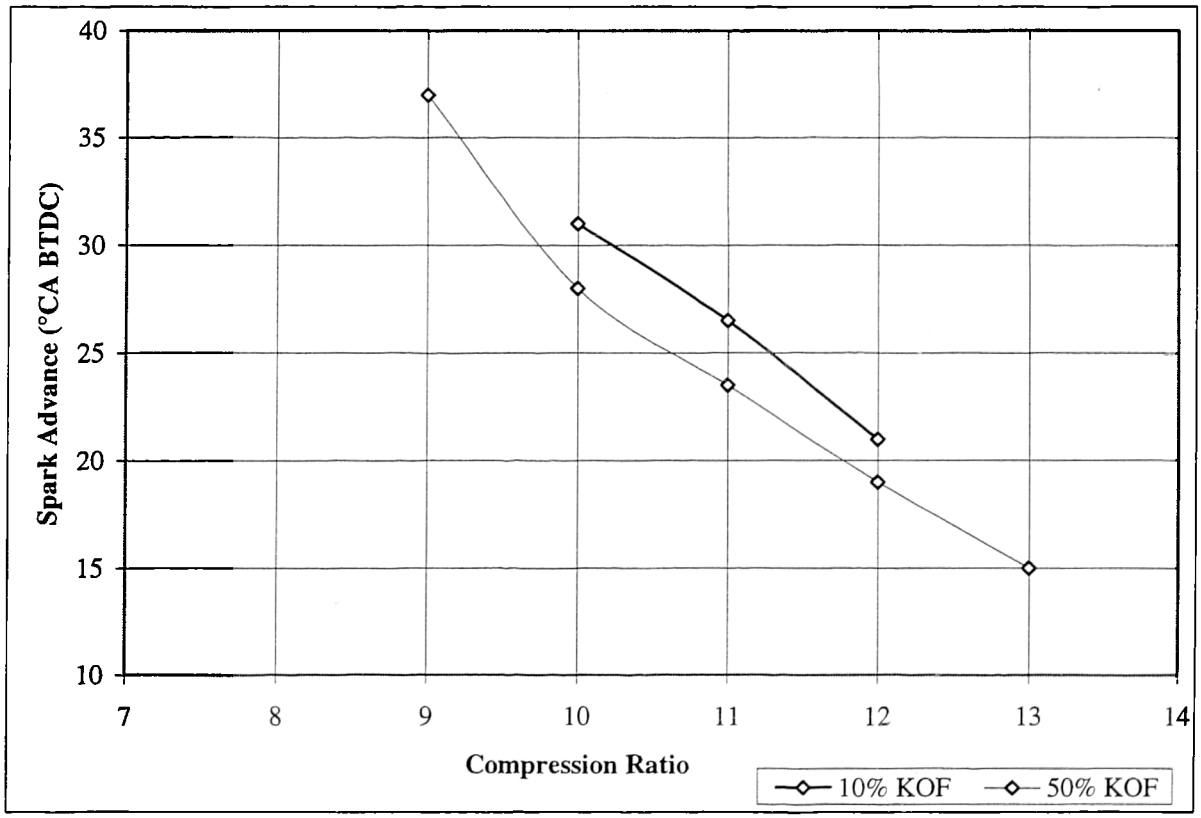

Figure 5.20 **Spark advance to cause knocking cycles as a function of compression ratio for the PRF 90 RON. 90% KOF are not recorded due to the destructive nature of knocking combustion for this particular fuel under those conditions.**

Chapter 6

Experimental Studies on the CAI Combustion of Gasoline Fuel

Chapter 6 Experimental Studies on the CAI Combustion of Gasoline Fuel

6.1 Introduction and Objectives

A detailed discussion of current and past research in the area of CAI combustion was presented in chapter 2. The most practical method that has emerged in recent times for gasoline engines uses burned gas recycling to provide the required heat and dilution control. Despite the superior qualities of this approach, only a limited amount of work has been done to document the effects of dilution using exhaust gases. Furthermore, most of this work has not studied the combined effects of air and exhaust gas dilution, which together determine the full range of possibilities for charge composition. CAI combustion and emissions characteristics are not only dependent on the composition of the charge, but also on its pressure and temperature histories. However, the effects of compression ratio and intake temperature, which together determine the temperature and pressure histories, are well documented. Of the experimental studies that do attempt to sufficiently vary the EGR and air dilution rates [24, 83], either the information given was insufficient [24], or the experimental techniques that were employed were questionable [83]. In the latter case, intake temperatures were adjusted to maintain ignition at TDC over the EGR and air dilution ranges. Thus, any combustion trends with dilution rate are modified by a varying temperature history, and the precise role of either intake temperature or dilution rate cannot be determined explicitly. This chapter details CAI combustion tests using standard gasoline fuel (BS EN 228) on the Ricardo E6 engine. Detailed measurements combined with a reasoned experimental approach provide a large amount of information on the combined EGR and air dilution effects on CAI combustion.

The aim of the tests is to study the interplay between air and EGR dilution under strictly controlled conditions. To this end, all other engine variables are fixed to the values shown in Table 6.1. The measured or dependant variables are obtained during testing using the DAQ system for heat release and knocking combustion detection, gas analysers for intake and exhaust compositions, and a thermocouple to measure exhaust gas temperature. Thus, each measured variable forms a surface over the two-dimensional air and exhaust gas dilution range. It is not possible to operate the engine under all of the EGR rate/Lambda

combinations specified in Table 6.1. In fact, one of the objectives of these tests is to define the two-dimensional region in which CAI combustion can be successfully attained.

	Parameter		Value
Independent Variables	EGR Rate		0-60%
	A/F Ratio (Lambda)		1.0-5.5
Fixed Conditions	Engine Speed	(rpm)	1500
	Compression Ratio		11.5:1
	Intake Manifold Pressure	(bar)	0.93 absolute
	Intake Charge Temperature	(°C)	320
	Coolant Tempretaure	(°C)	80
	Oil Temperature	(°C)	55
	Fuel		Gasoline (BS EN 228)
	Injection Timing	(°CA)	79 BTDC Compresion Stroke

Table 6.1 List of Experimental Parameters for CAI Combustion Tests on Gasoline Fuel.

6.2 Test Methodology

An unfortunate result of performing the tests as described in table 6.1 is that the combustion phasing is allowed to vary over the dilution ranges. In CAI combustion, all of the dependant (measured) variables have a greater or lesser relationship with the combustion timing. If it is over-advanced, the heat release rate is accelerated and knocking combustion and high NOx emissions can result. However, if it is over-retarded, heat release is slowed down and incomplete combustion can occur. In a practical engine, the independent parameters that seek to control combustion will do so to maintain optimum ignition timing under the prevailing conditions. Thus, the results that are obtained in these tests do not relate to those that could be expected in a practical CAI engine. While this maybe a drawback, the alternative route is to perform the tests in a similar fashion to Christensen et al. [83], where they controlled the intake gas temperature independently to maintain constant ignition timing. This technique does give realistic combustion and emissions characteristics, but only for a practical engine that uses both EGR dilution and intake temperature to control combustion. Such a control method is subject to the problems of intake thermal inertia and is unlikely to be practicable, as discussed in chapter 2. The current method has been employed in the absence of any better ones, so that the dilution effects on CAI combustion can be explicitly determined without the interference of other engine variables (e.g. intake temperature).

6.3 Experimental Procedure

6.3.1 Cold Start Procedure

CAI combustion using gasoline fuel at a compression ratio of 11.5 requires an intake charge and coolant temperatures in the region of 300°C and 80°C respectively. Thus, a warm-up procedure is required before CAI combustion can be achieved. There are two methods that can be used to heat-up the engine sufficiently:

(i) The engine can be motored, with the intake air and coolant heaters on. When both reach steady state, the fuel is switched on at a reasonably lean A/F ratio (λ = 3-5). CAI combustion gradually starts, and the combustion efficiency increases reaching steady state after a short period of time.

(ii) The engine is started in SI combustion mode, without intake heating, but with coolant heating. Heat transfer from the combustion chamber ensures that the coolant is heated to its steady state temperature quickly. After 1 hour of operation, the intake heater is switched on. Increased intake air temperature reduces its density, leading to richer A/F ratios. The injector duration is shortened to compensate for this. Further increases in intake temperature can force the engine into knocking combustion, so the ignition timing is retarded to TDC, and the A/F ratio is further increased. As the intake temperature approaches approximately 280°C, CAI combustion begins to occur in some cycles. Eventually CAI combustion takes over completely, and the ignition system is switched off.

In both of these methods, the oil heater is engaged from cold start until it reaches a temperature of 55°C, after which it is maintained by heat rejection from the engine. While method (i) is simpler, it takes longer because it does not benefit from the heat rejection of combustion until CAI combustion is attained. For this reason, method (ii) has been employed for all subsequent tests.

A preliminary test was conducted to determine the amount of time that the engine should be left operating in CAI combustion mode before measurements can safely be taken. Changes in combustion efficiency over time occur because the engine block and ancillaries are gradually warmed up during operation. These changes can be observed as reductions in

the exhaust HC concentration. As temperatures increase, full oxidation of the fuel is promoted resulting in lower HC emissions for the same engine operating conditions. Figure 6.1 shows how the exhaust HC concentration reduces over a period of six hours during a single test. Clearly, HC concentrations exponentially decay over time, with the majority of reduction occurring within the first hour of testing. From one hour onwards the measurements only change by a few percent. Thus, a period of one hour of SI operation followed by one hour of CAI operation should allow the system to stabilise prior to measurement.

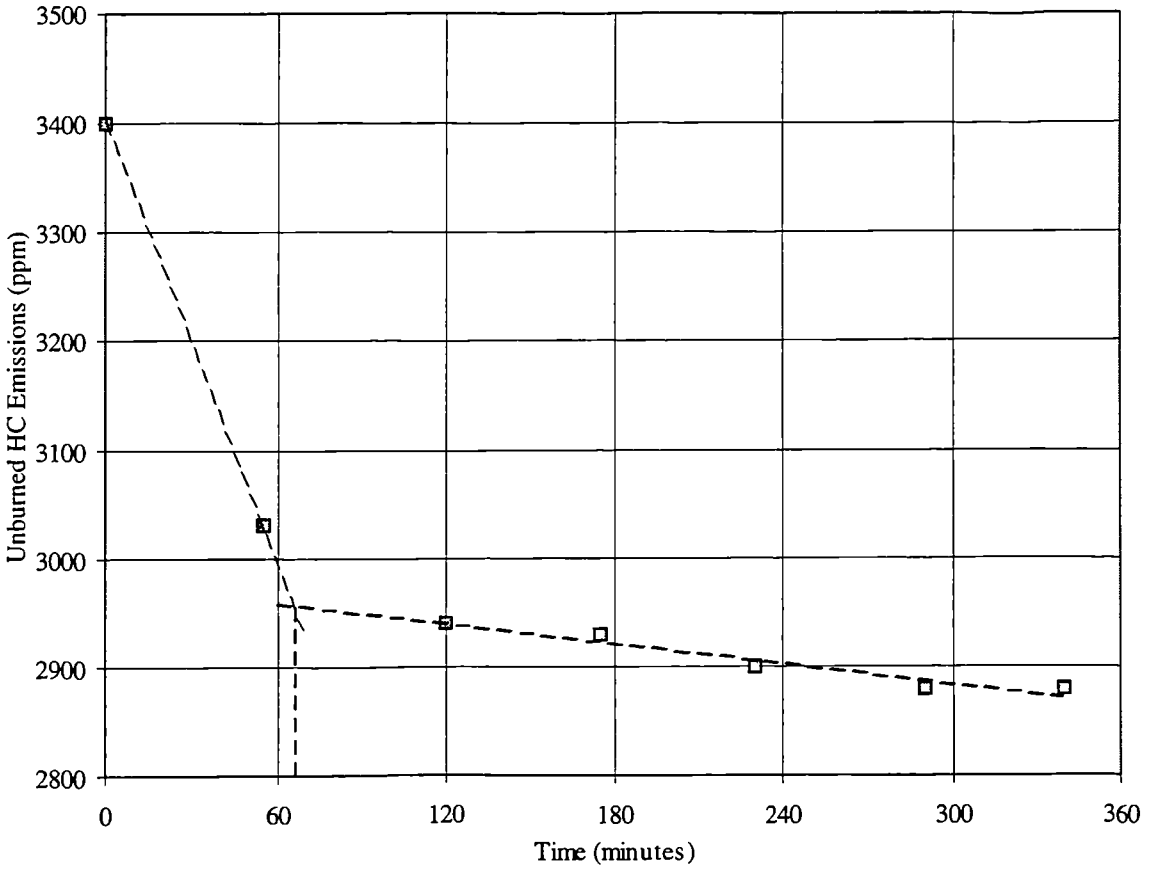

Figure 6.1 Unburned HC Emissions Over Time For CAI Combustion at WOT, $\lambda = 2.7$, EGR Rate = 0%, 95 RON PRF.

6.3.2 Test Procedures

Once the engine and ancillaries are fully warmed up and under stable and steady state operation, testing can commence. Firstly, the EGR gate valve is checked to ensure it is closed, and the fuelling is adjusted so that the engine is operating under incipient knocking conditions. Once this operating point has been established, the fuelling is reduced slightly so that no knock occurs. This operating condition is the start point for the test, indicated by

point A on Figure 6.2. The DAQ system is reset so that it uses the crankshaft clock input instead of the computer generated clock, which is only used for knocking combustion detection.

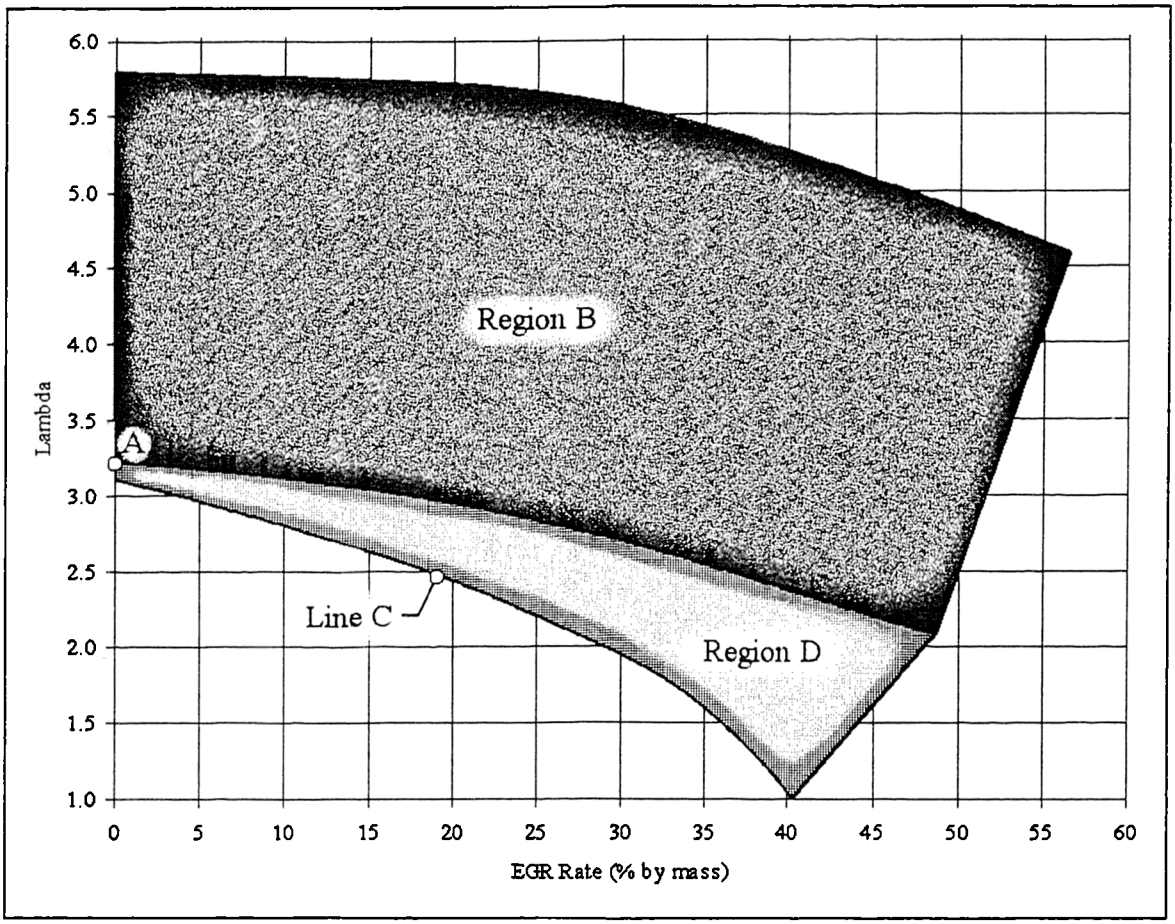

Figure 6.2 Lambda vs. EGR Rate Showing the Sequence of CAI Combustion Testing

The engine and measurement systems are left to stabilise for a few minutes. Readings of intake and exhaust CO_2, O_2, and CO are taken from the Richard Oliver K650 analyser and recorded on a spreadsheet on the computer. Similarly, measurements are taken from the THC and NOx analysers and recorded. The spreadsheet program contains the combustion equations detailed in Chapter 3, and automatically calculates and plots the operating point on a Lambda/EGR rate chart. The DAQ system is set to record 100 consecutive in-cylinder pressure cycles, and the data is saved to the hard drive for post-processing. The EGR gate valve is then cracked open, and the EGR rate increased to approximately 5%. This is determined approximately using the intake CO_2 measurement, and comparing it to the

previous exhaust CO_2 measurement. The engine is left to stabilise and the measurement process is repeated.

The EGR is increased in incremental steps and measurements are taken until combustion appears to exceed normal limits, usually indicated by a collapse in combustion stability. When this occurs, the EGR gate valve is closed, and the fuel rate leaned by approximately 0.5 of lambda, and the whole process is repeated. Thus, results are taken under progressively leaner conditions until the fuelling rate is so low that combustion suffers. This region is indicated by region B on Figure 6.2.

Once the lean limit has been explored, the fuelling and EGR rates are returned to the test start conditions (point A, Figure 6.2), just lean of incipient knocking combustion. The engine is allowed to stabilise and the exhaust and intake measurements are checked to ensure that they agree with those taken at the start of the test. This check ensures that the analysers and fuel injection system are still working correctly.

The next part of the chart to explore is the 'knock boundary', so named because 10% KOF occurs at all points on this boundary. From the start point, the fuelling rate is increased so that incipient knock is registered on the DAQ system. Measurements are taken for this point as before, then the EGR rate is increased. Increased EGR dilution leads to tempering of the heat release rate, so the fuel rate is slightly increased (reduce lambda) to bring operating conditions back onto the knock boundary. Measurements are taken and the process repeated until conditions reach stoichiometric values. This boundary is indicated by line C on Figure 6.2.

The final area of the chart to cover lies between the richer 'knock boundary' (line C, Figure 6.2) and the leaner conditions first explored (region B, Figure 6.2). Judgement is used to set the correct fuelling and EGR rates for individual points so that this region is properly explored. This region is indicated by region D on Figure 6.2.

This procedure generates anything between 80 and 150 measured points depending on fuel type (see Chapter 7), representing the full range of charge dilution conditions that can be attained under specific engine operating conditions.

6.4 Discussion of Results

6.4.1 General Characteristics

Investigation of the satisfactory operating region of standard gasoline was carried out for a range of A/F ratios and EGR rates. Figure 6.3 shows this region, with all the data points taken to define it. The region is limited by three boundaries: misfire, partial burn, and the knocking combustion limit.

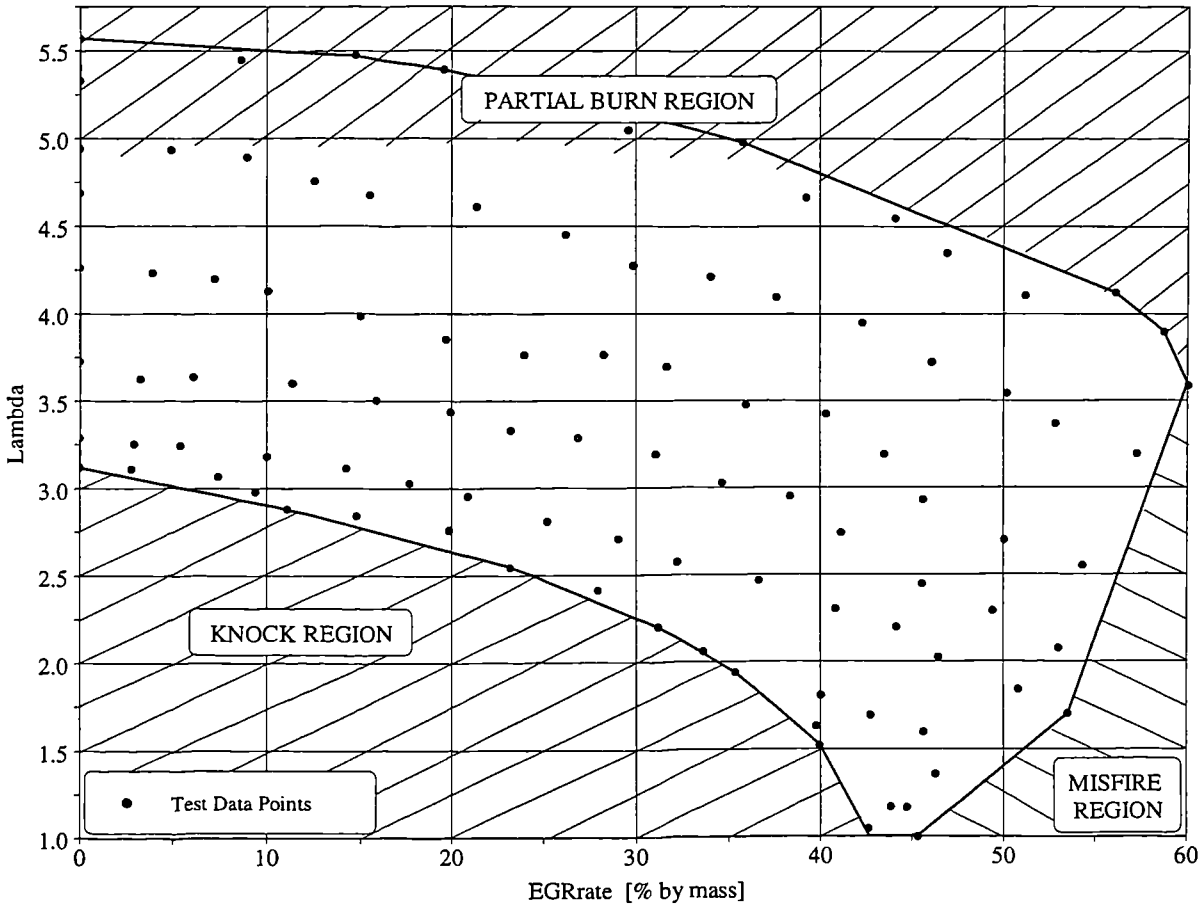

Figure 6.3 Region Defining Successful CAI Operation for Standard Gasoline

The misfire boundary is approached as EGR rates increase beyond acceptable levels. At higher EGR rates, the CO_2 and H_2O content of the intake charge is raised significantly, which tends to retard the ignition timing and eventually causes its failure in a small proportion of cycles. The misfire region is reached when misfire is observed in at least one cycle from the 100 taken for each test point. The engine's speed and torque output exhibit large oscillations under these conditions. This is because any misfire that occurs allows the unburned charge to be ejected into the exhaust manifold and recycled through the EGR

system. Thus, the EGR gases cycle between fully burned and unburned, and when mixed with the fresh intake gas, cause a cyclic variation in its composition, leading to large variations in the combustion heat release profiles.

The partial burn limit is approached as the fuelling rate is reduced excessively. It differs significantly from the misfire boundary because combustion initiation is not affected greatly by increased air dilution, and misfire never occurs. However, the reduced fuelling rate means that less fuel is used to heat the same amount of air during combustion. This results in a lower combustion temperature. Eventually, the combustion temperature becomes so low that the full oxidation of the fuel cannot occur, resulting in high concentrations of partially burned combustion products in the exhaust gas. The partial burn boundary is loosely defined during testing when the concentrations of unburned HC measured in the exhaust stream are seen to rise excessively (HC_{vol} > 5000ppm). However, post-processing of the volumetric unburned HC data provides a sounder basis for a quantitative definition of the partial burn boundary.

In the case of homogeneous CAI combustion, the entire charge behaves as the end-gas would in spark-induced knocking combustion. At any point on the knock boundary, if the EGR rate is increased then combustion is slowed and knocking combustion avoided. A similar result is achieved if the fuelling rate is reduced. The knocking boundary represents an important practical boundary to CAI combustion, since it affects the highest engine loads that are possible. If the knock region can be reduced in size towards the origin of figure 6.3, then higher engine loads can be achieved. The knocking combustion limit is the most rigorously defined of the three. A digital band-pass filter is used to isolate the vibrations of the engine structure that result from knocking combustion. As explained in section 3.3.1.2, the amplitude of the resulting signal is sampled and compared to a threshold value of 0.5 bar gauge. 100 consecutive engine cycles are recorded for each test point, and the engine is deemed to be 'knocking' if at least 10 (10%) of these cycles record a knocking amplitude above the threshold, defined as 10% Knock Occurrence Frequency (KOF).

6.4.2 Heat Release Analyses

6.4.2.1 Ignition Timing

Ignition timing is defined as the crank angle at which 10% of the charge mass has burned, as indicated by the heat release profiles. Although lower values (1%, 5%) of the mass fraction burned could have defined ignition, it is believed that measurements of smaller quantities of burned gases are subject to larger errors, which may increase the measured variability in ignition timings. Figure 6.4 shows the timing map generated over the dilution ranges for the data as taken in Figure 6.3.

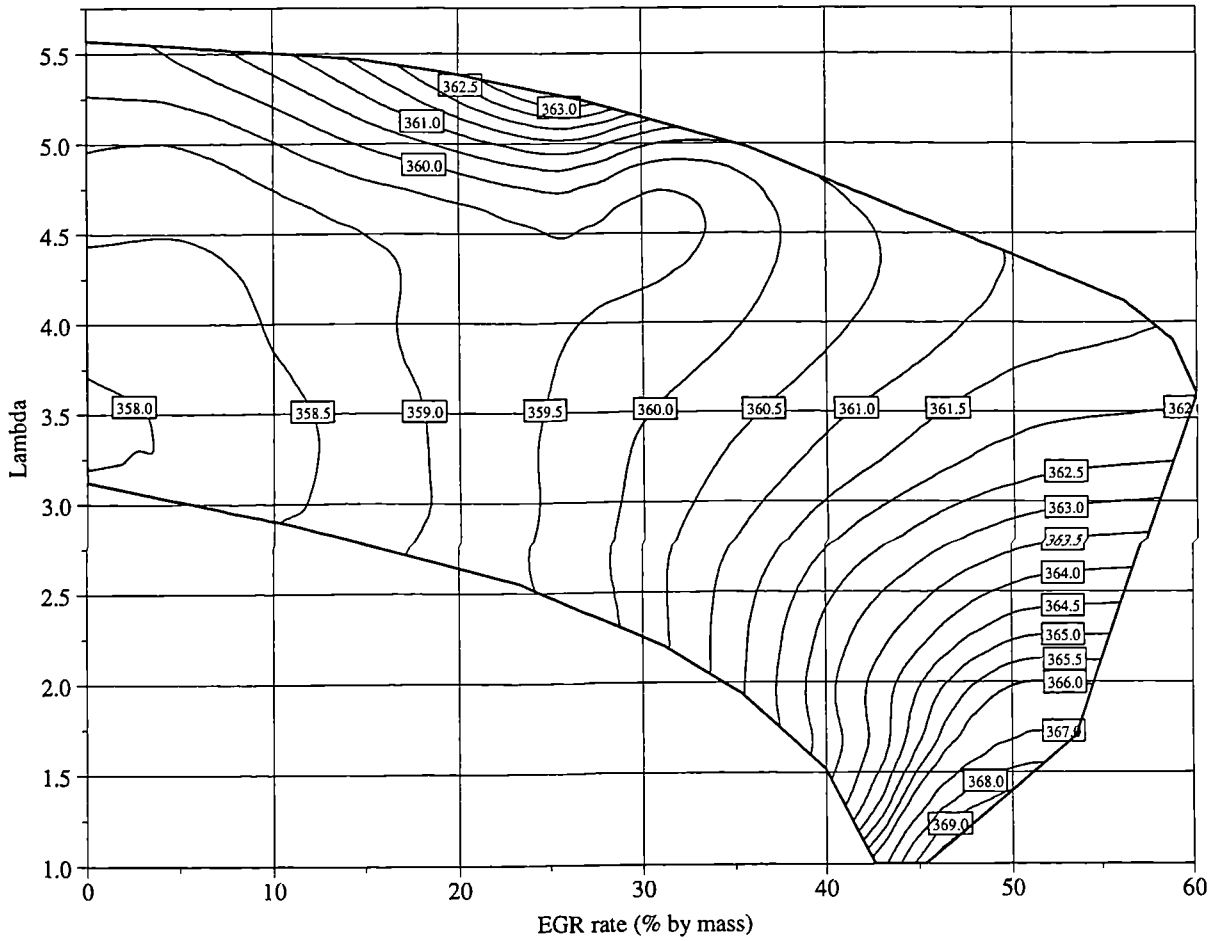

Figure 6.4 Ignition Timing (10% Burn Crank Angle), (°CA, TDC=360) for Standard Gasoline

As discussed already, ignition timing shows very little dependence on A/F ratio for the majority of the map, until EGR rates are in excess of approximately 40%. An interesting result of this trend is that as the fuel rate is increased at any point on the knock boundary

(10% KOF), the combustion phasing does not appear to advance. Therefore the cause of knocking must be due to some other parameter, and not on advancing ignition timing.

At the higher EGR rates, Ignition timing becomes a strong function of A/F ratio. The reason for this appears to be associated with the CO_2 and H_2O contents of the intake charge. As conditions approach stoichiometric, the concentrations of these species increase rapidly, tending to retard ignition. In similar fashion, as the charge is leaned at high EGR rates, the oxygen availability increases, and the H_2O and CO_2 concentrations are reduced, which tends to advance the ignition timing.

The maximum ignition retardation that can be tolerated is approximately 10° ATDC. When the average ignition timing occurs this late, a small number of cycles do not ignite at all. This happens as a combined result of the EGR excessively slowing the pre-combustion reactions that lead to autoignition, and the piston descending in the expansion stroke, which progressively lowers the charge temperature.

6.4.2.2 Autoignition Temperature

Autoignition temperatures of the CAI combustion process are interesting because ignition is not directly controlled as in SI and CI combustion, but relies on the charge composition, and its temperature and pressure histories. In this study, it is of particular interest to observe how the autoignition temperatures change with charge composition, if at all. Furthermore, because of the homogeneous nature of CAI combustion, it is possible to calculate the bulk charge temperature over the entire engine cycle, and correlate it to emissions data such as NOx and unburned HC. Calculation of the autoignition temperature for a particular engine condition relies on the ideal gas law relationship:

$$T_i = \frac{P_i . V_i}{n_t . \tilde{R}} \qquad \text{Equation 6.1}$$

Where T_i, P_i, and V_i are the respective temperature, pressure, and volume of the cylinder contents at a given point in the cycle (i). n_t is the total number of moles of gas trapped in the cylinder, and $\tilde{R}$ is the universal gas constant. Correct application of Equation 6.1 requires knowledge of the cylinder pressure and volume at autoignition, which can be

found from the heat release analyses in the previous section. Also, the number of trapped moles must be calculated based on the charge composition. To find n_t, the following relationships can be used:

$$a = \frac{n_f}{n_t} \qquad \text{Equation 6.2}$$

Where a is the molar fraction of fuel relative to the entire intake charge, which is calculated in Equation 3.17. n_f is the number of moles of fuel, which can be known by applying:

$$n_f = \frac{m_f}{\tilde{m}_f} \qquad \text{Equation 6.3}$$

Where m_f is the mass of fuel contained in the cylinder, calculated from the injector calibration. $\tilde{m}_f$ is the molecular weight of the fuel. Equations 6.2 and 6.3 can be combined to give:

$$n_t = \frac{m_f}{a.\tilde{m}_f} \qquad \text{Equation 6.4}$$

If autoignition temperatures are required, then n_t is sufficient for use in Equation 6.1. However, if the full cycle temperatures are required (during valve closure), then n_t must be modified according to the state of heat release to account for the change in number moles that occurs during combustion. Thus, the relationship:

$$n_t = n_{start}\left[1 + mfb.\left(\frac{n_P - n_R}{n_R}\right)\right] \qquad \text{Equation 6.5}$$

Where *mfb* varies between 0 and 1, and represents the heat release condition during compression and expansion. n_R and n_P are found from knowledge of the A/F ratio; the relationship between them is defined by the number of moles of reactants and products either side of the combustion Equation 3.13 respectively. This relationship shall be used later this chapter for NOx and unburned HC emissions correlations with temperature.

Autoignition temperatures for gasoline have been calculated according to Equations 6.1 and 6.4, and are presented in Figure 6.5. Autoignition temperatures lie in the region of 950 K to 1100 K for the entire range, reaffirming results from past investigations on this subject. The general trend is for the autoignition temperature to increase as stoichiometry is approached. To investigate this further, charge temperatures at IVC have been calculated and are presented in Figure 6.6.

Comparison of Figures 6.5 and 6.6 shows that the trends are almost identical. Thus, the autoignition temperature is intimately related to the charge temperature at IVC. Furthermore, the autoignition temperature results (figure 6.5) seem to correlate with the autoignition timing results (figure 6.4); the higher autoignition temperatures required by the near-stoichiometric charge under high EGR conditions are probably responsible for the delayed autoignition timing.

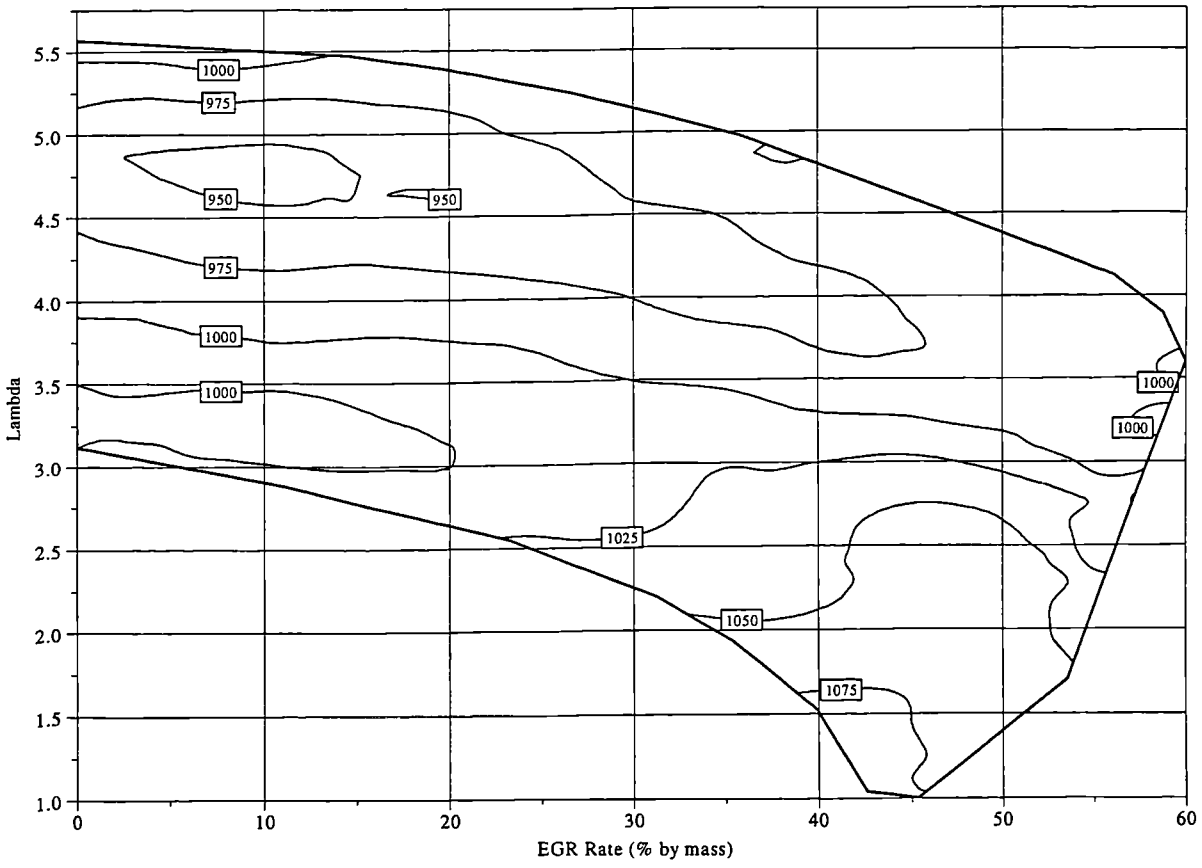

Figure 6.5 Autoignition temperatures (K) for Gasoline Fuel (at 10% MFB)

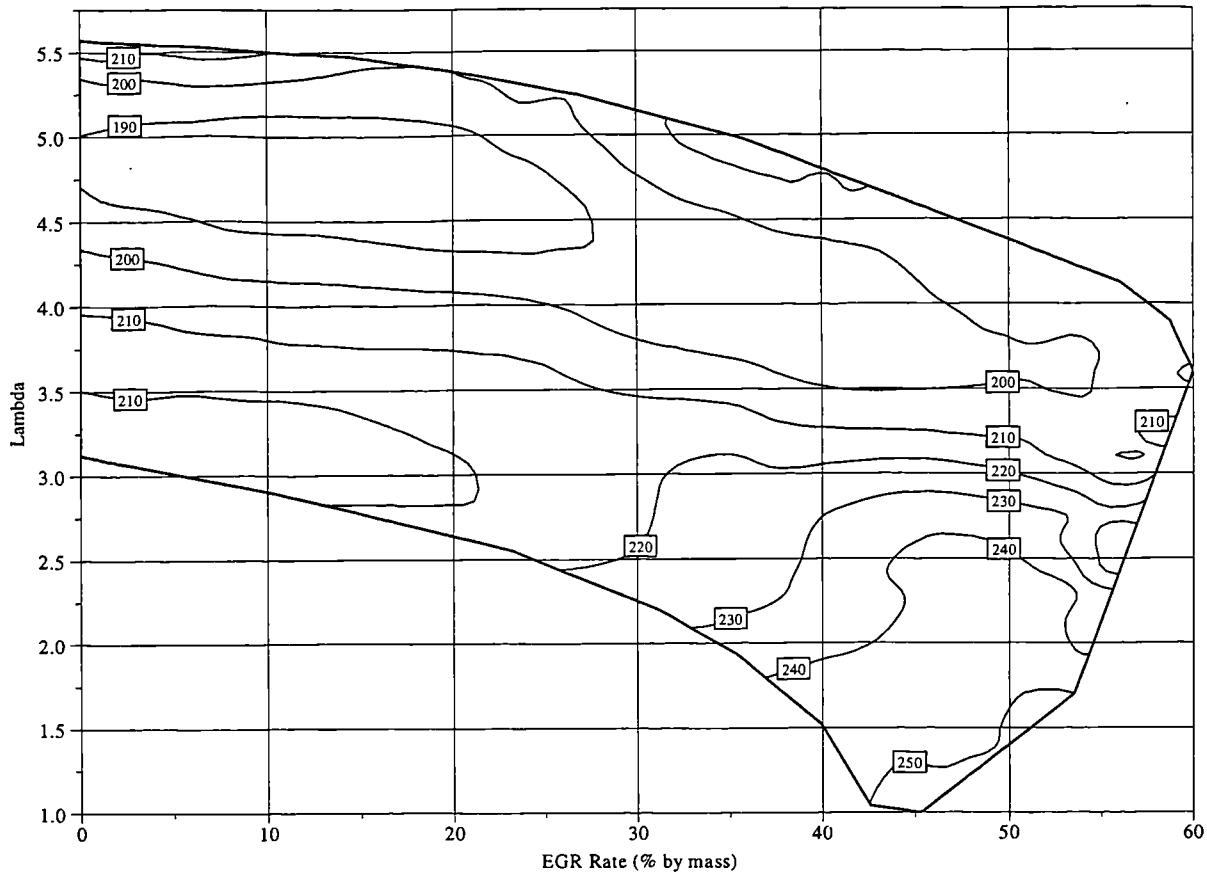

Figure 6.6 Charge Temperature (°C) Calculated at IVC for Gasoline Fuel

These results imply that despite a higher temperature history, a close-to-stoichiometric charge with substantial EGR requires slightly higher temperatures to achieve autoignition satisfactorily. Conversely, leaner mixtures undergo greater cooling during induction (lower temperature at IVC), but require lower temperatures to achieve autoignition. This observation may appear counter-intuitive due to the charge-cooling effects of increased fuel flow. However, intake temperatures are controlled to 320 °C in the intake port, 100 mm after the point of fuel injection. The very hot intake gas and manifold ensure that charge-cooling effects downstream of the thermocouple are minimised compared to engine operating conditions where ambient intake temperatures are used.

6.4.2.3 Combustion Duration

Figure 6.7 shows the combustion duration over the dilution ranges, defined as the crank angle period between 10% and 90% mass fraction burned. Unlike the ignition timing, combustion duration shows a strong relationship with air dilution up to the EGR rate of 40%; increasing the A/F ratio lengthens the duration. This chart clearly shows that as the fuelling rate is increased into the knock region, the combustion duration decreases to

extremely low values of 7 or 8 °CA. Thus the onset of knocking combustion occurs as a result of excessively high heat release rates, and not because of any changes in ignition timing. In SI combustion, while the onset of knock is linked to the heat release rate in the end-gas after autoignition, it is the spark event that effectively controls the end-gas conditions prior to its autoignition. Thus, in SI combustion, the onset of knock is dependent mainly on the ignition timing, which appears not to be the case for CAI combustion.

Beyond 40% EGR, combustion duration becomes almost entirely dependant on EGR rate. In this region, increases in the concentrations of inert EGR species such as CO_2 and H_2O are thought to affect combustion. On a molecular level, the presence of inert species obstructs the chain propagating and degenerate-branching reactions, slowing the overall reaction rate. Increasing the air dilution in this region reduces the rate at which the reactions are slowed with increasing EGR, because of the increased oxygen availability for oxidation, and the reduced presence of the inert species.

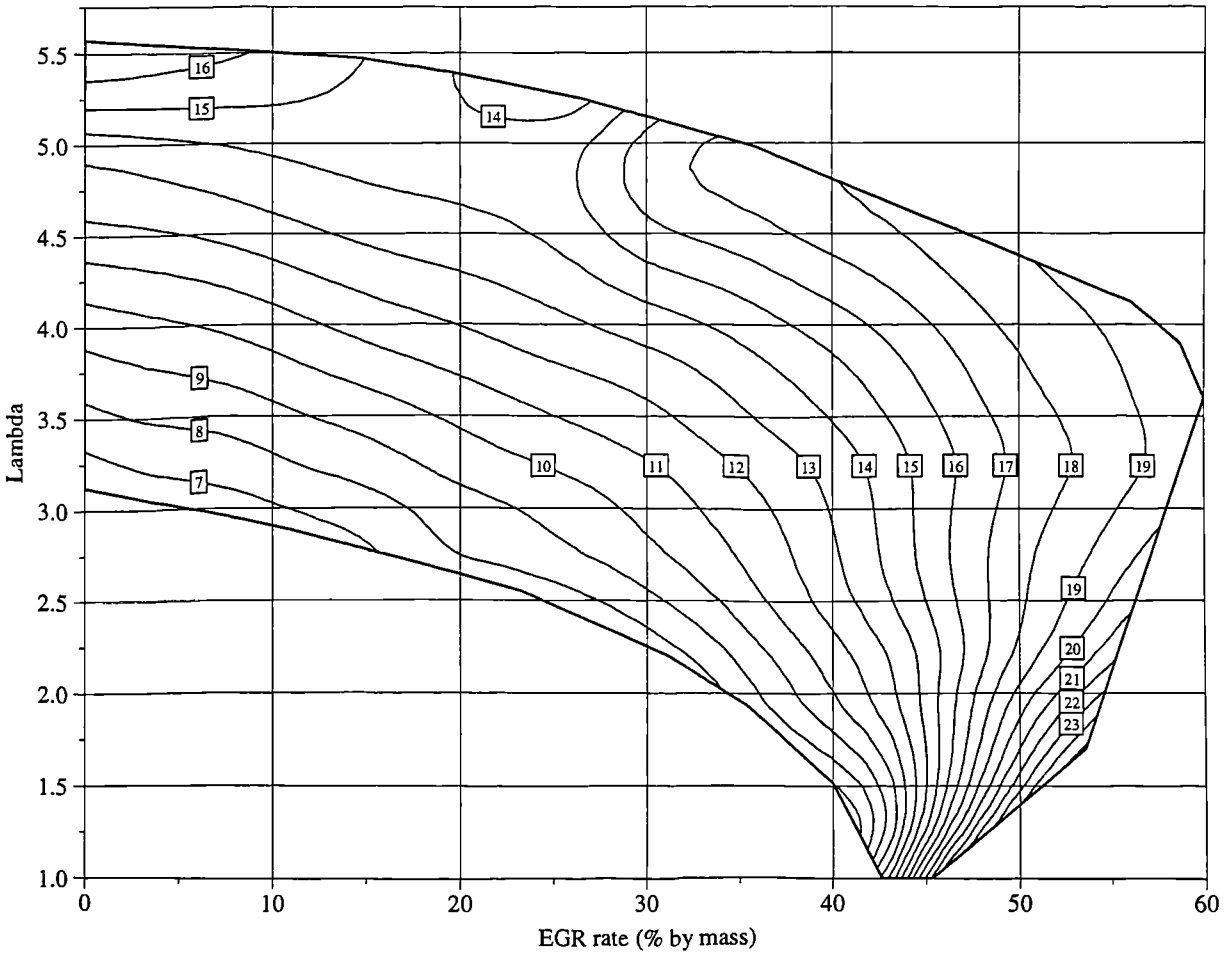

Figure 6.7 Combustion Duration (10-90% Burn), (°CA) for Standard Gasoline

Short combustion durations are a distinctive characteristic of CAI combustion, when one considers that homogeneous SI combustion normally takes in the order of 30-50 °CA in modern fast burn engines. Short combustion duration allows the actual engine cycle to be more efficient since it more closely matches the ideal air-standard Otto cycle, in which constant volume (no duration) combustion is desirable.

The density of the ignition timing and combustion duration isolines increases rapidly as conditions approach stoichiometric. This indicates inherent combustion instability under these conditions. Cyclic variations in the EGR rate and composition occur naturally in the system, and are unavoidable. However, these small variations can lead to relatively large changes in consecutive heat release profiles because of the density of the isolines. Although this is not a strong influence on combustion in the case of gasoline, more attention shall be drawn to this in chapter 7, when other fuels are considered.

6.4.3 Engine Load and Combustion Variability

6.4.3.1 IMEP Considerations

Figure 6.8 shows the trends of IMEP with air and EGR dilution. As expected, higher loads are achieved as the fuel rate is increased and the lambda value is reduced. Furthermore, for a constant A/F ratio, the highest load occurs at the minimum allowable EGR rate. Thus, the maximum load of 3.8 bar occurs under stoichiometric conditions, and at the minimum EGR rate (to avoid knocking combustion) of 43%. This load represents approximately one third of the maximum load attainable under WOT conditions when using a conventional, normally aspirated spark-ignition engine.

Minimum loads occur as the operating conditions approach the partial burn region at high A/F ratios. The minimum recorded value was approximately 0.6 bar IMEP. This value is roughly equal to the FMEP of a fully warmed modern production engine. Thus, the engine may only just be able to idle under these conditions.

The lean limit placed on the region investigated by Thring [24] was set when his engine reached 0 bar BMEP. This limit is a false one because the engine he used was of the single cylinder research type, having an unquantified FMEP. This is part of the reason why he did not make any comment as to the combustion quality under these ultra-lean conditions.

Conversely, a generally applicable limit is defined here, as the combustion itself is seen to deteriorate in a particular way when the charge is excessively diluted with air.

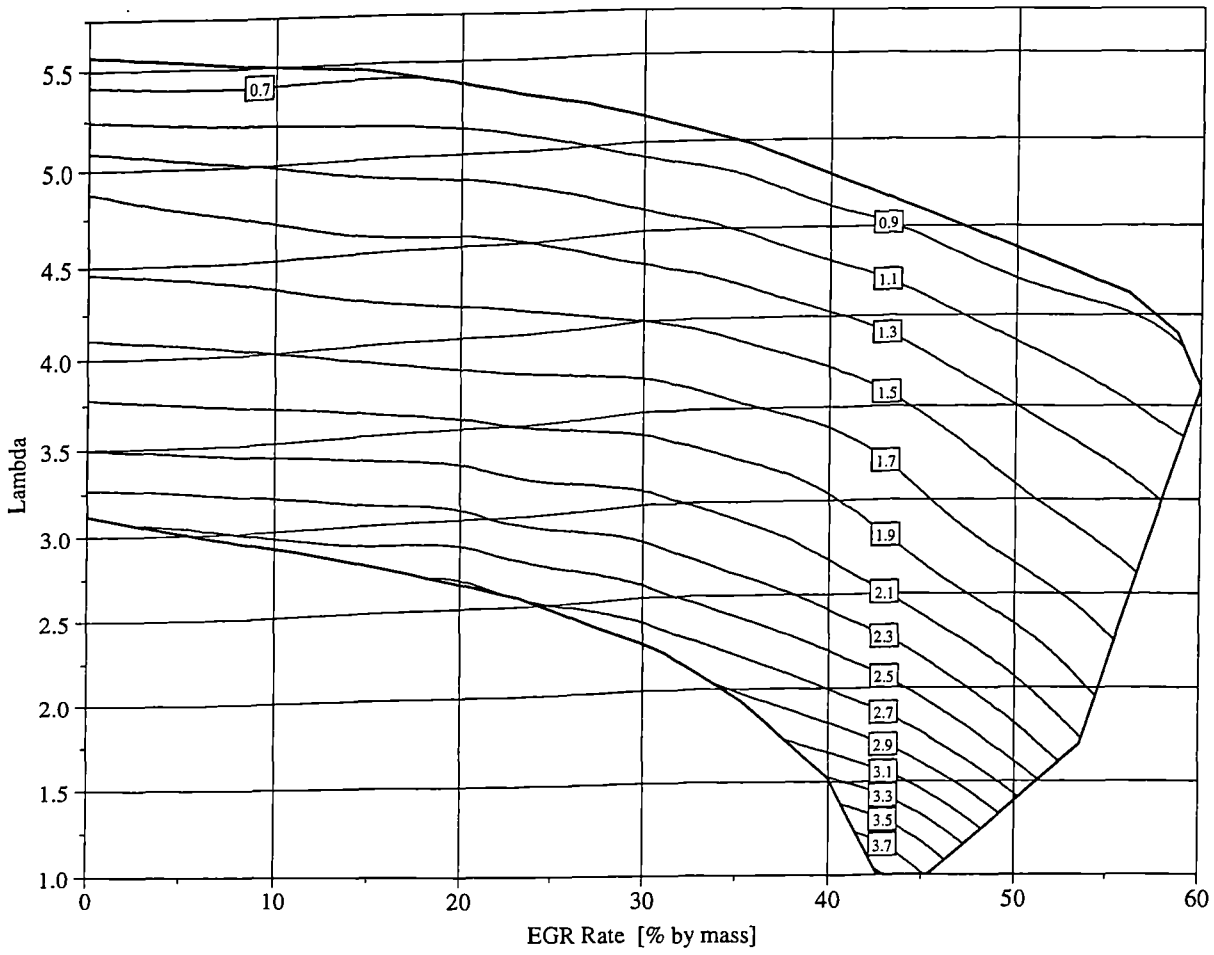

Figure 6.8 Net IMEP (bar) for Standard Gasoline

Another interesting point is that the engine load appears to show little or no resemblance to the ignition timing and combustion duration trends. This is distinctly different to SI combustion, where correct spark timing is of utmost importance to maintain MBT conditions. This would tend to indicate that correct combustion phasing is rather less important than some researchers would suggest, since a reasonable power output can still be achieved despite retarded ignition and relatively long combustion durations. This probably has a lot to do with the fact that the full range of ignition timings in the CAI region is relatively small at 12 °CA, and that the combustion durations are extremely short relative to the normal SI equivalents.

6.4.3.2 Combustion Stability

The COVimep trends with dilution are presented in figure 6.9. At values of lambda higher than about 4.0, combustion stability is clearly affected by increasing air dilution. Similarly, at EGR rates higher than 45% stability is also affected. The normal limit of driveability is approximately 5% COVimep. This would impose a maximum lambda of around 3.5, and a maximum EGR rate of 45% for CAI combustion to remain within tolerable limits under these engine conditions.

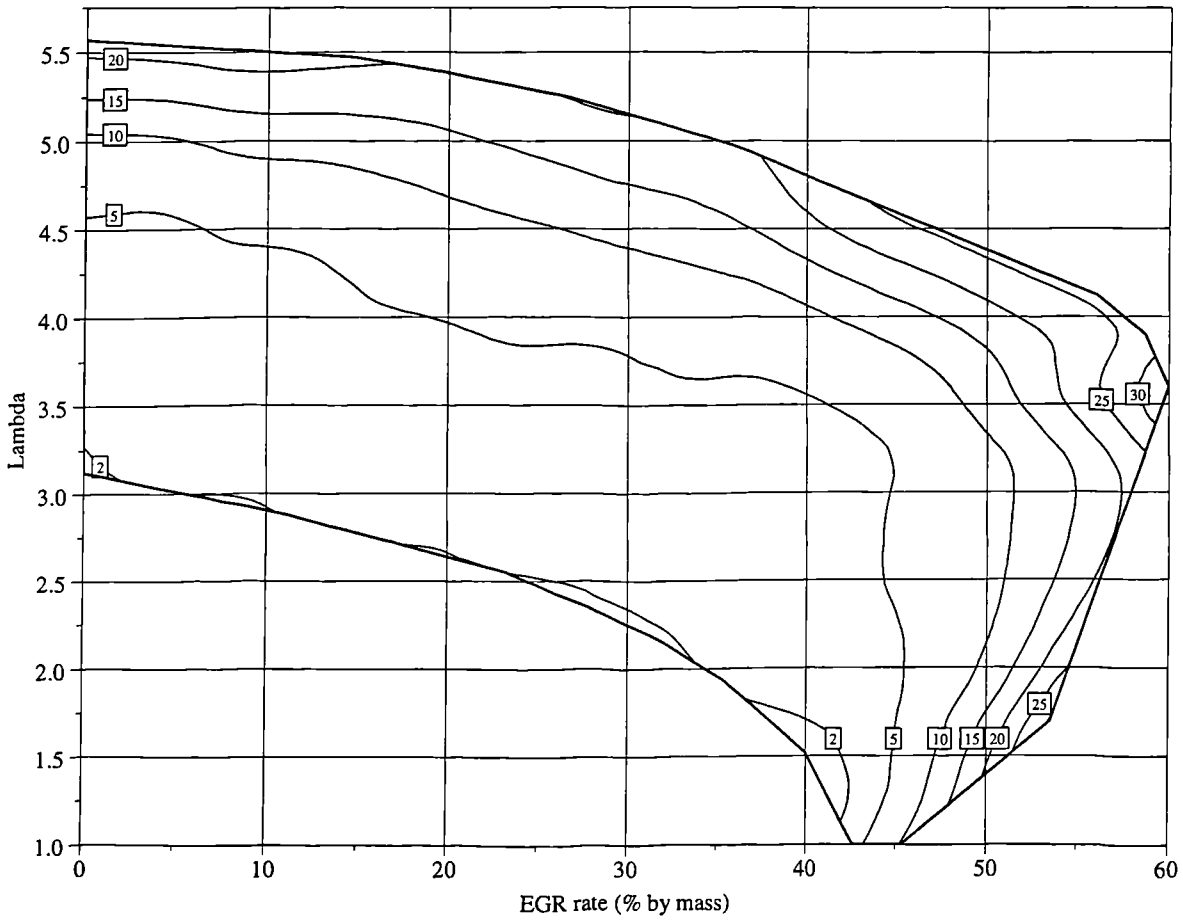

Figure 6.9 COVimep (%) for Standard Gasoline

The region of operation around lambda 1.0 is of particular interest for practical CAI combustion. In this area the exhaust gas temperatures are most likely to be high enough to maintain CAI combustion using hot residuals only, and there is enough exhaust dilution to prevent knocking combustion. The knock and misfire limits tend to converge in this region because of the rapid increase in combustion instability. In order to enlarge the 'practical' region of CAI it is necessary to shift the knock region to the left and the misfire region to the right. While it may be possible to do this through optimisation of the fuel blend, it can be asserted that the stratified residual approach already achieves this in a clever way.

Because the residuals are stratified, the fresh charge is initially exposed to a much lower concentration of residuals than would be the case if the cylinder contents were homogeneous. Also, at the charge/residual boundary the temperature is much higher because the residuals are concentrated in one area of the combustion chamber. So, ignition probably occurs when the charge composition is shifted left of the knock boundary. If combustion were to occur in a homogeneous manner in the same way as shown here, knocking combustion would ensue. However, the residual stratification also sets up temperature gradients that cause combustion to propagate, slowing the heat release rate and avoiding the high rates of pressure rise that lead to knock. Propagating CAI combustion was clearly demonstrated for the first time by Zhao et. al. [87], when they employed the residual stratification technique. Residual stratification also allows much higher global EGR rates, since locally the charge dilution is much lower. This allows more heat to be trapped in-cylinder, facilitating autoignition. Under these conditions the misfire limit is shifted to a higher global EGR rate, and the region of satisfactory combustion attained at close-to-stoichiometric conditions is extended considerably.

6.4.3.3 Rate of Pressure Rise

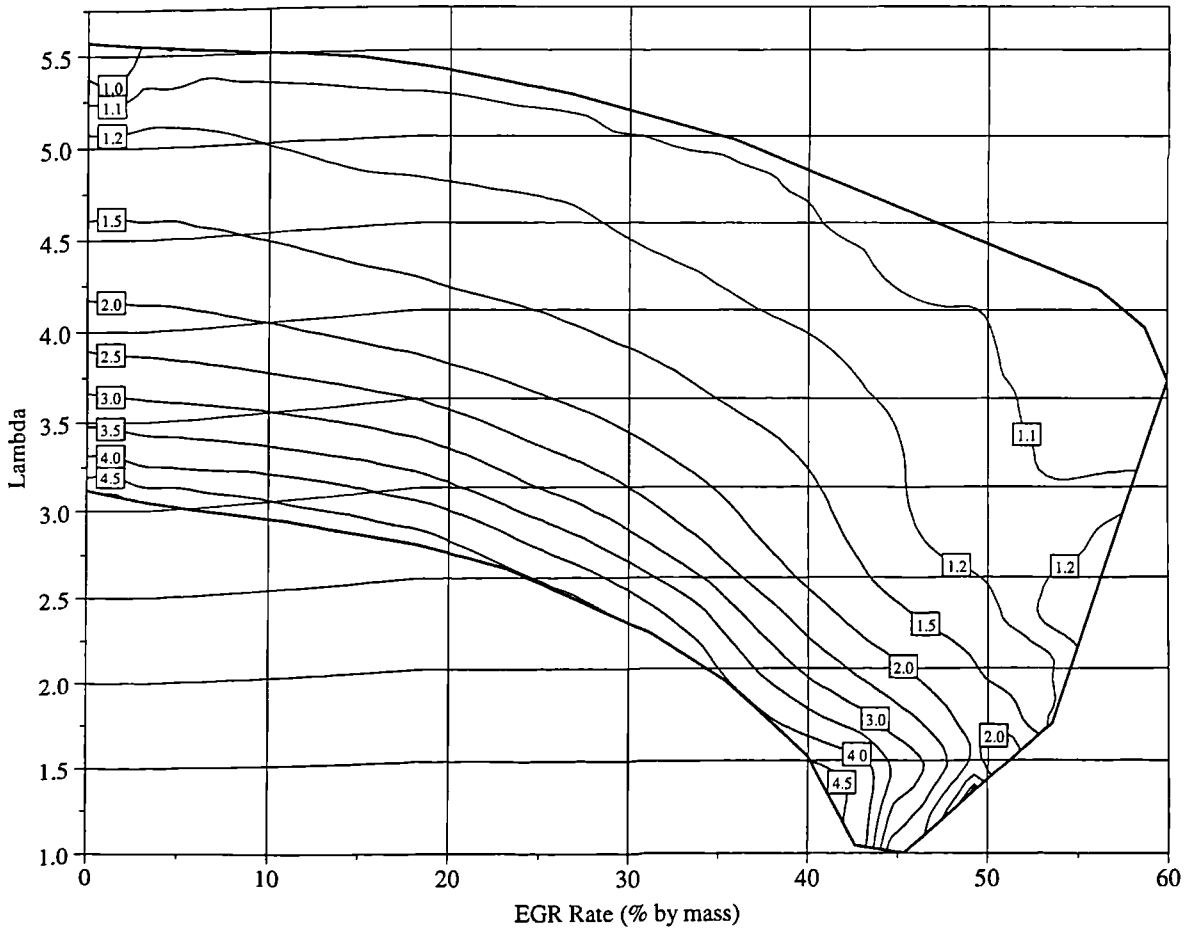

Figure 6.10 Maximum Rate of Pressure Rise (bar) for Standard Gasoline

The cylinder pressure data was post-processed to determine the maximum rate of pressure rise that occurs during combustion over the dilution ranges. The results of this analysis are presented in Figure 6.10. It is interesting that the isolines on this diagram appear to run parallel to the knock boundary for all A/F ratios and EGR rates. This would indicate that it is the value of pressure rise rate that determines whether the combustion causes engine knock. If the pressure rise rate exceeds 4.5-5.0 bar/°CA, then the DAQ system records 10% KOF at a filtered pressure threshold of 0.5 bar. Once again, the pressure rise rate is seen to fall rapidly as EGR is increased under stoichiometric conditions, showing that the inert species contained in the EGR have a profound effect on the heat release rate in this region.

6.4.4 Exhaust Gas Measurements

6.4.4.1 Exhaust Gas Temperature

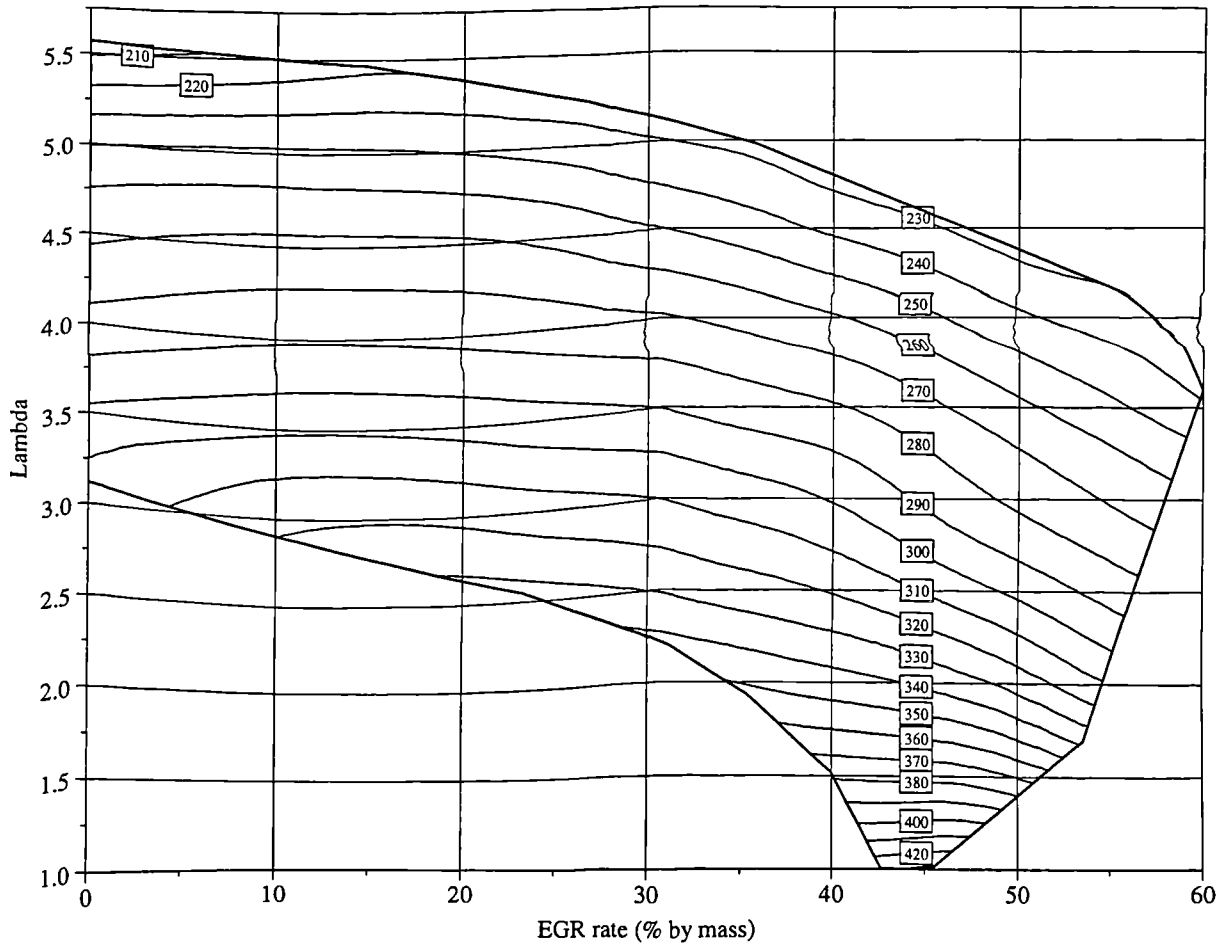

Figure 6.11 Exhaust Gas Temperatures (°C) for Standard Gasoline

Figure 6.11 shows the exhaust gas temperature trends with dilution, measured in degrees centigrade. Temperatures are much lower than those found in SI combustion, with minimum and maximum values of 200°C and 440°C respectively. Trends show that exhaust gas temperature scales approximately with engine load at moderate to high EGR rates. However, at low EGR rates (0-10%), temperatures are comparatively reduced. This effect cannot be attributed to changes in combustion timing or duration since they are relatively small over the 0-30% EGR range. Lower combustion efficiency is thought to be the cause, as HC emissions presented in the following section will support.

It is interesting that above lambda values of around 2-3, exhaust gas temperatures fall below the heated intake temperature of 320°C. Low exhaust temperatures are detrimental for two reasons:

(i) For practical CAI combustion, residual temperatures must be high enough to maintain autoignition from cycle to cycle.

(ii) Catalyst efficiencies deteriorate if exhaust temperatures are too low.

For these reasons, the low exhaust temperatures experienced with high rates of air dilution place the most stringent limits on the range in which a practical engine could be operated. Exhaust gas dilution is preferable to air dilution because it maintains higher combustion and exhaust temperatures, despite the detrimental effect of some EGR species on combustion when EGR rates become too high.

6.4.4.2 Exhaust Emissions

AFR	Engine Speed rpm	IMEP bar	ISFC g/kW.h	ISNOx g/kW.h	ISHC g/kW.h	ISCO g/kW.h
14.4	1501	1.5	382.8	1.6	4.7	28.0
14.4	1500	1.9	325.5	6.8	4.2	22.3
14.4	1501	3.2	266.1	10.5	3.0	17.4
14.4	1501	3.7	255.1	11.7	2.2	16.4
14.4	1501	4.3	248.5	13.0	2.3	16.6

Table 6.2 ISFC and Indicated Specific Emissions Taken from a Reference SI Engine (Zetec 1.8L) at a Number of Engine Loads and Using Standard Gasoline Fuel [101]

This section presents the trends in specific exhaust emissions that occur over the air and EGR dilution ranges. Table 6.2 shows the typical indicated specific fuel consumption and pre-catalyst exhaust emissions of a reference SI engine running at a constant speed of 1500rpm. The data was obtained on a production Zetec 1.8L engine, and kindly provided by researchers at the Ford Motor Company as part of their contribution to the 4SPACE project [101]. This data shall be used for comparison against the CAI combustion data, so that relevant conclusions can be drawn as to the benefits and drawbacks of the CAI combustion achieved during this work.

Unburned Hydrocarbon Emissions

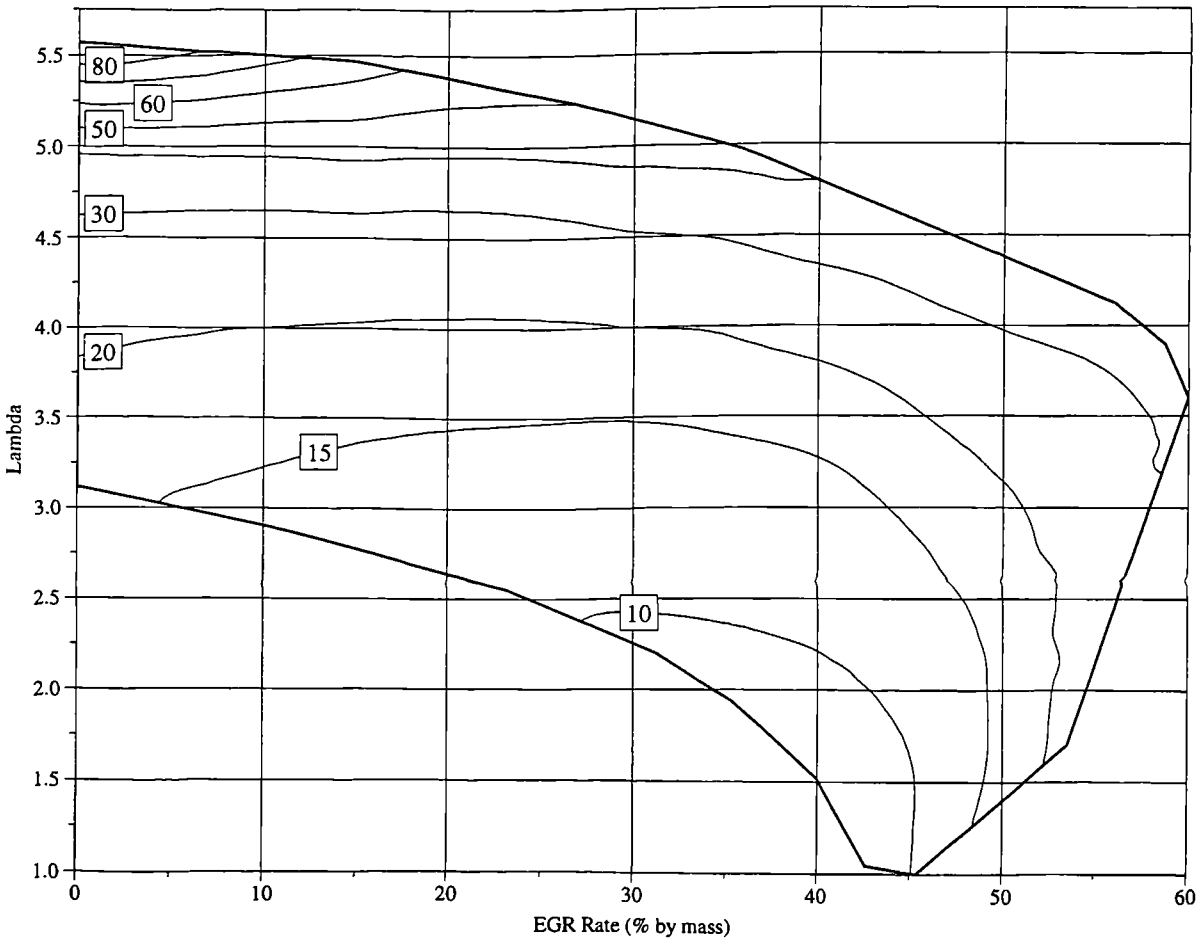

Figure 6.12 Indicated Specific HC Emissions (g/kW.h) for Standard Gasoline

Figure 6.12 shows the unburned HC emissions as measured by the FID analyser. Emissions are minimum at the highest load point (lambda 1.0, EGR rate 43%). As lambda is increased from this point, the emissions also increase. Emissions are highest when the air dilution is maximum, with no EGR. The reasons for these trends are threefold:

(i) A reduction in load is achieved by decreasing the fuel rate. Thus, the total heat release and average combustion temperature are also reduced. The charge spends less time at high temperature, which results in more incomplete combustion and higher HC emissions. This point is illustrated in Figure 6.15, where a reduction in load leads to a lower combustion temperature and higher unburned HC emissions.

(ii) In the region of lambda 3.0–4.5, HC emissions are reduced as EGR is increased from 0-25% (for constant lambda). Exhaust gas temperature trends are raised with increasing EGR rate in this region. The only possible explanation for these trends is that better combustion efficiency is obtained when small amounts of EGR are admitted to the intake manifold, compared to when there is none. This may occur as a result of the EGR containing significant quantities of unburned hydrocarbons, which are recycled and subsequently consumed during combustion.

(iii) At high EGR rates (>40%), combustion timing and duration are retarded and lengthened respectively, due to the high concentrations of inert species in the intake charge. A long combustion duration in particular contributes to higher HC emissions, since the maximum in-cylinder temperature is reduced. In addition, higher specific emissions are observed as a result of the comparatively lower loads achieved (for constant fuelling) when the timing is retarded and the combustion duration increased. These two effects are clearly shown in figure 6.13. In this figure, in-cylinder gas temperatures for EGR conditions of 32% and 51% are compared under constant fuelling conditions. Increasing the EGR results in retarded ignition and longer combustion duration, which lowers the IMEP from 2.37 bar to 2.22 bar, and lowers the peak combustion temperature by approximately 150K.

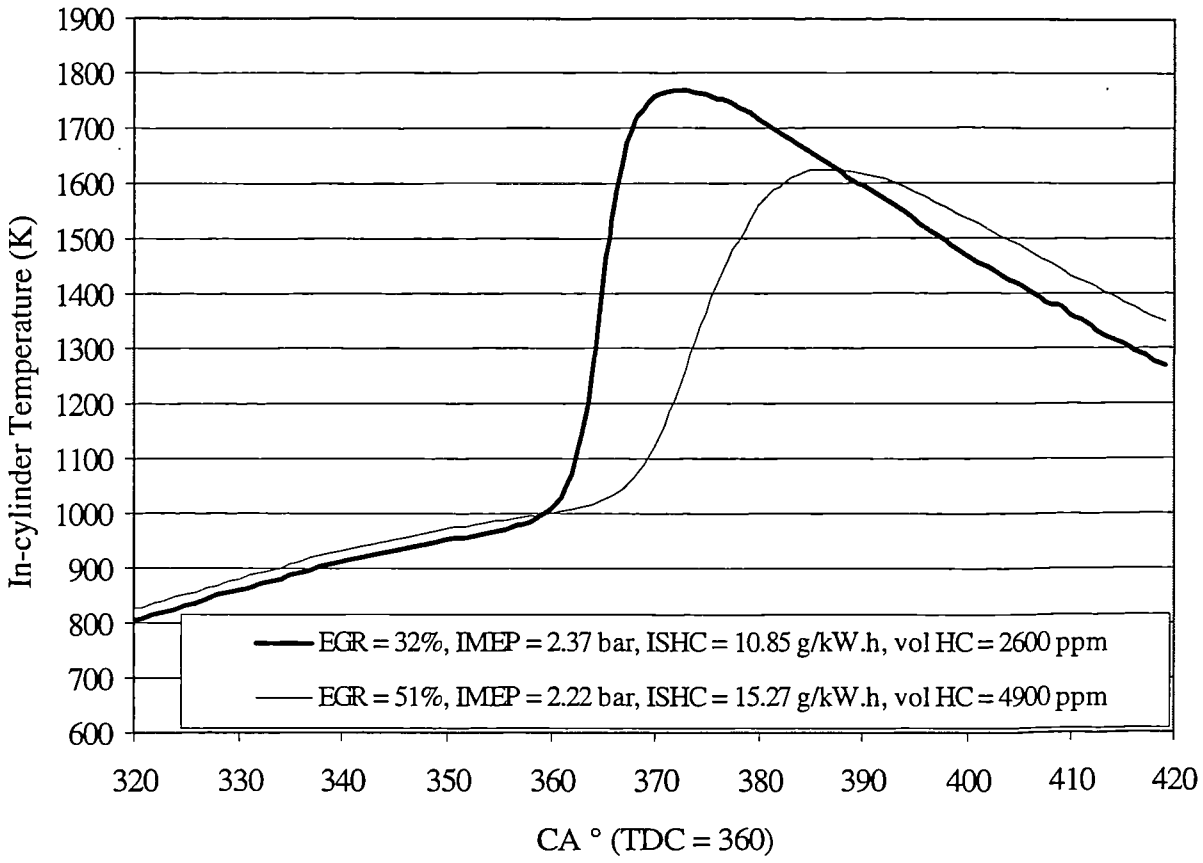

Figure 6.13 In-cylinder Charge Temperature (K) for two EGR conditions with Constant Fuel Rate (7.42 mg/cycle)

Comparable unburned HC emissions for SI operation given in Table 6.2 range from approximately 4.7 g/kW.h at low load (1.5 bar IMEP) to around 2.2 g/kW.h at the highest load attainable here (3.8 bar IMEP). Unburned HC emissions for gasoline CAI combustion exceed these values over the entire region. This represents one of the major drawbacks of CAI combustion. However, a standard oxidation or 3-way catalyst can be used effectively to remove most unburned hydrocarbons, providing exhaust gas temperatures are high enough.

NO_x emissions

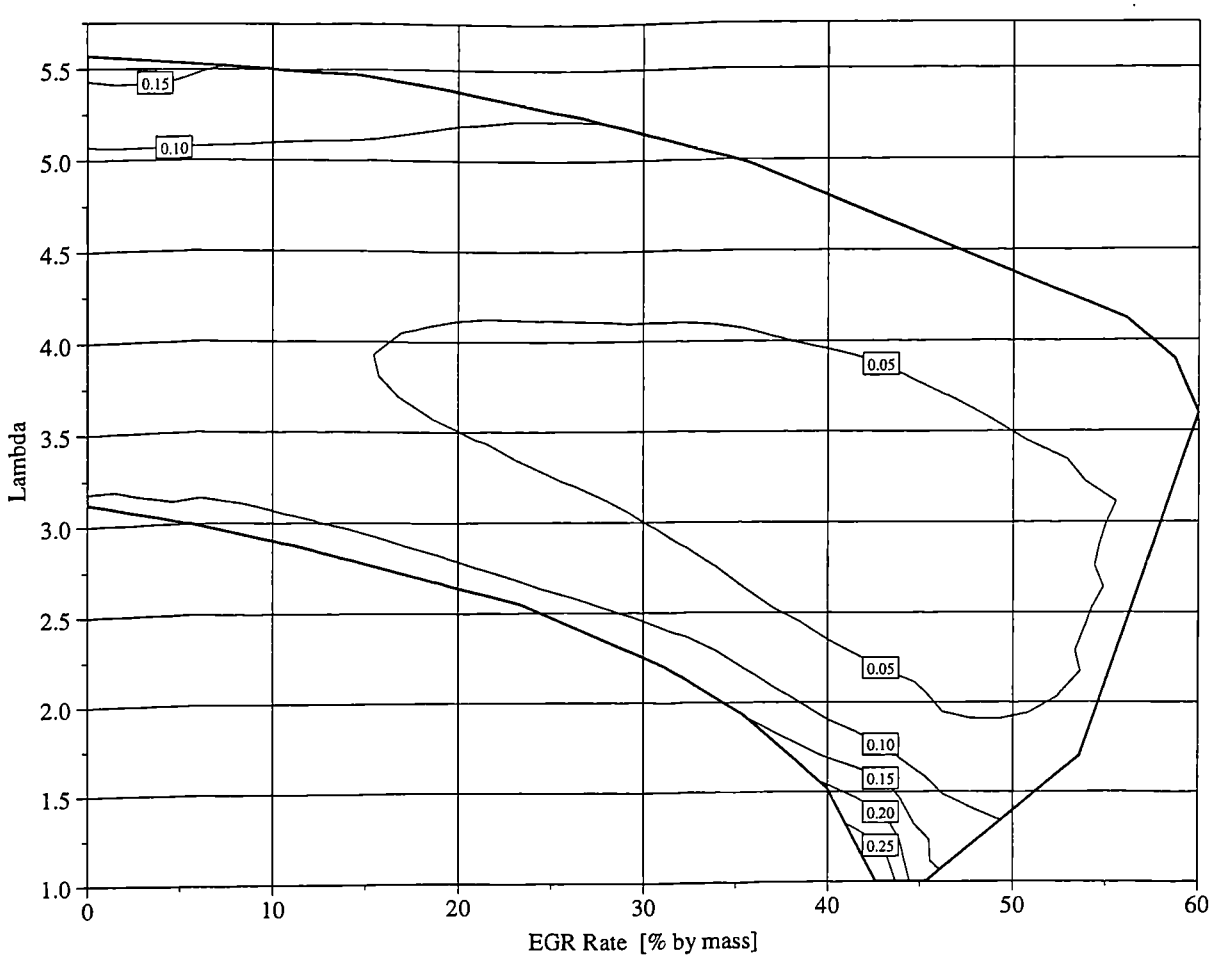

Figure 6.14 Indicated Specific NO_x Emissions (g/kW.h) for Standard Gasoline

NO_x emissions of a SI engine operating under comparable conditions range from 1.6 g/kW.h (at 1.5 bar IMEP) to around 12 g/kW.h (at 3.7 bar IMEP), scaling approximately with engine load. Figure 6.14 shows the NO_x emissions map generated for standard gasoline CAI combustion. As expected, NO_x emissions are highest as conditions approach the knock boundary, increasing further along this boundary as lambda is decreased to 1.0. Thus, NO_x emissions peak with load at approximately 0.3 g/kW.h. This represents a 97% reduction in emissions compared to SI operation under similar conditions.

Trends also show an increase in NO_x emissions at low EGR rates and high air dilution. This effect is attributable to extremely poor combustion efficiency in this region. Since specific emissions are highly dependent on the relative difference between fuel consumption and power output, higher specific NO_x emissions result if combustion is poor.

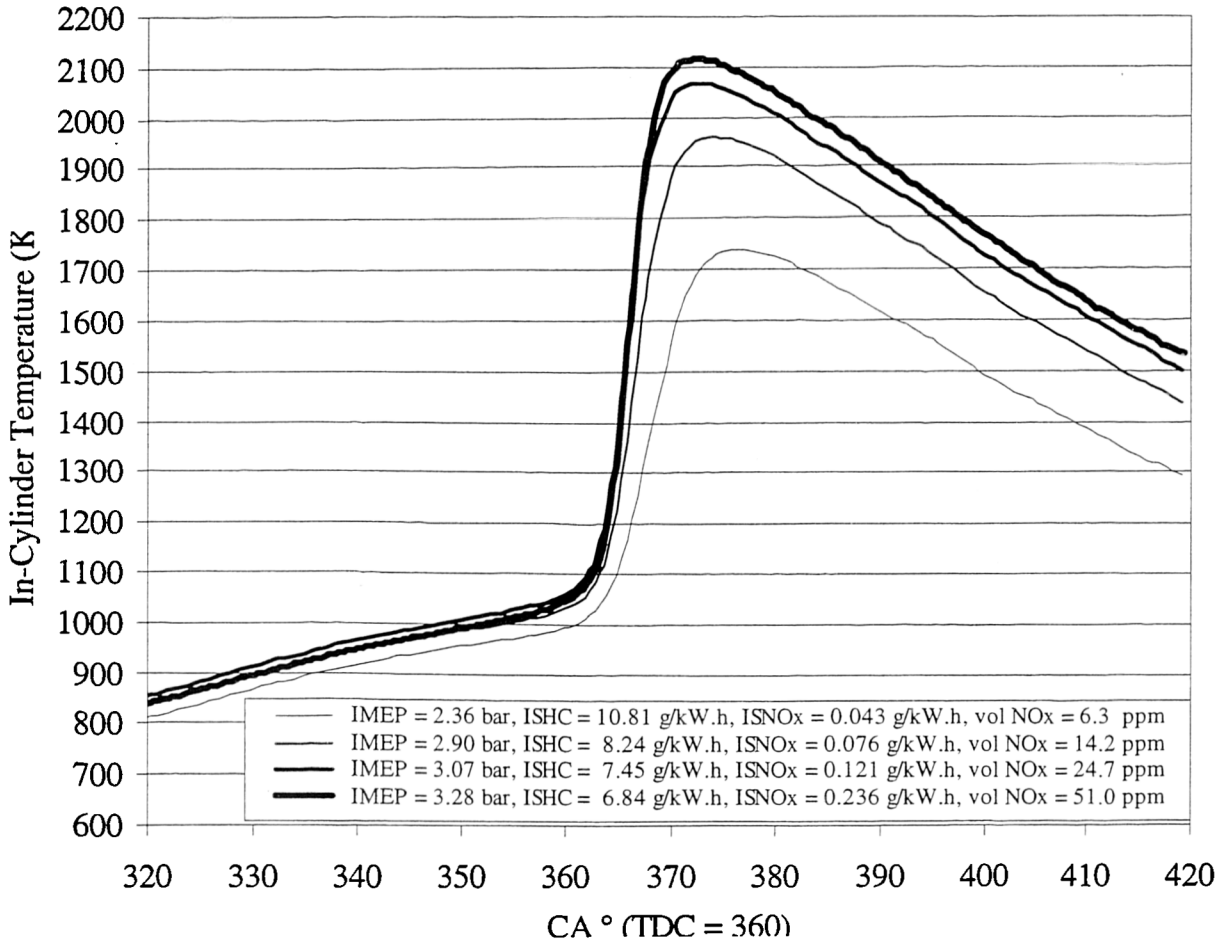

Figure 6.15 In-cylinder Charge Temperatures (K) for Four Load Conditions with Similar EGR Rates (40%)

An explanation for why the NOx emissions from CAI combustion are so low arises when one considers the in-cylinder gas temperatures during combustion. The in-cylinder NOx formation rate is known to be strongly dependant on oxygen availability and temperature. As local in-cylinder temperatures approach and exceed 1800 K, the kinetic reaction rates for NOx species increase exponentially. In SI and CI combustion regimes, the temperature of the thin-walled flames that govern combustion are normally in the range 2000 – 3000 K, well above that required for significant NOx formation. However, by the nature of homogeneous CAI combustion, the temperature throughout the cylinder contents is equal over the whole cycle (ignoring boundary effects). Thus, there is an absence of the single hot reaction zone seen in SI and CI combustion processes. In a homogeneous combustion process, it is only when the entire cylinder contents are raised above 1800K that significant NOx emissions are observed. This point is illustrated in Figure 6.15, which shows the in-cylinder gas temperatures for four different engine loads, all with similar EGR dilution rates. For the lowest load case, the concentration of NOx species in the

exhaust is 6.3 ppm, barely above ambient levels. However, as load is increased and peak cycle temperatures rise above 1800K, NOx emissions also increase.

CO Emissions

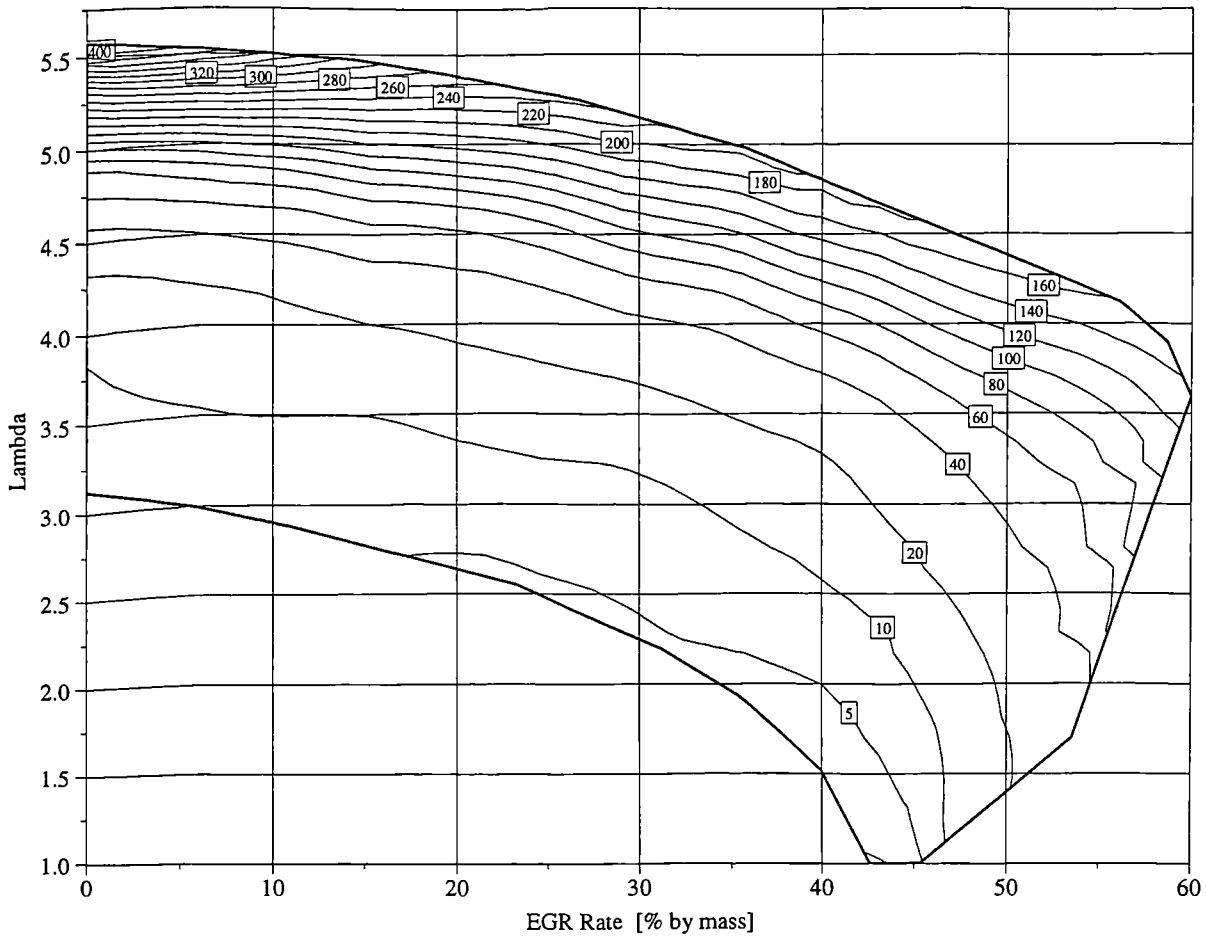

Figure 6.16 Indicated Specific CO Emissions (g/kW.h) for Standard Gasoline

Figure 6.16 shows the indicated specific CO emissions for the attainable gasoline CAI region. Clearly, CO emissions increase monotonically with distance from the knock boundary. This is a further indicator that partial combustion occurs more at higher air and EGR dilution rates. Comparable CO emissions for SI combustion under these operating conditions are approximately 28 g/kW.h at 1.5 bar IMEP, decreasing to 16.5 g/kW.h at approximately 4 bar IMEP. There is a large region close to the knock boundary where CAI combustion produces much lower emissions than SI combustion under equivalent load. In this region and at the highest load point (lambda 1.0, EGR rate 43%) CO emissions reach a minimum of 2 g/kW.h, representing a reduction of around 88 % on the SI combustion values.

However, since low loads are desirable in a CAI combustion mode (to eliminate pumping losses), CO emissions become important. Idling loads can only be achieved under high dilution conditions, and in the case of homogeneous CAI combustion, only with high air dilution. Under those conditions CO emissions can exceed 300 g\kW.h, indicating that ultra-lean combustion is not a desirable way to achieve low loads because of the massive reduction in combustion efficiency that occurs. If using air dilution is not desirable for low load and idle operation, and misfire prevents homogeneous EGR from providing the required dilution, then another method is required to achieve idling conditions. Residual stratification techniques achieve low load by maintaining extremely high global residual rates, while the combustible region of the charge is only subject to moderate residual rates. However, these techniques have not yet been developed sufficiently to allow idle CAI operation because residual temperatures fall too low when the fuelling is reduced excessively. Thus, to achieve idle at lower engine speeds, it may be necessary to formulate more suitable fuels, or provide a small degree of additional charge heating either locally in-cylinder, or globally in the intake manifold.

Indicated Specific Fuel Consumption

ISFC is used as an indicator of CO_2 emissions, and measures how efficiently the engine uses fuel to do useful work, not including frictional considerations. Figure 6.17 shows the ISFC map for the attainable CAI region. As with other parameters, ISFC is minimum at the highest load point, at a value of approximately 200 g/kW.h. So, fuel consumption is reduced to a minimum when both HC and CO emissions are at their lowest values, and the exhaust gas temperature and NO_x emissions are highest. Once again, it is interesting that ISFC trends seem to bear little relation to the combustion heat release profiles. At the highest load point, ignition timing is retarded to 6 °CA ATDC, and combustion duration as long as 15 °CA, which both would be considered less than optimal.

Comparable ISFCs for the reference SI engine range from around 330 g/kW.h (at 1.25 bar IMEP) to 250 g/kW.h (at 4 bar IMEP), primarily as a result of reduced pumping losses in this range. Therefore, at best a 20% reduction in fuel consumption and CO_2 emissions is achieved for similar load and speed.

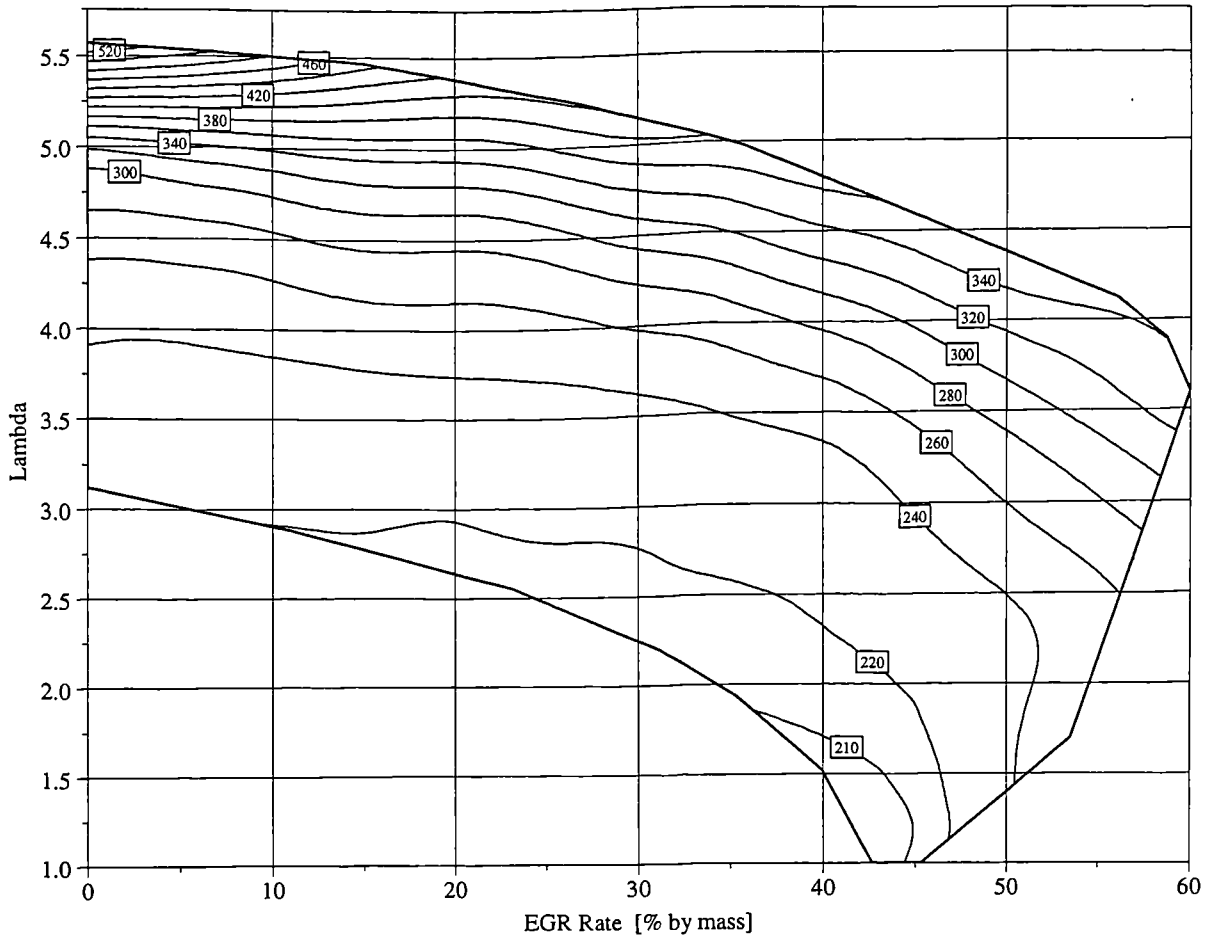

Figure 6.17 Indicated Specific Fuel Consumption (g/kW.h) for Standard Gasoline

However, ISFC for CAI combustion increases dramatically with air dilution, further reinforcing trends for HC and CO. Under low load, highly (air) diluted operation, the CAI combustion appears to show little or no improvement in fuel consumption over SI combustion, since the CAI combustion efficiency is seriously affected. These results lend further weight to the argument that excessive air dilution is not desirable for achieving low load operation.

6.5 Summary of Results

Review of the relevant literature has revealed a deficiency of detailed research pertaining to the combined EGR and air dilution effects on CAI combustion, despite recent developments using stratified residual gas strategies. This has provided the basis for a parametric study of the dilution effects on gasoline CAI combustion, looking at a wide range of combustion and emissions parameters. The measured variables have helped to define the acceptable CAI combustion operating region, highlighted differences between the homogeneous and stratified recycled gas approaches, and precisely defined the

advantages and disadvantages of homogeneous CAI combustion compared to normal SI combustion. Specifically, the results can be summarised as follows:

(i) Under the conditions chosen, CAI combustion was attained up to A/F ratios of 80:1 and EGR rates of 60%.

(ii) The region is bounded on three sides by the knock, misfire, and partial burn regions. Knock occurs when either the air or EGR dilution rates are too low to prevent excessive heat release. If the pressure rise rate exceeds 4.5-5.0 bar/°CA, then knocking combustion ensues. At high EGR rates, the increase in inert species retards ignition beyond acceptable limits, causing misfire in a small proportion of cycles. When excessive air dilution is used, CO and HC emissions levels rise dramatically, as does the ISFC. These parameters indicate that partial combustion occurs in this region, which is an undesirable effect.

(iii) The Combustion timing does not change significantly with increased air dilution, whereas its duration is lengthened monotonically. EGR dilution tends to retard ignition and increase combustion duration. The rates of change of timing and duration with EGR rate are highest when the charge composition is close-to-stoichiometric. This leads to an inherent instability in this region, since small changes in EGR rate can lead to large changes in the heat release profile.

(iv) Autoignition temperatures show some relationship with ignition timings. It appears that a close-to-stoichiometric charge moderately diluted with EGR loses less temperature during induction, and requires a higher temperature for autoignition. Conversely, a lean charge loses more temperature during induction, and requires a lower temperature to achieve autoignition.

(v) Despite conventional thinking, the heat release profiles do not seem to have strong relationships with important parameters such as IMEP and ISFC. However, combustion stability does seem to rely on reasonable combustion phasing and duration.

(vi) The ISFC can be improved by up to 20% compared to SI combustion, occurring under moderate load conditions (3.8 bar IMEP). The expected low-load

improvement in ISFC for CAI combustion was not materialised due to reduced combustion efficiency under high air dilution conditions.

(vii) Unburned hydrocarbon emissions are always at least twice those found from equivalent SI combustion, and under highly diluted conditions they are significantly worse. This problem is compounded by the low exhaust gas temperatures, which would tend to reduce the effectiveness of exhaust aftertreatment systems. Unburned HC emissions result from usual sources such as crevice volume and boundary layer quenching. However, further causes of unburned HC emissions have been identified, including:

1. High dilution leads to a reduced peak cycle temperature. At lower temperatures, kinetic reaction rates are reduced and the charge is eventually 'frozen'.
2. High dilution leads to retarded combustion. For similar fuelling conditions, retarded combustion tends to produce a lower load. This transfers directly to higher specific emissions.

(viii) As expected, NO_x emissions are highest when the load is highest. However, a reduction of approximately 97% over conventional SI combustion is still gained under these conditions. Analysis of the in-cylinder temperatures for various load conditions confirmed that CAI combustion generally produces low NOx because of its homogeneous nature; a shared global in-cylinder temperature ensures that reasonable loads can be attained without any part of the charge exceeding the minimum temperature for NOx formation (~1800 K) up to loads of about 2.5 bar IMEP at 1500 rpm. At higher loads NOx formation is observed, but emissions levels stay well below the equivalent SI values.

Chapter 7

Fuel Effects on CAI Combustion

Chapter 7 Fuel Effects on CAI Combustion

7.1 Introduction

There have been many studies documenting how CAI combustion is affected by changing the fuel composition. While the study by Duret and Lavy [86] was the most comprehensive of these, it failed to present a detailed account of their experimental approach and results, leaving the reader to accept their qualitative analysis. Christensen et al. [68, 82, 83] presented some detailed work investigating the heat release and emissions characteristics of several fuels including PRFs, natural gas, mixtures of commercial diesel and gasoline, and ethanol. While they presented insightful analyses, the majority of differences occurring between fuel types were explained in terms of the different charge temperature and pressure histories, resulting from varying intake charge temperatures and compression ratio to achieve fixed combustion phasing. Thus, they had difficulty separating fuel, dilution, and temperature effects explicitly.

The experimental approach used for gasoline fuel in the previous chapter was selected so that dilution effects could be determined with no interference from other engine operating conditions. In a similar fashion, if one wishes to study fuel effects only, then different fuels must be tested in exactly the same way as the gasoline was. The original conditions chosen for the gasoline tests (Tin = 320 °C, Rc = 11.5) were selected so that CAI combustion could also be achieved with a wide selection of other fuels. The range of fuels under investigation can be broadly divided into three types:

7.1.1 Primary Reference Fuels

Primary Reference Fuels (PRFs) comprise mixtures of isooctane (2-2-4 Trimethylpentane) and n-heptane, and are used to benchmark the autoignition resistance of automotive fuels for use in SI engines. A number of PRFs including 80, 90, 95, and 100 RON are tested over their attainable air and exhaust gas dilution ranges during the following tests. Detailed analysis should provide information on the effects of changing fuel octane on CAI combustion characteristics.

7.1.2 Gasoline Fuels

Light and heavy fraction fuels produced using the fuel fractionating system are tested. Unlike the SI tests detailed in chapter 5, the light fraction has been stored in liquid form as per section 5.2, and is injected in a similar way to all other fuels in these tests. This method has been selected so that the quality of operation of the fuel fractionating system does not affect the CAI combustion results in any way. Investigation of the light and heavy fractions will provide information on the following:

(i) How different blends of gasoline containing varying amounts of paraffins and aromatics perform under homogeneous CAI combustion conditions. This will give insight into how sensitive CAI combustion is to changes in fuel composition that can occur between regions around the world, as a result of varying crude oil processing requirements and techniques.

(ii) Whether the stratified fuel fractions concept can be useful for extending the speed/load operating region over current CAI combustion systems. The properties and composition of the light and heavy fractions are distinctly different, which may result in different attainable dilution ranges.

7.1.3 Alcohol Fuels

Methanol and Ethanol are viable replacements for current automotive fuels. Furthermore, many studies have shown that alcohols have distinctly different and advantageous CAI combustion characteristics when compared to hydrocarbon fuels. Detailed Investigation of the attainable dilution ranges of these alcohols may provide some insight into why they appear to be superior.

7.2 Experimental Technique

The tests on each fuel are carried out in exactly the same way as described in section 6.3 for gasoline. The full range of experimental conditions are summarised in table 7.1. Once again, the full dilution ranges presented cannot be achieved with all the fuels under the fixed conditions chosen. When combustion is observed to deteriorate as a result of misfire,

excessive partial burn, or knocking combustion for each fuel, the attainable ranges are individually defined.

	Parameter		Value
Independent Variables	Fuel		PRF 80, 90, 95, 100 RON, Light Fraction, Heavy Fraction, Methanol, Ethanol
	EGR Rate		0-75%
	A/F Ratio (Lambda)		1.0-8.25
Fixed Conditions	Engine Speed	(rpm)	1500
	Compression Ratio		11.5:1
	Intake Manifold Pressure	(bar)	0.93 absolute
	Intake Charge Temperature	(°C)	320
	Coolant Tempretaure	(°C)	80
	Oil Temperature	(°C)	55
	Injection Timing	(°CA)	79 BTDC Compresion Stroke

Table 7.1 List of Experimental Parameters for CAI Combustion Tests of Various Fuels

7.3 Discussion of Results

This section contains a predominantly qualitative discussion of the trends and differences that occur between different fuels and fuel types. Since there are a total of nine fuels under discussion for any one combustion or emissions characteristic, the figures have not been included with the text in this chapter. Instead, all figures are presented at the end of this chapter.

7.3.1 General Characteristics

Figures 7.1 to 7.9 show the number of data points taken for each fuel, and the dilution ranges over which they are taken. The knock, misfire, and partial burn regions discussed in chapter 6 are clearly in evidence for each fuel, with only one exception. When methanol is subjected to extreme homogeneous EGR rates (70-80%), it is not forced into misfire as all the other fuels are. Instead, it exhibits rapidly increasing partial burning, as CO and HC trends will reinforce. Reasons for this shall be given in later sections.

7.3.1.1 Partial Burn Regions

The air dilution to cause excessive partial burning varies greatly between different fuel types. The PRFs exhibit the most restrictive boundaries, followed by the gasolines, and then the alcohols. In the case of methanol, the partial burn boundary extends all the way from lambda 8.25, EGR rate 0% to lambda 1.0, EGR rate 70%, with the absence of the misfire region. Ethanol exhibits similar characteristics, although the trends are not as explicit. The alcohols are much more tolerant to both air and EGR dilution, indicated by their much wider operating regions.

7.3.1.2 Misfire Regions

The misfire boundaries for the three gasolines are similarly placed, indicating that despite their compositional differences, EGR affects combustion in a similar way for each. Considering the PRFs, the 80 RON PRF exhibits a higher tolerance to EGR than the 100 RON PRF, since higher EGR rates can be achieved prior to misfire. As explained already, methanol fuel never misfires despite extremely high EGR rates (>70%). Ethanol does exhibit misfire under close-to-stoichiometric conditions, but the EGR rates at which it occurs are vastly higher than for the hydrocarbon fuels.

7.3.1.3 Knock Regions

Figures 7.10 to 7.12 present the superimposed knock boundaries (10% KOF) for the gasoline fractions, PRFs, and alcohols respectively. While the knock boundary exists for every fuel tested, only the gasoline fractions (light, heavy and standard) exhibit similar knocking tendencies under these conditions. All of the PRFs exhibit a higher resistance to knock than the gasoline fuels, whereas the alcohols exhibit the lowest resistances among the fuels tested. So, not only do the gasolines not exhibit similar knock resistances to the PRFs having a similar octane rating, but also they appear to show higher knock resistance than the alcohols, which possess much higher RONs and MONs. Clearly, the propensity of a general fuel type to cause knocking combustion under these engine conditions has little or no relationship with its octane quality, as Duret and Lavy [86] also found in their two stroke studies.

The gasolines exhibit very similar knocking tendencies over a wide range of air and EGR dilution, despite having dissimilar octane qualities and composition. On the negative side, this shows that the stratified fuel fraction concept may not facilitate CAI combustion at high load operation, as is the case with gasoline fuels used today. However on the positive side, the difference in composition between the light and heavy fractions yields a similar knocking tendency, indicating that the fuels have more in common than not. Thus, differences in gasoline composition that occur across world markets are unlikely to affect how a CAI combustion system is calibrated for fuel. This subject is worthy of further attention, and shall be addressed in more detail later in this chapter.

Despite the lack of a direct relationship between RON and knocking combustion for most fuels tested, a trend does exist among the PRFs. Figure 7.11 shows that as the octane value is reduced, the air dilution required to avoid knocking combustion increases. In a similar fashion, as the octane value is reduced, the EGR dilution required to avoid knock increases. These trends are fundamentally controlled by the difference in oxidation kinetics between isooctane and n-heptane. Analysis of the heat release rates for each fuel in this region may provide further understanding of why the fuels behave differently.

7.3.2 Heat Release Analyses

7.3.2.1 Ignition Timing

The ignition timing trends for each of the nine fuels are presented in Figures 7.13 to 7.21. Considering the gasoline fractions (Figures 7.13 to 7.15), it is clear that they behave almost identically. Not only are the trends the same for each, but also the timings are almost numerically equal for any air or EGR dilution rate. This result is curious given the pronounced compositional differences between light and heavy fractions (Table 5.1), and their distinctly different spark-induced knocking combustion characteristics shown in Chapter 5.

Trends for the PRFs are shown in Figures 7.16 to 7.19. The timing trends with EGR and air dilution are similar to those of the gasoline fractions: air dilution affects ignition timing at higher EGR rates, when the concentration of oxygen in the intake is increased, and the concentrations of inert species (H_2O, CO_2) are reduced simultaneously. When EGR dilution is relatively low, timing appears to be dependent mainly on the EGR rate. While

this is true for the majority of the dilution range, trends differ significantly close to the knock region. For the PRFs, as the fuelling rate is increased close to the knock boundary, ignition timings rapidly advance. Conversely, the timing of combustion for the gasoline fractions shows little or no dependence on air dilution close to the knock region.

Unlike the gasoline fractions, combustion cannot be achieved under stoichiometric conditions for any of the PRFs. In each case, the knock and misfire limits converge much more sharply at a charge composition leaner than lambda 1.0. At the point where the knock and misfire limits converge, combustion oscillates wildly between 10% KOF and complete misfire. The fact that this can occur for any fuel is of interest, because this effect severely limits the maximum loads that can be attained under CAI combustion conditions. An explanation arises when the differences in timing diagrams between the gasoline fractions and PRFs are examined. The gasolines generally exhibit more advanced timing for a given air and EGR dilution rate. Also, EGR seems to retard timings at a similar rate for both types of fuels. Thus, if the ignition timing for the PRF is comparatively retarded under no EGR conditions, then when EGR is included the misfire limit is reached sooner. Among the PRFs, the ones containing more n-heptane tend to show more advanced ignition timings. Similarly, the misfire and knock limits converge at EGR rates of 37%, 35%, 31%, and 25% for the 80, 90, 95, and 100 RON fuels respectively. This shows that there is a strong relationship between the most advanced timing attainable under no EGR conditions and the highest EGR rate attainable to just avoid knock and misfire.

So, for the gasoline fractions, the temperature and pressure histories of the charge are sufficiently severe to give more advanced ignition timings, and prevent EGR dilution retarding combustion excessively when stoichiometric conditions are sought. Using the same argument, if the pressure and temperature histories of the PRFs were made more severe, then their ignition would occur earlier, and allow stoichiometric combustion to be achieved with moderate EGR rates.

Timing maps for the alcohols are presented in Figures 7.20 and 7.21. The trends are strikingly different from those of the hydrocarbon fuels. In the case of methanol, it would appear that EGR has no effect on ignition timing over the entire map. This result is extremely important because it shows that methanol has a very high tolerance of EGR dilution, making it an ideal fuel for CAI combustion, as other researchers have also found. This is the reason why no misfire region was observed when testing methanol. Increased

air dilution has a relatively weak advancing effect on combustion in the region lambda 1.0-3.0. The Ethanol ignition timings behave in a similar way, but trends with EGR are appreciable. For both of these fuels, ignition timings are much more advanced over the majority of the region than for the hydrocarbon fuels, which shows immediately why their regions are considerably larger. Methanol and ethanol contain 50% and 33% oxygen by mass respectively. It would appear that this oxygen available in immediate proximity to the fuel aids considerably in its autoignition, especially when the charge contains high concentrations of inert species. It would be an interesting exercise to consider the reasons for this in terms of autoignition chemistry.

7.3.2.2 Autoignition Temperature

Autoignition temperature trends for all of the fuels are presented in Figures 7.22 to 7.30. There are slight differences among the gasoline fractions (Figures 7.22 to 7.24), but on the whole trends are similar. Maximum autoignition temperatures always occur in the close-to-stoichiometric region, and range from about 1075 to 1100K. However, while minimum ignition temperatures generally occur in an area slightly rich of the partial burn region, light fraction gasoline exhibits a considerably lower minimum autoignition temperature of around 840 K, compared to the standard and heavy fractions, which show minimums of 950 K and 960 K respectively. So, it would appear that under ultra-lean conditions, the light fraction auto-ignites at the lowest temperatures, followed by standard gasoline, and then the heavy fraction. However, the fact that minimum ignition temperatures occur rich of the partial burn region is slightly puzzling, and cannot be explained satisfactorily. One can only surmise that partial burning has a significant effect on the performance of the combustion equations used to calculate the molar fraction of fuel (a) in the intake charge, which may lead to erroneous results.

Trends for the PRFs (Figures 7.25 to 7.28) are similar to the gasolines, exhibiting maximum temperatures under the richest conditions attainable. However, minimum autoignition temperatures never dip below 975 K for any of the PRFs. Generally speaking autoignition occurs around 975 K to 1050 K for most conditions, which is in agreement with previous work.

The alcohols (Figures 7.29 and 7.30) show similar trends to the hydrocarbon fuels. As already discussed, the knocking combustion boundary for these fuels occurs at

considerably higher (air and/or EGR) dilution than for the hydrocarbon fuels. This would suggest that for the intake temperature conditions chosen, the alcohols are more easily forced into autoignition, and the autoignition temperature should be comparatively lower. However, the results presented here suggest the opposite. Ethanol autoignition temperatures range from 1040 K to 1160 K, approximately 100 K higher than those for standard gasoline. Minimum and maximum autoignition temperatures for methanol are comparable to gasoline's at 960K and 1075K respectively, over the attainable range for gasoline. However, the maximum autoignition temperatures for Methanol occur under close-to-stoichiometric conditions at very high EGR rates, and approach 1400K!

To further investigate these phenomena, charge temperatures at IVC have been calculated, and presented in Figures 7.31 to 7.39. For the gasoline fuels (Figures 7.31 to 7.33), maximum IVC temperatures occur at close-to-stoichiometric conditions, and are in the region of 250°C to 260°C, which is realistic for a port charge temperature controlled to 320°C. Considering the PRFs (Figures 7.34 to 7.37), IVC temperatures appear to be in general agreement excepting two cases:

(i) For the 80 RON PRF, as stoichiometry is approached, the IVC temperature increases to around 260°C, which is 30°C above any of the others in this region.
(ii) The 100 RON PRF exhibits significantly lower IVC charge temperatures than the other PRFs, in the order of 10°C to 40°C.

These discrepancies are of concern because the convective coefficient that governs heat transfer from the charge during the induction process should be equivalent for all of the PRFs for a given air and exhaust gas dilution rate, which should lead to similar IVC temperatures. In both cases, it is conceivable that a slightly erroneous injector calibration could cause the changes in IVC temperatures observed. However, the calculated IVC temperatures lead to higher calculated autoignition temperatures for the 80 RON PRF, and lower autoignition temperatures for the 100 RON PRF. This is particularly problematic because the autoignition temperature for n-heptane is known to be some 200 K lower than that for isooctane, in direct contradiction to the results presented here.

Further problems arise when one considers the alcohol fuels' IVC charge temperatures (Figures 7.38 and 7.39). As for all fuels, the autoignition temperature trends follow the IVC charge temperature trends closely, showing little regard for ignition timing. For both

ethanol and methanol, there are regions (when EGR rates are very high) in which the calculated IVC charge temperature exceeds the temperature measured in the intake port (320°C). In the case of methanol, temperatures reach in excess of 440°C, a full 120°C increase between the top and bottom of the induction stroke! The only explanation for these results is that a significant heat release occurs during induction, which partially burns some of the fuel, and raises the charge temperature. This is conceivable because the intake temperatures are initially so high. A mechanism such as this would also explain why the 80 RON PRF exhibits higher IVC temperatures than PRFs containing less n-heptane, because n-heptane is more reactive than isooctane at lower temperatures. However, if a fuel is prone to heat release at relatively low temperatures, then why does it then require much higher temperatures to achieve autoignition? Results from the analysis of autoignition temperatures for the PRFs and alcohol fuels are difficult to explain, and since the same technique was used for the gasoline fuels as well, the same question is asked for all of the fuels tested here.

To determine if the calculation technique was in error, a completely separate method was developed for the calculation of n_t, the number of moles trapped in cylinder at IVC. This uses the relationship

$$n_t = \frac{m_t}{\tilde{m}_t} \qquad \text{Equation 7.1}$$

where m_t is the mass trapped *in-cylinder*, which can be found from knowledge of the A/F ratio, EGR rate, and the fuel flow rate. $\tilde{m}_t$ is its molecular weight of the intake charge, found from application of combustion Eqaution 3.17. However, when this analysis was undertaken, the calculated number of moles was exactly the same as before, for all fuels and under all conditions. This has assured the validity of either method to calculate the trapped number of moles, which leaves either the combustion calculations (Equation 3.17), or the analyser measurements of individual species as possible causes for error.

The Richard Oliver K650 analyser is used to measure concentrations of O_2, CO_2, and CO. The analyser was used according to the manufacturers instructions, and they have assured that there are no issues regarding the accuracy of measurement for different fuel types. The THC analyser uses the FID technique, which is known to vary in accuracy depending on

the type of fuel being tested (see Table 3.1). However, a short investigation using the combustion equations (Equation 3.17) showed that if the volumetric concentration of unburned HCs in the exhaust is doubled (from 2500 ppm to 5000 ppm), this changes the number of trapped moles calculated by approximately 2%. Thus the calculations are relatively insensitive to unburned HC concentration, and the accuracy of the FID technique for particular fuels is inconsequential.

As part of the measurement system commissioning, the calculations for A/F ratio were checked against outputs from both the Richard Oliver K650 analyser, and a UEGO device. Under stoichiometric conditions, all three techniques were in close agreement to within a few percent. As conditions are leaned, differences between the calculations and the UEGO device increased to a maximum of around 10% under ultra-lean conditions (λ = 5-6). However, problems with the autoignition temperature analysis arise under close-to-stoichiometric conditions, where the three techniques are in general agreement for the calculation of A/F ratio, so it is unlikely that the combustion equations are to blame for the effects observed.

In summary, the autoignition temperature results using the ideal gas law and detailed combustion equations are inconclusive. Generally speaking, the analysis provides reasonable data, which is comparable to previous work. However, there are specific conditions that appear to show unrealistic autoignition and IVC charge temperatures. Further investigation is required, using more suitable techniques such as Laser Raman Scattering, which would allow for the direct measurement of in-cylinder gas temperatures.

7.3.2.3 Combustion Duration

Combustion duration charts for each of the fuels are presented in Figures 7.40 to 7.48. Once again, trends for the gasoline fractions (Figures 7.40 to 7.42) are almost identical, both qualitatively and quantitatively. Durations are lowest along the knock boundary, reaching a minimum when no EGR is used. Under close-to-stoichiometric conditions, durations increase rapidly with EGR rate, supporting results from the previous chapter.

The PRFs (Figures 7.43 to 7.46) show similar trends to the gasolines, with combustion durations increasing with air dilution at low EGR rates. This trend is reversed at high EGR rates for reasons already explained. For all of the hydrocarbon fuels, the combustion

duration isolines tend to converge as stoichiometry is approached. However, it is notable that the isolines for the PRFs containing more n-heptane are progressively less dense in the high load regions of each map. This is further indication that the lower octane PRFs are more tolerant to increasing EGR under the conditions chosen.

This time the trends for the alcohol fuels (Figures 7.47 and 7.48) are much more like those observed for the hydrocarbon fuels. When EGR rates are low, combustion duration is dependent mainly on air dilution. However, as the EGR rate increases beyond about 40%, the durations eventually become entirely dependent on the EGR rate. It is notable that the duration trends with air dilution at high EGR rates are not in evidence for methanol as they were for the hydrocarbon fuels, while the ethanol durations only show a weak relationship with air dilution in this region. This is further evidence that the combustion of alcohols under high EGR conditions is not sensitive to oxygen concentration in the intake gas, probably because a large proportion of the oxygen used for combustion occurs naturally in the fuel.

7.3.3 Engine Load and Combustion Variability

7.3.3.1 IMEP Considerations

Trends in IMEP for all of the fuels are shown in Figures 7.49 to 7.57. Trends appear to be very similar for all fuels, despite their vastly different heat release profile trends. This adds further weight to the argument that the engine load shows very little dependence on combustion phasing or duration, but is a strong function of fuelling rate. Highest loads are obtained by the gasoline fractions under stoichiometric conditions, each at around 3.8 bar IMEP. The PRFs exhibit lower maximum loads because stoichiometric combustion is not possible. However, the maximum attainable load does increase with octane, since the higher octane fuels require less air and/or EGR dilution to prevent knocking combustion. Thus, the maximum load seen for the 100 RON PRF approaches that of the gasolines, despite lean operation. The maximum loads attainable for the alcohols are also reduced compared to the gasolines, at 3.6 and 3.4 bar IMEP for ethanol and methanol respectively. Loads are limited because the air and/or exhaust gas dilution required to inhibit knocking combustion is higher than that for the gasolines. Fundamentally this can be attributed to more advanced autoignition timing and faster subsequent heat release of the alcohols.

Low loads are achieved when the air dilution rates are very high. The very large regions exhibited by the alcohols mean that they are much more suited to excessive air dilution. The required idling load of modern production engines is somewhere in the region 0.6-0.9 bar IMEP. These values sit comfortably in the methanol CAI region, giving further indication that it is the most suitable fuel of the ones tested here. Under those load conditions, the hydrocarbon fuels are beginning to exhibit high degrees of partial burning, with accompanied losses in combustion efficiency and increases in fuel consumption.

7.3.3.2 Combustion Stability

COVimep trends for each of the fuels are presented in Figures 7.58 to 7.66. Once again the gasoline fractions (Figures 7.58 to 7.60) exhibit identical trends, as if they were all the same fuel. The limit of driveability (5% COVimep) is exceeded beyond approximately lambda 4, and EGR rates of 40% in each case.

All of the fuels exhibit increasing COVimep with air and EGR dilution. The PRF COVimep trends (Figures 7.61 to 7.64) are also very similar to one another. It is notable that at the highest loads attainable for these fuels, in most cases the combustion stability is already unacceptable. This occurs as a result of the misfire and knock boundaries converging sharply under lean conditions. For these fuels to exhibit stable combustion under high load (stoichiometric) conditions, it would be necessary to increase the intake temperature considerably, so that combustion is less effected by the EGR dilution. The effect of partial burning is particularly noticeable for these fuels; COVimep values rapidly accelerate under high air dilution conditions, especially for the lower octane PRFs.

While the alcohol fuels (Figures 7.65 and 7.66) show similar trends to those of the hydrocarbons, the combustion stability for any given dilution condition is vastly improved. This is most beneficial to combustion under the highest load conditions, where values of COVimep of only 1% and 3% are observed for methanol and ethanol respectively.

7.3.3.3 Rate of Pressure Rise

In the previous chapter, it was asserted that the rate of in-cylinder pressure rise was the most important parameter for determining the onset of knocking combustion. The pressure rise rates for all of the fuels are presented in Figures 7.67 to 7.75. Trends show that the

pressure rise rate has a similar qualitative dependence on air and EGR dilution for all of the fuels; in each case the isolines run roughly parallel to the knock boundary. As expected, the numerical values of pressure rise rate are different for each fuel at a given air and EGR dilution rate. However, at each knock boundary the pressure rise rate always falls within 4.5-5.5 bar/°CA, regardless of fuel or dilution rates. Thus, a strong relationship between points at which a 10% KOF occurs, and the rate of pressure rise that is observed at these points has been established.

Using this idea, it may be possible to avoid knocking combustion simply by limiting the maximum rate of pressure rise. Obviously this can be achieved through changes in the air or exhaust gas dilution rates, or by changing fuel composition. However, other approaches could include innovative approaches to engine design, such as proposed by Galvin [94]. Their idea involves the use of a sprung piston to store energy during combustion, releasing it later in the expansion stroke. A set of Bellville washers are sited between the part of the piston connected to the gudgeon pin, and the top of the piston which houses the sealing rings. This system has been realised for efficiency improvements in SI engines, achieved by reducing the maximum in-cylinder pressure, temperature, and associated heat losses to the cylinder head. However, such a design could equally be used to limit the maximum rate of pressure rise in a CAI engine, possibly allowing higher loads to be obtained without the onset of destructive knocking combustion.

7.3.4 Exhaust Gas Measurements

7.3.4.1 Exhaust Gas Temperature

The exhaust gas temperature trends with dilution for each of the fuels are presented in Figures 7.76 to 7.84. As with all other characteristics so far, the gasoline fractions (Figures 7.76 to 7.78) exhibit little or no difference in exhaust gas temperatures.

For all fuels, temperatures are highest as conditions approach stoichiometric, and lowest when the air dilution rates are high. The maximum temperatures for the hydrocarbon fuels seem to be equal at approximately 420 °C, despite the limited lean-of-stoichiometric combustion of the PRFs. There is one exception to this trend; the 95 RON PRF (Figure 7.81) exhibits a maximum exhaust gas temperature of 380°C at lambda 1.75, EGR rate 35%. This represents a difference of 5.8% (in Kelvin) from exhaust gas temperatures of the

other hydrocarbon fuels. It is unlikely that this is the result of normal experimental error. However, it is equally unlikely that this shows a real and significant trend. In the absence of further data to prove or disprove the results for the 95 RON PRF, no further conclusions can be drawn.

The alcohols (Figures 7.77 and 7.78) show slightly lower maximum exhaust gas temperatures of 380 °C at their respective highest load points, when compared to the hydrocarbon fuels. This difference may be attributed to more advanced combustion phasing for both of the alcohols in the region. Under high air dilution conditions, the exhaust gas temperatures for the alcohols do not fall off as sharply as those for the hydrocarbon fuels. Since the alcohol fuels are much more resistant to partial burning, their combustion efficiency is higher than the hydrocarbon fuels under comparable conditions. Higher combustion efficiency leads to a higher total heat release, raising the exhaust gas temperature.

7.3.4.2 Exhaust Emissions

Unburned Hydrocarbon Emissions

Trends for the indicated specific unburned HC emissions are given in Figures 7.85 to 7.93 for each fuel respectively. Trends for all fuels appear to be very similar, with minimum emissions obtained under the highest load operation, and always in the region of 5-10 g/kW.h. The highest emissions are observed when air dilution is also highest, due to the reduction in combustion temperature that prevents complete oxidation in this region. However, the hydrocarbon fuel trends with both air and EGR dilution are much more severe than those for the alcohol fuels, which in part accounts for the alcohols attaining a much wider acceptable operating region. The full explanations for hydrocarbon emissions using gasoline fuel given in chapter 6 are just as relevant for all of the fuels presented in this section.

NO_x Emissions

NO_x trends for each of the fuels are presented in Figures 7.94 to 7.102. For once, the gasoline fuels (Figures 7.94 to 7.96) do not appear to be in strict agreement. While all three gasolines show similar trends, the light fraction emissions are approximately halved when

compared to the other two under similar conditions. NO_x emissions in SI, CI, or CAI combustion are known to be dependent on two factors: oxygen availability and combustion temperature. The oxygen availability is a function of the air and EGR dilution rates, which are the same for similar points on each map. Furthermore, since all of the measured parameters presented so far for the gasolines are almost identical across their dilution ranges, one can assume that their combustion temperatures are similar also. An explanation arises when the absolute quantities of measured NO_x concentrations are considered. The exhaust NO_x concentrations measured for the light fraction are markedly lower than for the other two gasolines. However for the majority of the dilution ranges, measurements are below 20 ppm for all three fuels. Even under the highest load conditions, emissions barely reach 100 ppm. Given that the analyser is calibrated over a range of 0-1500 ppm, a difference in measurement of 75 ppm only represents a 5% error. So, a very small error in the calibration would be enough to cause the absolute differences in NO_x readings observed.

The PRF fuels (Figures 7.97 to 7.100) exhibit similar trends to the gasolines, only more pronounced. Most notably, maximum NO_x emissions tend to increase with octane, reaching values in excess of 1g/kW.h for isooctane at its highest load point. This appears to be related to the proximity of the knock boundary to the origin of the chart for each fuel. Isooctane is more resistant to knocking combustion than the other fuels, and so it requires less dilution to limit its heat release rate. However, combustion temperature increases under lower dilution conditions, which raises the NO_x emissions. So, isooctane exhibits the highest NO_x emissions along its knock boundary, followed by the 95, 90, and then the 80 RON PRFs.

A similar argument can be given for the NO_x trends exhibited by the alcohols (Figures 7.101 and 7.102). For these fuels, the dilution rates required to avoid knocking combustion are much higher than for the other fuels, and consequently the NO_x emissions barely rise above ambient levels along their knock boundaries. NO_x emissions are highest when the combustion efficiency suffers in the partial burn region, as a result of the specific emissions' dependency on the specific fuel consumption.

CO Emissions

CO emission trends are presented in Figures 7.103 to 7.111. The trends shown for the gasoline fuels (Figures 7.103 to 7.105) are very similar, although absolute values differ significantly for a given dilution condition. Close to the knock region, values are very similar. However, as the partial burning region is approached, the light fraction CO emissions tend to increase more rapidly than the other two. This may be attributed to varying oxidation kinetics, but equally it could be as a result of the change in fuel volatility and subsequent charge homogeneity. However, there is no definite trend with fuel composition, since both the heavy fraction and standard gasoline exhibit lower emissions. Consequently no definite conclusions can be drawn.

The PRF fuels (Figures 7.106 to 7.109) exhibit similar trends to the gasolines, although their rate of increase in CO emissions with air dilution is much higher. Minimum CO emissions occur at the highest load point for each of the hydrocarbon fuels, and are always in the region of 3-5 g/kW.h.

CO trends for the alcohols (Figures 7.110 and 7.111) are markedly different than those for the hydrocarbon fuels. Firstly, the rate of increase in CO emissions as air dilution rates exceed lambda 5.0 are much lower, giving further indication of their wider operating region. But more importantly, as EGR rates increase beyond 60%, CO trends become highly dependant on the EGR rate. This effect is only moderate for the hydrocarbon fuels, and shows that the partial burning region extends much further for the alcohols. For methanol in the region lambda 6.0-8.0, CO emissions become extremely high; way beyond what can be considered acceptable. So it is not only the COVimep that limits lean methanol combustion, but CO emissions as well.

Indicated Thermal Efficiency

In chapter 6, the efficiency of gasoline CAI combustion was expressed in terms of ISFC. When comparing a number of different fuels, ISFC is not sufficient because it is not a dimensionless parameter. For example, ISFC measures the gravimetric quantity of a fuel to deliver a specific mean effective pressure. Gasoline and methanol have vastly different heating values and stoichiometric A/F ratios, which results in approximately twice the quantity of methanol required to deliver the same IMEP as gasoline. Thus for the same

combustion efficiency, methanol exhibits roughly twice the ISFC of gasoline, giving an unrealistic comparison. However, if the ISFC is normalised to the heating value of the fuel (Q_{HV}), then an expression for the dimensionless indicated thermal efficiency (η_i) of the engine can be defined thus:

$$\eta_i = \frac{1}{ISFC.\ Q_{HV}} \qquad \text{Equation 7.1}$$

Table 7.2 gives the (lower) heating values for the nine fuels tested here. No data exists for the light and heavy fraction fuels, so a heating value equal to that of standard gasoline has been assumed. While the extent to which this assumption can be relied on is unknown, it will allow qualitative comparisons between the gasolines to be made.

Fuel	Q_{HV} MJ/kg
Standard Gasoline	~42.70
Light Fraction Gasoline	42.70
Heavy Fraction Gasoline	~42.70
80 RON PRF	44.71
90 RON PRF	44.68
95 RON PRF	44.66
100 RON PRF	44.65
Ethanol	27.73
Methanol	21.10

Table 7.2 Lower heating values (at 298.15 K) for a variety of fuels. From Stone [95].

The indicated thermal efficiencies for each of the fuels are presented in Figures 7.112 to 7.120. The efficiency trends for the gasoline fractions (Figures 7.112 to 7.114) are very similar, as has been shown for most of the other operating characteristics. Highest efficiencies are observed when the intake composition contains most fuel. As the air dilution rate is increased from this point, efficiency tends to reduce in a fairly linear fashion. Also, as the EGR rate is increased from the highest load point, efficiencies suffer slightly. Maximum efficiency for standard gasoline is approximately 41%. The light and heavy fractions show similar maximum values, indicating that their ISFCs are comparable in this region.

Once again trends for the PRFs (Figures 7.115 to 7.118) closely resemble those of the gasolines, showing similarly orientated isolines. However, maximum indicated efficiencies are comparatively reduced by up to 7% in all cases except for the 95 RON PRF, which exhibits a maximum efficiency of 41%. There is no obvious reason for this anomaly. In general, the higher octane PRFs are able to achieve higher efficiencies for equivalent dilution rates.

The trends for the alcohol fuels (Figures 7.119 and 7.120) are similar to the others, except that efficiency becomes more of a function of EGR rate at rates higher than 60%. In both alcohol fuel cases, the rate of decrease in efficiency with increased air dilution is much lower than for any of the hydrocarbon fuels, which is further proof of their much wider operating region. Highest efficiencies are again in the region of 41%.

It is clear that while all of the fuels show similar trends in indicated thermal efficiencies, these trends are not a function of combustion phasing in any case. Thus, it can be asserted that the timing of heat release and its duration are of secondary importance to the attainment of satisfactory CAI combustion. So in practice, a production CAI engine will be optimised for performance characteristics such as knocking combustion, efficiency, and engine out emissions by changing the global and local in-cylinder charge temperature and/or pressure histories, with little attention paid to the timing of heat release, which is one of the most important parameters in current SI and CI technologies.

7.4 Further Investigation of the Gasoline Fractions

The most surprising results presented in previous sections are that the gasoline fractions do not appear to show any significant difference in combustion or emissions characteristics when they are used in CAI combustion. Results presented in chapter 5 showed that these fuels exhibited a marked difference in spark-induced knocking combustion characteristics, which one would expect to translate to CAI combustion. A reasonable explanation must be found for this behaviour.

The original octane tests performed by Saybolt UK Ltd. showed that the light and heavy fractions produced by the online system had RONs of 93.5 and 98, and MONs of 85 and 86.5 respectively. So, while the fractions exhibited a significant research octane number spread of 4.5, the motoring octane number spread is much smaller at only 1.5. The reason

for the different values lies in the fundamental differences between the RON and MON tests, and how these tests change the autoignition chemistry of paraffinic and aromatic hydrocarbons. The engine conditions for both methods are summarised in table 7.3.

Engine Parameter		Research Method	Motor Method
Engine Speed	rpm	600	900
Intake Temperature	°C	52	149
Spark Advance	°CA BTDC	13	19-26

Table 7.3 Experimental engine conditions for Research and Motor Octane rating methods (reproduced from Leppard [44])

The lower engine speed of the research method places the cylinder charge under more severe conditions because more time is allowed for autoignition to occur. However, the overriding factor is the difference in intake temperatures between the two methods. The higher intake temperature of the motoring method raises the entire temperature history. Paraffinic and aromatic fuels respond to this change in different ways. The autoignition chemistry of paraffins is generally less sensitive to temperature changes because of their negative temperature coefficient (NTC) behaviour. When in the NTC region, increases in temperature do not lead to increases in charge reactivity. Thus, if the temperature history of a paraffinic charge includes the NTC region, reactions that lead to autoignition of the end-gas are delayed, delaying autoignition itself. The effect of delaying autoignition gives the flame front more time to arrive, which may preclude autoignition altogether. However, aromatic hydrocarbons do not exhibit NTC behaviour, so as the charge temperature history is raised, so are the rate of the kinetic reactions that lead to autoignition.

In practical terms this behaviour is recorded as a difference in fuel sensitivity, which is the arithmetic difference between RON and MON values measured for that fuel. Aromatic fuels tend to exhibit higher fuel sensitivities than paraffinic fuels, because the increase in intake temperature between the two tests makes the end-gas of the aromatic charge comparatively more reactive. This is the fundamental reason for why the fractions exhibit similar MONs, despite having dissimilar RONs; the heavy fraction starts with a RON of 98, but it has a higher sensitivity to the change in test conditions, and its ON undergoes a larger reduction. So, under high intake temperature conditions the two fractions tend to behave in a similar manner when operated in SI combustion mode. If the intake temperature were raised higher than that for the MON test, one could expect that at some

point the two fuels would exhibit exactly the same ON. The intake temperature condition used for the CAI tests presented here is 320°C, over twice that of the MON test. Therefore, one could reasonably expect that little difference in the CAI combustion characteristics between each fuel will be observed. This is the most compelling reason for the similarity between gasoline fraction trends presented in this chapter.

So, if the high intake temperature chosen has adversely affected results for the gasoline fuels, then further tests must be performed to ascertain if the fuels can be made to behave differently under lower temperature conditions. If they do, then the stratified fuel fraction concept may still be useful for the control of CAI combustion.

7.4.1 Scope and Test Conditions

The purpose of these further tests is to ascertain whether the gasoline fuel fractions behave differently when operated with lower intake temperature conditions. To this end, it is not necessary to build a full map of the combustion parameters over the air and EGR dilution ranges for each fuel. In previous tests the position of the knocking boundary has proved to be a good indicator of the size of the attainable CAI range. In particular, ignition timing results under no EGR and 10% KOF conditions can indicate the size of the EGR dilution range for hydrocarbon fuels. In the following section each fuel shall be tested along the knocking boundary only, and similarities or differences between each fuel shall be inferred.

The intake temperature used for these tests should ideally be as low as possible, so as to get the greatest difference between these test conditions and previous ones. However, The maximum compression ratio at which the Ricardo E6 can operate is 17.8:1. Under these conditions, a minimum intake temperature of approximately 135 °C is required to give a sufficiently large knocking boundary for the comparison between fuels. If lower intake temperature conditions are used, then ignition timings are retarded and the EGR required for complete misfire is reduced, effectively shifting the misfire boundary towards the origin of the dilution chart. Unfortunately, these conditions are somewhat similar to those of the MON test, and so a large difference between the combustion characteristics of each fuel is not expected. However, these temperature conditions are much more realistic of those experienced by the cylinder charge in a CAI engine that uses burned gas recycling to

initiate combustion. Thus, the tests will probably give more realistic results than if ambient intake temperatures were used.

7.4.2 Discussion of Results

Results along the knock boundary for the light, standard, and heavy fraction gasolines have been generated with the engine operating at a compression ratio of 17.8, and intake temperature of 135 °C. Knock boundaries for each gasoline fuel under these conditions and the previous ones (CR = 11.5, Tin = 320°C) are presented for comparison in Figure 7.121.

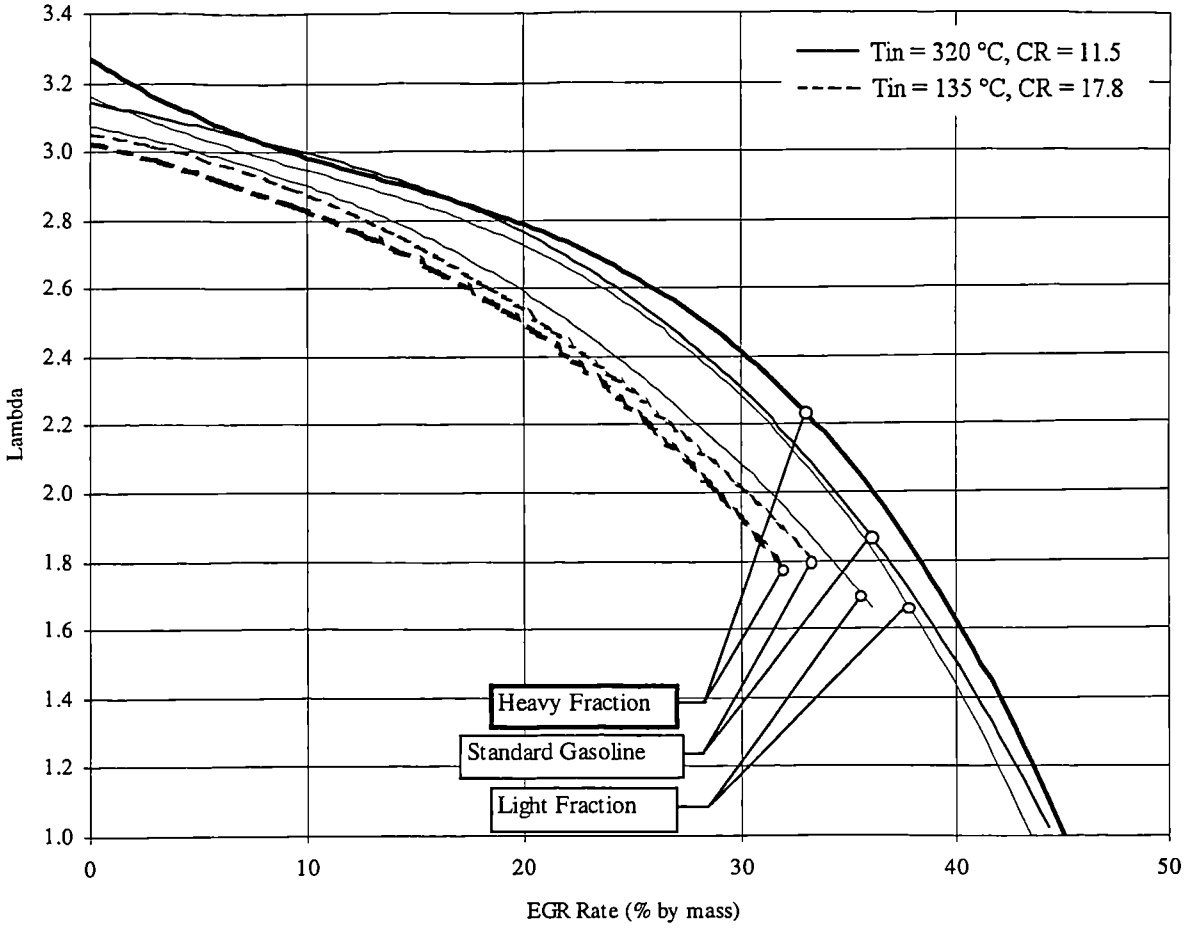

Figure 7.121 Knock boundaries for light, standard, and heavy fraction gasolines under two engine operating conditions

The knock boundaries for the gasolines tested at low temperature are slightly closer to the origin of the chart than in previous tests. This occurs as a result of the particular combination of intake temperature/compression ratio chosen. If the intake temperature chosen was higher, then the dilution required to limit the heat release rate and avoid

knocking combustion would be higher, effectively shifting each boundary away from the origin of the chart.

As before, the knock boundaries for the low temperature tests are very close together, indicating that the fuels are behaving in a similar fashion. There is a slight trend showing that the light fraction requires more dilution than standard gasoline, which in turn requires more dilution than the heavy fraction. This was expected due to the NTC behaviour of parrafins, but the proximity of each knock boundary to the other is disappointing, and indicates that CAI combustion is unlikely to benefit from application of the stratified fuel fraction concept using the current gasoline fuel. On the other hand, these results show that CAI combustion is not sensitive to gasoline composition over a wide range of conditions, and so strict control over fuel composition between regions and fuel companies is probably not required to ensure correct engine operation.

The knock boundaries for the fuels tested under low temperature conditions are truncated at EGR rates of 32-36%. This occurs as a result of the intake temperature/compression ratio conditions chosen. At the 10% KOF, 0% EGR point, combustion timing (10% MFB) for each fuel is in the region of 2 °CA ATDC. This comparatively retarded timing under no EGR conditions ensures that when EGR is introduced, the misfire limit is reached much sooner than in previous tests. Furthermore, the similarities of combustion timing (to within 0.5 °CA) at this point indicate that the attainable dilution ranges for each fuel are also likely to be very similar.

7.5 Summary

A number of fuels including three blends of gasoline, four primary reference fuels, and two alcohols have been tested to establish their attainable CAI combustion regions. For each fuel, its region is defined by measured combustion and emissions parameters to give minimum and maximum permissible air and EGR dilution rates. A qualitative comparison between fuels for each of the measured parameters has been undertaken, and the results can be summarised as follows:

(i) All fuels tested exhibit knock and partial burning characteristics in a similar way. However, while the hydrocarbon fuels distinctly show misfire-limited operation at high EGR rates, the alcohol fuels appear to be more tolerant of EGR. In the case of

methanol, no misfire region is observed. Instead, the partial burn region extends much further.

(ii) When the gasoline fractions were tested under high intake temperature conditions, they behaved in almost exactly the same way for nearly all of the parameters measured. Similarities have been attributed to a convergence of autoignition behaviour that occurs under high temperature conditions. The fractions behaved slightly differently under lower temperature conditions.

(iii) Ignition timing trends for the hydrocarbon fuels were similar over the dilution ranges. However, the alcohol fuels only showed a weak ignition timing relationship with increasing EGR rate. In the case of methanol, ignition timing is independent of EGR rate. This result is very important because it shows why researchers have previously found methanol to be a superior fuel for CAI combustion. Moreover, it explains why methanol can operate under a wider set of engine conditions without including any effect that radicals may have in aiding autoignition. The presence of radicals in methanol EGR has been used by some researchers in the past to explain its superiority. However, while the EGR used in this study certainly contains a proportion of stable intermediate combustion products, it cannot contain radicals because they would be consumed in the intake manifold, if not a lot sooner.

(iv) Analyses of autoignition temperatures are inconclusive. Generally speaking, the calculated temperatures were reasonable, and comparable to work presented by previous authors. However, under some conditions calculations showed that some of the fuels exhibited excessive IVC charge temperatures, leading to high autoignition temperatures. The only reasonable explanation for this behaviour is that some heat release occurs during induction, as a result of the high intake temperature used. However, if the fuel is prone to heat release at the intake temperature, then one could reasonably expect a lower autoignition temperature towards the end of the compression stroke, which was never the case. More likely is that the analytical technique used is inaccurate or unsuitable.

(v) The rate of pressure rise experienced by the in-cylinder charge seems to be closely related to the degree of knock observed. Thus, if the pressure rise rate can be reduced, so can knocking combustion. This can be achieved by changes in the

intake composition or temperature, but equally it can be achieved by innovative engine concepts.

(vi) For any fuel, highest efficiency appears to be attained at the highest load conditions at which the engine can be operated. If the intake temperature and compression ratio are sufficiently severe, then significant EGR rates can be used and stoichiometric combustion achieved. Thus, for the gasoline blends and the alcohols, best efficiency coincides with stoichiometric combustion that is diluted just enough to avoid knocking combustion. At this point, CO and HC emissions are *minimised* also. High combustion temperatures can lead to significant NO_x emissions, but they only ever reached in the order of 15% of those found under comparative SI combustion conditions for any of the fuels.

(vii) Most of the improvement in engine efficiency comes from the reduction in pumping work facilitated by CAI combustion under highly diluted operation. It is thought that some of the efficiency improvement also comes from CAI combustion approximating the air standard cycle better than SI or CI processes, since ignition always occurs close to TDC, and combustion durations never exceed 20 °CA.

(viii) Researchers in the past have asserted that control over the combustion phasing is the fundamental issue that needs to be addressed, partly because ignition timing is of utmost importance for the optimisation of SI and CI engines. However, the work presented here suggests that combustion phasing is more of a side effect. To optimise a CAI engine, one must set the charge composition to achieve a compromise for best efficiency, emissions, and power output, not to achieve best combustion phasing. Thus, if one sets the goal of optimum ignition timing for calibrating a CAI engine, it is likely that the engine's efficiency and emissions will suffer.

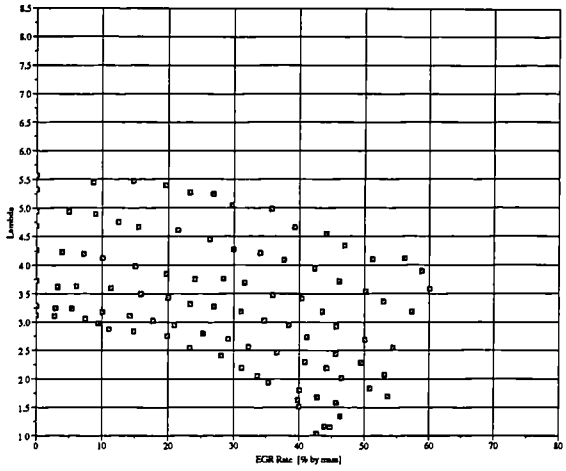

Figure 7.1 Data points for CAI combustion of gasoline fuel

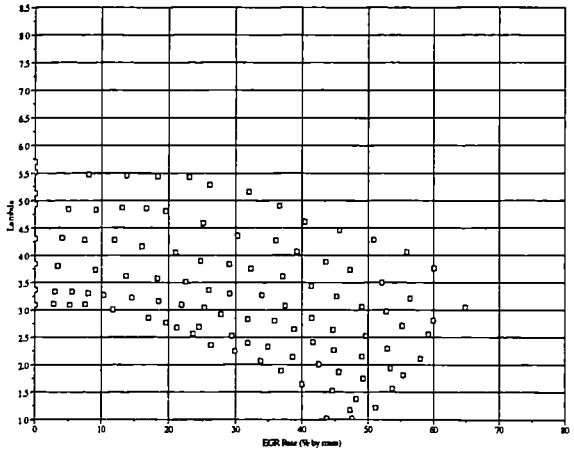

Figure 7.2 Data points for CAI combustion of light fraction gasoline fuel

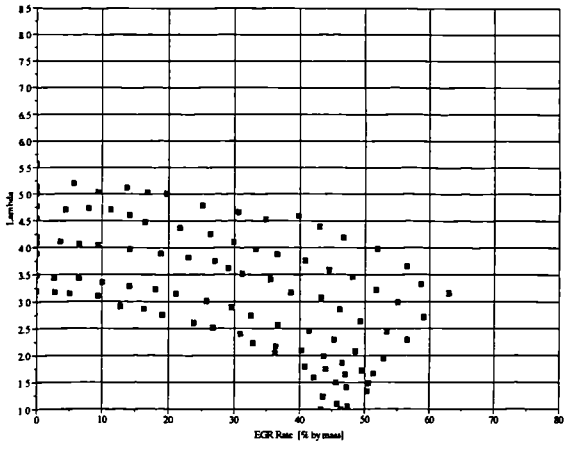

Figure 7.3 Data points for CAI combustion of heavy fraction gasoline fuel

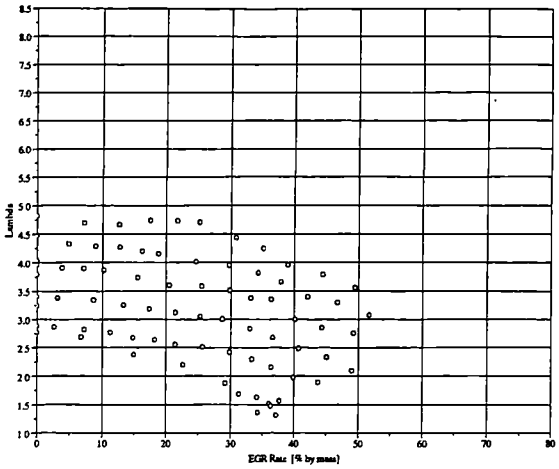

Figure 7.4 Data points for CAI combustion of 80 RON PRF

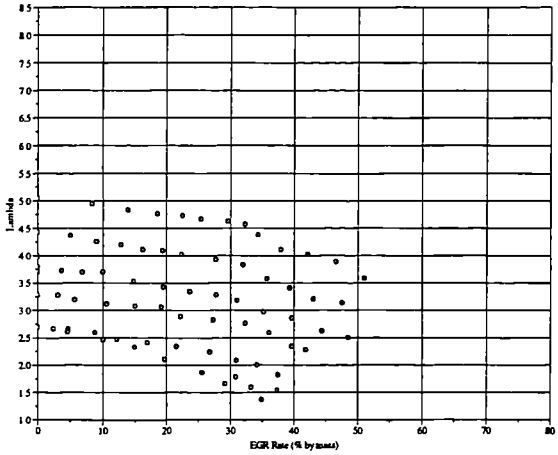

Figure 7.5 Data points for CAI combustion of 90 RON PRF

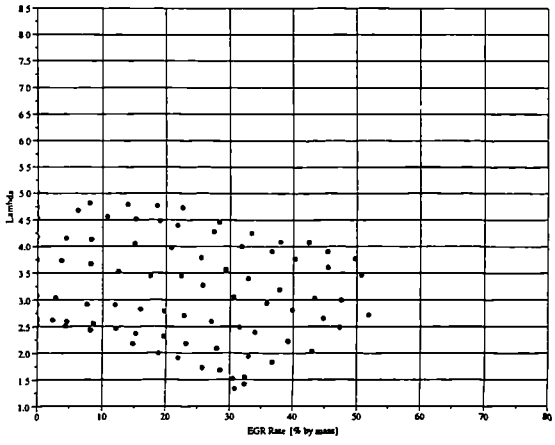

Figure 7.6 Data points for CAI combustion of 95 RON PRF

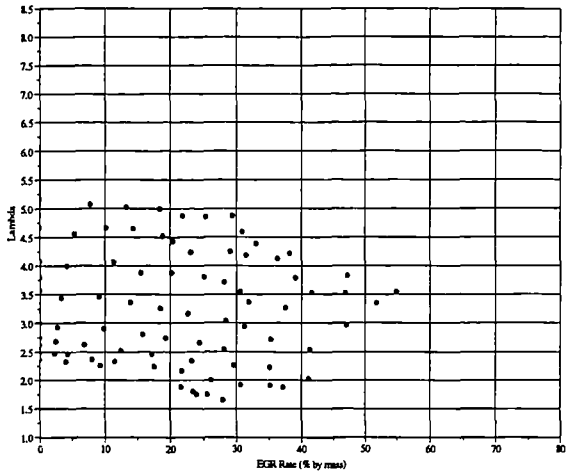

Figure 7.7 Data points for CAI combustion of 100 RON PRF

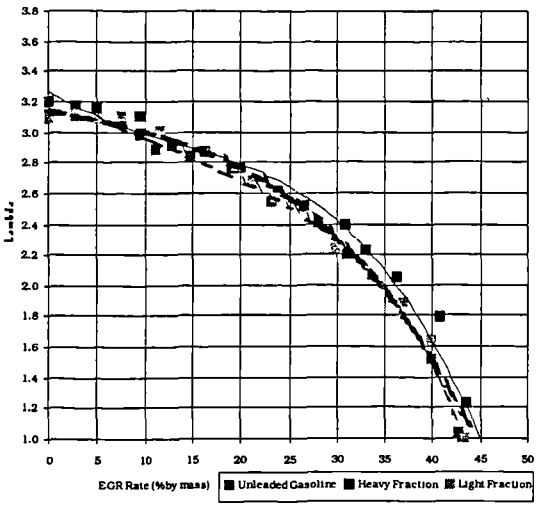

Figure 7.10 Superimposed knock boundaries (10% KOF) for gasoline, heavy fraction, and light fraction (Tin = 320°C, Rc = 11.5)

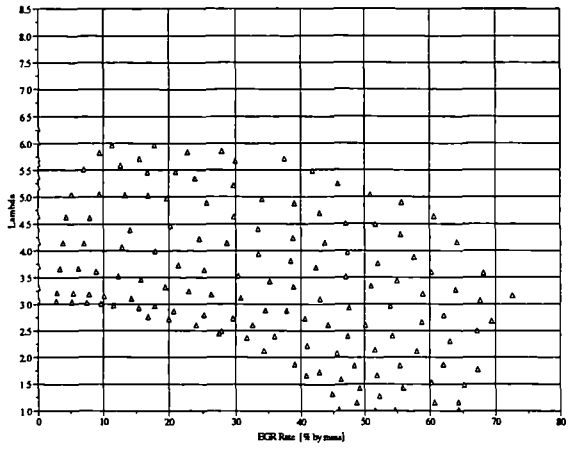

Figure 7.8 Data points for CAI combustion of Ethanol

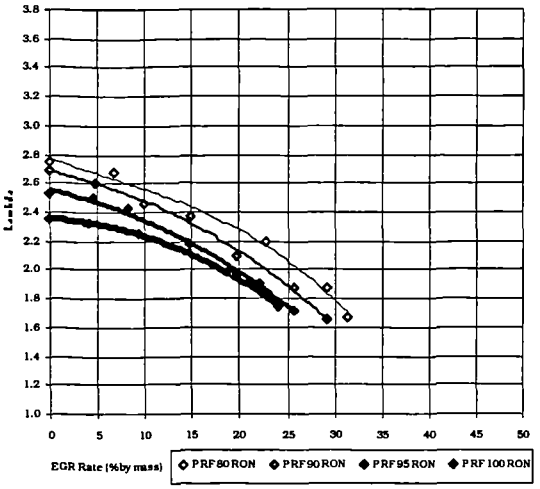

Figure 7.11 Superimposed knock boundaries (10% KOF) for 80, 90, 95, and 100 RON PRFs (Tin = 320°C, Rc = 11.5)

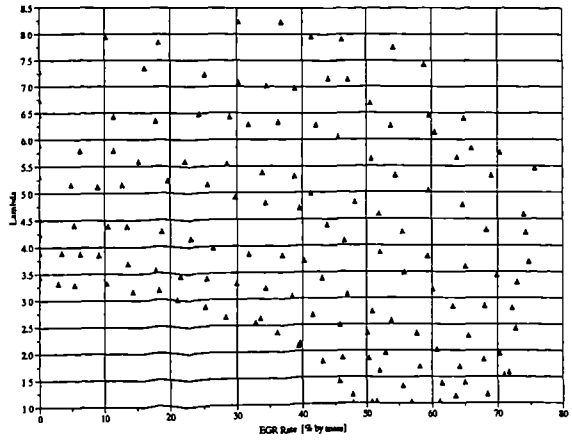

Figure 7.9 Data Points for CAI combustion of Methanol

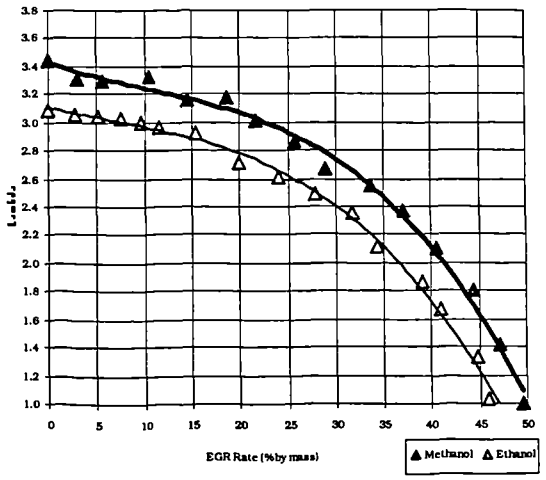

Figure 7.12 Superimposed knock boundaries (10% KOF) for ethanol and methanol (Tin=320°C, Rc=11.5)

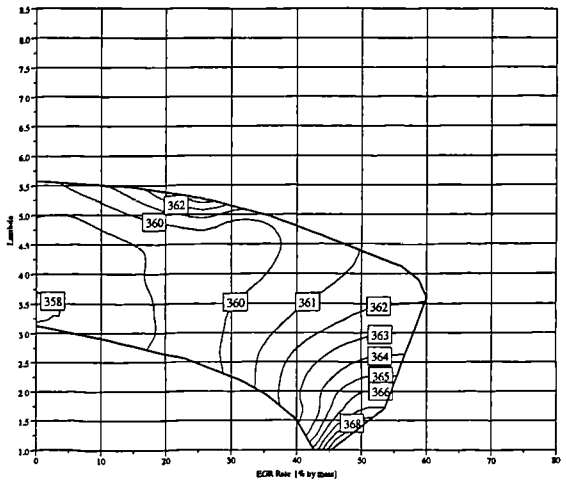

Figure 7.13 Ignition timing (10% MFB) for gasoline CAI combustion (°CA)

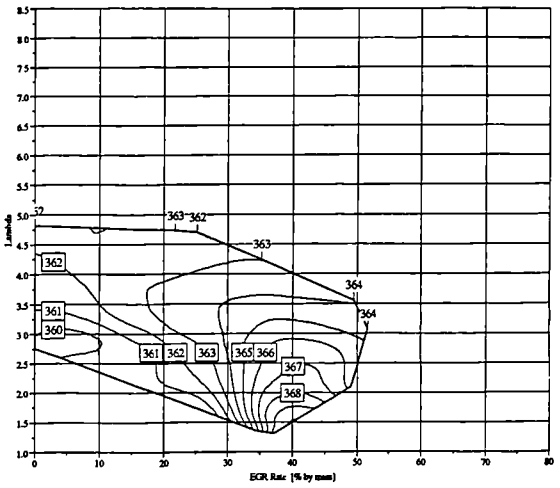

Figure 7.16 Ignition timing (10% MFB) for 80 RON PRF CAI combustion (°CA)

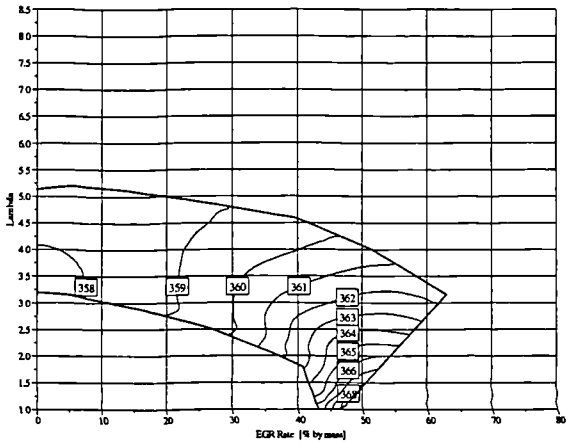

Figure 7.14 Ignition timing (10% MFB) for heavy fraction CAI combustion (°CA)

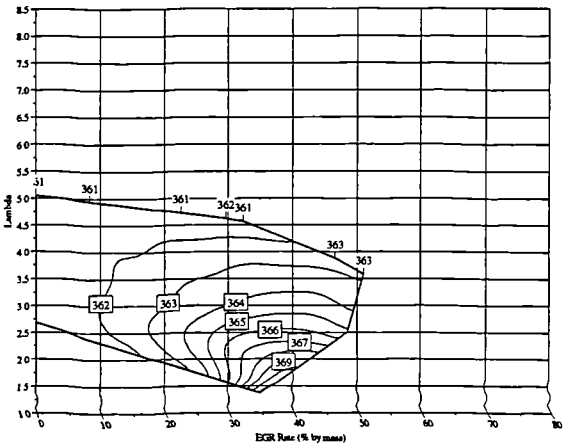

Figure 7.17 Ignition timing (10% MFB) for 90 RON PRF CAI combustion (°CA)

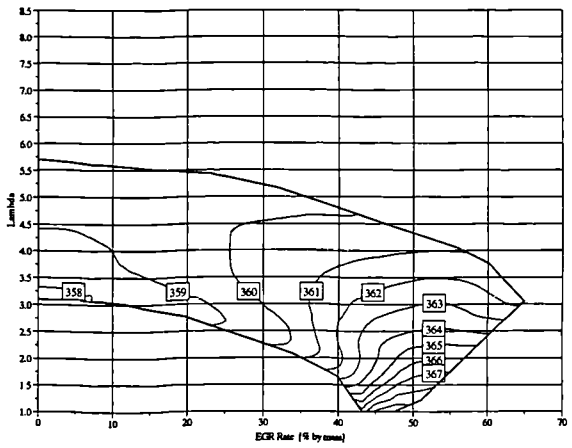

Figure 7.15 Ignition timing (10% MFB) for light fraction CAI combustion (°CA)

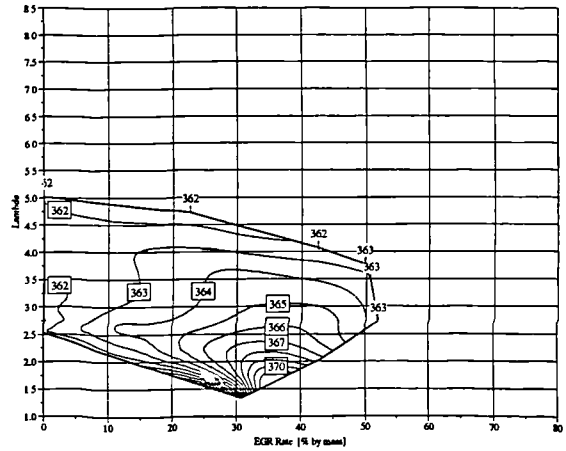

Figure 7.18 Ignition timing (10% MFB) for 95 RON PRF CAI combustion (°CA)

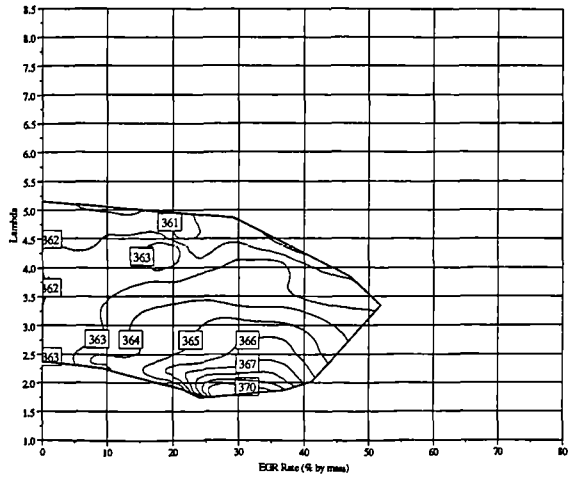

Figure 7.19 Ignition timing (10% MFB) for 100 RON PRF CAI combustion (°CA)

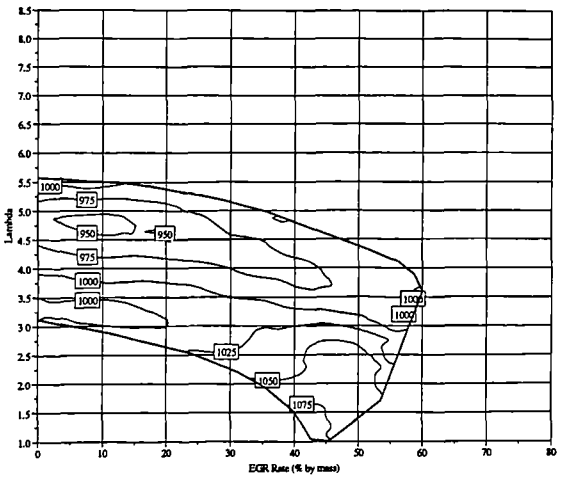

Figure 7.22 Autoignition temperature (K) for gasoline fuel

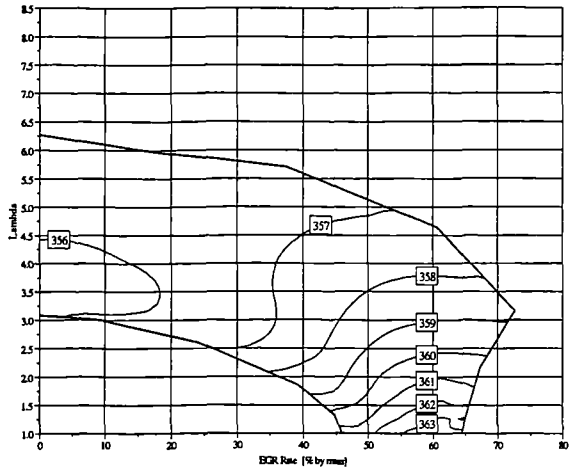

Figure 7.20 Ignition timing (10% MFB) for Ethanol CAI combustion (°CA)

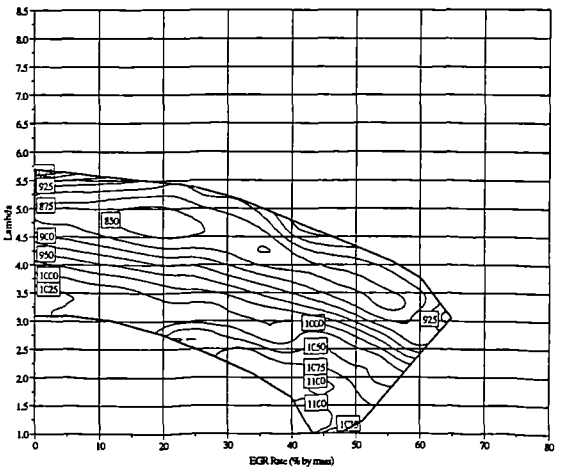

Figure 7.23 Autoignition temperature (K) for light fraction gasoline fuel

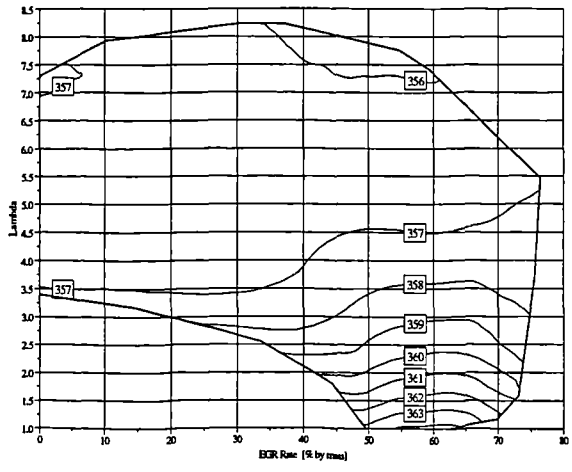

Figure 7.21 Ignition timing (10% MFB) for methanol CAI combustion (°CA)

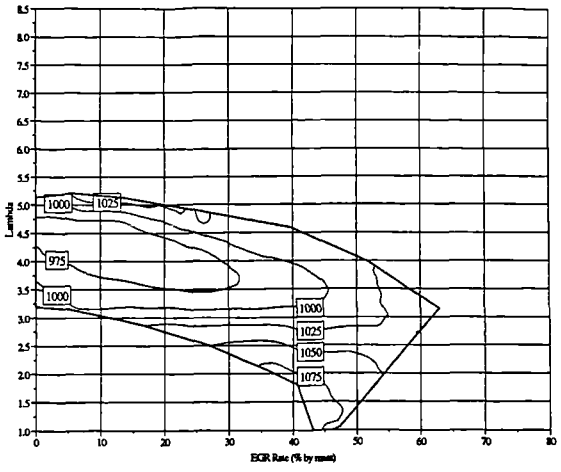

Figure 7.24 Autoignition temperature (K) for heavy fraction gasoline fuel

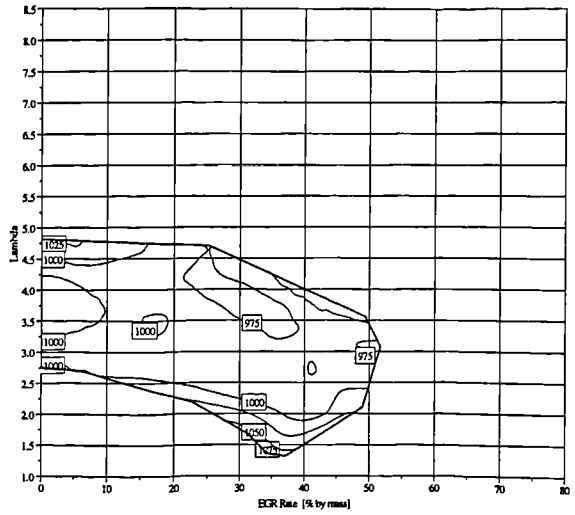

Figure 7.25 Autoignition temperature (K) for 80 RON PRF

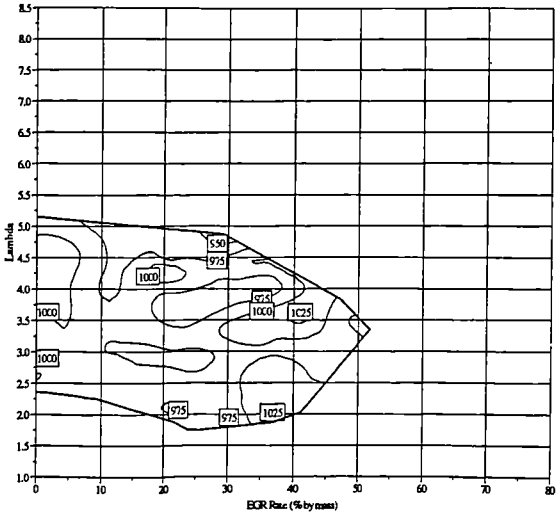

Figure 7.28 Autoignition temperature (K) for 100 RON PRF

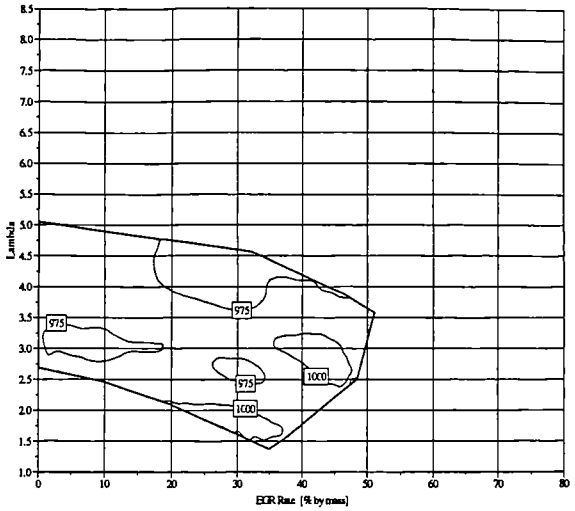

Figure 7.26 Autoignition temperature (K) for 90 RON PRF

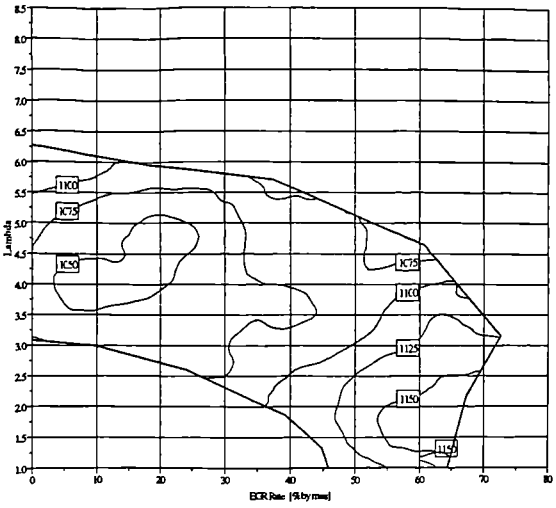

Figure 7.29 Autoignition temperature (K) for ethanol fuel

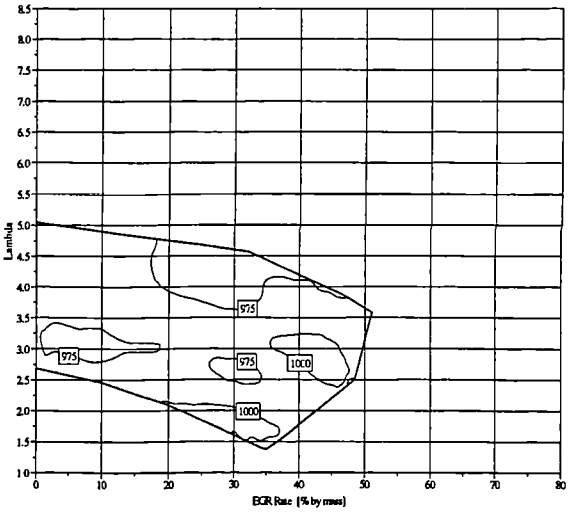

Figure 7.27 Autoignition temperature (K) for 95 RON PRF

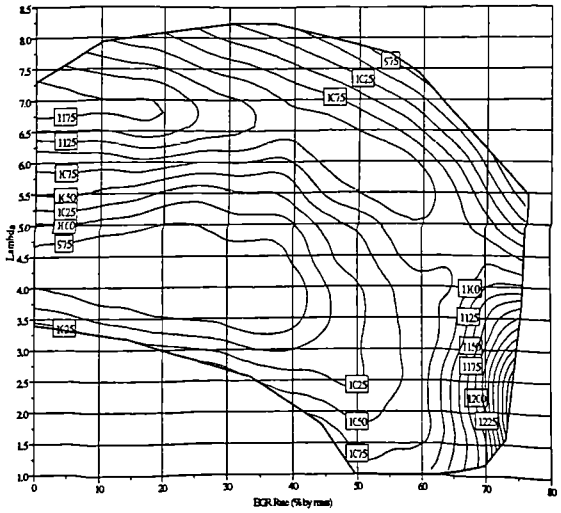

Figure 7.30 Autoignition temperature (K) for methanol fuel

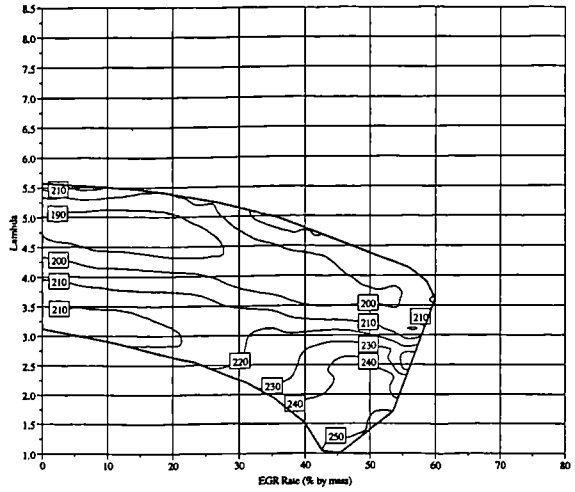

Figure 7.31 Charge temperature at IVC (°C) for gasoline fuel

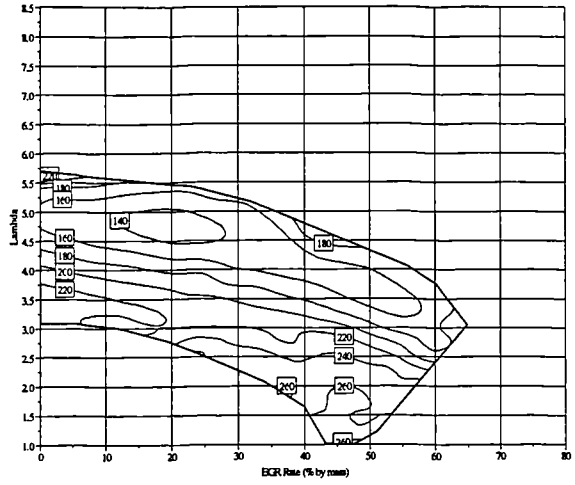

Figure 7.32 Charge temperature at IVC (°C) for light fraction gasoline fuel

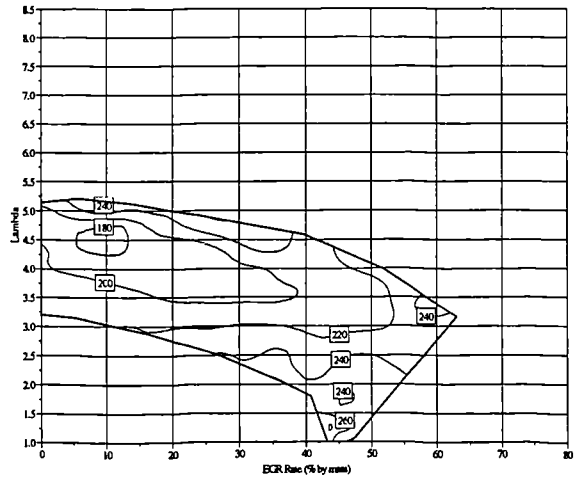

Figure 7.33 Charge temperature at IVC (°C) for heavy fraction gasoline fuel

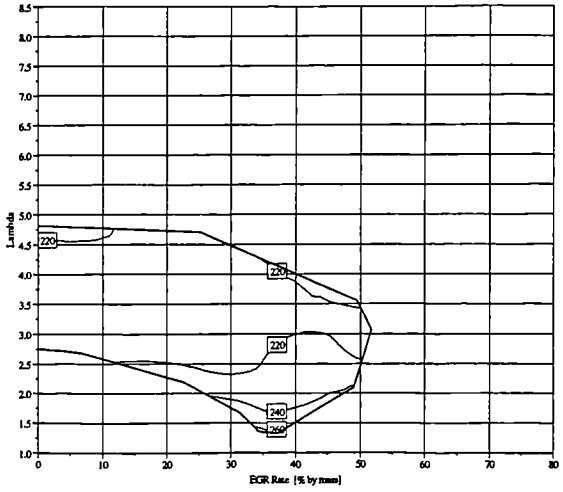

Figure 7.34 Charge temperature at IVC (°C) for 80 RON PRF

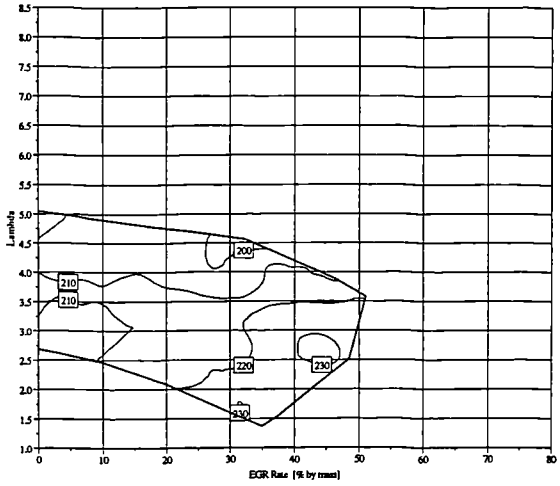

Figure 7.35 Charge temperature at IVC (°C) for 90 RON PRF

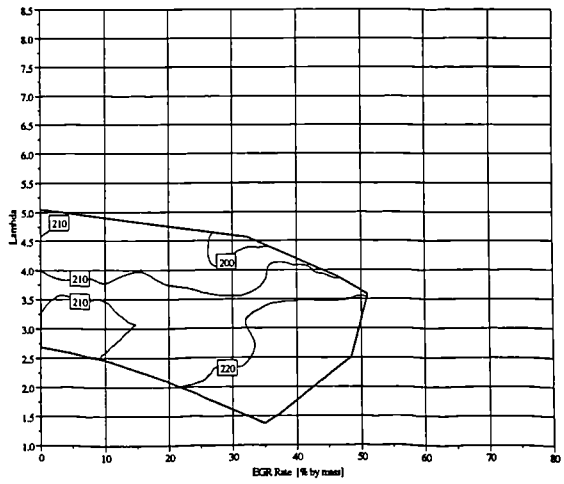

Figure 7.36 Charge temperature at IVC (°C) for 95 RON PRF

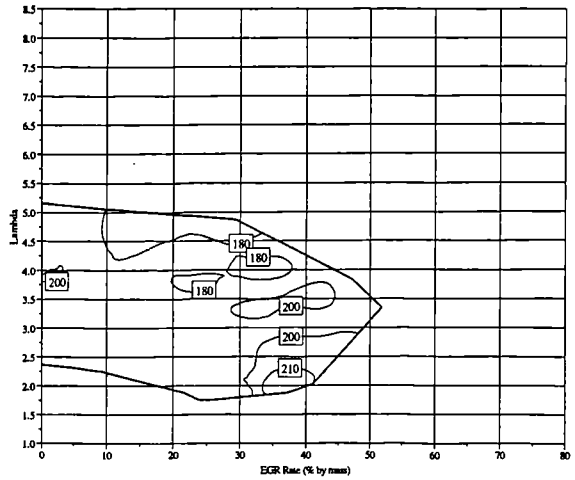

Figure 7.37 Charge temperature at IVC (°C) for 100 RON PRF

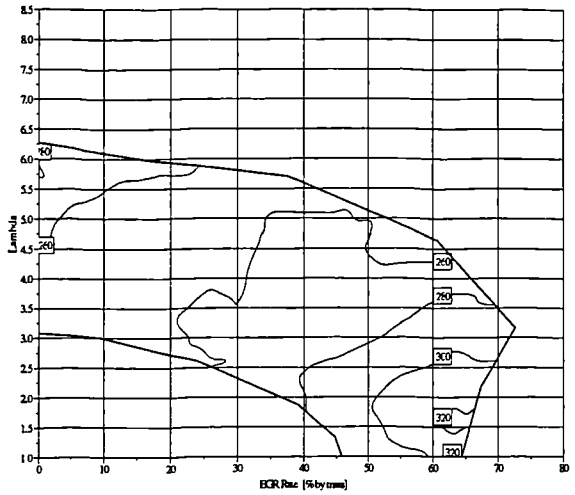

Figure 7.38 Charge temperature at IVC (°C) for ethanol fuel

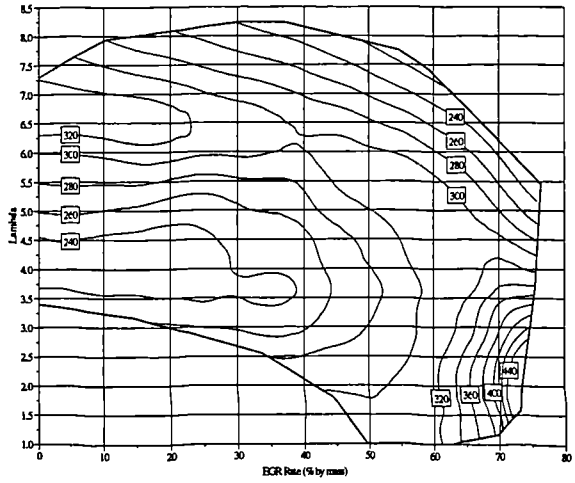

Figure 7.39 Charge temperature at IVC (°C) for methanol fuel

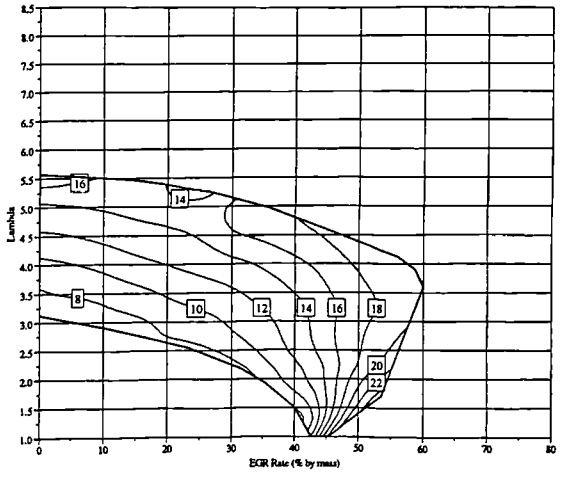

Figure 7.40 Combustion duration (10-90% MFB) for gasoline CAI combustion (°CA)

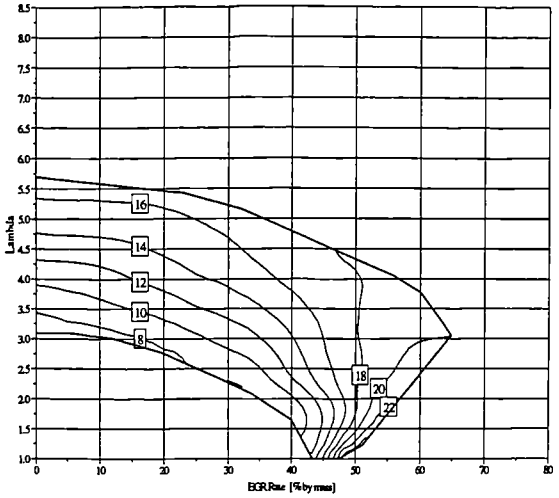

Figure 7.41 Combustion duration (10-90% MFB) for light fraction CAI combustion (°CA)

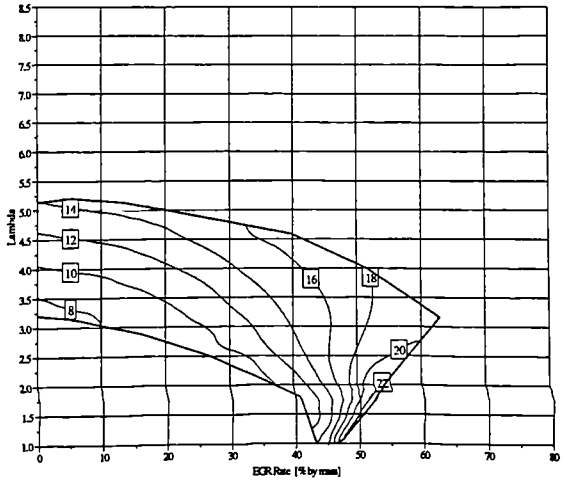

Figure 7.42 Combustion duration (10-90% MFB) for heavy fraction CAI combustion (°CA)

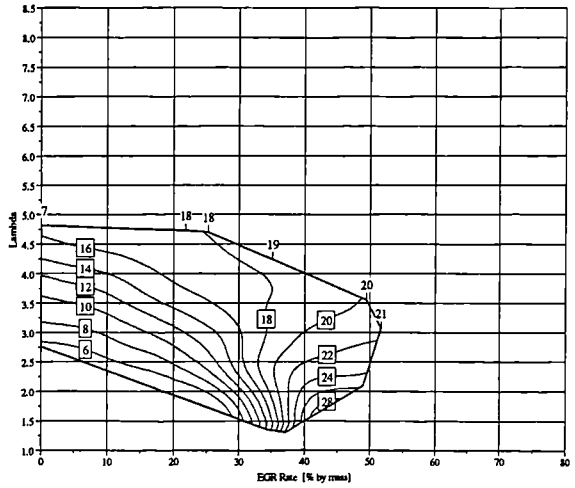

Figure 7.43 Combustion duration (10-90% MFB) for 80 RON PRF CAI combustion (°CA)

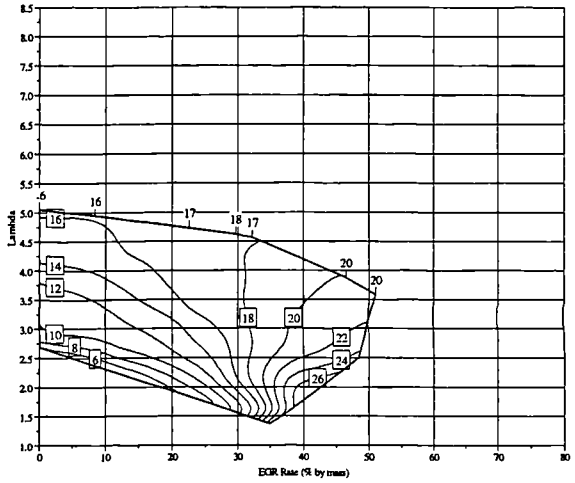

Figure 7.44 Combustion duration (10-90% MFB) for 90 RON PRF CAI combustion (°CA)

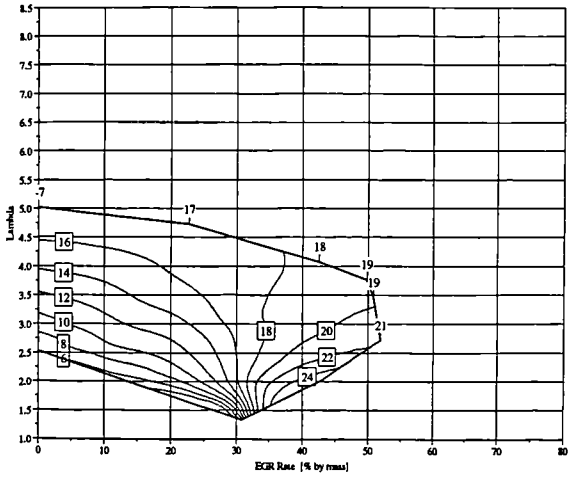

Figure 7.45 Combustion duration (10-90% MFB)for 95 RON PRF CAI combustion (°CA)

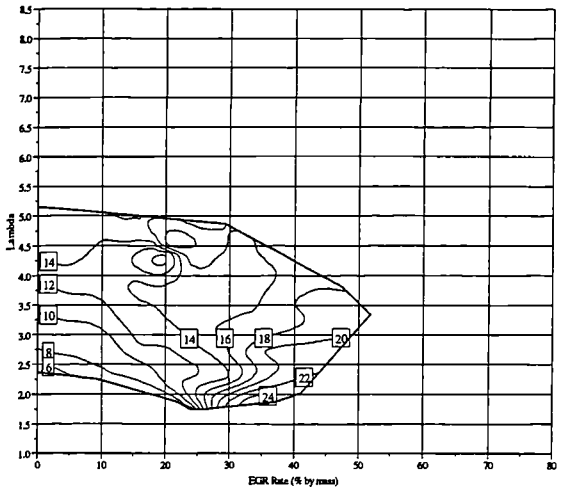

Figure 7.46 Combustion duration (10-90% MFB) for 100 RON PRF CAI combustion (°CA)

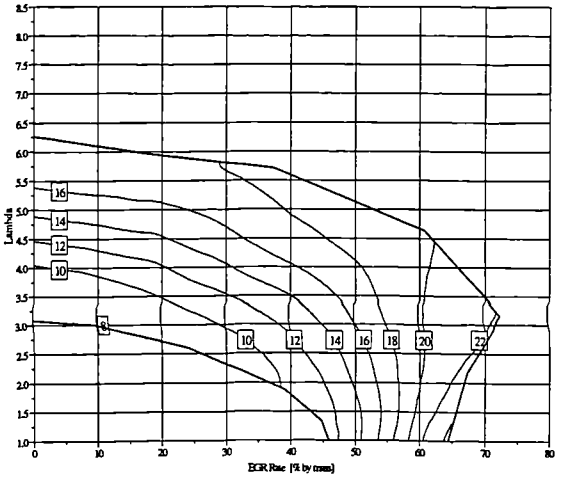

Figure 7.47 Combustion duration (10-90% MFB) for ethanol CAI combustion (°CA)

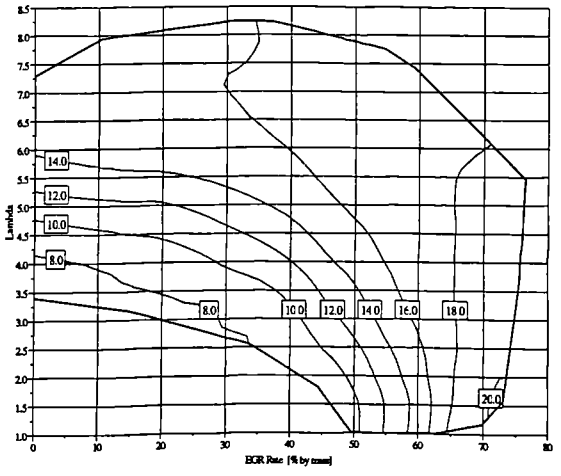

Figure 7.48 Combustion duration (10-90% MFB) for methanol CAI combustion (°CA)

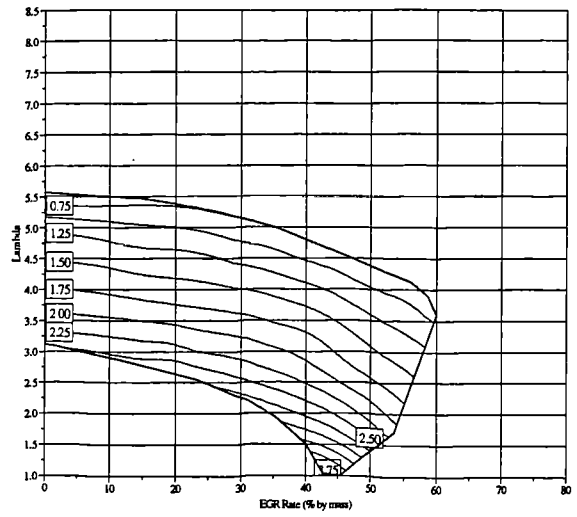

Figure 7.49 IMEP for gasoline CAI combustion (bar)

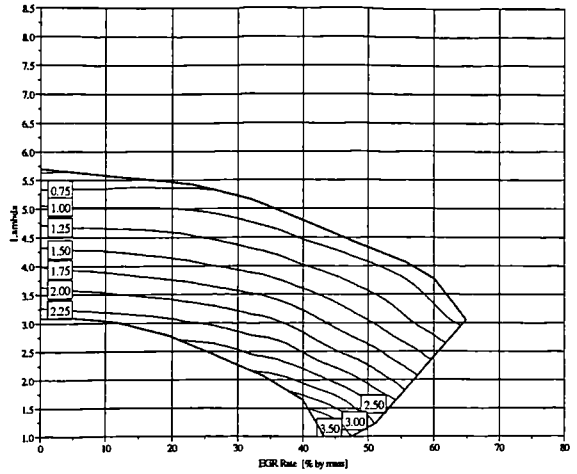

Figure 7.50 IMEP for light fraction CAI combustion (bar)

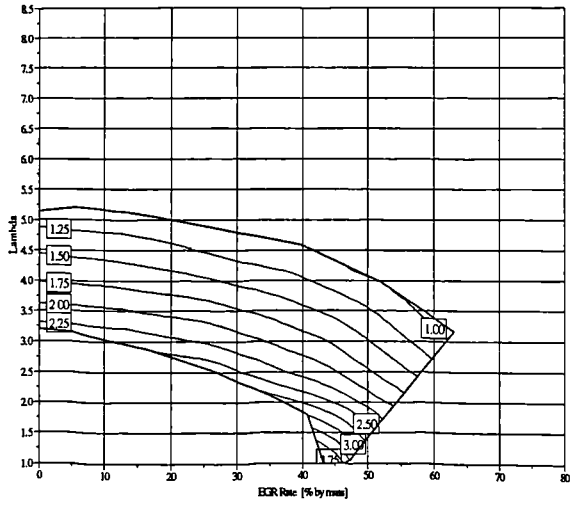

Figure 7.51 IMEP for heavy fraction CAI combustion (bar)

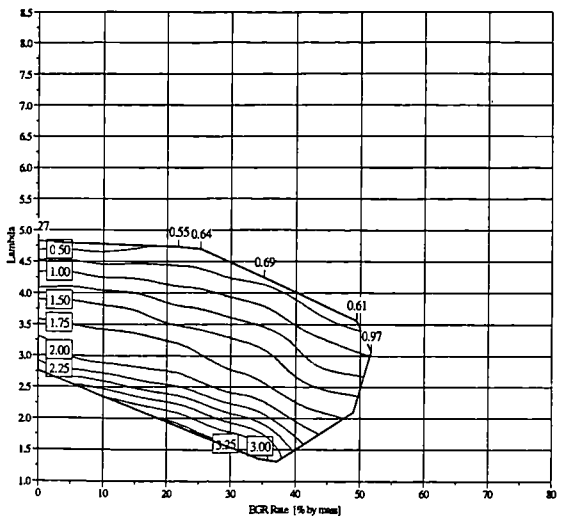

Figure 7.52 IMEP for 80 RON PRF CAI combustion (bar)

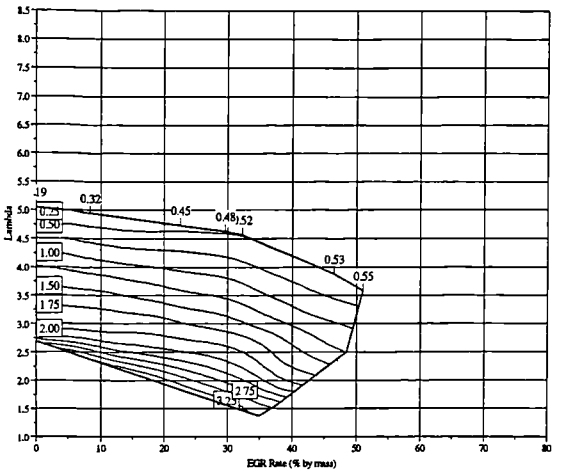

Figure 7.53 IMEP for 90 RON PRF CAI combustion (bar)

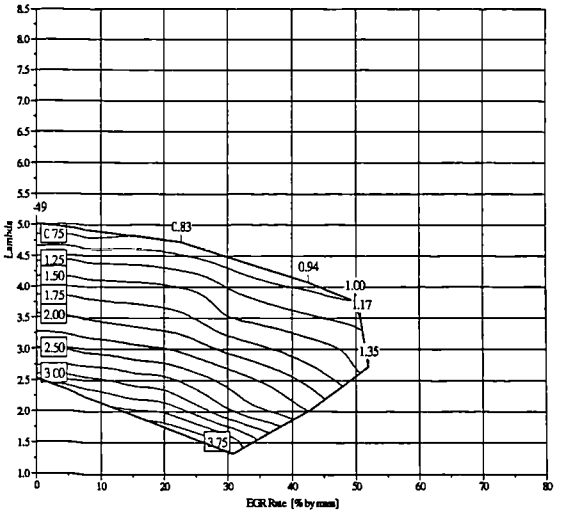

Figure 7.54 IMEP for 95 RON PRF CAI combustion (bar)

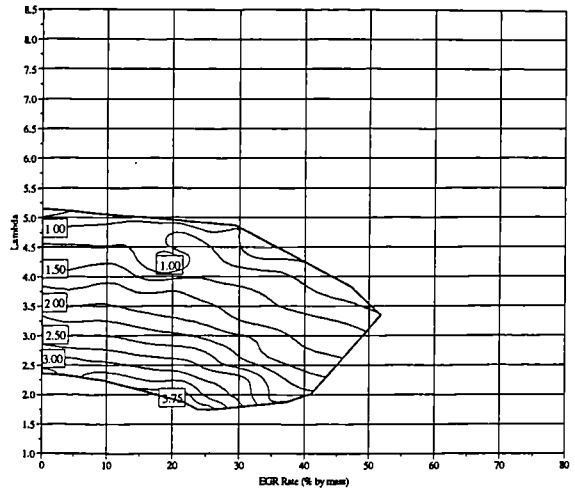

Figure 7.55 IMEP for 100 RON PRF CAI combustion (bar)

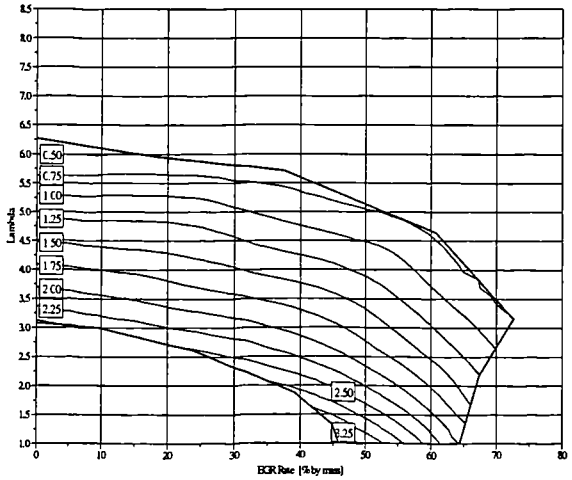

Figure 7.56 IMEP for ethanol CAI combustion (bar)

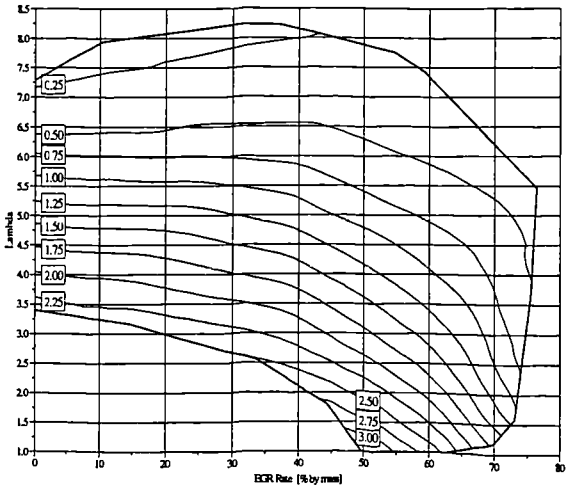

Figure 7.57 IMEP for methanol CAI combustion (bar)

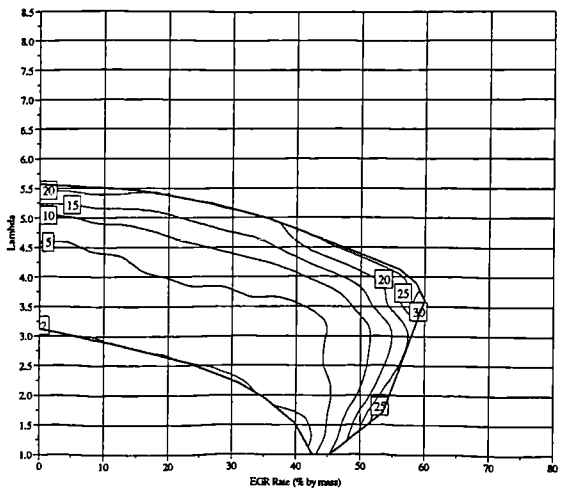

Figure 7.58 COVimep for gasoline CAI combustion (%)

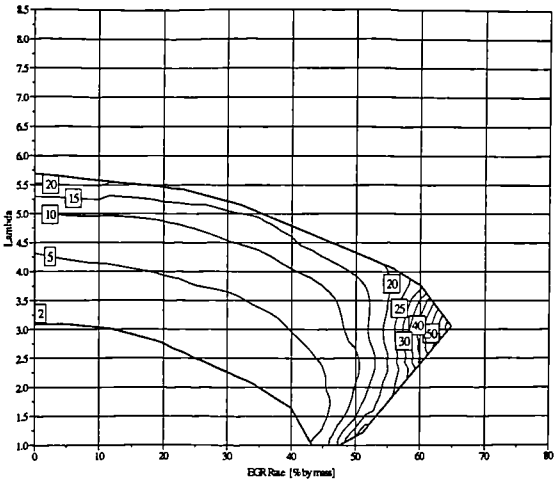

Figure 7.59 COVimep for light fraction CAI combustion (%)

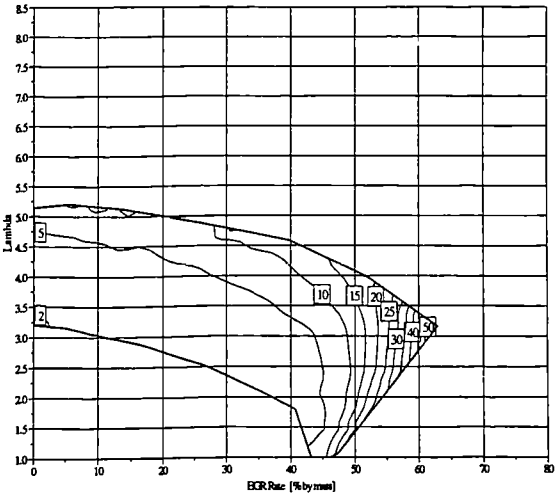

Figure 7.60 COVimep for heavy fraction CAI combustion (%)

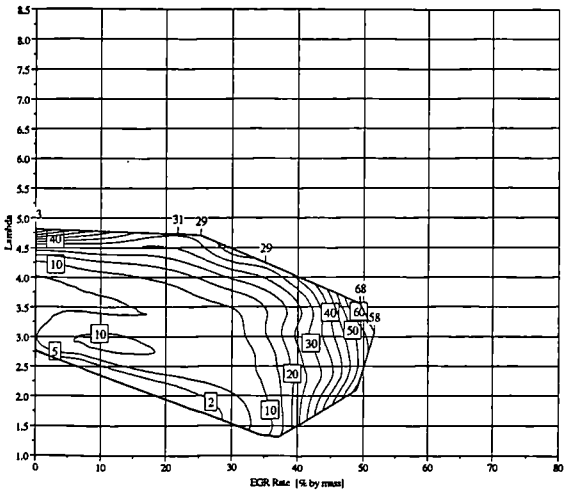

Figure 7.61 COVimep for 80 RON PRF CAI combustion (%)

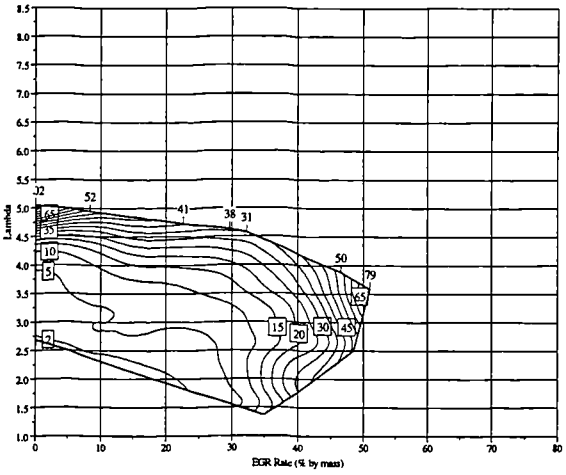

Figure 7.62 COVimep for 90 RON PRF CAI combustion (%)

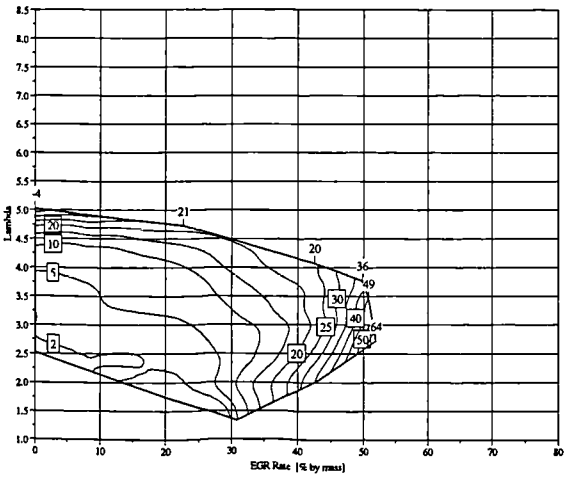

Figure 7.63 COVimep for 95 RON PRF CAI combustion (%)

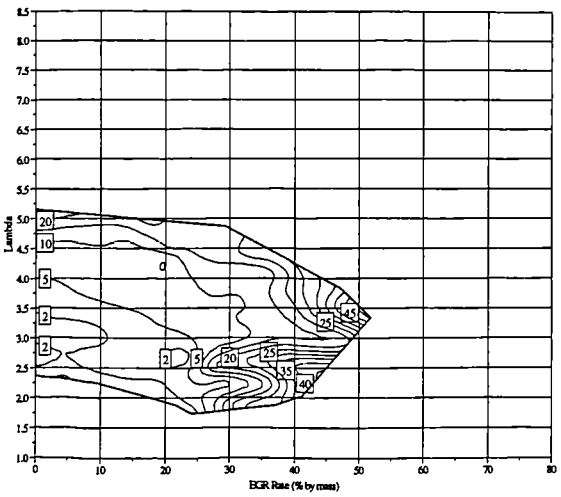

Figure 7.64 COVimep for 100 RON PRF CAI combustion (%)

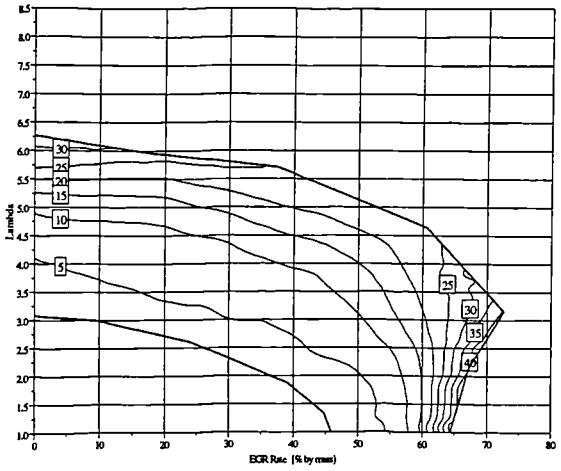

Figure 7.65 COVimep for ethanol CAI combustion (%)

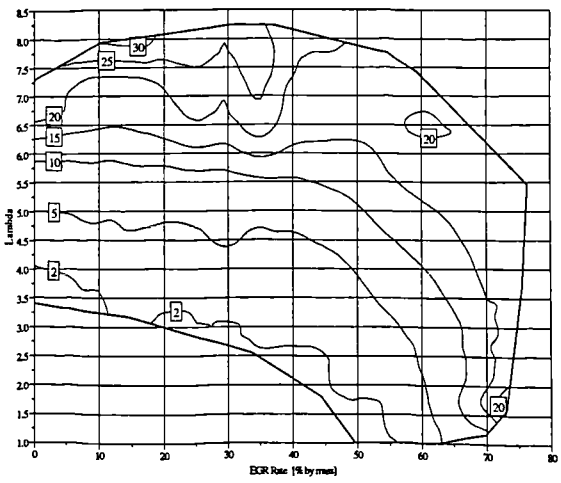

Figure 7.66 COVimep for methanol CAI combustion (%)

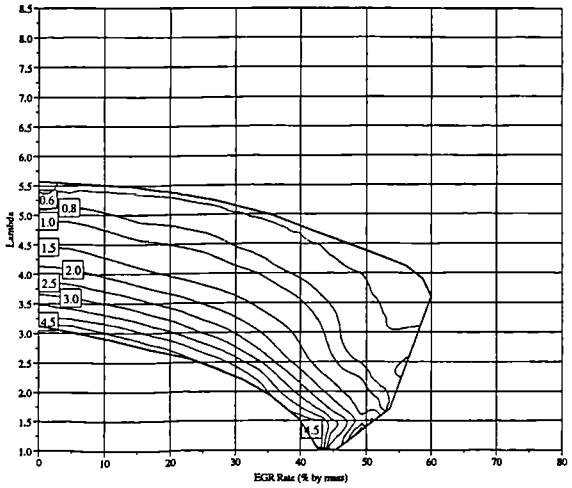

Figure 7.67 Maximum rate of pressure rise for gasoline CAI combustion (bar/°CA)

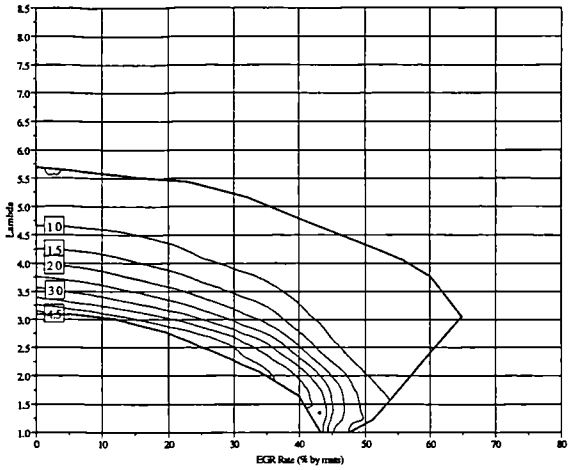

Figure 7.68 Maximum rate of pressure rise for light fraction CAI combustion (bar/°CA)

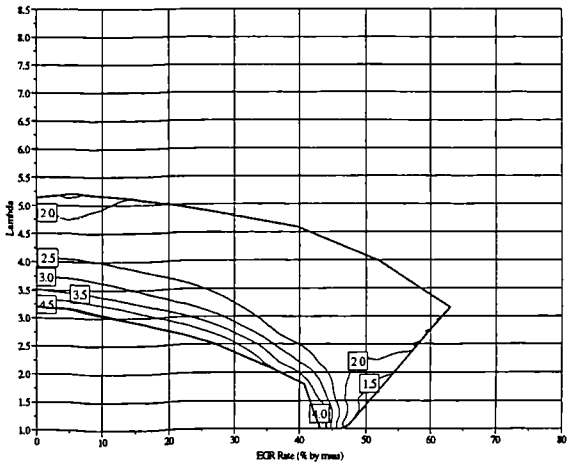

Figure 7.69 Maximum rate of pressure rise for heavy fraction CAI combustion (bar/°CA)

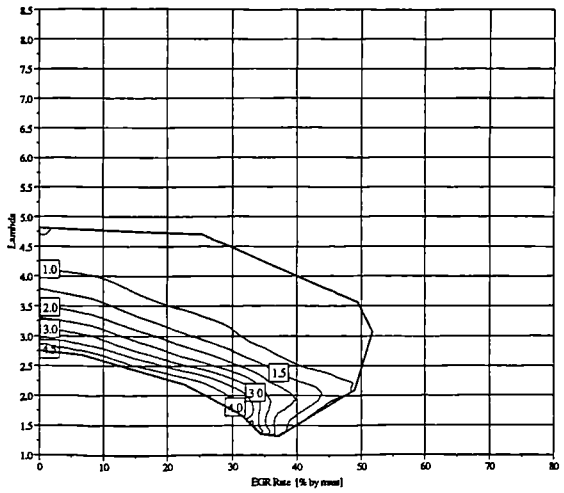

Figure 7.70 Maximum rate of pressure rise for 80 RON PRF CAI combustion (bar/°CA)

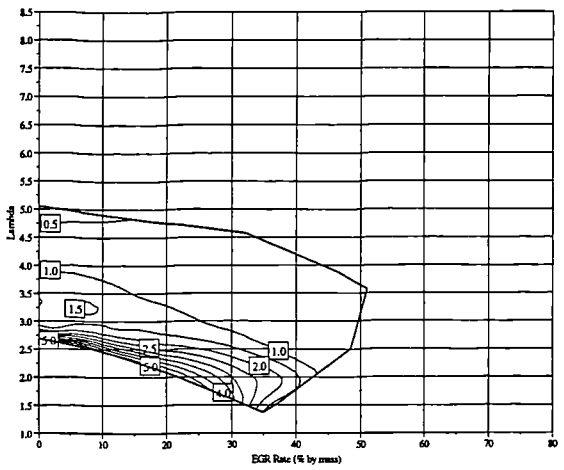

Figure 7.71 Maximum rate of pressure rise for 90 RON PRF CAI combustion (bar/°CA)

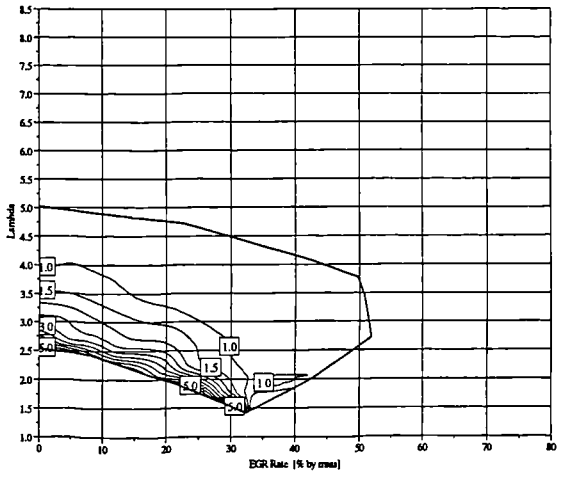

Figure 7.72 Maximum rate of pressure rise for 95 RON PRF CAI combustion (bar/°CA)

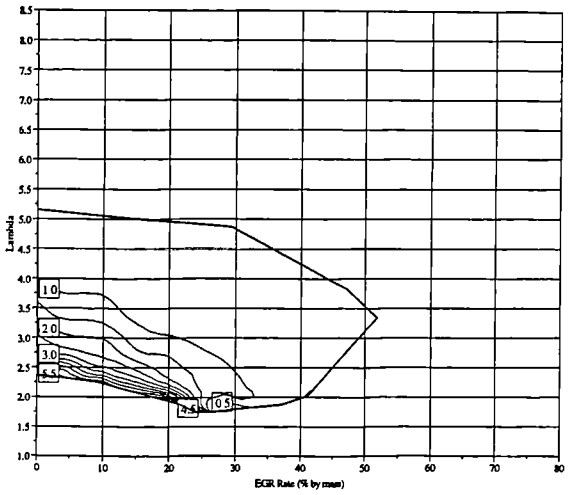

Figure 7.73 Maximum rate of pressure rise for 100 RON PRF CAI combustion (bar/°CA)

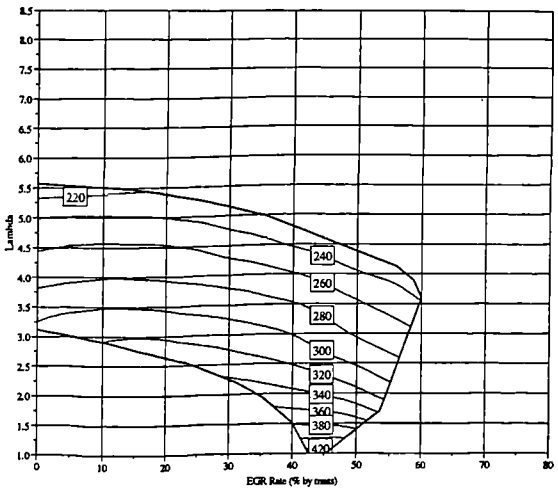

Figure 7.76 Exhaust gas temperature for gasoline CAI combustion (°C)

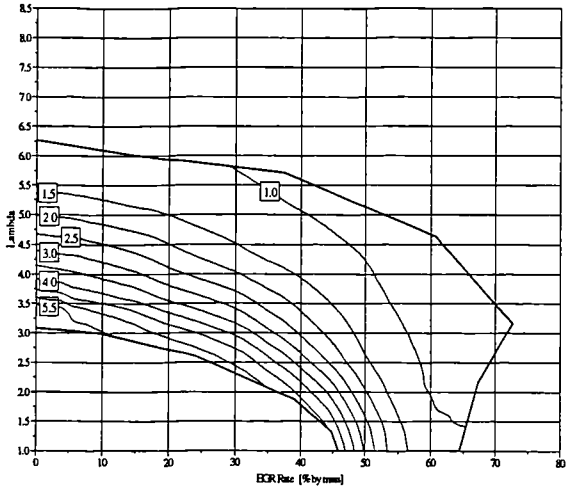

Figure 7.74 Maximum rate of pressure rise for ethanol CAI combustion (bar/°CA)

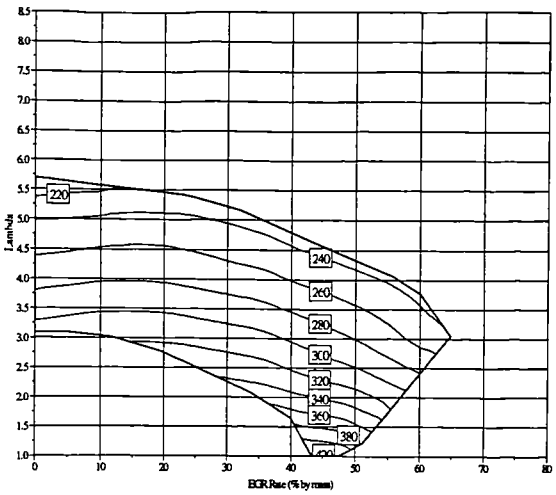

Figure 7.77 Exhaust gas temperature for light fraction CAI combustion (°C)

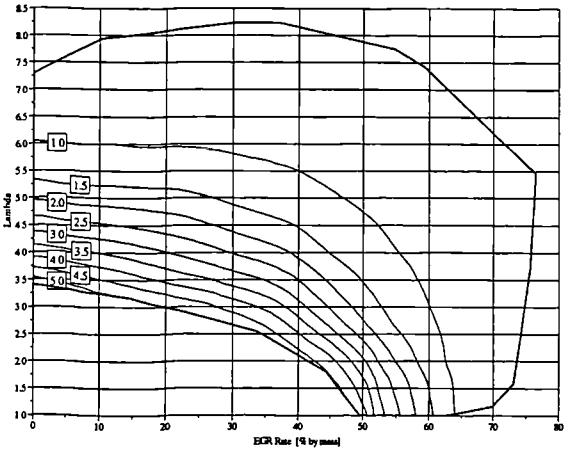

Figure 7.75 Maximum rate of pressure rise for methanol CAI combustion (bar/°CA)

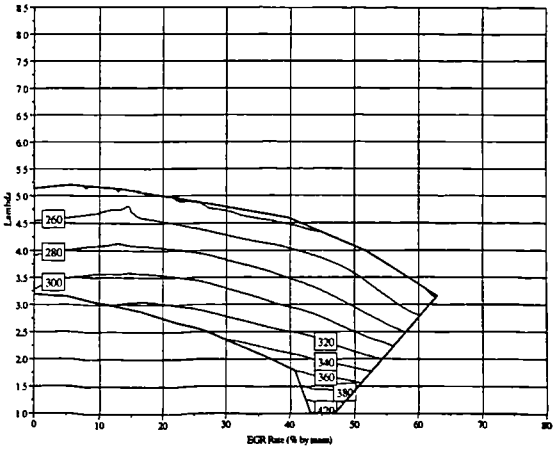

Figure 7.78 Exhaust gas temperature for heavy fraction CAI combustion (°C)

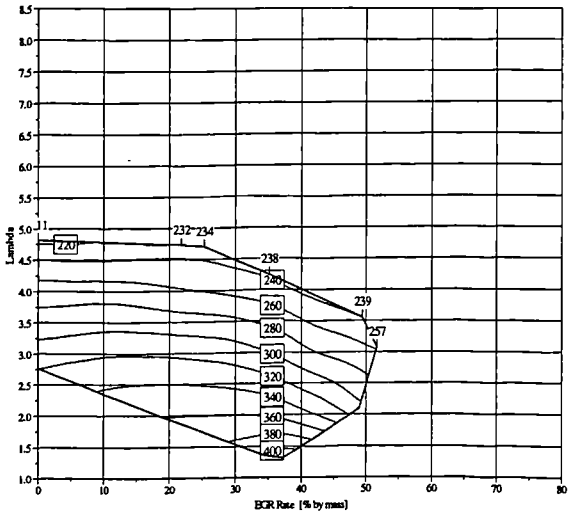

Figure 7.79 Exhaust gas temperature for 80 RON PRF CAI combustion (°C)

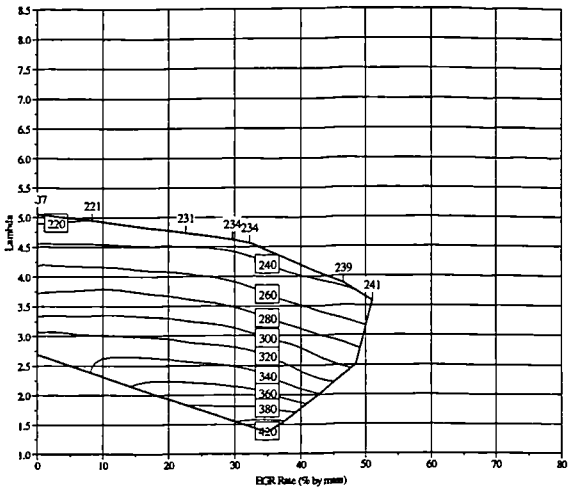

Figure 7.80 Exhaust gas temperature for 90 RON PRF CAI combustion (°C)

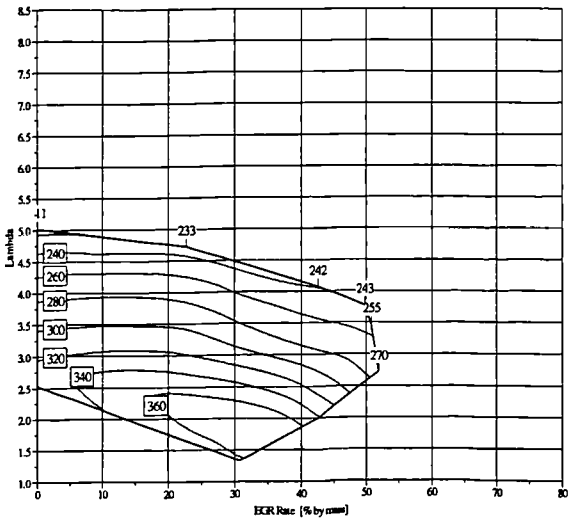

Figure 7.81 Exhaust gas temperature for 95 RON PRF CAI combustion (°C)

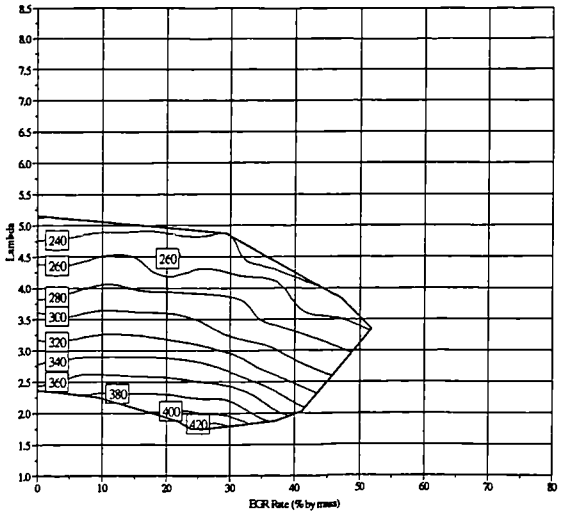

Figure 7.82 Exhaust gas temperature for 100 RON PRF CAI combustion (°C)

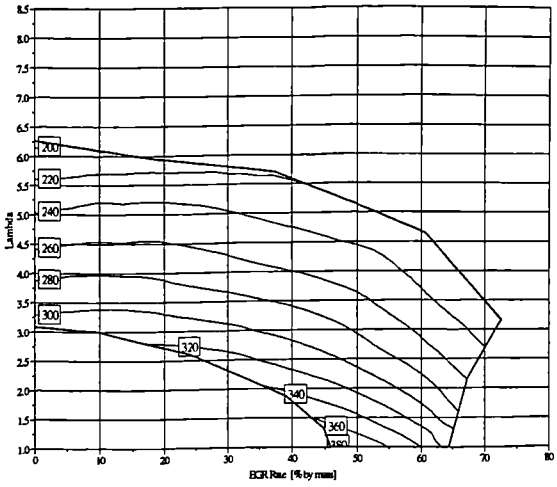

Figure 7.83 Exhaust gas temperature for ethanol CAI combustion (°C)

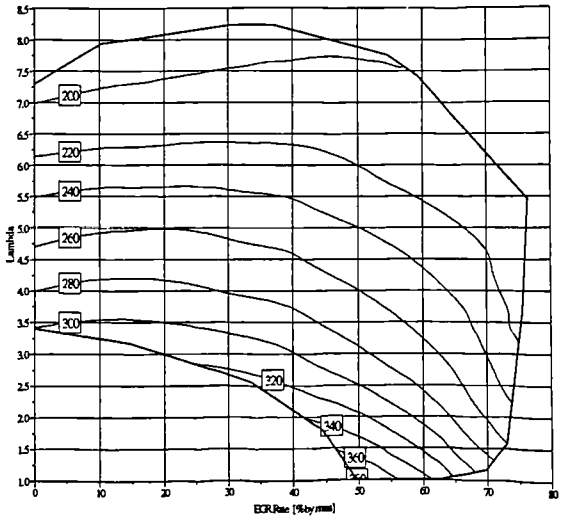

Figure 7.84 Exhaust gas temperature for methanol CAI combustion (°C)

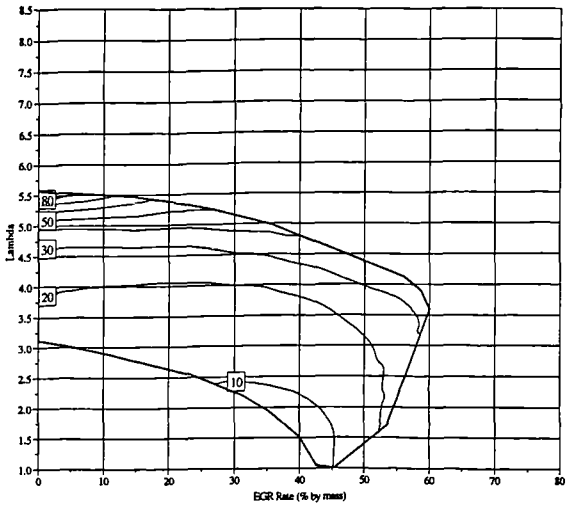

Figure 7.85 Indicated specific unburned HC emissions for gasoline CAI combustion (g/kW.h)

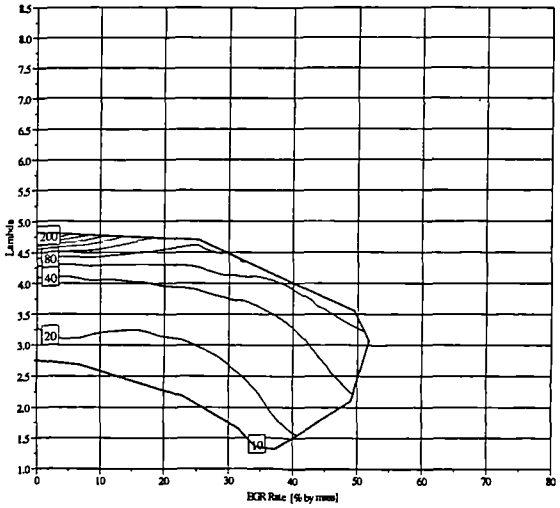

Figure 7.88 Indicated specific unburned HC emissions for 80 RON PRF CAI combustion (g/kW.h)

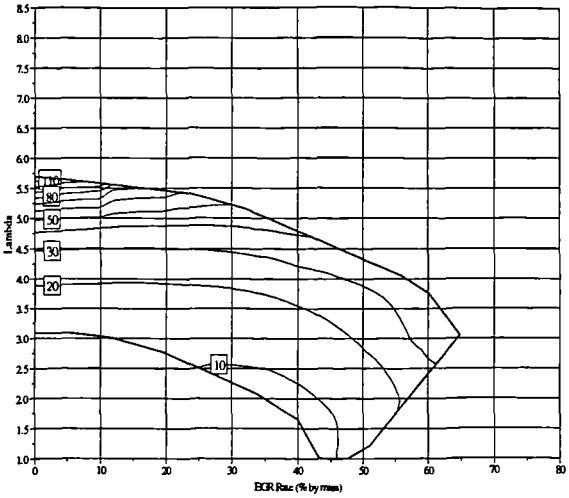

Figure 7.86 Indicated specific unburned HC emissions for light fraction gasoline CAI combustion (g/kW.h)

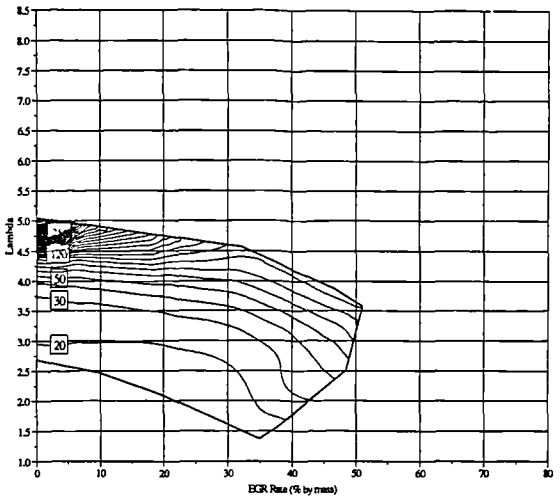

Figure 7.89 Indicated specific unburned HC emissions for 90 RON PRF CAI combustion (g/kW.h)

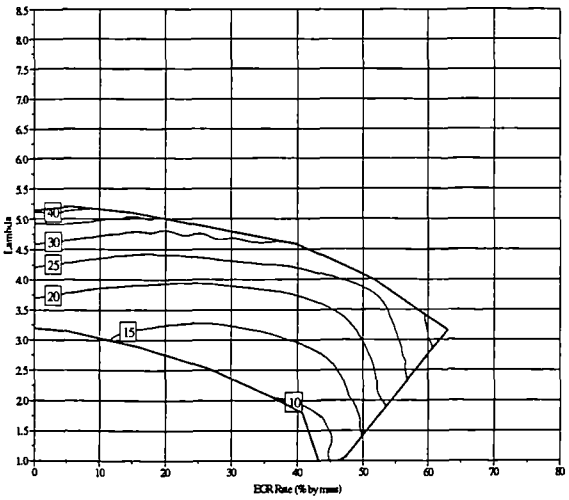

Figure 7.87 Indicated specific unburned HC emissions for heavy fraction gasoline CAI combustion (g/kW.h)

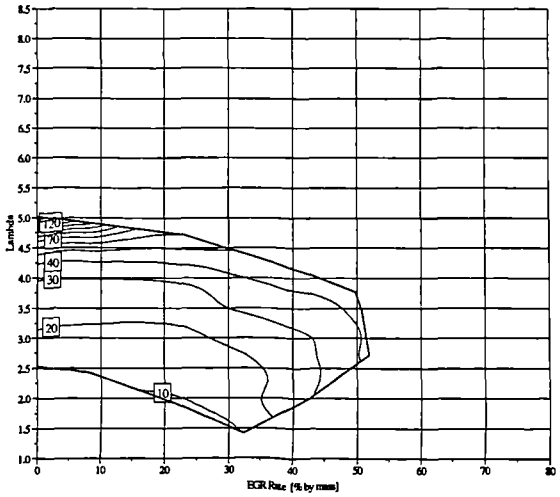

Figure 7.90 Indicated specific unburned HC emissions for 95 RON PRF CAI combustion (g/kW.h)

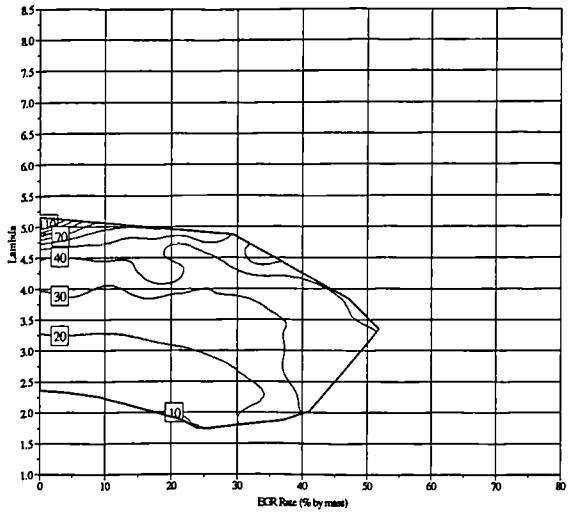

Figure 7.91 Indicated specific unburned HC emissions for 100 RON PRF CAI combustion (g/kW.h)

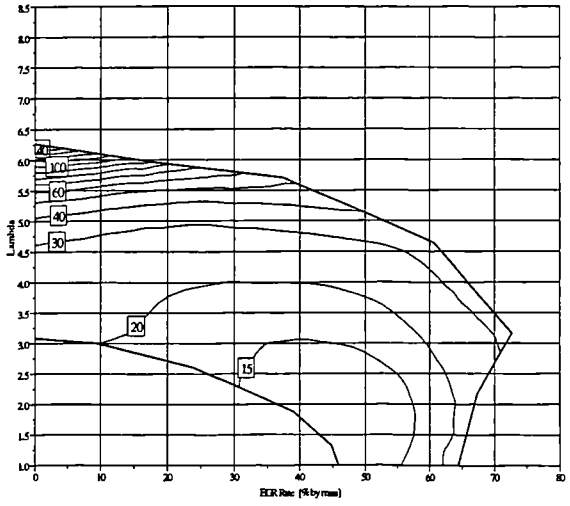

Figure 7.92 Indicated specific unburned HC emissions for ethanol CAI combustion (g/kW.h)

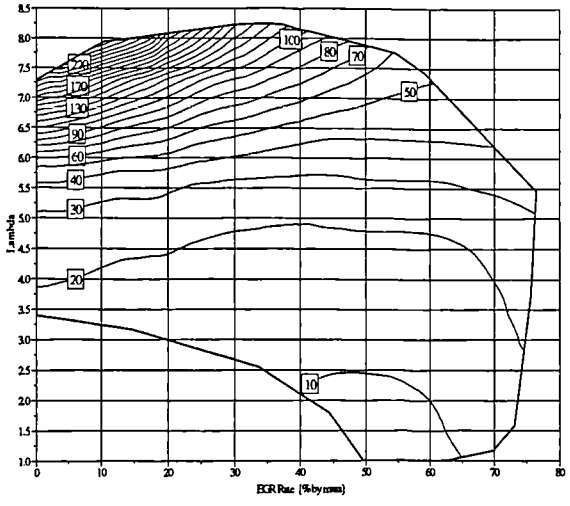

Figure 7.93 Indicated specific unburned HC emissions for methanol CAI combustion (g/kW.h)

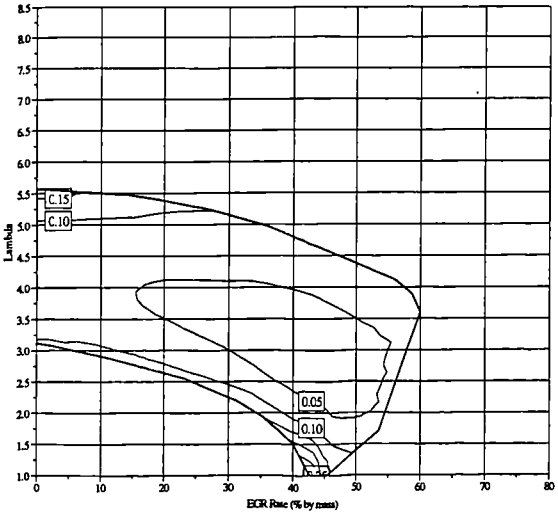

Figure 7.94 Indicated specific NO_x emissions for gasoline CAI combustion (g/kW.h)

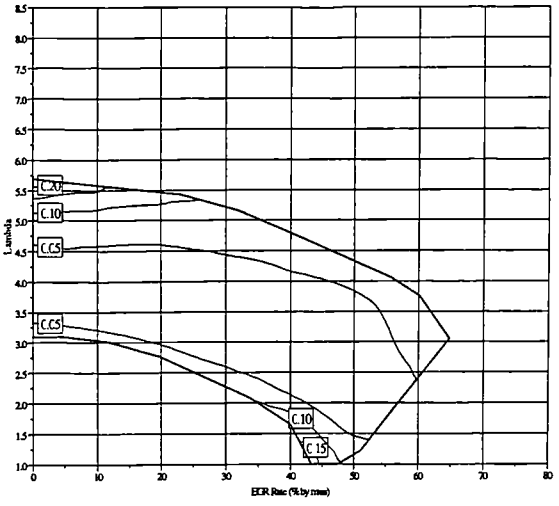

Figure 7.95 Indicated specific NO_x emissions for light fraction gasoline CAI combustion (g/kW.h)

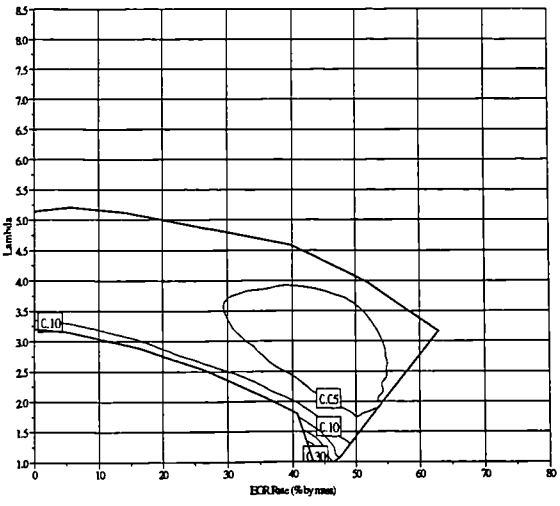

Figure 7.96 Indicated specific NO_x emissions for heavy fraction gasoline CAI combustion (g/kW.h)

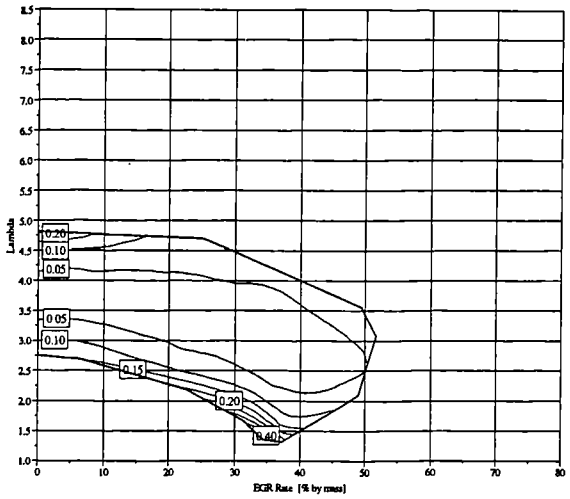

Figure 7.97 Indicated specific NO_x emissions for 80 RON PRF CAI combustion (g/kW.h)

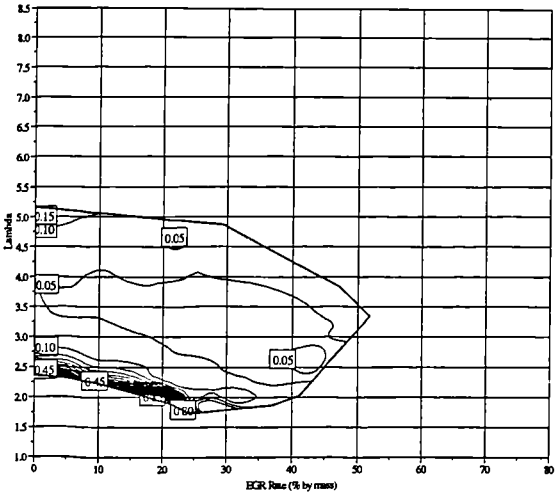

Figure 7.100 Indicated specific NO_x emissions for 100 RON PRF CAI combustion (g/kW.h)

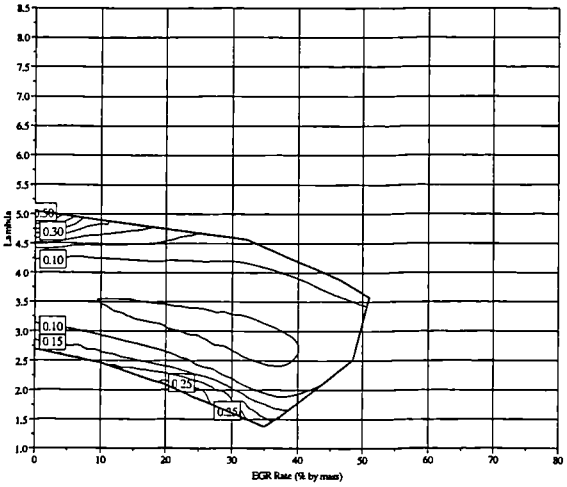

Figure 7.98 Indicated specific NO_x emissions for 90 RON PRF CAI combustion (g/kW.h)

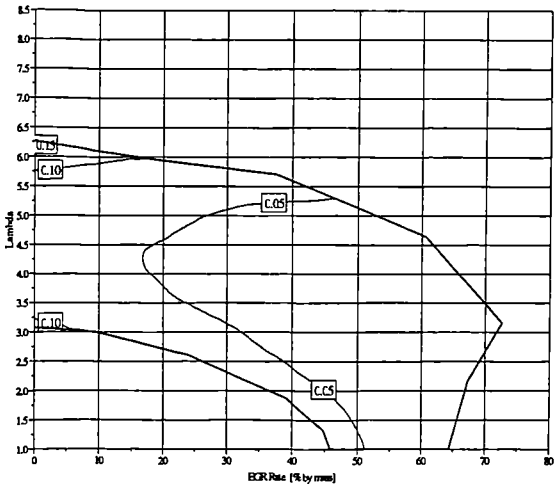

Figure 7.101 Indicated specific NO_x emissions for ethanol CAI combustion (g/kW.h)

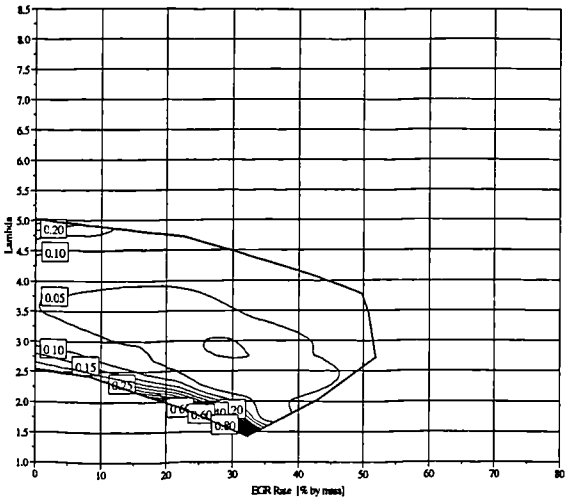

Figure 7.99 Indicated specific NO_x emissions for 95 RON PRF CAI combustion (g/kW.h)

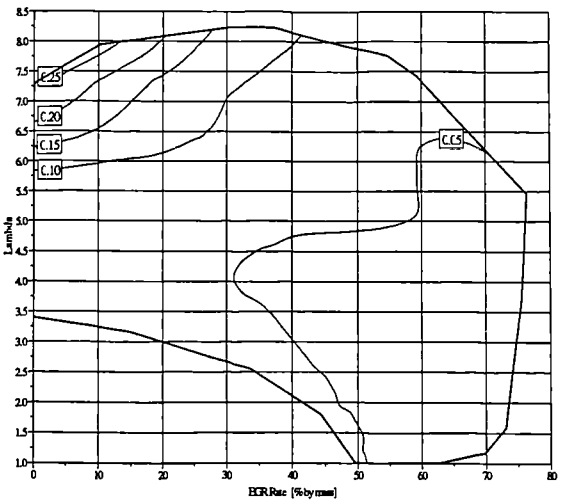

Figure 7.102 Indicated specific NO_x emissions for methanol CAI combustion (g/kW.h)

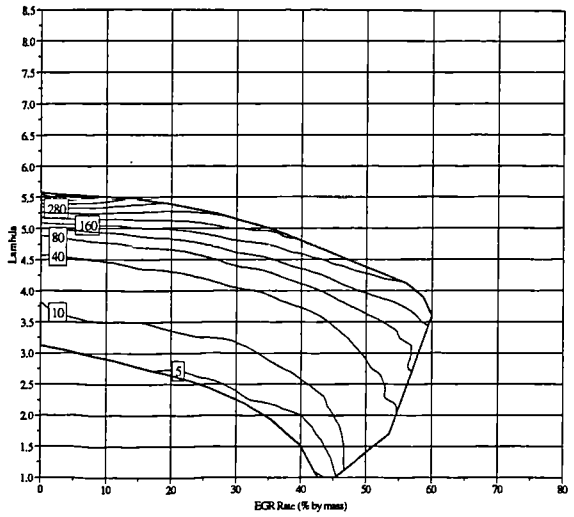

Figure 7.103 Indicated specific CO emissions for gasoline CAI combustion (g/kW.h)

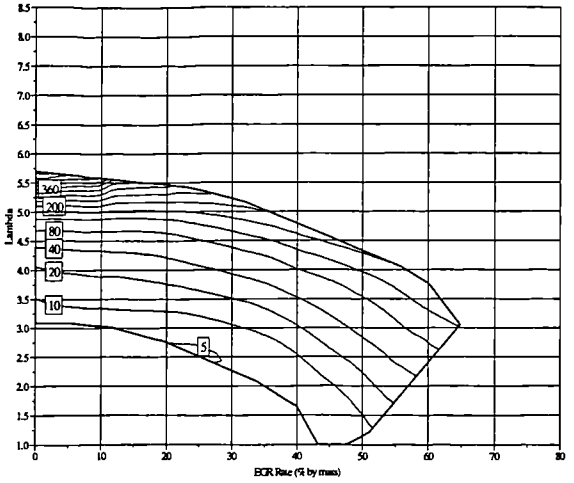

Figure 7.104 Indicated specific CO emissions for light fraction gasoline CAI combustion (g/kW.h)

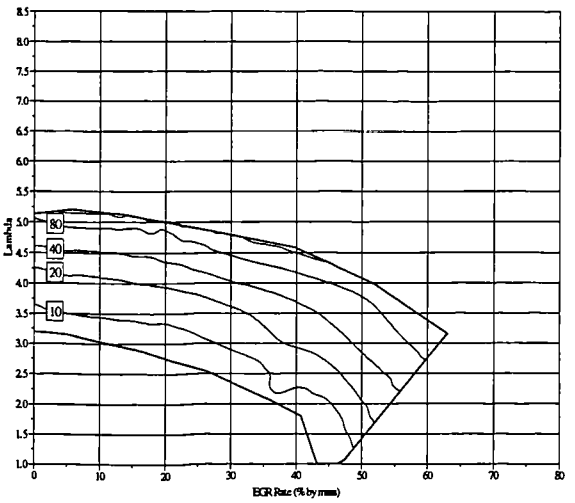

Figure 7.105 Indicated specific CO emissions for light fraction gasoline CAI combustion (g/kW.h)

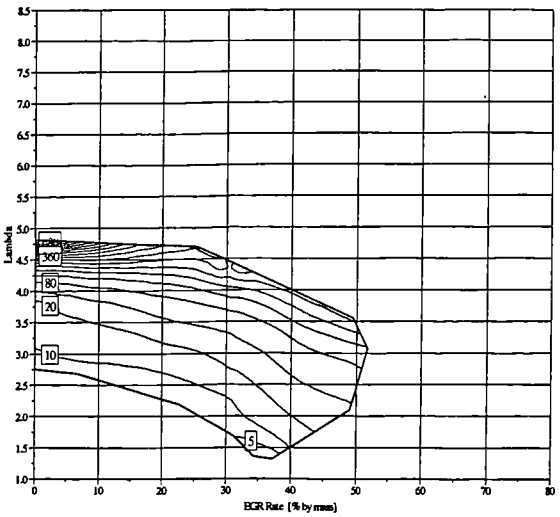

Figure 7.106 Indicated specific CO emissions for 80 RON PRF CAI combustion (g/kW.h)

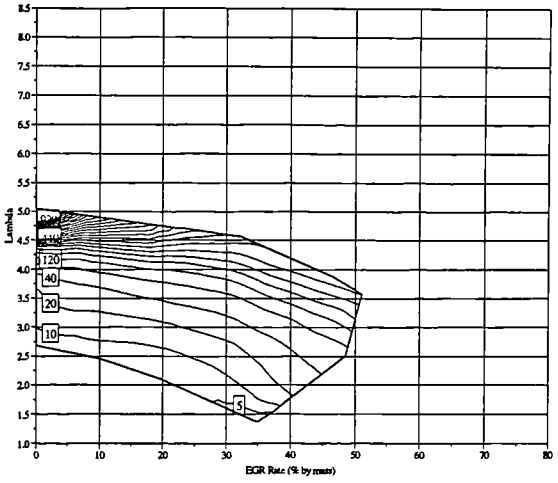

Figure 7.107 Indicated specific CO emissions for 90 RON PRF CAI combustion (g/kW.h)

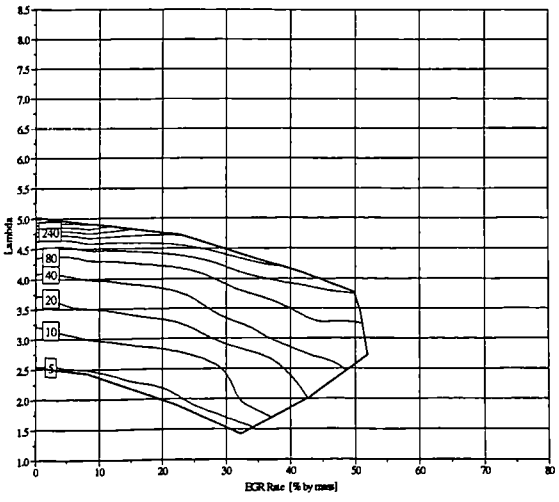

Figure 7.108 Indicated specific CO emissions for 95 RON PRF CAI combustion (g/kW.h)

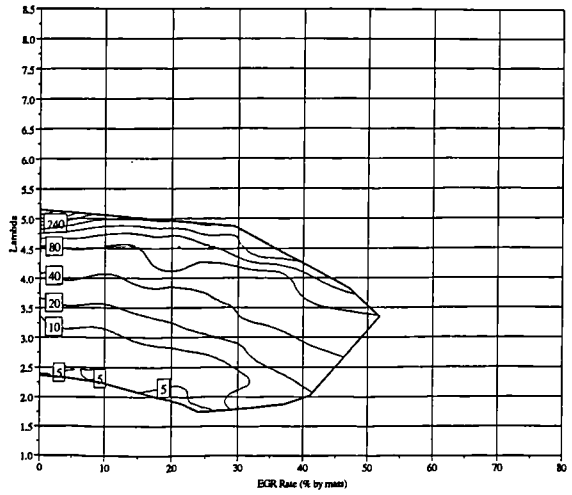

Figure 7.109 Indicated specific CO emissions for 100 RON PRF CAI combustion (g/kW.h)

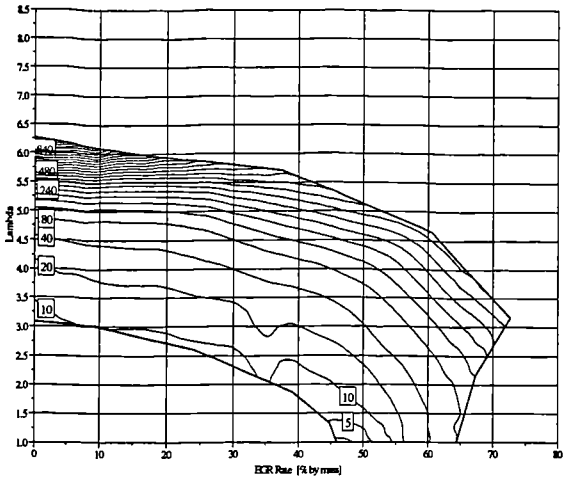

Figure 7.110 Indicated specific CO emissions for ethanol CAI combustion (g/kW.h)

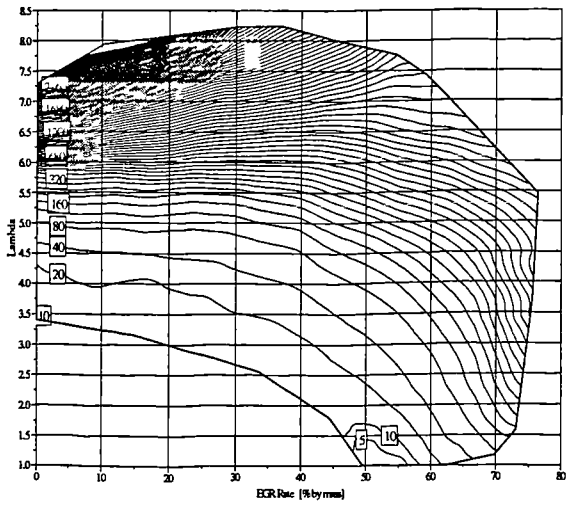

Figure 7.111 Indicated specific CO emissions for methanol CAI combustion (g/kW.h)

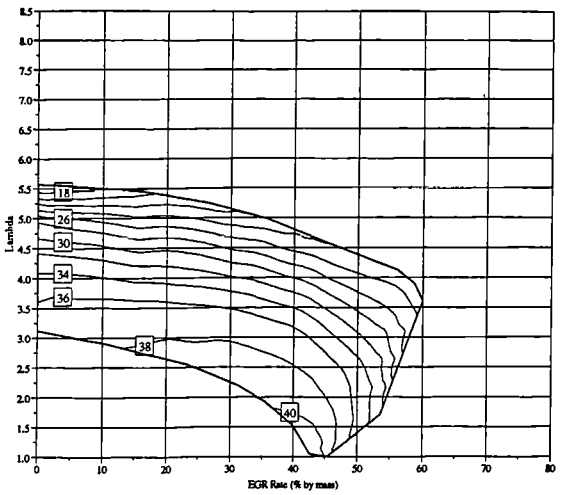

Figure 7.112 Indicated thermal efficiency for gasoline CAI combustion (%)

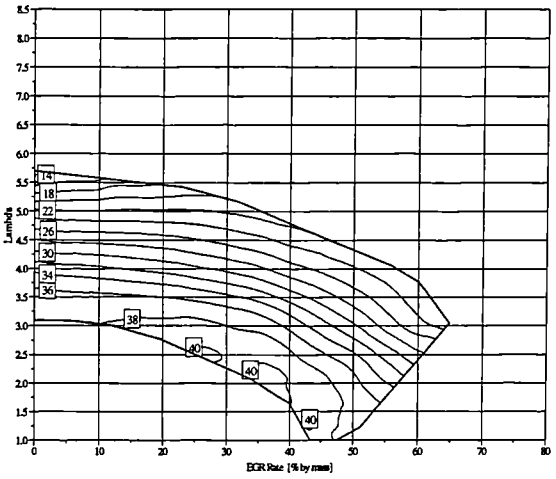

Figure 7.113 Indicated thermal efficiency for light fraction CAI combustion (%)

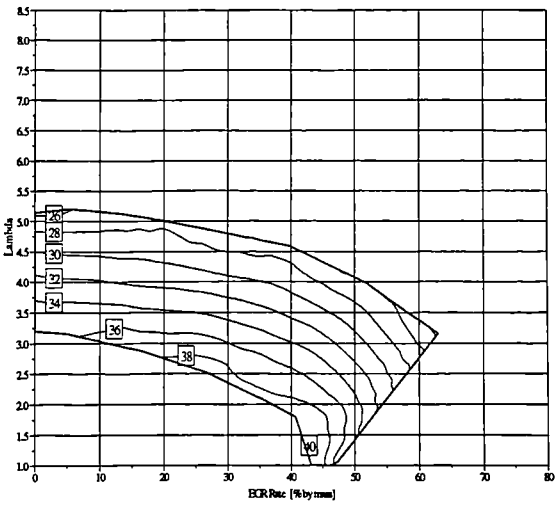

Figure 7.114 Indicated thermal efficiency for heavy fraction CAI combustion (%)

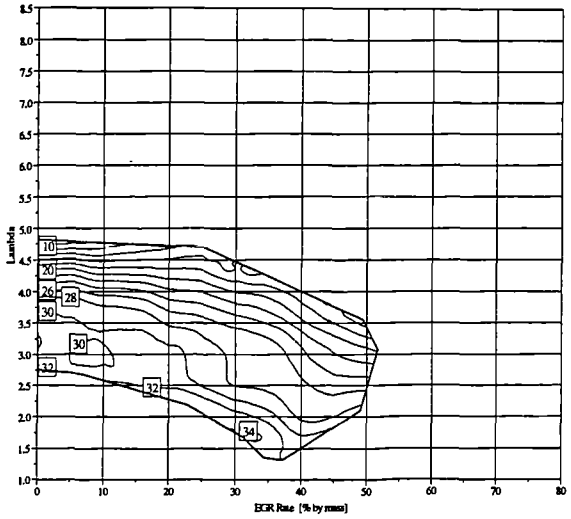

Figure 7.115 Indicated thermal efficiency for 80 RON PRF CAI combustion (%)

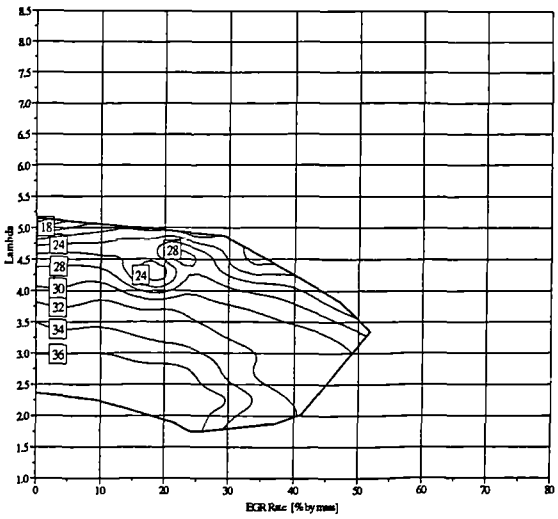

Figure 7.118 Indicated thermal efficiency for 100 RON PRF CAI combustion (%)

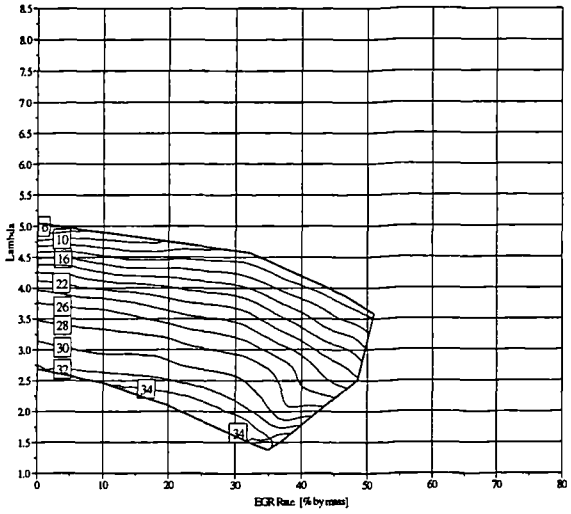

Figure 7.116 Indicated thermal efficiency for 90 RON PRF CAI combustion (%)

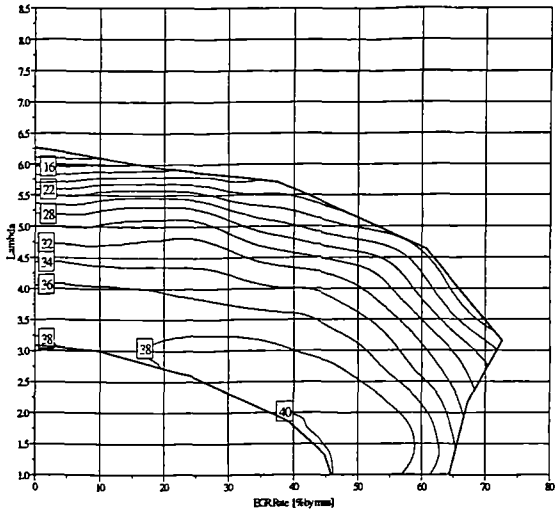

Figure 7.119 Indicated thermal efficiency for ethanol CAI combustion (%)

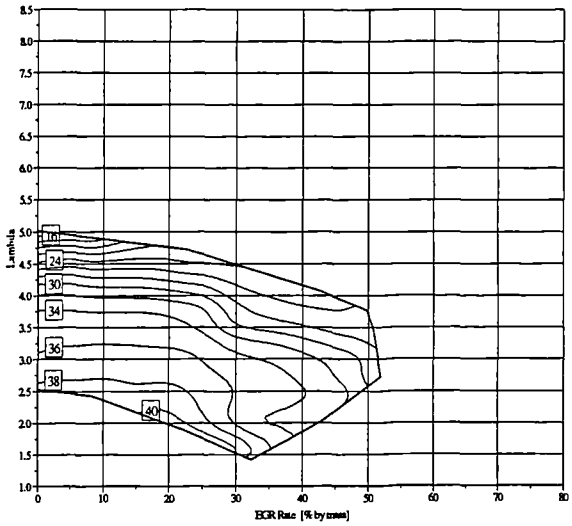

Figure 7.117 Indicated thermal efficiency for 95 RON PRF CAI combustion (%)

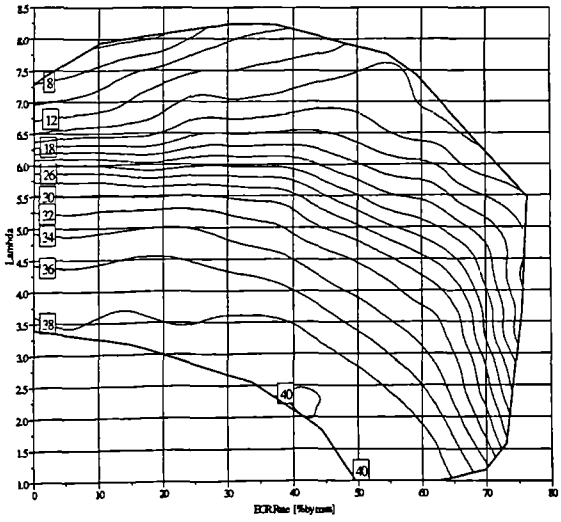

Figure 7.120 Indicated thermal efficiency for methanol CAI combustion (%)

Chapter 8

Conclusions and Recommendations for Further Work

Chapter 8 Conclusions and Recommendations for Further Work

8.1 Conclusions

8.1.1 Stratified Fuel Fraction Engine (STRAFFE) Concept

The STRAFEE concept as proposed by the Ford Motor Company has been evaluated through development and testing of an online gasoline fuel fractionating system in both SI and CAI combustion modes. The prototype system was shown to operate satisfactorily under steady state conditions, producing a stable flow of light and heavy fractions to the intake manifold of the engine. Unfortunately, there appears to be a trade-off between the stability of vapour (light fraction) production and the system's thermal inertia. To maintain a stable light fraction flow, the thermal mass of the system must be kept relatively high, which compromises its behaviour under transient engine operating conditions.

Compositional, octane, and spark-induced knocking combustion tests performed on the gasoline fractions showed that they are significantly different. Results indicated that if the STRAFFE concept is employed in a modern fast-burn engine, then the compression ratio of the engine may be increased by up to 1.0. This can be achieved through the combined effects of a faster burning light fraction, and a higher-octane heavy fraction.

Conversely, CAI combustion tests performed over a range of A/F ratios and EGR rates, and at two intake temperature/compression ratio conditions, have shown that the fractions behave almost identically, with similar normal and knocking combustion characteristics. Thus, a CAI engine is unlikely to benefit from employment of the STRAFFE concept. However, this result also shows that CAI combustion is relatively insensitive to the precise gasoline formulation, and so strict controls on the gasoline fuel composition for a CAI engine may not be required.

8.1.2 CAI Combustion Tests

4-stroke CAI combustion systems that employ recycled burned gases to achieve the required heat and dilution conditions appear to be the most promising for practical applications. However, review of the relevant literature showed that the effects of air and

exhaust gas dilution has not been fully and rigorously investigated. The tests performed in this work set out to document the effects of dilution on homogeneous CAI combustion of a wide range of candidate fuels. Detailed data on the heat-release, load, and emissions trends exhibited by these fuels over the dilution ranges has been presented and compared qualitatively and quantitatively. Conclusions from this work are as follows:

(i) Knocking combustion limited high load operation for all of the fuels tested. The air and EGR dilution conditions required to cause similar knocking characteristics varied significantly between fuels, except between the gasoline fractions. The PRFs generally required less dilution, and the alcohol fuels more. However, the onset of knocking combustion was accompanied by an increase in in-cylinder pressure-rise rate, which was found to be numerically similar for all of the fuels. Thus, a means of avoiding knock and allowing higher loads to be attained is simply to limit the pressure rise rate.

(ii) Low load operation could only be achieved under ultra-lean conditions for all of the fuels tested. This is because the effect of EGR is to retard ignition and/or increase the combustion duration excessively, so the required dilution to achieve low loads cannot be attained. Unfortunately, lean conditions lead to higher unburned hydrocarbon and CO emissions, which in turn reduces combustion and thermal efficiencies. It is thought that these emissions rise as a result of lowering combustion temperature, which is inevitable for homogeneous combustion as the fuelling rate is decreased. Thus, lean operation is not considered as a practical means of achieving low loads in a CAI engine.

(iii) Excessive EGR rates lead to misfire in hydrocarbon fuels, since ignition is monotonically retarded with increasing EGR dilution. The EGR rate to cause misfire for a particular fuel depends intimately on the intake temperature/compression ratio conditions chosen. In the cases of the PRFs, and the gasoline fractions under low intake temperature conditions, the misfire and knocking combustion boundaries converge under lean conditions. At these conditions, combustion is extremely unstable and variable, as indicated by COVimep trends. Thus, high load combustion is unstable if the intake temperature/compression ratio conditions are not sufficiently severe.

(iv) Combustion trends with increasing EGR are markedly different for the alcohol fuels. Most significantly, the ignition of methanol shows almost no relationship with EGR rate, and misfire never occurs. Methanol also exhibits a much wider overall operating region, indicating that the minimum intake temperature/compression ratio conditions required to achieve CAI combustion are much lower than for the hydrocarbon fuels. Thus, in systems that employ recycled burned gases to provide the heat and dilution for CAI combustion, the required temperature of the exhaust gases and the degree of charge stratification are much less onerous than for hydrocarbon fuels. In the past researchers have asserted that the presence of radicals in the recycled gases aids methanol autoignition, and more so than for gasoline. However, these results show that methanol is more superior to gasoline for CAI combustion for other reasons, since the significantly cooled EGR used here cannot contain radicals. It would appear that its superiority stems from its composition and autoignition chemistry. Methanol contains more oxygen than ethanol, which itself exhibits only a small dependence of ignition timing on EGR. It appears that the oxygen contained within the fuels must play a significant role in their more suitable autoignition characteristics.

(v) Highest efficiencies for all of the fuels were obtained under the highest load conditions, when unburned HC and CO emissions were lowest, and NO_x emissions were also highest. It is interesting that these conditions do not coincide with optimal combustion timing (close to TDC). Thus, in a CAI engine using recycled burned gases, the fuelling rate and valve timing and profiles are used to obtain best emissions, ISFC, and power in much the same way that the throttle and spark ignition systems are used in a SI engine for the same reasons. Ignition timing in a CAI engine is a consequence of the conditions chosen to achieve good engine operation, and not necessarily something that needs to be optimised.

The tests performed here have given great insight into various aspects of homogeneous CAI combustion, with particular relevance to dilution effects. It is hoped that this work will provide future researchers in the field with useful information for the development of CAI combustion systems, fuels, and kinetic models. To this end, the author has co-authored four technical papers [96-99] that set out the main results of this work in a more digestible format.

8.2 Recommendations for Further Work

Considerable progress was made towards realising the STRAFFE concept, and understanding the effects of air and exhaust gas dilution on CAI combustion for a range of research and real-world fuels. However, there are a number of aspects of this research that can be extended upon.

8.2.1 Stratified Fuel Fraction Engine (STRAFFE) Concept

The fuel fractionating system has been developed to prototype stage, so that steady state tests could be performed on the light and heavy fraction fuel streams. However, compositional and octane analysis performed by Saybolt UK Ltd. showed that the fractions produced by the system are not as well defined as can be achieved under ideal conditions. It is suggested that optimisation of the fractionating system be undertaken. A starting point for this process is to design a more efficient heat exchanger than the simple coil-in-fuel currently used.

Transient operation of the fractionating system has been identified as problematic due its thermal inertia. Further work is required to determine the system's transient behaviour and optimise it. However, it remains to be seen if the transient response can only be improved at the expense of stability of vapour production. These problems arise because of the 'online' nature of the current system. An alternative system could be developed similar to that proposed by Jehlik et al. [100]. In such a system, fuel fractions would be produced 'offline' and stored for use by the engine in two separate reservoirs. Decoupling the production of the fractions from their metering to the engine allows a much more flexible system, which will accommodate transient requirements easily. However, it may also require that the light fraction be stored, which is not an easy task since it leaves the vaporisation chamber as a vapour.

The STRAFFE concept has not been tested in its entirety. To fully prove the concept, the fractionating system must be installed on an engine that has the capability to deliver the fuel fractions such that the in-cylinder charge is stratified in the correct pattern.

8.2.2 CAI Combustion

A parametric study of fuels, and air and EGR dilution has been undertaken here. To give further insight into how homogeneous CAI is affected by engine conditions, it is suggested that similar tests be performed for a range of compression ratios for fixed intake charge temperature, and vice versa. Similarly, parameters such as coolant and oil temperatures, and engine speed can be further investigated.

Results from the investigation of autoignition temperatures were inconclusive using the calculation technique presented. Direct measurement of in-cylinder temperature would be desirable. The measured gas temperature for a number of fuels and engine operating conditions would provide researchers with more information on the most suitable fuel types for CAI combustion, and facilitate the design of optimised fuels for use in real applications.

Significant differences between alcohol and hydrocarbon fuels have been detected. Experimental investigations could look at blends of gasoline and methanol to see if similar autoignition characteristics can be achieved to methanol alone. It may transpire that the blending autoignition characteristics of methanol are non-linear in the same way that the blending octane characteristics of individual hydrocarbons contained within gasoline are non-linear. A blend of gasoline and methanol is a much more economically attractive fuel than having to use methanol alone.

The autoignition chemistry of methanol fuel is relatively simple because it is a single compound. It is well within the capabilities of modern computers to develop kinetic models that describe how methanol behaves under CAI combustion conditions. Such an investigation would be extremely useful to determine why it behaves so differently to hydrocarbon fuels. It would also provide information on how best to design a fuel to meet the requirements of CAI combustion more effectively.

References

1. "Climate Change UK Programme", UK Department of the Environment Transport and the Regions, February 2001.

2. "The Kyoto Protocol to the United Nations Framework Convention on Climate Change", UNFCCC Document No. FCCC/CP/1997/7/Add.1, March 1998.

3. "California Exhaust Emissions Standards and Test Procedures for 2001 and Subsequent Model Passenger Cars, Light-Duty Trucks, and Medium-Duty Vehicles", California Environmental Protection Agency Air Resources Board (CARB), August 1999.

4. Information on Euro II – Euro IV emissions regulations, provided by the UK Vehicle Certification Agency (VCA), obtained from http://www.vcacarfueldata.org.uk/ , 2001.

5. Johnson, T. V., "Mobile emission control technologies in review", Int. Conf. On 21st Century Emissions Technology, IMechE Conference Transactions 2000-2, ISBN 1 86058 322 9, 2000.

6. Weiss, M., Heywood, J., et. al., "On the Road in 2020: A Life Cycle Analysis of New Automobile Technologies", MIT Energy Laboratory Report EL00-003, MIT, Cambridge, MA, October 2000.

7. Kishi, N., et. al., "Technology for Reducing Exhaust Gas Emissions in Zero Level Vehicles (ZLEV)", SAE 1999-01-0772, 1999

8. Kitagwa, H., et. al., "L-4 Development for a Super Ultra Low Emissions Vehicle (SULEV)", SAE 2000-01-0887, 2000.

9. Stone, R., "Introduction to Internal Combustion Engines", Third Edition, p.171, Macmillan Press, ISBN 0-333-74013-0, 1999.

10. Searles, R. A., "Emission catalyst technology – challenges and opportunities in the 21st century" Int. Conf. On 21st Century Emissions Technology, IMechE Conference Transactions 2000-2, ISBN 1 86058 322 9, 2000.

11. Salvat, O., et. al., "Passenger Car Serial Application of a Particulate Filter System on a Common Rail Direct Injection Diesel Engine", SAE Paper 2000-01-0473, 2000.

12. Oppenheim, A. K., "The Knock Syndrome: Its Cures and its Victims", SAE Paper 841339, 1984

13. Gussak, L. A., et. al. "High Chemical Activity of Incomplete Combustion Products and a Method of Pre-chamber Torch Ignition for Avalanche Activation of Combustion in Internal Combustion Engines" SAE Paper 750890, 1975.

14. Gussak, L. A., et. al. "The Application of LAG-Process in Pre-chamber Engines", SAE Paper 790692, 1979.

15. Onishi, S., "A New Combustion Method of Two-Stroke Engine" A Fundamental Study on the Automobile Emission Control, Education Ministry of Japan, Dec. 22, 1976.

16. Onishi, S., Hong Jo, S., Shoda, K., Do Jo, P., and Kato, S., "Active Thermo-Atmosphere Combustion (ATAC) - A New Combustion Process for Internal Combustion Engines", SAE Paper 790501, 1979.

17. Noguchi, M., Tanaka, Y., Tanaka, T., and Takeuchi, Y., "A Study on Gasoline Engine Combustion by Observation of Intermediate Reactive Products during Combustion", SAE Paper 790840, 1979.

18. 'Honda readies Activated Radical Combustion two-stroke engine for production motorcycle', Automotive Engineer, pp. 90-92, SAE Publications, January 1997.

19. Shawcross, D., Pumphrey, C., and Arnall, D., "A Five-Million Kilometre, 100 Vehicle Fleet Trial, of an Air-Assist Direct Fuel Injected, Automotive 2-Stroke Engine", SAE Paper 2000-01-0898, 2000.

20. Najt, P. M., and Foster, D. E., "Compression-Ignited Homogeneous Charge Combustion", SAE Paper 830264, 1983.

21. Lavy, J., Dabadie, J., Angelberger, C., Duret, P. (IFP), Willand, J., Juretzka, A., Schaflein, J. (Daimler-Chrysler), Ma, T. (Ford), Lendresse, Y., Satre, A.(PSA Peugeot Citroen), Schulz, C., Kramer, H. (PCI - Heidelberg University), Zhao, H., Damiano (Brunel University), "Innovative Ultra-low NOx Controlled Auto-Ignition Combustion Process for Gasoline Engines : the 4-SPACE Project", SAE Paper 2000-01-1837, 2000.

22. Kimura, S., Aoki, O., Ogawa, H., Muranaka, S., Enomoto, "New Combustion Concept for Ultra-Clean and High Eficiency Small DI Diesel Engines", SAE Paper 1999-01-3681, 1999.

23. Kimura, S., Aoki, O., Kitahara, Y., Aiyoshizawa, E., "Ultra-Clean Combustion Technology Combining a Low-Temperature and Premixed Combustion Concept for Meeting Future Emission Standards", SAE Paper 2001-01-0200, 2001

24. Thring, R. H., "Homogeneous Charge Compression-Ignition (HCCI) Engines", SAE Paper 892068, 1989.

25. Ishibashi, Y., Asai, M., "Improving the Exhaust Emissions of Two-Stroke Engines by Applying the Activated Radical Combustion", SAE Paper 960742, 1996.

26. Aoyama, T., Hattori, Y., Mizuta, J., Sato, Y., "An Experimental Study on Premixed-Charge Compression Ignition Gasoline Engine", SAE Paper 960081, 1996.

27. Duret, P., and Venturi, S., "Automotive Calibration of the IAPAC Fluid Dynamically Controlled Two-Stroke Combustion Process", SAE Paper 960363, 1996.

28. Ricardo, H., "Recent Research Work on the Internal Combustion Engine" SAE Trans., Vol. 17, Pt. 1, 1922.

29. Strehlow, R. A., "Combustion Fundamentals", McGraw-Hill, ISBN 0-07-066599-0, 1984.

30. Withrow, L., Boyd, T. A., Ind. and Eng. Chem., Vol. 23, p. 539

31. Miller, C. D., SAE Quart. Trans.,Vol. 1, p. 98, 1947

32. Male, T., Third Symposium on Combustion, Flame and Explosion Phenomena, Williams and Wilkins, Baltimore, p. 721, 1949.

33. Kono, M., Shiga, S., Kumagai, S., Iinuma, K., "Thermodynamic and Experimental Determinations of Knock Intensity by Using Spark-Ignited Rapid Compression Machine", Combustion and Flame Vol. 54, pp. 33-47, 1983.

34. Chun, K. M., Heywood, J. B., "Characterisation of Knock in a Spark-Ignition Engine", SAE Paper 890156, 1989.

35. Lee, W., Schaefer, H. J., "Analysis of Local Pressures, Surface Temperatures and Engine Damages under Knock Conditions", SAE Paper 830508, 1983.

36. Zhao, H, Collings, N., Ma, T., "Characterisation of Knock and its Effect on Surface Temperatures", SAE Paper 920514, 1992.

37. Stone, R., "Introduction to Internal Combustion Engines", Third Edition, p.150, Macmillan Press, ISBN 0-333-74013-0, 1999.

38. Dickinson, H. C., "The Cooperative Fuel Research and its Results", SAE Trans., 24, 262-265, 1929.

39. Campbell, J.M., Lovell, W. G., and Boyd, T. A., "Detonation Characteristics of Some of the Fuels Suggested as Standards of Anti-Knock Quality", SAE Trans., 25, 126-131, 1930.

40. Horning, H. L., "The Cooperative Fuel-Research Committee Engine", SAE Trans., 26, 436-440, 1931.

41. Boyd, T. A., "Pathfinding in Fuels and Engines" SAE Quart. Trans., 4, 182-195, 1950.

42. Glassman, I., Combustion, Academic Press, 1977.

43. Heywood, J. B., "Internal Combustion Engine Fundamentals", p.464, McGraw-Hill, ISBN 0-07-100499-8, 1988.

44. Leppard, W. R., "The Chemical Origin of Fuel Octane Sensitivity", SAE Paper 902137, 1990.

45. Litzinger, T. A., "A review of Experimental Studies of Knock Chemistry in Engines", Prog. Energy Combust. Sci., Vol. 16, pp. 155-167, 1990.

46. Heywood, J. B., "Internal Combustion Engine Fundamentals", p.469, McGraw-Hill, ISBN 0-07-100499-8, 1988.

47. Lovell, W. G., "Knocking Characteristics of Hydrocarbons", Industrial and Engineering Chemistry, Vo. 40, No. 12, pp. 2388-2438, 1948.

48. Owen, K., Coley, O., "Automotive Fuels Reference Book", p. 112, Second Edition, SAE Publications, ISBN 1-56091-589-7, 1995.

49. Mackinven, R., "A Search for an Ashless Replacement for Lead in Gasoline", Jahrestagung, DGMK, West Germany, 1974.

50. Kawabata, Y., Sakonji, T., Amano, T., "The Effect of NOx on Knock in Spark-ignition Engines", SAE Paper 1999-01-0572, 1999.

51. Brooks, D. B., "Ozone, Knock-Inducer Extraordinary" J. Ind. Petroleum Technology, Vol. 19, pp. 835-844, 1933

52. Axelsson, E., Brezinsky, K., Dryer, F. L.,Pitz, W. J., and Westbrook, C. K., Twenty-First Int. Symp. On Comb., p.783, The Combustion Institute, Pittsburg, 1987.

53. Kirsch, L. J., and Quinn, C. P., J. Chem. Phys. 82, 459, 1985

54. Heywood, J. B., "Internal Combustion Engine Fundamentals", p.237, McGraw-Hill, ISBN 0-07-100499-8, 1988.

55. Russ, S., "A Review of the Effect of Engine Operating Conditions on Borderline Knock", SAE Paper 960497, 1996.

56. Gluckstein, M. E., Walcutt, C., "End-Gas Temperature-Pressure Histories and Their Relation to Knock", SAE Trans. 69, pp. 529-553, 1961.

57. Taylor, C. F., "The Internal Combustion Engine in Theory and Theory and Practice Volume 2: Combustion, Fuels, Materials, and Design", The MIT Press, 1985.

58. Leppard, W. R., "Individual Cylinder Knock Occurrence and Intensity In Multi-Cylinder Engines", SAE Paper 820074, 1982.

59. Caris, D. F., Nelson, E. E., "A New Look at High Compression Engines", Sae Transactions, Vol. 67, pp.112-124, 1959.

60. Thring, R. H., Overington, M. T., "Gasoline EngineCombustion – The High Ratio Compact Chamber, SAE Paper 820166, 1982.

61. Caris, D.F., Mitchel B.J., McDuffie, A.D., Wyczalek, F.A., "Mechanical Octanes for Higher Efficiency", SAE Transactions, Vol. 64, pp. 76-100, 1956.

62. Heywood, J. B., "Internal Combustion Engine Fundamentals", p.467, McGraw-Hill, ISBN 0-07-100499-8, 1988.

63. Pucher, G. R., Gardiner, D. P., Bardon, M. F., and Battista, V., "Alternative Combustion Systems for Piston Engines Involving Homogeneous Charge Compression Ignition Concepts - A review of Studies Using Methanol, Gasoline and Diesel Fuel.", SAE Paper 962063, 1996.

64. Yui, S., Ohnishi, S., "A New Concept of Stratified Charge Two-Stroke Engine – Yui and Ohnishi Combustion Process (YOCP)" SAE Paper 690468, 1969.

65. Jo, S. H., Jo, P. D., Gomi, T., Ohnishi, S., "Development of a Low Emission and High Performance 2-Stroke Gasoline Engine (NiCE)", SAE Paper 730463, 1973.

66. Stanglmaier, R. H., and Roberts, C. E., "Homogeneous Charge Compression Ignition (HCCI): Benefits, Compromises, and Future Engine Applications", SAE Paper 1999-01-3682, 1999.

67. Ryan III, T. W., Callahan, T. J., "Homogeneous Charge Compression Ignition of Diesel Fuel", SAE Paper 961160, 1996.

68. Christensen, M., Hultqvist, A., and Johansson, B., "Demonstrating the Multi Fuel Capability of a Homogeneous Charge Compression Ignition Engine with Variable Compression Ratio", SAE Paper 1999-01-3679, 1999.

69. Olsson, J., Johansson, B., "Closed Loop Control of an HCCI Engine", SAE Paper 2001-01-1031, 2001.

70. Bruestle, C., Schwarzenthal, D., "VarioCam Plus – A Highlight of the Porsche 911 Turbo Engine", SAE Paper 2001-01-0245, 2001

71. Ekenburg, M., "SAAB Combustion Concept – A High Fuel Economy Concept Meeting Future World Emissions Regulations", SAE Paper 2001-01-0246, 2001.

72. Kreuter, P., Heuser, P., Reinicke, J., Stein, P., Erz, R., Peter, U., "Meta CVD System – An Electro Mechanical Cylinder and Valve Deactivation System", SAE Paper 2001-01-0240, 2001.

73. Li, J., Zhao, H., Ladommatos, N., Ma, T., "Research and Development of Controlled Auto-ignition (CAI) Combustion in a 4-Stroke Multi-Cylinder Gasoline Engine", SAE Paper 2001-01-3608, 2001.

74. Law, D., Allen, J., Kemp, D., Williams, P., "4-stroke active combustion (controlled auto-ignition) investigations using a single cylinder engine with Lotus active valve train (AVT)", Int. Conf. 21st Century Emissions Technology, IMechE 2000.

75. Law, D., Kemp, D., Allen, J., "HCCI Mode of Combustion in a Single Cylinder 4-Stroke Engine Fitted With Active Valve Train", SAE Paper 2001-01-0251, 2001.

76. Christensen, M., Johansson, B., Amneus, P., Mauss, F., "Supercharged Homogeneous Charge Compression Ignition", SAE Paper 980787, 1998

77. Lida, N., "Combustion Analysis of Methanol-Fuelled Active Thermo-Atmosphere Combustion (ATAC) Engine Using Spectroscopic Observation", SAE Paper 940684, 1994.

78. Fergusen, C. R., "Internal Combustion Engines Applied Thermosciences", John Wiley and Sons, New York, 1986.

79. Heywood, J. B., "Internal Combustion Engine Fundamentals", p.413, McGraw-Hill, ISBN 0-07-100499-8, 1988.

80. Matekunas, F. A., "Modes and Measures of Cyclic Combustion Variability", SAE Paper 830337, SAE Trans. Vol. 92, 1983.

81. Lida, N., Ichikura, T., Kase, K., Yoshiteru, E., "Self-Ignition and combustion stability in a methanol fuelled low heat rejection ceramic ATAC engine – analysis of cyclic variation and high wall temperatures and lean burn operation", JSAE Paper 0389-4304/97, 1997.

82. Christensen, M., Johansson, B., Einewall, P., "Homogeneous Charge Compression Ignition (HCCI) Using Isooctane, Ethanol, and Natural Gas – A Comparison with Spark Ignition Operation", SAE Paper 972874, 1997.

83. Christensen, M., Johansson, B., "Influence of Mixture Quality on Homogeneous Charge Compression Ignition", SAE Paper 982454, 1998.

84. Flowers, D., Aceves, S., Smith, R., Torres, J., Girard, J., and Dibble, R., "HCCI in a CFR Engine: Experiments and Detailed Kinetic Modelling", SAE Paper 2000-01-0328, 2000

85. Nakano, M., Mandokoro, Y., Kubo, S., Yamazaki, S., "Effects of exhaust gas recirculation in homogeneous charge compression ignition engines", Int J Engine Research, Vol. 1 No. 3, pp. 269-279, IMechE 2000

86. Duret, P., Lavy, J., "Gasoline Controlled Auto-Ignition (CAI^{TM}): potential and prospects for future automotive application", Int. Conf. 21st Century Emissions Technology, IMechE 2000.

87. Zhao, H., Williams, J., Damiano, L., Bryce, D., Ladommatos, N., "Development of a specially designed optical engine and laser diagnostics for stratified charge and controlled auto-ignition combustion studies", Proceedings of the IMechE, 2000.

88. Zhao, H., Peng, Z., Ladommatos, N., "The Effects of EGR on Controlled Autoignition (CAI) Combustion in a Four-Stroke Gasoline Engine", Proceedings of the IMechE, 2000.

89. Davis, S.G., Law, C. K., "Determination of and Fuel Structure Effects on Laminar Flame Speeds of C_1 to C_8 Hydrocarbons", Combustion Science and Technology, pp. 427-449, 1998.

90. Heywood, J. B., "Internal Combustion Engine Fundamentals", p.150, McGraw-Hill, ISBN 0-07-100499-8, 1988.

91. Stone, R., "Introduction to Internal Combustion Engines", Third Edition, p.526, Macmillan Press, ISBN 0-333-74013-0, 1999.

92. Cheng, W. K., Summers, T., Collings, N., "The fast response flame ionisation detector", Progress in Energy and Combustion Science, Vol. 24, No. 2, pp. 89-124, 1998.

93. Heywood, J. B., "Internal Combustion Engine Fundamentals", Equation 4.68, p.152, McGraw-Hill, ISBN 0-07-100499-8, 1988.

94. "Piston Have Springs In Their Steps", Eureka Innovative Engineering Design, pp. 24-25, June 1999.

95. Stone, R., "Introduction to Internal Combustion Engines", Third Edition, p.597, Macmillan Press, ISBN 0-333-74013-0, 1999.

96. Oakley, A., Zhao, H., Ladommatos, N., Ma, T., "Experimental Studies on Controlled Auto-Ignition (CAI) Combustion in a 4-Stroke Gasoline Engine" Int. Conf. 21st Century Emissions Technology, IMechE 2000.

97. Oakley A., Zhao, H., Ladommatos, N., Ma, T., "Experimental Studies on Controlled Auto-Ignition (CAI) Combustion of Gasoline in a 4-Stroke Engine", SAE Paper 2001-01-1030, 2001.

98. Oakley, A., Zhao, H., Ladommatos, N., Ma, T., "Feasibility Study of an Online Gasoline Fractionating System For Use in Spark-Ignition Engines", SAE Paper 2001-01-1193, 2001.

99. Oakley, A., Zhao, H., Ladommatos, N., Ma, T., "Dilution Effects on the Controlled Auto-Ignition (CA) Combustion of Hydrocarbon and Alcohol Fuels", SAE Paper 2001-01-3606, 2001.

100. Jehlik, F., Jones, M., Shepherd, P., Johnson, K., McClanahan, M., Norbeck, J., "Development of a Low-Emission, Dedicated Ethanol-Fuel Vehicle with Cold-Start Distillation System", SAE Paper 1999-01-0611, 1999.

101. "4-Stroke Powered gasoline Auto-ignition Controlled combustion Engine (4SPACE) project: Final Report", BRITE EURAM III Project. Partners: IFP, Ford, Daimler-Chrysler, PSA Peugeot Citroen, PCI - Heidelberg University, Brunel University. 1998-2001.

Appendix A Calculating the gravimetric EGR rate and A/F ratio from inlet and exhaust compositions only.

A.1 Variables

a	Wet molar fraction of injected fuel
b	H/C ratio of fuel
c	O/C ratio
d	Wet molar fraction of inlet air (not including excess air in EGR)
f	Wet molar fraction of exhaust products in inlet mixture (including excess air)
g	Wet molar fraction of CO_2
h	Wet molar fraction of CO
j	Wet molar fraction of O_2 (associated with exhaust gas and EGR)
k	Wet molar fraction of N_2 (associated with exhaust gas and EGR)
l	Wet molar fraction of H_2O
n_R	Number of moles of reactants
n_P	Number of moles of products
m	Wet molar fraction of NO
q	Wet molar fraction of NO_2
s	Wet molar fraction of unburned hydrocarbons (measured as CH_4)
t	Wet molar fraction of H_2
v	Wet molar fraction of O_2 in the intake gas (including excess O_2 contained in EGR)
x	Generic wet molar fraction

subscripts

i	Associated with the inlet
e	Associated with the exhaust

superscripts

‘	Denotes a dry molar fraction (as measured in all cases except HC and NO_x)

The combustion equation can be written explicitly as:

$$n_R[aCH_bO_c + d(O_2 + 3.773N_2) + (g_iCO_2 + h_iCO + j_iO_2 + k_iN_2 + l_iH_2O + m_iNO + q_iNO_2 + s_iCH_4 + t_iH_2)] \Rightarrow n_P(g_eCO_2 + h_eCO + j_eO_2 + k_eN_2 + l_eH_2O + m_eNO + q_eNO_2 + s_eCH_4 + t_eH_2)$$

Equation A1

Let the volumetric EGR rate

$$f = \frac{x_i}{x_e} \quad \Rightarrow \quad x_i = f.x_e$$

Equation A2

The same is true for the relationship between all exhaust products and EGR components. Thus, equation A1 can be rewritten

$$n_R[aCH_bO_c + d(O_2 + 3.773N_2) + f(g_eCO_2 + h_eCO + j_eO_2 + k_eN_2 + l_eH_2O + m_eNO + q_eNO_2 + s_eCH_4 + t_eH_2)] \Rightarrow n_P(g_eCO_2 + h_eCO + j_eO_2 + k_eN_2 + l_eH_2O + m_eNO + q_eNO_2 + s_eCH_4 + t_eH_2)$$

Equation A3

Collecting EGR and exhaust gas species on the RHS:

$$n_R[aCH_bO_c + d(O_2 + 3.773N_2)] = (n_P - n_Rf)(g_eCO_2 + h_eCO + j_eO_2 + k_eN_2 + l_eH_2O + m_eNO + q_eNO_2 + s_eCH_4 + t_eH_2)$$

Equation A4

Assumptions: These calculations shall be used for lean combustion only. Thus, the term $t_e \rightarrow 0$. Also, when operating in CAI combustion NO_x emissions are negligible, so m_e, $q_e \rightarrow 0$. Even in SI mode, the inaccuracy incurred by not including NO_x concentrations is very small.

Omitting those terms:

$$n_R[aCH_bO_c + d(O_2 + 3.773N_2)] = (n_P - n_R f)(g_e CO_2 + h_e CO + j_e O_2 + k_e N_2 + l_e H_2O + s_e CH_4)$$

Equation A5

The fuel composition is known (b,c), as are the dry concentrations of CO_2, CO, and O_2 in the inlet and exhaust (f, g_e', h_e', j_e'). The variables (d'+j_i'), g_e', h_e', j_e', and s_e are measured using the appropriate analysers. The general relationship

$$x = (1 - l)x'$$

Equation A6

defines the dependence of wet and dry (measured) molar fractions on the H_2O molar fraction in the inlet or exhaust (wet). Providing l_e can be found, d, g_e, h_e, and j_e are known. Solution requires assuming 100 moles of dry exhaust products (n_P = 100).

Thus, The unknowns are a, d, n_R, k_e, and l_e. 5 exclusive equations are required for solution of the combustion equation A5.

A.2.1 Solving for Exhaust H_2O concentration (l_e)

Carbon balance from equation A5:

$$n_R a = (n_P - n_R f)(g_e + h_e + s_e)$$

Equation A7

Hydrogen balance from equation A5:

$$n_R ab = (n_P - n_R f)(2l_e + 4s_e)$$

Equation A8

Replacing ($n_R a$) in equation A8 for equation A7

$$(n_P - n_R f)(g_e + h_e + s_e)b = (n_P - n_R f)(2l_e + 4s_e)$$

Rearranging

$$l_e = \frac{b}{2}(g_e + h_e + s_e) - \frac{4s_e}{2}$$ Equation A9

Calculations of g_e and h_e are further dependent on l_e because measured molar concentrations are dry. However, n_e is measured wet. Applying equation A6, replacing into equation A9, and rearranging

$$l_e = \frac{b}{2}(1 - l_e)(g_e' + h_e') - \frac{s_e}{2}(b - 4)$$

Rearranging in terms of l_e

$$l_e = \frac{b(g_e' + h_e') + s_e(b - 4)}{[2 + b(g_e' + h_e')]}$$ Equation A10

Thus the wet molar concentration of H_2O in the exhaust can be calculated from measured concentrations of CO_2, CO, and CH_4 in the exhaust stream, and knowledge of fuel composition.

Note: Equation A10 is analogous to the equation presented by Heywood [93]. Important differences are that (i) lean mixture means that CO concentrations are very low, and (ii) hydrocarbons are measured here as CH_4, not converted to concentrations of unburned HC with the same C/H ratio as the intake fuel.

A.2.2 EGR Considerations

Since there is a negligible (≈400ppm) concentration of CO_2 in ambient air, it can be assumed that any measured concentrations of CO_2 in the intake gas are as a result of EGR. So, from equation A2

$$f = \frac{g_i}{g_e}$$ Equation A11

Furthermore, g_i' is not only measured dry, but before fuel is added to the mixture. So, developing equation A6 gives

$$g_i = (1 - l_i - a)g_i' \qquad \text{Equation A12}$$

$$g_e = (1 - l_e)g_e' \qquad \text{Equation A13}$$

Replacing equations A12 and A13 into equation A11 gives

$$f = \frac{(1 - l_i - a)g_i'}{(1 - l_i)g_e'} \qquad \text{Equation A14}$$

As with equation A11, l_i and l_e are related thus

$$f = \frac{l_i}{l_e} \qquad \text{Equation A15}$$

Replacing equation A15 into equation A14 and rearranging gives

$$ae_i' + f[(1 - l_e)g_e' + l_e g_i'] = g_i' \qquad \text{Equation A16}$$

Equation A16 is the first of four simultaneous equations that are used in conjunction with equation A10 for the calculation of unknowns

A.2.3 Relationships Between Intake and Exhaust Oxygen Concentrations

The O_2 concentration in the intake gas (v_i') is measured dry, and before fuel is added to the mixture. This measurement includes oxygen contained in the intake air and any excess oxygen in the EGR as a result of lean or incomplete combustion. Thus, the relationship

$$v_i' = d' + j_i' \qquad \text{Equation A17}$$

can be formed by considering where each constituent of the dry measurement comes from. Furthermore, as with equation A12, measurements are made prior to the injection of fuel. Therefore

$$d = (1 - l_i - a)d'$$

$$j_i = (1 - l_i - a)j_i'$$

Replacing into equation A17 gives

$$d = (1 - l_i - a)v_i' - j_i \qquad \text{Equation A18}$$

Furthermore, general equations A2 and A6 provide the relationships

$$f = \frac{j_i}{j_e}$$

$$j_e = (1 - l_e)j_e'$$

These relationships combined with equation A15 allow further development of equation A18

$$d = (1 - fl_e - a)v_i' - fj_e$$

$$d = (1 - fl_e - a)v_i' - f(1 - l_e)j_e'$$

Expanding terms

$$d = v_i' - fl_e v_i' - av_i' - fj_e' + fj_e' l_e$$

Regrouping in terms of unknowns

$$-v_i' a - d + f(l_e j_e' - l_e v_i' - j_e') = -v_i' \qquad \text{Equation A19}$$

This form of the equation is most suitable for our purposes, since v_i' and j_e' are directly measured at the analyser, and l_e is calculated previously using equation A10.

A.2.4 Oxygen Balance (from equation A5)

$$n_R(ac+2d)=(n_P-n_Rf)(2g_e+h_e+2j_e+l_e)$$ Equation A20

Rearranging in terms of unknowns

$$ac+2d+f(2g_e+h_e+2j_e+l_e)-\frac{n_P}{n_R}(2g_e+h_e+2j_e+l_e)=0$$

g_e, h_e, and j_e are measured dry, so equation A6 applies. However, l_e is calculated wet in equation A10. Including these relationships gives

$$ac+2d+f[(1-l_e)(2g_e'+h_e'+2j_e')+l_e)]-\frac{n_P}{n_R}[(1-l_e)(2g_e'+h_e'+2j_e')+l_e)]=0$$

Equation A21

A.2.5 Carbon Balance (from equation A5)

Although the carbon balance has been used previously in the derivation of equation A10 for the determination of exhaust H_2O concentration, neither the carbon balance nor the hydrogen balance have yet been used in the formulation of the simultaneous equations. Therefore, it is possible to use either method again. The carbon balance has been chosen arbitrarily.

From equation A7

$$n_Ra=(n_P-n_Rf)(g_e+h_e+s_e)$$ Equation A7

rearranging gives

$$a+f(g_e+h_e+s_e)-\frac{n_P}{n_R}(g_e+h_e+s_e)=0$$

Using relationships provided by equation A6 gives

$$a + f[(1-l_e)(g_e'+h_e') + s_e] - \frac{n_P}{n_R}[(1-l_e)(g_e'+h_e') + s_e] = 0 \qquad \text{Equation A22}$$

A system of four simultaneous equations have been developed (A16, A19, A21, A22) with four unkowns (a, d, f, and n_R^{-1}). All other variables are either measured directly or calculated. The simplest solution method is by matrix algebra.

$$\begin{bmatrix} g_i' & 0 & (1-l_e)g_e'+l_e g_i' & 0 \\ -v_i' & -1 & l_e j_e'-l_e v_i'-j_e' & 0 \\ c & 2 & (1-l_e)(2g_e'+h_e'+2j_e')+l_e & -n_P[(1-l_e)(2g_e'+h_e'+2j_e')+l_e] \\ 1 & 0 & (1-l_e)(g_e'+h_e')+s_e & -n_P[(1-l_e)(g_e'+h_e')+s_e] \end{bmatrix} \begin{bmatrix} a \\ d \\ f \\ n_R^{-1} \end{bmatrix} = \begin{bmatrix} g_i' \\ -v_i' \\ 0 \\ 0 \end{bmatrix}$$

Equation A23

A.3 Calculation of A/F ratio

Once the 4 unknowns have been given by equation 23, the A/F ratio can be calculated simply

$$A/F \;\; Ratio = \frac{\dot{m}_a}{\dot{m}_f} = \frac{n_R(c+g_i)(32+3.773*28.16)}{n_R[a(12.011+1.008b+16c)+fs_e(12.011+4*1.008)]}$$

Rearranging for Simplicity

$$A/F \;\; Ratio = \frac{138.25(c+f(1-l_e)g_e')}{a(12.011+1.008b+16c)+16.043fs_e} \qquad \text{Equation A24}$$

A.4 Calculation of Gravimetric EGR rate

All of the EGR rate data presented in this report is done so on a gravimetric basis. Many CAI combustion studies that have considered EGR have presented measurements on a volumetric basis. While this is fine for entirely homogeneous combustion (such as is presented here), it has become clear that when burned gas residuals are used to initiate and control the combustion event, a volumetric representation of EGR is not sufficient to express the EGR rate. This is because the mass of EGR used is dependent on its temperature and pressure for a known volume, and these quantities may well not be known. So, it has been decided that EGR presented on a gravimetric basis is of more use to future researchers in the field, even though the gravimetric and volumetric rates are approximately numerically equal in this study (due to charge homogeneity). The gravimetric EGR rate can be calculated from the following expression

$$EGR_m = \frac{\dot{m}_{EGR}}{\dot{m}_{EGR} + \dot{m}_r}$$ Equation A25

where m_{EGR} and m_R are the masses of the EGR and reactant (intake air and injected fuel) components respectively.

$$\begin{aligned} m_{EGR} &= n_R f(g_e m_{CO_2} + h_e m_{CO} + j_e m_{O_2} + k_e m_{N_2} + l_e m_{H_2O} + s_e m_{CH_4}) \\ &= n_R f(44.01 g_e + 28.01 h_e + 32 j_e + 28.16 k_e + 18.016 l_e + 16.043 s_e) \end{aligned}$$

Using equation A6 to relate wet and dry species concentrations

$$m_{EGR} = n_R f[(1-l_e)(44.01 g_e' + 28.01 h_e' + 32 j_e') + 28.16 k_e + 18.016 l_e + 16.043 s_e]$$

Equation A26

Calculating reactant mass

$$m_R = n_R(am_{CH_bO_c} + d(m_{O_2} + 3.773m_{N_2})$$
$$= n_R[a(12.011 + 1.008b + 16c) + d(32 + 3.773 * 28.16)$$

Equation A27

Equations A26 and A27 are then replaced into A25 to calculate the gravimetric EGR rate.

The simplest way to employ these A/F ratio and EGR calculations is by programming a spreadsheet to perform them automatically. The computer used for data acquisition of pressure data has also been used for this. An extensive spreadsheet has been developed, used to manually log all of the inlet and exhaust species concentrations during experimentation. It also has facility for the input of fuel composition, required for the A/F ratio and λ calculations. The software then automatically calculates the unknowns of equation A23, λ, and the gravimetric EGR rate, and plots the results on a relevant chart for immediate review.